UNIVERSITÄT ZU LÜBECK

From the Institute of Nutritional Medicine

of the University of Lübeck

Director: Prof. Dr. med. Christian Sina

Mucosal p32/gC1qR/HABP1 regulates mitochondrial metabolism and hence goblet cell differentiation - implications for ulcerative colitis

Dissertation

for Fulfillment of

Requirements

for the Doctoral Degree

of the University of Lübeck

from the Department of Natural Sciences

Submitted by

Annika Sünderhauf

from Berlin, Germany

Lübeck 2021

First referee: Prof. Dr. med. Christian Sina

Second referee: Prof. Dr. med. Peter König

Date of oral examination: 6th of July 2021

Approved for printing. Lübeck, 9th of August 2021

In memories of my beloved father, Andreas Sünderhauf, who paved my way and who would have been incredibly proud.

Results of the present work were partly published in advance in the following articles:

- Sünderhauf, A., Hicken, M., Schlichting, H., Skibbe, K., Ragab, M., Raschdorf, A., Hirose, M., Schaffler, H., Bokemeyer, A., Bettenworth, D., Savitt, A.G., Perner, S., Ibrahim, S., Peerschke, E.L., Ghebrehiwet, B., Derer, S., and Sina, C. (2021). Loss of mucosal p32/gC1qR/HABP1 triggers energy deficiency and impairs goblet cell differentiation in ulcerative colitis. Cell Mol Gastroenterol Hepatol.
- Sünderhauf, A., Raschdorf, A., Hicken, M., Schlichting, H., Fetzer, F., Brethack, A.K., Perner, S., Kemper, C., Ghebrehiwet, B., Sina, C., and Derer, S. (2020). GC1qR Cleavage by Caspase-1 Drives Aerobic Glycolysis in Tumor Cells. Front Oncol *10*, 575854.
- Hirose, M., Kunstner, A., Schilf, P., Sünderhauf, A., Rupp, J., Johren, O., Schwaninger, M., Sina, C., Baines, J.F., and Ibrahim, S.M. (2017). Mitochondrial gene polymorphism is associated with gut microbial communities in mice. Sci Rep 7, 15293.

All experiments which were not directly conducted by the author or under her supervision by the technical assistants Maren Hicken, Heidi Schlichting and Ann-Kathrin Brethak from the Institute of Nutritional Medicine, University Hospital Schleswig-Holstein, Campus Lübeck, Germany are marked as such. Text passages with no or minor changes were only taken over from the previously published articles if they were originally phrased by the author.

Table of contents

List of figures

Supplementary figures

List of tables

Supplementary tables

Abbreviations

-/-	homozygous gene knockout
+/-	heterozygous gene knockout
aa	amino acids
ADP	Adenosine diphosphate
Aim2	absent in melanoma 2
ANCA	antineutrophil-cytoplasmatic antibodies
AOM	azoxymethane
Asc	apoptosis-associated speck like protein containing a CARD
ASCA	antibodies directed against *Saccharomyces cerevisiae*
ARF	ADP ribosylation factor
ATCC	American Type Cell Culture Collection
ATOH1	atonal basic helix-loop-helix transcription factor 1
ATP	adenine triphosphate
ATP8	ATPase 8
B6	C57BL/6J
°C	degree Celsius
C1q	complement component 1q
C1qbp	C1q binding protein
CARD	caspase recruitment domain
CD	Crohn's disease
cDNA	complementary DNA
CO_2	carbon dioxide
CoA	coenzyme A
CRC	colorectal cancer
CRISPR	clustered regularly interspaced short palindromic repeats
CXCL	CXC ligand
ctrl	control
DAPI	4',6-Diamidin-2-phenylindol
DLB	denaturating lysis buffer
DNA	deoxyribonucleic acid
DNP	2,4-Dinitrophenol
DSS	dextran sodium sulfate
ECAR	extracellular acidification rate
ELISA	enzyme-linked immunosorbent assay
et al.	*et alii*
$FADH_2$	flavin adenine dinucleotide (reduced)
FBS	fetal bovine serum
FMT	fecal microbiota transplantation
g	gramm
GAB	goblet cell autoantibodies
gC1qR	receptor of the globular heads of C1q
GFHP	glucose-free high protein
GWAS	genome-wide association studies
HABP1	hyaluronan-binding protein 1

HBSS	Hank's Balanced Salt Solution
HEPES	4-(2-hydroxyethyl)-1-piperazineethanesulfonic acid
Hes1	hairy/enhancer of split 1
HRP	horseradish peroxidase
HSP	heat shock protein
IBD	inflammatory bowel disease
IEC	intestinal epithelial cell
IgA	immunglobulin A
IL	interleukin
kc	keratinocyte chemoattractant
kcal	kilocalorie
kDa	kilodaltons
Klf4	Krueppel-like factor 4
l	liter
Lgr5	leucine-rich repeat-containing G-protein coupled receptor 5
LPS	lipopolysaccharide
M	mol/liter
MAB	mucosa attached bacteria
MAPK	mitogen-activated protein kinase
min	minute(s)
ml	milliliter
mm	millimeter
mM	millimol/liter
mRNA	messenger RNA
MTX	methotrexate
Muc	Mucin
µg	microgram
µl	microliter
µm	micrometer
NADH	nicotinamide adenine dinucleotide (reduced)
NEAA	non-essential amino acids
NF-*k*B	nuclear factor kappa b
NLB	non-denaturating lysis buffer
NLR	NOD-like receptor
Nlrc4	NOD-containing protein-like receptors family CARD-containing protein 4
Nlrp6	NLR protein 6
nm	nanometer
OCR	oxygen comsumption rate
ON	overnight
OCNT2	organic carnitine transporter 2
OXPHOS	oxidative phosphorylation
PAMPs	pathogen-associated molecular patterns
PBS	phosphate Buffered Saline
PCR	polymerase chain reaction
PFA	paraformaldehyde
pH	negative decimal logarithm of the H^+ ion concentration
PCR	polymerase chain reaction

PRR	pathogen-recognition receptors
PVDF	polyvinylidene difluoride
qPCR	quantitative PCR
ROS	reactive oxygen species
rRNA	ribosomal RNA
RT	room temperature
sec	second(s)
SCFA	short chain fatty acid(s)
SD	standard deviation
SDS	sodium dodecyl sulfate
SEM	standard error of the mean
siRNA	silencing RNA
SPDEF1	SAM pointed domain-containing Ets transcription factor 1
TBS	tris-buffered saline
TBS-T	tris-buffered saline with Tween20
TGF	transforming growth factor
Th	T helper
TLR	toll-like receptor
TNBS	trinitrobenzenesulfonic acid
TNF	tumor-necrosis factor
Tomm22	translocase of the outer membrane of mitochondria
U	units
UC	ulcerative colitis
UCP2	uncoupling protein 2
VDAC-1	voltage-dependent anion channel 1
wt	wild-type
w/o	without
w/v	weight per volume
xg	standard gravity

Abstract

Cell differentiation in intestinal crypts is driven by a metabolic switch from glycolysis to mitochondrial oxidation. Furthermore, mitochondrial and goblet cell dysfunction have been attributed to the pathology of ulcerative colitis (UC). In the present work, it was hypothesized that the multifunctional protein p32/gC1qR/HABP1, which has been described to critically maintain oxidative phosphorylation (OXPHOS), is involved in goblet cell differentiation and hence in the pathology of UC.

Ex vivo, colonic goblet cell differentiation in relation to p32 expression and mitochondrial function was studied in tissue biopsies from UC patients in remission and active disease *versus* non-inflammatory bowel disease controls. Functional studies were performed in goblet cell-like HT29-MTX cells as well as in Hap1-*p32*-knockout, HAP1-p32-mutant and parental HAP1-*p32*-wildtype cells *in vitro.* Mitochondrial respiratory chain complex V-deficient, ATP8-mutant mice were utilized as a confirmatory model. Nutritional intervention studies utilizing a glucose-free, high-protein diet were performed in C57BL/6 mice.

In vitro, p32 was found to be essential for maintenance of mitochondrial OXPHOS function. Of major interest, in UC patients in remission, colonic goblet cell differentiation was significantly decreased compared to controls in a p32-dependent manner. Plasma/serum L-lactate and colonic pAMPK level were increased, pointing at high glycolytic activity and energy deficiency. Consistently, *p32* silencing in mucus-secreting HT29-MTX cells abolished butyrate-induced differentiation and induced a metabolic shift towards glycolysis. In ATP8-mutant mice, colonic p32 expression correlated with loss of differentiated goblet cells, resulting in a thinner mucus layer. Conversely, feeding mice an isocaloric glucose-free, high-protein diet increased mucosal energy supply that promoted colonic p32 level, goblet cell differentiation and mucus production. Upon inflammasome activation, caspase-1 was found to cleave p32 at two distinct sides, resulting in loss of the mitochondrial leader sequence and thus a shift in cell metabolism from mitochondrial OXPHOS towards glycolysis. *In vitro,* cell proliferation was induced upon caspase-1 dependent p32-cleavage while goblet cell differentiation was abrogated. This mechanism was found to be relevant during active UC, since level of non-cleaved p32 and goblet cell numbers were decreased in a caspase-1 dependent manner in colonic biopsies of UC patients.

Taken together, this thesis describes two novel p32-dependent molecular mechanism which might highly impact the development and pathology of UC and which may be therapeutically regulated by nutritional intervention. On the one hand, mucosal p32 enables colonic goblet cell differentiation by driving mitochondrial OXPHOS, a mechanism impaired in UC. Whereas during active inflammation caspase-1 mediated cleavage of p32 induces a metabolic switch from OXPHOS towards glycolysis enabling high cell proliferation rates.

Zusammenfassung

In intestinalen Krypten wird die Zelldifferenzierung durch eine Verschiebung des Metabolismus von Glykolyse zu mitochondrialer Oxidation angetrieben. Des Weiteren ist eine Dysfunktion der Mitochondrien und der Becherzellen mit der Pathogenese von Colitis ulcerosa (CU) assoziiert. In der vorliegenden Arbeit wurde die These aufgestellt, dass das multifunktionale Protein p32/gC1qR/HABP1, welches laut Literatur substantiell an der Aufrechterhaltung der oxidativen Phosphorylierung (OXPHOS) beteiligt ist, eine wichtige Rolle in der Becherzelldifferenzierung und somit der Pathogenese von CU spielt.

Die Becherzelldifferenzierung im Kolon wurde in Bezug auf die p32-Expression und Mitochondrienfunktion *ex vivo* in Gewebebiopsien von CU Patienten in Remission und mit aktiver Erkrankung sowie Kontrollproben von Patienten ohne chronisch entzündliche Darmerkrankung, untersucht. *In vitro* erfolgten funktionale Studien an becherzellartigen HT29-MTX Zellen sowie Hap1-*p32*-defizienten, HAP1-p32-mutierten und parentalen HAP1-*p32*-Wildtyp Zellen. Zur Bestätigung der Ergebnisse wurden Mäuse mit einer Mutation im Komplex V der mitochondrialen Atmungskette (ATP8-mut) verwendet. An C57BL/6 Mäusen erfolgten Studien zur Ernährungsintervention unter Verwendung einer glukosefreien, proteinreichen Diät.

In vitro wurde festgestellt, dass p32 für die Aufrechterhaltung der mitochondrialen OXPHOS-Funktion essentiell ist. Interessanterweise war die Differenzierung von Becherzellen aus dem Kolon in CU Patienten in Remission im Vergleich zur Kontrollgruppe in Abhängigkeit von der p32-Expression signifikant verringert. Plasma/Serum L-Laktat und die Phosphorylierung von AMPK waren erhöht als Anzeichen einer hohen Glykolyseaktivität und einer Energiedefizienz. Ebenso verhinderte die RNA-Interferenz von *p32* die Butyrat-induzierte Differenzierung von Mukus-sezernierenden HT29-MTX Zellen und bewirkte eine Verschiebung des Metabolismus hin zur Glykolyse. In ATP8-mut Mäusen korrelierte die Expression von p32 im Kolon mit dem Verlust von differenzierten Becherzellen, was in einer dünneren Mukusschicht resultierte. Im Gegenzug steigerte eine isokalorische glukosefreie, proteinreiche Diät das mukosale Energieangebot was wiederum die p32-Expression, die Becherzelldifferenzierung und die Mukusproduktion förderte. Im Zuge der Inflammasomaktivierung wurde p32 an zwei spezifischen Stellen durch Caspase-1 gespalten, was in einem Verlust der mitochondrialen Leitsequenz und somit zu einer Verschiebung des Zellmetabolismus von mitochondrialer OXPHOS hin zur Glykolyse führte. Die Caspase-1 abhängige Spaltung von p32 induzierte Zellproliferation in *in vitro* Experimenten, während die Becherzelldifferenzierung inhibiert wurde. Dieser Mechanismus erwies sich als relevant in aktiver CU, da das Expressionsniveau von ungespaltenem p32 und die Anzahl von Becherzellen in Kolonbiopsien von CU Patienten in Abhängigkeit von aktiver Caspase-1 reduziert waren.

Zusammengenommen beschreibt die vorliegende Arbeit zwei neue p32-abhängige Mechanismen, welche die Entstehung und Pathogenese von CU stark beeinflussen und therapeutisch durch Ernährungsinterventionen reguliert werden könnten. Einerseits ermöglicht mukosales p32 die Becherzelldifferenzierung im Kolon durch Aufrechterhaltung der mitochondrialen OXPHOS, ein Mechanismus, der in CU beeinträchtigt ist. Andererseits induziert die Caspase-1 vermittelte Spaltung von p32 unter aktiver Entzündung eine metabolische Verschiebung von OXPHOS hin zu Glykolyse, infolgedessen hohe Zellproliferationsraten ermöglicht werden.

1 Introduction

1.1 The intestinal crypt

The human gastrointestinal tract comprises all organs of the digestive system between mouth and anus, including esophagus, stomach and intestine. The intestine itself can be anatomically subdivided into two segments: a) the small intestine, combining duodenum, jejunum and ileum, and b) the large intestine, including cecum, ascending to sigmoid colon as well as rectum and anal canal. Facing the lumen, the epithelium together with the underlying lamina propria and the muscularis mucosae form the mucosa. The single-cell layered columnar epithelium itself is responsible for the absorption, processing, transcellular transport, sensing as well as secretion of various compounds. It also serves as a physical barrier by separating the luminal content from underlying structures. The epithelial layer is completely renewed within three to five days and thus depicts the highest cellular turnover rate in the body (Darwich et al., 2014). Meanwhile, the lamina propria presents a thin layer of loose connective tissue, which lies beneath the epithelium and harbors a variety of cell types, including fibroblasts and different immune cells. Separating the lamina propria from the submucosa, the muscularis mucosae consists of several thin layers of smooth muscle fiber, which mediate transport of food content through the gut by contractile peristaltic waves (Rao and Wang, 2010).

Within the epithelium, the intestinal crypt comprises a basic unit of functionally different cells, which originate from the same pool of stem cells. In both, the small and large intestine, crypts are clearly structured in three sections, the stem cell niche at the bottom of the crypt, the transit amplifying zone and the differentiated cell zone at the top of the crypt (Clevers, 2013) (Figure 1). In contrast to the colonic crypt, the crypts of Lieberkühn in the small intestine, extend as small, finger-like protrusions into the lumen, forming so-called villi, thereby increasing the surface area for absorption of nutrients (Lieberkühn, 1745).

Each crypt base contains multiple leucine-rich repeat-containing G-protein coupled receptor 5 positive ($LGR5^+$) stem cells which eventually produce four main cell types, including enterocytes, goblet cells, enteroendocrine cells and Paneth cells, which are restricted to the small intestine (Cheng and Leblond, 1974) (Figure 1). Besides this model of stem cell identity referred to as “stem cell zone model”, a second paradigm for the small intestinal crypt has been proposed by Potten in 1977, the “+4 model” (Potten, 1977). Here, stem cells are proposed to reside within a ring of 16 cells at the +4 position directly above the Paneth cells. Even if both of these stem cell models are still under discussion, theories combining aspects of one and the other are emerging (Barker, 2014).

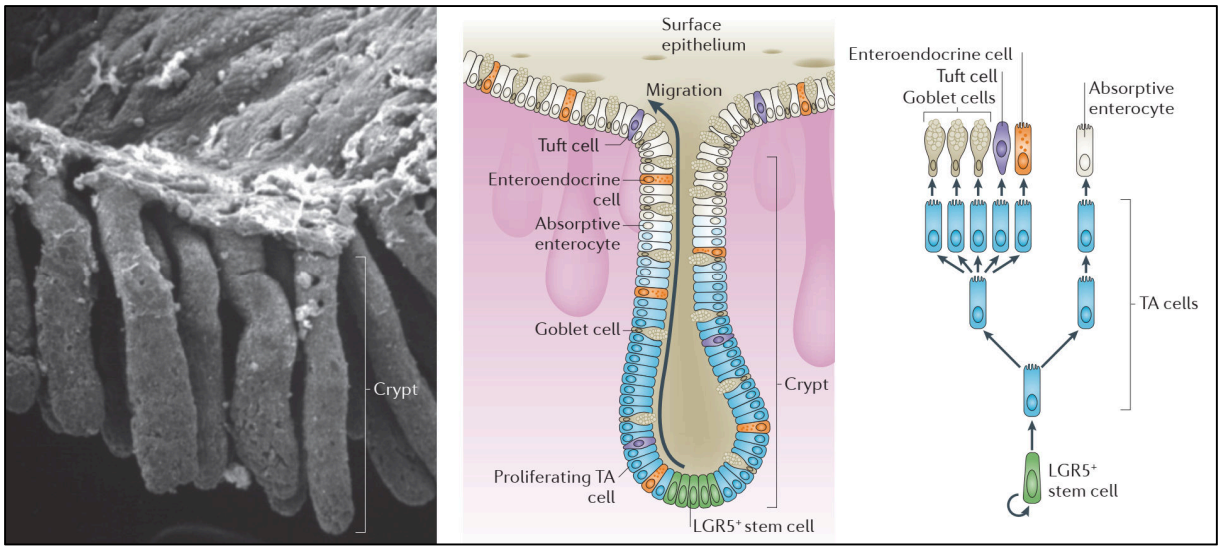

Figure 1: The colonic crypt architecture. LGR5$^+$ stem cells at the bottom of the crypt give rise to rapidly proliferating cells in the transit amplifying (TA) zone, which then differentiate into mature lineages including enterocytes, goblet cells, enteroendocrine cells and tuft cells in the upper part of the crypt (middle and right panel). Left panel: Scanning electron microscopy of colonic crypts. *Taken from:* Barker: Adult intestinal stem cells: critical drivers of epithelial homeostasis and regeneration (Figure 1b), Nature Reviews 2014 (Barker, 2014).

Enterocytes are the most abundant cells in the intestinal epithelium. Their main role is the absorption of nutrients as well as secretion of hydrolytic enzymes into the lumen. Furthermore, enterocytes take up luminal antigens, which are either degraded *via* the lysosome, released into the interstitial space after transcytosis or processed and presented to T cells in the submucosa. Tight junctions in between cells serve as regulators of paracellular transport of antigens (Snoeck et al., 2005). Goblet cells are scattered in between the enterocytes from the middle of the crypt to the tip of the crypt or villus. Their main function is to produce and secrete mucins, which form the intestinal mucus layer, separating the luminal content from the epithelium. Goblet cell numbers increase from proximal (small intestine) to distal (colon), similar to the increase in luminal microbes (Cheng, 1974). Apart from its barrier function, growing evidence supports the involvement of goblet cells in maintaining tolerance under steady state conditions by transporting antigens to antigen presenting cells of the lamina propria (McDole et al., 2012). Enteroendocrine cells comprise different cellular subtypes, which produce various hormones that have key functions in regulating food digestion and absorption, insulin secretion and appetite (Gribble and Reimann, 2019). They represent a minority of cells found in the small intestine and the rectum, with even lower frequency and diversity in the colon (Sjolund et al., 1983). In the small intestine, Paneth cells additionally locate to the crypt base, residing between stem cells. They contribute to antimicrobial defense *via* secretion of antimicrobial peptides such as defensins and lysozyme. Finally, two recently discovered cell types, named microfold cells and tuft cells, which are rare in their mucosal appearance, have been found to also derive from crypt-based stem cells (de Lau et al., 2012). Microfold cells are found at sites of gut-associated lymphoid tissue within the small

intestinal epithelium and allow for transcytosis of antigens across the epithelial cell layer towards the immune cell-harboring lamina propria (Mabbott et al., 2013). On the other hand, tuft cells function in concert with the hematopoietic compartments in mounting an efficient immune type 2 response (Howitt et al., 2016). Decision on cell fate as well as cell proliferation and differentiation in the intestinal crypt are highly regulated systems, depending on various external stimuli, the expression of a complex and highly hierarchical network of transcription factors and distinct metabolic requirements.

1.1.1 Energy generation in the intestinal crypt

In the intestinal mucosa, cells of different type and state gain their energy required for maintenance of cellular processes from distinct metabolic pathways. Generally, three main mechanisms can be distinguished: glycolysis, β-oxidation and oxidative phosphorylation (OXPHOS). Hereby, energy homeostasis is seldom maintained by only one metabolic pathway, but mostly by a combination of mechanisms, with shifting emphasis on one or the other depending on differentiation and activation status of the cell (Rath et al., 2018; Stringari et al., 2012).

Cells of the lower third of the crypt, including the stem cell niche and the transit amplifying zone, mainly rely on glycolysis for energy generation (Figure 2) (Ito and Suda, 2014; Stringari et al., 2012). Glycolysis is an oxygen-independent metabolic pathway taking place in the cytosol. In its process one molecule of glucose is converted into two molecules of pyruvate *via* a series of catalytic reactions. Most other monosaccharides can also be metabolized to intermediates of the glycolysis pathway. During glycolysis, energy is generated in the form of four molecules adenosine triphosphate (ATP) and two molecules of the cofactor nicotinamide adenine dinucleotide in its reduced state (NADH). The latter function primarily as electron donors in the electron transport chain as part of the OXPHOS system or as co-substrates in various enzymatic reactions (Alberts et al., 2015). Of note, cells located at the crypt base display a high free to bound NADH ratio (i.e. $NADH/NAD^+$), characterizing a glycolytic metabolic phenotype in a hypoxic environment (Stringari et al., 2012). Under anaerobic conditions pyruvate is fermented towards lactate, while in the presence of oxygen, pyruvate is metabolized to acetyl coenzyme A (acetyl CoA), a molecule which is finally oxidized in the citric acid or Krebs cycle. Oxidation of both, pyruvate and acetyl CoA, takes place in the mitochondrial matrix. The citric acid cycle itself generates NADH and the hydroquinone form of flavin adenine dinucleotide ($FADH_2$), which can be subsequently used for ATP production *via* the OXPHOS system. Finally, instead of entering the citric acid cycle as acetyl CoA, pyruvate can also be converted to form the amino acid alanine (Alberts et al., 2015).

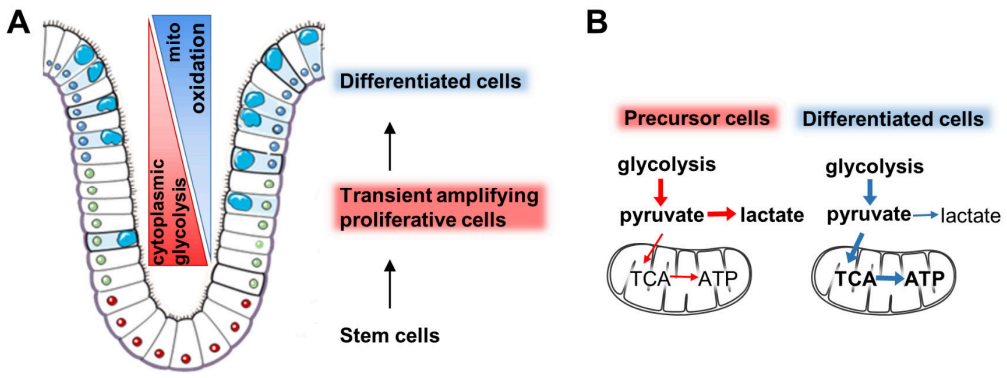

Figure 2: Energy generation in the colonic crypt. A) Proliferating cells in the lower part of the colonic crypt mainly rely on cytoplasmic glycolysis, while differentiated cells in the upper part of the crypt obtain their energy from mitochondrial (mito) oxidation, including β-oxidation and oxidative phosphorylation. The schematic model was generated by modifying images from Servier Medical Art (Reef et al., 2007). **B)** High rates of glycolysis of precursor cells in the transient amplifying zone result in high production of lactate but low level of generated ATP per molecule glucose compared to differentiated intestinal epithelial cells.

As an alternative to completing the classical glycolytic pathway, glucose molecules, in the form of glucose – 6 – phosphate, can enter the cytosolic pentose phosphate pathway. Firstly, in the oxidative phase the reducing agent NADPH is generated, which is needed in a range of anabolic reactions, such as lipid and nucleic acid synthesis. Subsequently, 5-carbon sugars (pentoses), which are used for the synthesis of nucleic and aromatic amino acids, are produced in the non-oxidative phase (Alfarouk et al., 2020). Both metabolic pathways, glycolysis and the pentose phosphate pathway are active, especially in highly proliferating cells, such as cancer cells and potentially cells of the transit amplifying zone, even in the presence of sufficient oxygen. While glycolysis is utilized for rapid production of ATP, the pentose phosphate pathway generates NADPH and 5-carbon sugars. All these products are required for anabolic processes enabling high cellular proliferation rates (Alfarouk et al., 2020; Vander Heiden et al., 2009; Warburg, 1956).

In contrast to stem cells and rapidly proliferating, undifferentiated cells in the lower part of the crypt, differentiated post-mitotic cells in the upper third of the crypt maintain their energy level by mitochondrial oxidation, including OXPHOS and β-oxidation (Kaiko et al., 2016; Stringari et al., 2012; Xu et al., 2013). Hereby, the switch in energy generation has to be perceived as a metabolic trajectory, which occurs in parallel to the cellular differentiation gradient within the crypt, rather than as a sudden cut off (Figure 2) (Stringari et al., 2012).

Mitochondrial OXPHOS provides for the vast amount of usable energy obtained from the breakdown of carbohydrates or fats. Compared to cytosolic glycolysis, accounting an overall production of two to four molecules of ATP, OXPHOS generates 32 to 34 ATP molecules. During OXPHOS, NADH and $FADH_2$ transfer their electrons along complex I to IV of the electron transport chain, thereby generating a proton gradient across the inner mitochondrial membrane. During the final step of the OXPHOS

system, the ATPase synthase couples the energetically favorable flow of protons back across the membrane for the synthesis of ATP (Cooper, 2000).

B-oxidation, the prime pathway for the degradation of fatty acids is taking place at the inner mitochondrial membrane, although very long chain fatty acids or oxidized in peroxisomes. Within mitochondria, the β-carbons of fatty acids undergo oxidation to carbonyl groups, facilitated by the mitochondrial trifunctional enzyme complex. This process generates the co-enzymes acetyl CoA, NADH and $FADH_2$. The energy yield obtained during ß-oxidation depends on the length of the fatty acid utilized as substrate and requires final oxidation in the citric acid cycle or during OXPHOS (Houten and Wanders, 2010). In the human and murine colonic mucosa, short chain fatty acids (SCFA), microbial derived butyrate in particular, serve as the main substrate for ß-oxidation (Roediger, 1980b). Nevertheless, long chain fatty acids have also been recently reported to be oxidized by the intestinal epithelium (Smith et al., 2020). Of special interest, butyrate inhibits stem and progenitor cell proliferation and metabolization of butyrate by differentiated colonocytes in the upper part of the crypt prevents it from reaching stem and progenitor cells at the crypt bottom (Kaiko et al., 2016). Despite extensive research on cell metabolism in the intestinal epithelium, it is not yet understood which factors drive the metabolic switch from cytosolic glycolysis to the mitochondrial oxidation system and the transition of transient amplifying cells into post-mitotic differentiated cells.

1.1.2 Intestinal goblet cells

Differentiation of cells occurs along the described metabolic trajectory of shifting energy metabolism in the intestinal epithelial crypt (Stringari et al., 2012). One cell type that is highly involved in the maintenance of intestinal barrier integrity is the goblet cell. Cells of this entity are highly specialized in the secretion of mucins, which forms a physical barrier separating luminal bacteria from the colonic epithelium (Johansson et al., 2008) (Figure 3).

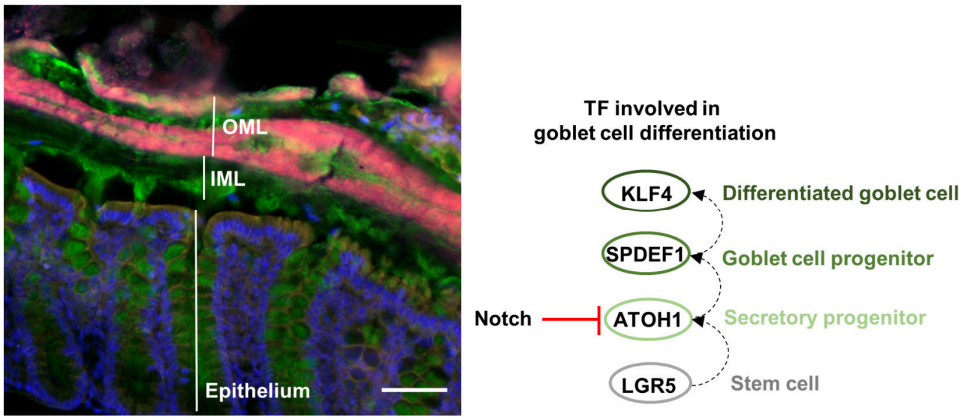

Figure legend follows on next page

Figure 3: Mucins secreted by goblet cells form the intestinal mucus barrier.(left) The inner mucus layer (IML) is devoid of bacteria, while the outer mucus layer (OML) serves as a habitat for the microbiota. Mucus was stained applying a polyclonal antibody against mucin 2 (Clone H-300), and a corresponding AlexaFluor-488 labeled secondary antibody (green). Bacteria were visualized by fluorescent *in situ* hybridization, applying a DY480XL-labeled probe against bacterial 16S ribosomal RNA (EUB 338) (red). Samples were counterstained with DAPI (blue). Fluorescent microscopy staining was performed by Heidi Schlichting under the supervision of the author at the Institute of Nutritional Medicine, Lübeck, Germany. (right) Transcription factors (TF) involved in goblet cell differentiation are displayed along the differentiation axis from crypt bottom to the tip of the crypt.

Differentiation in the intestinal crypt is controlled by the expression of lineage-restricting transcription factors (Clevers, 2013) (Figure 3). Constantly dividing, $LGR5^+$ stem cells produce progenitor cells, which move upwards, leave the stem cell niche and enter the transit amplifying zone. Secretory precursor cells in the transit amplifying zone are characterized by high expression of atonal basic helix-loop-helix transcription factor 1 (ATOH1, also referred to as HATH1 in humans and Math1 in mice). Further down the differentiation line goblet cell precursor cells exhibit high level of SAM pointed domain-containing Ets transcription factor 1 (SPDEF1) (Noah et al., 2010). Meanwhile, Notch signaling and expression of transcription factor hairy/enhancer of split 1 (HES1) define cells of the absorptive lineage and negatively regulate secretory cell differentiation (van Es et al., 2005). Moving upwards within the crypt, cells of the secretory or absorptive lineage enter terminal differentiation. Terminally differentiated goblet cells in the upper third of the colonic crypt are defined by high expression of the transcription factor Krueppel-like factor 4 (KLF4). Notably, *klf4* deficient mice display a decrease of about 90% of colonic goblet cells and abnormal mucin and goblet cell appearance in the presence of inconspicuous cell proliferation and normal presentation of all other cell entities (Katz et al., 2002).

1.1.2.1 Formation of the intestinal mucus layer

KLF4-expressing, terminally differentiated goblet cells are particularly specialized in the production and secretion of mucins, with mucin (MUC) 2 being the most abundant one in the colon and small intestine. These large, complex and highly glycosylated proteins are stored in secretory vesicles and are released into the intestinal lumen by exocytosis upon vesical fusion with the apical membrane (Bansil and Turner, 2018). After secretion, the densely packed mucins expand 100-1,000 times in volume by incorporating large amounts of water into their net-like structure (Bansil and Turner, 2018). The mucus layer covering the epithelium of the small and large intestine differ in composition and function. In the small intestine the mucus layer is non-attached, forms a discontinuous layer and is penetrable for bacteria (Atuma et al., 2001). In contrast, colonic mucus is composed of two structurally and functionally different strata: a firm inner layer which is continuously renewed within hours and a loose outer layer (Johansson et al., 2008). The mucosa-attached inner layer has been shown to exclude the majority of bacteria, providing a first line of defense and functioning as a size exclusion filter through which small molecules, such as ions, water and nutrients can diffuse and reach the enterocytes

(Cone, 2009). On the other hand, the loose outer layer serves as a habitat for the intestinal commensal microbiota (Johansson et al., 2008) (Figure 3). In contrast to the fecal microbiota, composition of this mucosal or mucus-attached microbiota remains poorly understood. Recent studies suggest a remarkable difference in bacterial composition between feces and mucus. The outer mucus layer in both mice and humans is mainly colonized by bacteria which utilize mucin as a substrate, such as *Bacteroides fragilis*, *Akkermansia muciniphila* and Bifidobacteriaceae (Ouwerkerk et al., 2013). Interestingly, these mucin-degrading bacteria promote mucus secretion and protect from inflammation rather than reducing the mucus layer thickness (Earley et al., 2019). While the mucus layer itself serves as a nutritional source for certain bacterial strains, constitution of the mucus layer is dependent on the dietary intake of the host. Deprivation of dietary fibers has been reported to result in a mucus-eroding microbiota, promoting barrier disruption and lethal colitis upon infection with Citrobacter rodentium (Desai et al., 2016). In general, the gut microbiota has been demonstrated to be pivotal for the formation of a functional mucus barrier. The mucus layer of germ-free mice depicted lower relative amounts of Muc2 and an increased penetrability compared to conventionally raised mice (Johansson et al., 2015). In line, mice lacking Muc2 present with bacterial invasion into the epithelium resulting in increased risk of developing spontaneous colitis and colon cancer (Van der Sluis et al., 2006).

1.1.2.2 Immunogenic properties of intestinal goblet cells

Besides its major role in barrier maintenance through the secretion of mucus, an immunogenic function has been recently attributed to goblet cells. On the one hand, goblet cells have been reported to display endocytic and antigen delivering properties (McDole et al., 2012). On the other hand, sentinel goblet cells trigger mucin exocytosis in response to toll-like-receptor (TLR)-dependent inflammasome-mediated activation (Birchenough et al., 2016).

Despite the presence of a physical barrier due to the mucus layer and epithelium, the immune system underlying the epithelium is not ignorant of the luminal content, but instead achieves oral tolerance by continuously monitoring innocuous luminal antigens in the steady state (Pabst and Mowat, 2012). Several pathways enable the traverse of luminal substances through the epithelium including paracellular leak, transcellular permeability, transport by M cells, and the extension of transepithelial dendrites by antigen-presenting cells of the lamina propria (Schulz and Pabst, 2013). Additionally, a process referred to as goblet cell-associated antigen passage describes the uptake and transfer of luminal antigens to antigen presenting cells of the lamina propria by goblet cells (McDole et al., 2012). Under steady state conditions, this process has been reported to occur in the small intestine and distal colon, the sides of luminal tolerance, but not in the adult proximal colon (Knoop et al., 2017).

Interestingly, goblet cell-associated antigen passage is rapidly inhibited in the small intestine of mice during pathogenic infections (Kulkarni et al., 2018).

A second system which appears to mediate innate immune signalling in goblet cells is the inflammasome complex. Colonic goblet cells in the mouse express TLRs as potent inducers of inflammasome priming (Murphy and Weaver, 2017), the inflammasome activation sensors Aim2 (absent in melanoma 2), Nlrc4 (nucleotide-binding oligomerization domain (NOD)-containing protein-like receptors family caspase recruitment domain (CARD)-containing protein 4), Nlrp6 (NOD-like receptor (NLR) protein 6) and the core inflammasome components ASC (adaptor molecule apoptosis-associated speck-like protein containing a CARD), Caspase-1 and Caspase-11 (Volk et al., 2019). Of special interest, Wlodarska *et al*. reported Nlrp6$^{-/-}$ and Casp1/11$^{-/-}$ mice to be highly susceptible to *Citrobacter rodentium* infection compared to wild-type controls (Wlodarska et al., 2014) and the severity of *C. rodentium* infection can be linked to inner mucus layer integrity (Bergstrom et al., 2017).

Formation of the inflammasome is a multi-step process, which is preceded by a priming step that induces the translation of pro-forms of the inflammatory cytokines IL-1ß and IL-18. Several bacterial components such as LPS and flagellin may trigger inflammasome priming. Of note, treatment of colonic explants with the corresponding stimuli resulted in Muc2 secretion of goblet cells in the upper part of the crypt (Birchenough et al., 2016). Assembly of the inflammasome complex itself can be induced by several different events including reduced intracellular potassium, increased level of reactive oxygen species (ROS) and lysosome disruption. All of these activating signals result in dissociation of heat shock protein (HSP) 90 and co-chaperone SGT1 from NLR proteins, thereby enabling assembly of the core inflammasome complex. Several active NLR molecules assemble *via* aggregation of their leucine-rich repeat domains, which then induces the pyrin domains of NLR proteins to interact with the adaptor protein ASC. ASC itself is composed of an N-terminal pyrin domain and a *C*-terminal CARD domain. Both of these domains are able to form polymeric filaments after interaction with NLR proteins. The outward facing CARD domains interact with inactive pro-caspase 1 molecules, thereby enabling autocleavage and the release of active Caspase1 molecules. Finally, Caspase1 activates IL-1ß and IL18 by proteolytic cleavage, resulting in the release of these pro-inflammatory cytokines into the extracellular space (Murphy and Weaver, 2017).

One goblet cell subpopulation, which appears to be especially susceptible for bacterial antigen endocytosis and inflammasome activation are so called sentinel goblet cells. They display distribution of less than one cell per crypt in apical regions. Of special interest, antigen-triggered, Nlrp6 inflammasome-dependent activation of sentinel goblet cells triggered rapid Muc2 exocytosis as well as Muc2 release from adjacent goblet cells in the upper part of the crypt in colonic explants

(Birchenough et al., 2016). This mechanism is assumingly highly important upon prior mucus barrier disruption, when invading bacteria need to be expelled from the epithelial crypt.

Whether the inflammasome is also required for baseline goblet cell function and formation of the colonic mucus barrier has been a topic of controversy. Wlodarska *et al.* reported in 2014, that *Nlrp6*$^{-/-}$ as well as *Caspase1/11*$^{-/-}$ mice present with defective mucus secretion and mucus layer formation in the colon already at baseline level (Wlodarska et al., 2014). Meanwhile, confirmation experiments performed in mice lacking either specific inflammasome activation receptors (*Nlrp3*$^{-/-}$, *Nlrc4*$^{-/-}$ and littermate-controlled *NLRP6*$^{-/-}$) or canonical and non-canonical inflammasome components (*Caspase1/11*$^{-/-}$ and *Caspase11*$^{-/-}$) by Volk *et al.* did not result in an altered mucus layer compared to wild-type animals (Volk et al., 2019).

Despite contradicting data on the involvement of the inflammasome compartment on goblet cell function in the non-inflamed state, goblet cells most certainly function as antigen sensing and presenting cells that react to bacteria penetrating the inner mucus layer, thereby contributing to intestinal immunity.

1.2 P32/HABP1/gC1qR

One highly conserved protein, that has been described to be indispensable for OXPHOS function is p32, also referred to as hyaluronan-binding protein 1 (HABP1) or receptor of the globular heads of the complement component 1q (gC1qR). The rather complex nomenclature of this protein arose from its historic discovery, where it was independently described from three different working groups in distinct contexts. D' Souza and Datta purified in 1985 a hyaluronan-binding protein using hyaluronan affinity chromatography which they referred to as HABP1 (Genbank ID 9786126) (D'Souza and Datta, 1985). The according complementary DNA (cDNA) sequence matched with the cDNA sequence of p32, which Krainer *et al.* identified as a subunit of the human pre-messenger RNA (mRNA) splicing factor 2 in 1991 (Krainer et al., 1991). Initially, the cDNA sequence identified by Krainer *et al.* was lacking the 5' end sequence encoding the first 73 amino acids (aa) and thereby the first exon of the full-length p32 protein. A mistake, which was corrected two years later by Honoré *et al.*, who described p32 to be synthesized as a pro-protein of 282 amino acids that is post-translationally processed by removal of the initial 73 aa to a mature protein of 209 aa (Genbank ID L04636) (Honore et al., 1993). The sequence of p32 and HABP1 was further found to be identical to that of the human gC1qR or C1q binding protein (C1QBP), which was identified by Ghebrehiwet *et al.* in 1994 (Ghebrehiwet et al., 1994). For reasons of simplicity the present work will refer to p32/HABP1/gC1qR as p32 from here onwards.

The human *p32* gene is located on chromosome 17q13.3 (Guo et al., 1997) and presents with a high degree of identity to the rat and mouse p32 sequence (89.9% cDNA sequence identity) (Lynch et al.,

1997). A homologue for the *p32* gene has been further reported in birds (chicken 80% sequence homology to human *p32*), helminths (*Caenorhabditis elegans*), yeast (*Saccharomyces cerevisiae*) and unicellular organisms (*Trypanosoma brucei*) (Sengupta et al., 2004). The spliced mRNA of the human reference sequence of *p32* encompasses 849 nucleotides and six exons encoding the 282 amino acids 33 kDa full-length pre-protein. Meanwhile, the mature p32 protein has a calculated molecular weight of 23.7 kDa, lacking the *N*-terminal 73 amino acids of the full-length protein. These 73 amino acids are encoded by the first exon of the cDNA sequence and harbor a mitochondrial leader sequence. Experiments by Dedio *et al.* have shown that especially the first 33 amino acid residues of p32 are essential for guiding the pre-protein to the mitochondria (Dedio et al., 1998). The mechanism by which the p32 protein loses the *N*-terminal 73 residues and matures from the pre-protein is still not fully understood. Nevertheless, cleavage of targeting signals of precursor proteins in the mitochondrial matrix by the mitochondrial processing peptidase during or after import is a general mechanism conserved in mammals and fungi (Luciano and Geli, 1996). While p32 predominantly localizes to the mitochondria due to its 33-residue *N*-terminal mitochondria-targeting signal sequence, it has also been reported to appear at several other cellular compartments including the cell surface and the extracellular space (Ghebrehiwet et al., 1994; Muta et al., 1997; Saha and Datta, 2018). P32 has been further described to present as an unusual acidic, single chain protein that is able to form a doughnut-shaped quaternary structure comprising three monomers (Jiang et al., 1999).

Over the last decades p32 has been reported to bind to and interact with a large number of different proteins. P32-involvement in a range of processes and at different sub-cellular locations with so far unknown functions and binding partners is continuously emerging. Especially mitochondrial energy metabolism as well as inflammation and cancer development have been proven fields that are highly controlled by p32 function.

1.2.1 P32 and its role in cellular metabolism

In 1997, p32 was proposed for the first time to play an important role in maintenance of mitochondrial OXPHOS. Disruption of the yeast homologue of p32 resulted in growth retardation of yeast cells in glycerol but not in glucose medium, indicating involvement of p32 in mitochondrial energy metabolism (Muta et al., 1997). During the following decades, several research groups reported down-regulation of p32 in various human and murine cell lines to result in the suppression of mitochondrial activity and a shift in energy metabolism from OXPHOS towards glycolysis (Fogal et al., 2010; Hu et al., 2013). Data generated in mice heterozygous for *p32* supported *in vitro* experiments by displaying impaired mitochondrial OXPHOS and a compensatory increase in energy generation *via* fatty acid oxidation and glycolysis (Liu et al., 2017). Meanwhile, a homozygous knockout for *p32* in mice results in embryonic lethality, further supporting the notion that p32 is indispensable for cell survival (Liu et al., 2017; Yagi

et al., 2012). Interestingly, overexpression of p32 in a murine fibroblast cell line did not lead to an increase in cellular fitness, but induced growth perturbation and initiation of apoptosis (Chowdhury et al., 2008). This artificial increase of p32 above physiologic levels further resulted in inhibition of respiratory chain complex I, an increase in generation of reactive oxygen species and subsequent mitochondrial dysfunction underlining the importance of balanced p32 expression.

While the exact role of p32 in maintaining mitochondrial function is yet not fully understood, cumulative data indicate that p32 regulates mitochondrial protein translation. P32 appears to operate as a chaperone protein and RNA binding factor for translation of mitochondrially encoded proteins, including many mitochondrial-encoded respiratory chain complex subunits (Hillman and Henry, 2019; Yagi et al., 2012). P32 has been further reported to control RNA splicing by inhibiting phosphorylation and thereby RNA-binding and spliceosome formation of alternative splicing factor 1/pre-mRNA-splicing factor 2 (Petersen-Mahrt et al., 1999). Finally, mitochondrial morphology was shown to be dependent on p32 expression level (Hu et al., 2013). Overexpression of p32 increased mitochondrial fibrils and silencing RNA (siRNA)-mediated p32 knockdown enhanced mitochondrial fragmentation accompanied by loss of fusion proteins. Of note, maintenance of mitochondrial fusion and fission dynamics is essential for the control of energy metabolism in response to changing requirements of the cell (Detmer and Chan, 2007; Palmer et al., 2011).

As mentioned above, terminally differentiated intestinal epithelial cells in the upper third of the intestinal crypt generate ATP mainly by utilizing the OXPHOS system (Stringari et al., 2012). Therefore, the hypothesis of this thesis was, that goblet cells are highly affected by reduced OXPHOS activity and thus alterations in p32 expression and function.

1.2.2 P32 and its role in inflammation, infection and tumor development

Apart from its role in mitochondrial metabolism, p32 has been reported to be involved in several other cellular processes regulating inflammation, infection and tumor development.

When expressed on the cell surface or in soluble form, p32 acts as a receptor for the globular heads of the complement component 1q. Both, inhibition and activation of the classical complement cascade have been reported depending on the circumstances. Pre-incubation of C1q with recombinant p32 before addition to C1q-depleted serum inhibited formation of C1 immune complexes, suppressed induction of the classical complement pathway and abolished subsequent cell lysis (Ghebrehiwet et al., 1994; Peterson et al., 1997). Meanwhile, p32 was proposed to support C1q dependent classical complement pathway activation on platelets (Peerschke et al., 2006). Two other systems involved in inflammatory responses have been found to be modulated by p32, the coagulation cascade and fibrin polymerization. Cell surface bound as well as soluble p32 was reported to bind to high molecular

weight kininogen, subsequently resulting in the generation of bradykinin, an inflammation promoting peptide (Peerschke et al., 1998). Furthermore, p32 inhibited fibrin polymerization and thereby fibrin clot formation, which is part of the first line wound repair following injuries or inflammation (Lu et al., 1999).

One of the first binding partners attributed to p32 has been hyaluronan a component of the extracellular matrix, which plays a role in tumor cell adhesion, cell migration, T-and B-cell activation and is a confirmed biomarker (D'Souza and Datta, 1985; Franzmann et al., 2003). P32 has been reported to be enriched in cancers of various origin, including breast, prostate, thyroid, pancreatic, gastric, esophageal, lung and colon cancer (Bar et al., 2013; Chen et al., 2009; Gao et al., 2016; Kim et al., 2017; Rubinstein et al., 2004; Yu et al., 2013). In line, loss of p32 decreases cellular respiration and tumorigenesis (Fogal et al., 2010). The exact role of p32 in tumor development and progression is still unknown. Interaction with hyaluronan, regulation of cell metabolism and/or binding to an ADP ribosylation factor (ARF) might be responsible in driving tumor growth. The region of mammalian *p14ARF-p16INK4a* encoding the *C*-terminal half of ARF is frequently mutated in human cancers. Mitochondrial p32 is a required for the induction of mitochondria related apoptotic cell death mediated by ARF (Itahana and Zhang, 2008).

In addition to its regulation of immune and metabolic pathways, p32 has been reported to bind to several proteins of pathogenic origin including bacterial, parasitic and viral proteins. Among the most prominent ones are Epstein Barr virus, Herpes simplex and Human Immunodeficiency Virus, *Staphylococcus aureus*, *Listeria monocytogenes* and *Plasmodium falciparum* (Braun et al., 2000; Liu et al., 2015b; Magallon-Tejada et al., 2016; Nguyen et al., 2000; Pednekar et al., 2016; Van Scoy et al., 2000). The resulting function of pathogen-p32 interaction is rather diverse, with involvement in cell adhesion, virus internalization, replication or inhibition being proposed, but seldom proven *in vivo*.

So far it is still unknown, what decides the subcellular localization and consequent function of p32 within or outside the cell. Considering the vast range of potential interaction partners, localization of p32 might be detrimental for cell fate.

1.3 Ulcerative Colitis – an overview

Ulcerative colitis (UC) is one of the two main subentities of inflammatory bowel disease (IBD), which comprises a group of chronic, relapsing-remitting immune mediated inflammatory disorders of the human gastrointestinal tract. UC shares common features including clinical, pathophysiological and epidemiological appearance with Crohn's disease (CD), the second major subtype of IBD. Both diseases may present with symptoms like abdominal discomfort or cramps, blood or pus containing diarrhea that persist over an extended period of time and weight loss. However, while inflammation in CD may

affect any part of the gastrointestinal tract from mouth to anus, UC is localized to the large intestine. Furthermore, CD may include transmural lesions affecting deeper linings of the bowel wall, while UC is mainly restricted to the mucosa. Periods of remission, times when symptoms disappear, are common in both diseases and can last for years. UC and CD can affect men and women of all ages, with first-time occurrence being highest among young adults (Hoffmann et al., 2009). The exact pathophysiology of both IBD subentities, is still not fully understood, with genetic (Anderson et al., 2011; Duerr, 2007; Graham and Xavier, 2020; Halme et al., 2006; Liu et al., 2015a; Yang et al., 1993), immune-mediated (Hufford and Kaplan, 2014; Peters et al., 2017; Tatiya-Aphiradee et al., 2018; Xu et al., 2014) and environmental factors (Abegunde et al., 2016; Ananthakrishnan et al., 2014; James et al., 2015; Jantchou et al., 2010; Racine et al., 2016) contributing to disease onset and recurrence.

The prevalence of IBD has been constantly rising over the last decades, with numbers being the highest in the Unites States, followed by the United Kingdom and Norway. Meanwhile, comparable low numbers are documented for countries in Africa and South East Asia. In 2017, 6.8 million cases of IBD have been reported worldwide. The age-standardized prevalence rate increased from 79.5 per 100 000 population in 1990 to 84.3 per 100 000 population in 2017 (Collaborators, 2020). The incidence for IBD, in particular UC, is especially rising in developing countries adapting a westernized life style (Rogler et al., 2012). The rise in IBD prevalence is accompanied by an increasing financial burden of direct health care costs (including treatment, hospitalization, and surgery-related costs) and indirect costs (*e.g.* work productivity) (van der Valk et al., 2014; van Gennep et al., 2020). In order to lower the individual and social burden caused by IBD, there is a high demand for research on disease origin, pathology and treatment options.

The diagnostic procedure for UC combines interpretation of clinical symptoms, results from endoscopy and histology as well as determination of inflammatory parameters in blood and stool samples (Hoffmann et al., 2009). For the macroscopic-endoscopic assessment of disease activity, several scoring systems are available. The Mayo score is one of the most common, classifying the endoscopic presentation from Mayo 0: normal findings or inactive disease to Mayo III: severe colitis with ulcerations and spontaneous bleeding (Schroeder et al., 1987). Furthermore, the Montreal classification subdivides inflammation in UC according to its intestinal expansion reaching from proctitis: restricted to the rectum, over left sided colitis: inflammation distal of the left flexure, to pancolitis: inflammation proximal of the left flexure (Silverberg et al., 2005).

In the histopathological assessment, UC presents as a disorder of the mucosal architecture in the intestine. Distortion of crypt architecture and crypt abscesses are often combined with inflammatory cell infiltration to the lamina propria. Basal plasmacytosis, describing accumulation of plasma cells near

the mucosal base, is common. Contrasting CD, inflammatory activity in untreated UC is restricted to the mucosa and continuously increases towards the rectum (Geboes, 2008).

Classical inflammatory parameters such as increased leucocyte or C-reactive protein level in serum samples are often only increased under severe inflammatory activity in UC. Meanwhile, fecal calprotectin has been proven as a valid inflammatory parameter for diagnostics and monitoring (Hoffmann et al., 2009).

Correct diagnosis of UC and distinction from CD, infectious or non-steroidal anti-inflammatory drug-associated colitis is essential for the choice of treatment option. A causal medical treatment for UC is currently not available, due to the complex nature of disease origin. Choice of therapy is dependent on disease activity and progress, previous treatment and extraintestinal manifestations. Aminosalicylates, like mesalazine or sulfasazine, are nowadays often the first choice of treatment. They include a group of polypotent drugs, with several proposed anti-inflammatory modes of actions like inhibition of leucocyte recruitment into the bowel wall and reduction of interleukin (IL)-1 (Greenfield et al., 1993). Additionally or alternatively, thiopurines, Janus kinase-inhibitors, a range of biologica, immunosuppressive drugs like azathioprine and methotrexate (MTX) as well as corticosteroids are available for maintenance of remission in UC. If patients stop responding to medical treatment, proctocolectomy may present as a curative approach (Dignass and Esters; Staff, 2020; Ungaro et al., 2017).

Finally, modification of nutritional habits in order to maintain remission or prevent disease initiation in UC has found increasing support in the scientific community. The European Society for Clinical Nutrition and Metabolism stated in their guidelines from 2017 that “a diet rich in fruits and vegetables, rich in omega-3 fatty acids and low in n-6 fatty acids is associated with a decreased risk of developing Crohn’s disease or ulcerative colitis and is therefore recommended (Forbes et al., 2017)”. Recommendations were based on a systematic literature review and opinions of experts in the field.

1.3.1 Pathophysiological hallmarks of ulcerative colitis

Loss of intestinal epithelial and mucus barrier integrity leading to bacterial translocation is commonly accepted as a major cause of inflammation in UC. Lack of mucins or an abnormal composition of mucins may result in a leaky mucus barrier, allowing bacteria to get into direct contact with epithelial cells in the mucosa (Johansson, 2014; Johansson et al., 2014). Meanwhile, a damaged epithelial barrier with defective regulation of tight junctions increases permeability between the intestinal lumen and the immune-cell harboring lamina propria (Martini et al., 2017) (Figure 4). As a result, high numbers of translocating bacterial antigens induce an inflammatory cascade by binding to pattern recognition receptors (PRR), including TLRs and NLRs on innate immune cells, namely macrophages and dendritic

cells. Resulting release of chemokines leads to attraction of neutrophils. Furthermore, activation of nuclear factor kappa b (NF-*k*B) and components of the inflammasome complex stimulates the transcription of proinflammatory genes, leading to increased production of proinflammatory cytokines, namely tumor necrosis factor (TNF)-α and IL-6, IL-12, IL-23 and IL-1β. Whether this cytokine profile leads to maturation of T helper (Th) 1 cells or Th2 cells is still a topic under discussion (Heller et al., 2005; Kobayashi et al., 2020). Natural killer T-cells release IL-13 that mediates epithelial-cell cytotoxicity, apoptosis, and epithelial-barrier dysfunction. In the presence of transforming growth factor (TGF)-ß and IL-4 or IL36γ, Th0 cells differentiate towards Th9 cells, which inhibit cell proliferation of epithelial cells, impair tissue-repair mechanisms and further disrupt tight junctions (Hufford and Kaplan, 2014). Furthermore, IL36γ inhibits the formation of anti-inflammatory regulatory T cells (Harusato et al., 2017) and IL36 induces fibrogenesis in fibroblasts (Scheibe et al., 2019). Additionally, circulating lymphocytes bearing integrin-α4β7 bind to mucosal vascular addressin cell adhesion molecule 1 on colonic endothelial cells of the microvasculature, leading to increased entry of gut-specific T cells into the lamina propria. Finally, upregulation of inflammatory chemokines, such as CXC ligand (CXCL) 1, CXCL3, CXCL8 and CXCL10 leads to recruitment of circulating monocytes, which perpetuates the cycle of inflammation (Figure 4) (Kobayashi et al., 2020).

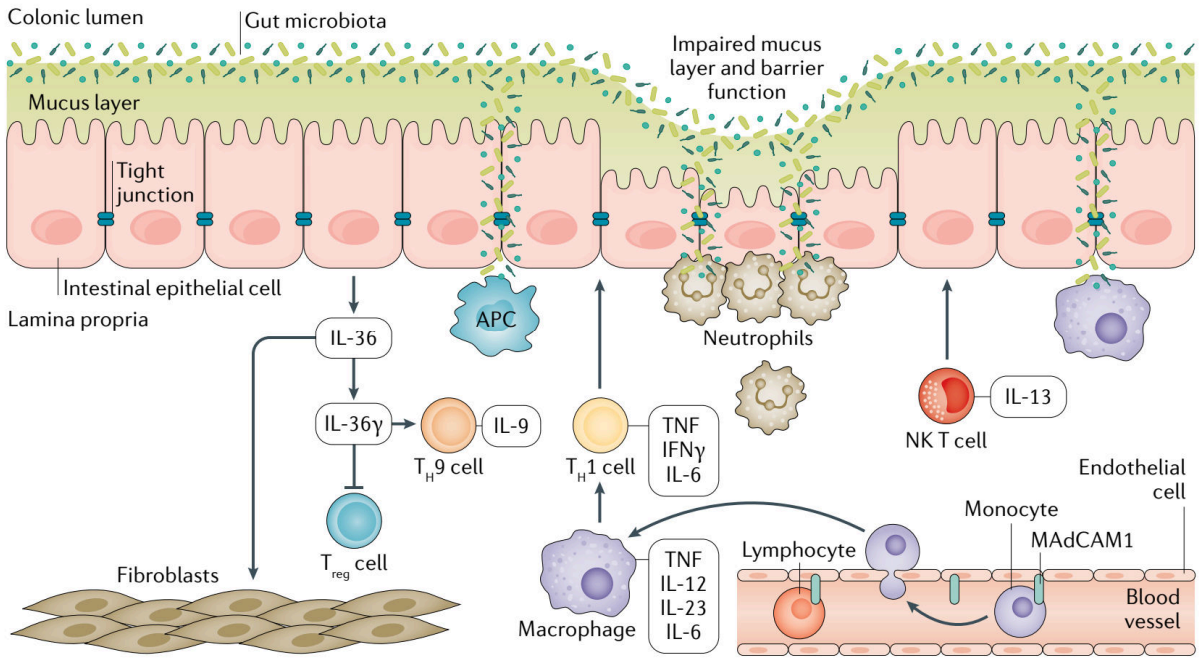

Figure 4: **Pathophysiology of ulcerative colitis.** Graphical summary of inflammatory cascades activated upon mucus and epithelial barrier disruption in UC. IL: interleukin, T_{reg} cell: regulatory T cells, T_H cell: T helper cell, NK T cell: natural killer T cell, MadCAM-1: mucosal vascular addressin cell adhesion molecule 1. *Taken from:* Kobayashi *et al.*: Ulcerative colitis, Nature reviews disease primer, 2020 (Kobayashi et al., 2020).

Activation of the inflammasome, as a central system to sense and react to invading pathogens, has been controversially discussed in the context of IBD (Davis et al., 2011; Guo et al., 2020). Different laboratories have reported conflicting results when inducing colonic inflammation in mice. The majority of laboratories reported exacerbated inflammatory phenotypes in mice deficient for *NOD2*, *Nlrp3*, *Nlrp6*, *Nlrp12*, *Nlrc4* and *ASC* upon colitis induction, supporting the idea of a protective role of the inflammasome in maintaining intestinal homeostasis (Allen et al., 2012; Carvalho et al., 2012; Couturier-Maillard et al., 2013; Elinav et al., 2011; Hirota et al., 2011; Zaki et al., 2010). On the contrary, some groups also reported a proinflammatory and pathogenic role for NLRP3 in the context of colitis (Bauer et al., 2010; Seo et al., 2015). Alterations in experimental outcomes in inflammasome research are most likely due to differences in intestinal microbiota composition, which is shaped by housing conditions, diet, mouse strains and disease model and triggers a specific PRR-response (Guo et al., 2020).

Up to now, the question which circumstances drive the epithelial barrier and mucus disruption in UC is still unsolved. Genetic factors, dysregulation of the immune system, dysbiosis and environmental factors such as diet are discussed as factors triggering disease onset.

1.3.2 Genetics and autoimmunity in the development of ulcerative colitis

From the genetic perspective, genome-wide association studies (GWAS) have shed new light on the field of complex genetic diseases during the last decade. With increasing numbers of IBD cases included in GWAS, more and more disease-related loci become identified (Jostins et al., 2012). Risk loci often overlap between CD and UC, indicating a tight relationship between the diseases also on a genetic level. A meta-analysis of six GWAS studies recently confirmed the presence of 47 risk loci associated with UC, of which 2/3 were shared with CD (Anderson et al., 2011). Major European risk variants include NOD2 and the IL-23 receptor, while TNF superfamily member 15 dominates in East-Asian populations (Liu et al., 2015a). Increased life-time risks for the development of UC in certain religious and most likely genetic subentities (Yang et al., 1993) as well as in first degree relatives compared to the general population support the idea that genetics indeed plays a role in UC disease development. Nevertheless, compared to CD, studies in twins have shown a lower concordance rate in UC (Halme et al., 2006) and early GWAS identified a larger number of susceptibility genes for CD compared to UC, indicating that genetic contribution is weaker in UC than in CD (Duerr, 2007). Molecular pathways associated with UC disease development and recurrence based on identified risk or protective loci or chromosomal regions, include epithelial barrier function, microbe-sensing, cytokine networks, apoptosis and autophagy as well as transcriptional regulation. Nevertheless, in many cases identified risk loci for both UC and CD are solely based on association studies, with the need to convert data to causal disease mechanisms (Finucane et al., 2018). Proving causality has been traditionally achieved

by knock-out or knock-in studies of respective genes in mice or cells in order to induce and study a disease phenotype. Furthermore, clustered regularly interspaced short palindromic repeats (CRISPR)-based genome editing approaches have enabled the experimental silencing and investigation of non-coding regions of the genome, such as enhancers, or the introduction of single specific coding variants implicated in UC (Cong et al., 2013). During the last decade murine and human intestinal organoid models have advanced the functional characterization of disease-associated genes. Organoid systems from primary intestinal tissue have been exploited to define gene function in a system that incorporates physiological relevant features of the *in vivo* intestinal epithelium, like a polarized epithelial layer, a functional lumen and presence of the different cell types of the intestinal crypt (Spence et al., 2011). All of these models hold great potential for identifying functional roles of IBD risk genes and variants.

Besides genetic susceptibility, autoimmunity is discussed as a second component contributing to the pathogenesis of UC. In more detail, it is questionable whether the immune reaction during acute UC is solely mediated against foreign pathogens entering the lamina propria after mucosal barrier disruption or additionally also against self-antigens. The most frequent serologic markers for IBD are antineutrophil-cytoplasmatic antibodies (ANCA) and antibodies directed against *Saccharomyces cerevisiae* (ASCA). Perinuclear or atypical ANCA can be found in 60-70% of UC patients but only in 10-15% of CD patients, *vice versa* ASCA are present in a high percentage of CD patients (60-70%) and in a low percentage of UC patients (10-15%) (Mitsuyama et al., 2016; Quinton et al., 1998; Reese et al., 2006). Other antibodies, directed against components of intestinal microbes, such as mannan in yeast, flagellin in flagellated bacteria and outer-membrane protein OmpC of *Escherichia Coli,* also display low positive rates in UC (~10%) compared to CD (> 55%) (Mitsuyama et al., 2016). Furthermore, autoantibodies directed against Glycoprotein 2, a receptor for FimH-expressing bacteria on intestinal M cells (Ohno and Hase, 2010), have been reported to be upregulated in both CD and UC, possibly inhibiting the mucosal immune response to invasive bacteria (Derer et al., 2020). Meanwhile, a second group of UC specific autoantibodies, which has received little attention in the literature and none in the clinic so far are anti-intestinal goblet cell autoantibodies (GAB). Depending on the autoantigenic targets chosen for testing, GAB appear with a prevalence of 12-46% and high specificity for UC (Conrad and Stöcker, 2014). This observation strengthens the role of goblet cell involvement in UC but not CD disease origin and pathology. Nevertheless, evidence for classical antibody-mediated autoimmunity in UC is lacking. Both, high titer of ANCA and GAB are likely a result of an aberrant immune response, rather than direct effectors involved in disease pathogenesis and therefore mainly applicable as non-invasive biomarkers (Conrad and Stöcker, 2014; Dotan, 2007).

1.3.3 The intestinal microbiome and nutrition in the development of ulcerative colitis

Despite the fact, that antibodies directed against microbes of the intestinal tract seem to have a subordinate role in UC, the intestinal microbiota composition appears of high importance in the development of intestinal inflammation. An imbalance between protective and potentially harmful bacteria, also called dysbiosis, has long been associated with chronic inflammatory diseases of the gastrointestinal tract (Sartor, 2001). However, recent advances in microbiome analysis as well as metabolomics enable assignment of specific bacterial species and metabolic pathways to UC. Intestinal dysbiosis in UC has been proposed in several publications, while the association of individual microbes to disease subtypes is rather inconsistent across studies (Walters et al., 2014). In general, microbes of the intestinal tract most likely act in concert with each other, rather than as individual infectious agents. Intestinal homeostasis is constantly balanced by the gut associated lymphoid tissue, generating either tolerance for dietary or microbial antigens or an active immune response against potential pathogens. Interestingly, both an exacerbated or diminished immune response may lead to breakdown of intestinal homeostasis and inflammation (Asquith and Powrie, 2010). In a meta-study of fecal microbiome analysis in IBD, both UC and CD patients tended to have lower microbial diversity compared to controls, while no consistent pattern was found across data sets that distinguished between IBD subgroups. Furthermore, a general depletion of microbial genera in patients *versus* controls, especially of butyrate producing *Clostridiales,* was observed for both IBD subtypes *(Duvallet et al., 2017)*. Additionally, a reduction in abundance of *Akkermansia muciniphila,* a mucolytic bacterium promoting mucus secretion, has been reported in both fecal samples and mucosal biopsies of patients suffering from UC (James et al., 2015; Png et al., 2010; Vigsnaes et al., 2012).

Potentially, metabolic activity of the microbiota might be even more important in disease pathology of UC than its composition. UC patients appear to have diminished ability to produce SCFAs even in the presence of sufficient fibers and starch as substrates (James et al., 2015). In this context, a systematic review and meta-analysis including 12 studies on SCFAs in IBD patients revealed a decrease in acetate, valerate and total SCFA but not propionate or butyrate. Nevertheless, a detailed analysis on butyrate levels displayed an inverse correlation of butyrate with disease status with low butyrate levels during active disease and high butyrate levels during remission state (Zhuang et al., 2019). In mice models, butyrate has been described to downregulate inflammation by inducing expression of tight junction proteins and differentiation of regulatory T-cells in the lamina propria and reduction of TNF-α expression (Furusawa et al., 2013; Wang et al., 2016). Even if experimental studies in mice and sequencing analyses in humans support a strong involvement of the intestinal microbiota and its metabolomics products in disease pathology, establishing a cause-effect relationship between dysbiosis and IBD has been proven difficult in humans.

Microbial colonization has an important effect on shaping the immune system, but at the same time, chronic inflammation promotes dysbiosis by altering the oxidative and metabolic environment of the gut. Inflammation as an oxidative state might for example favor the outgrowth of aerotolerant taxa such as Proteobacteria and Actinobacteria (Ni et al., 2017). Additionally, the impact of drugs applied in maintenance therapy in UC (*e.g.* mesalazine, azathioprine, steroids and antibiotics), on gut microbiota is not known. Nevertheless, animal studies as well as successful use of antibiotics and fecal microbiota transplantation (FMT) in specific cases of UC support the notion that an imbalanced intestinal microbiota is involved in UC disease pathogenesis. Antibiotic treatment appears to be supportive in the achievement of remission in patients with active UC or CD (Khan et al., 2011), while data on the efficacy of antibiotic usage in the maintenance of remission in UC is rather scarce and inconclusive (Ledder and Turner, 2018). A meta-analysis including 41 studies on FMT in UC conducted until 2017 supported the notion that FMT is effective in inducing remission in UC patients (Paramsothy et al., 2017), further validating importance of the microbiota in intestinal inflammation. In line, various murine colitis models have shown intestinal bacterial load as well as composition to be highly involved in severity of inflammation (Gkouskou et al., 2014). Nevertheless, a transfer from data on potential harmful or disruptive bacterial strains received from mouse experiments is difficult, since they fail to account for variables such as medication exposure, smoking and diet that are inherent in human research.

Several aspects of a modern, westernized lifestyle can be linked to alterations in microbial colonization of the gut, including caesarian section, early and extensive use of antibiotics, improved sanitation in industrialized countries and a decline in parasite infections (Manichanh et al., 2012). One of the most discussed environmental aspects in the context of IBD is adaptation of a westernized diet rich in sugars, fats, animal products and highly processed foods, low in fibers and with an increased overall calorie intake. Although no specific diet has been shown to directly cause, prevent, or treat IBD, long term dietary patterns indeed affect the intestinal microbiota (Kostic et al., 2014; Wu et al., 2011). In complex diseases like UC it has proven difficult to unravel individual dietary risk factors, since certain dietary patterns often appear in clusters like *e.g.* a diet rich in sugars, fats and food additives. Two large prospective studies found high animal protein intake, in specific red meat consumption, but not carbohydrate intake to be associated with an increased risk for UC (Jantchou et al., 2010; Jowett et al., 2004). Meanwhile the European Prospective Investigation into Cancer and Nutrition (EPIC) study cohort including 366,351 participants found an association between high-sugar and low-fiber intake and UC (Racine et al., 2016). The protective value or risk of dietary fat intake in UC appears to depend on the type of fat, with long-chain n-3 polyunsaturated fatty acids potentially having protective properties and trans unsaturated fatty acids having detrimental characteristics (Ananthakrishnan et al., 2014). In mice genetically susceptible to *Escherichia coli* infections, a high fat/high sugar diet has

been described to decrease butyrate production and expression of the butyrate receptor GPR43 accompanied by an increased permeability of the intestinal mucus barrier (Martinez-Medina et al., 2014). These data suggest that diet might indeed alter the microbial SCFA production capacity, resulting in impairment of the intestinal mucus barrier (Johansson et al., 2014; Pullan et al., 1994).

1.3.4 Goblet cell function and mucosal energy metabolism in ulcerative colitis

Of special interest, reduced numbers of goblet cells in line with intestinal mucus depletion have been suggested as major histological hallmarks of UC (Johansson, 2014; Pullan et al., 1994). In line, expression analysis of goblet cell differentiation factors revealed that the transcription factor KLF4 is upregulated in both, intestinal biopsies of patients with CD and non-IBD controls, during active inflammation. This was not the case for patients suffering from UC, thereby potentially lacking induction of goblet cell differentiation for barrier function during active disease (Gersemann et al., 2009). Another study which supports an imbalance between cell proliferation and differentiation in UC was published by Sinha *et al.* in 2003. Here, a small study cohort of 12 patients with mild to moderate UC received rectal enemas with epidermal growth factor (EGF), a potent mitogenic peptide, in a randomized, double-blind clinical trial. Compared to the control group, which received carrier alone, EGF-treated patients displayed significantly improved disease activity, sigmoidoscopic and histologic scores (Sinha et al., 2003).

As described in section 1.1.1 of this thesis, differentiated cells in the intestinal crypt mainly rely on energy generation by mitochondrial oxidation, while cell proliferation is driven by cytosolic glycolysis. Of note, epithelial energy-deficiency was postulated as a major pathological hallmark of UC already 30 years ago (Roediger, 1980a). When Roediger assessed metabolic performance of isolated colonocytes, he found oxidation of butyrate to be significantly reduced in UC compared to healthy controls (Roediger, 1993). Furthermore, two independent studies reported reduced mitochondrial respiratory chain complex activity accompanied by mucosal ATP depletion in UC patients (Santhanam et al., 2012; Sifroni et al., 2010). Interestingly, in all three studies mitochondrial dysfunction was already present in non-inflamed tissue of UC patients, implicating defective mitochondria as a pathophysiological cause rather than a consequence of the disease.

Taken together, the pathology of UC is driven by multiple individual aspects whereby environmental factors like *e.g.* nutrition presumably contribute to a larger extend to disease manifestation and recurrence than the individual genetic make-up (Peters et al., 2017). Defining specific environmental factors as potentially disease-driving has yet been proven difficult, due to the complex and heterogeneous nature of the disease, lack of prospective studies and insufficient transferability of data generated in animal experiments to the individual human situation. Nevertheless, bearing in mind that UC represents a disease that is usually restricted to the epithelium of the large intestine it is very likely

that colonocytes are highly involved in its pathogenesis. As disruption of the mucus barrier is widely accepted as a first step in the pathogenesis of UC, mucus-producing colonic goblet cells were the main focus of the present thesis.

2 Objective

Within the intestinal crypt, mitochondria maintain the energy gradient, which is necessary for efficient cell differentiation and proliferation and thereby critical in the determination of intestinal epithelial cell (IEC) fate (Ito and Suda, 2014; Stringari et al., 2012; Xu et al., 2013). UC is characterized by distortion of the colonic mucus barrier mucosal architecture (Geboes, 2008), strongly suggesting mitochondrial dysfunction to play a key role in both the onset and recurrence of the disease.

In order to enable the development of novel therapeutic and preventive strategies for UC it is of absolute necessity to fully decipher the molecular background behind disease development. Therefore, the main goal of the present thesis was to delineate molecular mechanisms behind mitochondrial dysfunction in intestinal epithelial cells, defective goblet cell differentiation and mucus depletion frequently observed in UC (Gersemann et al., 2009; Johansson, 2014; McCormick et al., 1990; Pullan et al., 1994; Roediger, 1980a, 1993; Santhanam et al., 2012; Sifroni et al., 2010). In this context, expression of p32, a main driver of OXPHOS (Fogal et al., 2010; Hu et al., 2013; Liu et al., 2017; Muta et al., 1997) was hypothesized to be dysregulated in the colonic crypt of patients with UC, thereby possibly impairing terminal differentiation and thus mucus secretion of goblet cells.

The following specific aims were part of this thesis:

- **Aim A:** Verifying the role of p32 in maintaining mitochondrial OXPHOS by utilizing CRISPR/Cas9-induced p32 knockout and corresponding parental cells.
- **Aim B:** Studying the expression pattern of p32 and the goblet cell differentiation status in colonic tissue from UC patients compared to non-IBD controls in the absence of inflammation.
- **Aim C:** Deciphering possible dependencies of goblet cell differentiation on mitochondrial metabolism in a mucus producing cell line *in vitro* as well as *ex vivo* in mice with defective respiratory chain complex V activity.
- **Aim D:** Identifying a nutritional intervention, which supports mitochondrial function, goblet cell differentiation and hence mucus secretion in the intestine *in vivo*.
- **Aim E:** Delineating the role of p32 in regulating the cellular metabolism during active inflammation in UC.

3 Methods

All materials, including mice strains and cell lines, instruments and software, which were required for implementation of the performed methods are listed in the appendix in section 7.1 Material.

3.1 Human study cohort

Tissue biopsies from the terminal ileum and colon were obtained during endoscopy as part of regular patient management in the medical department 1, University Hospital Schleswig-Holstein Campus Lübeck, Germany during the years 2004 and 2009 and in 2020. Blood samples were collected at the University Hospital Schleswig-Holstein Campus Lübeck, at the University Hospital Münster, North Rhine-Westphalia, Germany and at the University Hospital Rostock, Mecklenburg Western Pomerania, Germany. Characteristics of histologically confirmed UC patients and non-IBD controls at time of endoscopy or sample collection are listed in table 1 and 2, respectively. The control group included patients who presented for a regular check-up or underwent endoscopy due to non-IBD related reasons and presented without macroscopic and histologic evidence of mucosal inflammation. Diagnosis of UC and classification of patients into remission and disease flare was based on clinical, endoscopic and histopathologic findings. Categorization into inflamed and non-inflamed tissue was based on histopathologic presentation and activation of inflammasome component caspase-1. Groups were matched according to age and gender. Non-IBD controls or UC patients with reported colon cancer were excluded from the study. All patients gave informed consent for sample donation and protocols were approved by the ethics committees of the University of Lübeck (0-073; 03-043; AZ 13/084A; AZ 05-112), the University of Münster (AZ 2016-305-b-S) and the University of Rostock (A 2017-0137).

Table 1: Patients' characteristics of native and paraffin-embedded biopsies. n.i.: non-inflamed, i.: inflamed.

	mRNA expression			Immunohistochemistry analysis		
Total number of patients included	39			24		
Non-IBD	11 (28.2%)			10 (41.7%)		
UC remission non-inflamed	18 (46.2%)			9 (37.5%)		
UC inflamed	10 (25.6%)			5 (20.8%)		
Gender ratio women : men (unknown)						
Non-IBD	4 (36.4%) : 6 (54.5%) (1 (9.1%))			5 (50.0%) : 5 (50.0%)		
UC remission non-inflamed	9 (50.0%) : 9 (50.0%)			7 (77.8%) : 2 (22.2%)		
UC inflamed	5 (50%) : 5 (50%)			3 (60.0%): 2 (40.0%)		
Mean age ± SD (unknown)						
Non-IBD	62.2 ± 19.0 (1)			53.4 ± 11.3		
UC remission non-inflamed	52.4 ± 16.2 (1)			60.0 ± 13.5		
UC inflamed	38.51 ± 13.4			51.6 ± 7.7		
Origin of biopsies	**Non-IBD**	**UC n.i.**	**UC i.**	**Non-IBD**	**UC n.i.**	**UC i.**
Caecum	-	4 (22.2%)	-	-	-	-
Colon ascendens	2 (18.2%)	2 (11.1%)	-	-	-	-
Flexura hepatica	1 (9.1%)	-	-	-	-	-
Colon transversum	1 (9.1%)	1 (5.6%)	-	1 (10.0%)	-	
Colon descendens	-	1 (5.6%)	1 (10%)	3 (30.0%)	3 (33.3%)	1 (20.0%)
Colon sigmoideum	6 (54.5%)	9 (50.0%)	9 (90%)	6 (60.0%)	6 (66.7%)	4 (80.0%)
Rectum	1 (9.1%)	1 (5.6%)	-	-	-	-
Colon unclassified	-	-	-	1 (10.0%)	1 (11.1%)	-
Medication	**Non-IBD**	**UC n.i.**	**UC i.**	**Non-IBD**	**UC n.i.**	**UC i.**
Mesalazine/Mesalazine klysmen	-	12 (66.7%)	5 (50%)	-	5 (55.6%)	2 (40.0%)
Prednisone	-	6 (33.3%)	7 (70%)	1 (10.0%)	-	2 (40.0%)
Azathioprine	-	5 (27.7%)	1 (10%)	-	-	-
Sulfasalazine	-	2 (11.1%)	1 (10%)	-	1 (11.1%)	-
Tacrolimus	-	2 (11.1%)	-	-	-	1 (20.0%)
Budesonide klysmen	-	-	-		-	2 (40.0%)
Metronidazole	-	-	3 (30%)	1 (10%)	-	1 (20.0%)
Sirolimus	-	1 (5.6%)	-	-	-	-
Hydrocortisone rectal foam	-	1 (5.6%)	-	-	-	-
Olsalazine	-	1 (5.6%)	-	-	-	-
Ciprofloxacin	-	-	-	3 (30.0%)	1 (11.1%)	1 (20.0%)

Table 2: Patients' characteristics of serum/plasma samples and native biopsies utilized for western blotting experiments.

	Serum/plasma	Western blot analysis	
Total number of patients included	**33**	**9**	
Non-IBD	17 (51.5%)	5 (55.6%)	
UC remission	16 (48.5%)	4 (44.4%)	
Gender ratio women : men			
Non-IBD	9 (52.9%) : 8 (47.1%)	3 (60.0%) : 2 (40%)	
UC remission	7 (43.8%) : 9 (56.3%)	1 (25%) : 3 (75%)	
Mean age ± SD (unknown)			
Non-IBD	30.3 ± 9.7	49.8 ± 24.2	
UC remission	43.8 ± 7.7 (10)	60.15 ± 17.04	
Origin of biopsies	Not applicable	**Non-IBD**	**UC**
Caecum		-	1 (25.0%)
Colon ascendens		1 (20.0%)	1 (25.0%)
Flexura hepatica		1 (20.0%)	--
Colon descendens		1 (20.0%)	1 (25.0%)
Colon sigmoideum		1 (20.0%)	-
Rectum		1 (20.0%)	1 (25.0%)
Medication	**UC**	**UC**	
Mesalazine/Mesalazine klysmen	15 (93.8%)	2 (50%)	
TNF-α inhibitors	8 (50.0%)	-	
Prednisone	1 (6.3%)	2 (50%)	
Vedolizumab	3 (18.8%)	-	
Budesonide klysmen	2 (12.5%)	-	
Thiopurines	2 (12.5%)	-	
Hydrocortisone rectal foam	-	1 (25%)	
Ciprofloxacin	-	1 (25%)	
Sulfasalazine	-	1 (25%)	
Tacrolimus	-	1 (25%)	

3.2 Animal experiments

All animal experiments were approved by the ethics committee, Schleswig-Holstein, Germany (C57BL/6J-mt $^{FVB/NJ}$: V 242 – 63560/2017 (5-1/18); dietary intervention: V 242 – 27664/2018 (64-5/17)). Mice were maintained at the University of Lübeck under specific pathogen-free conditions at a regular

12-hour light–dark cycle with free access to food (Altromin #1324, Lage, Germany, if not indicated differently) and water. Procedures involving animals and their care were conducted in accordance with national and international laws and regulations.

C57BL/6J wild-type (B6-wt) mice were obtained from Jackson Laboratory and bred in the animal facility of the University of Lübeck. The conplastic strain C57BL/6J-mt$^{FVB/NJ}$, which carries a mutation in the mitochondrially encoded ATP synthase membrane subunit 8 (ATP8-mutant), was generated as described previously (Yu et al., 2009a) and was maintained by repeated backcrossing of female conplastic offspring with male B6-wt mice. Dr. rer. nat. Misa Hirose under the supervision of Prof. Dr. med. Saleh Ibrahim, both from the Institute of Experimental Dermatology and Center for Research on Inflammation of the Skin, University of Lübeck, Schleswig-Holstein, Germany, was in charge of breeding and backcrossing of B6-wt and ATP-8 mutant mice. All mice included in the result section 4.6 were kindly provided by them. Here, untreated 2.5 to 4 month old male ATP8-mutant mice and corresponding B6-wt controls were sampled in three independent rounds. The author of this thesis performed first tissue sampling of n = 6 mice/group and all subsequent molecular analyses. Meanwhile, prepared cDNA samples from colonic tissue from mice sampled in the second and third round was kindly provided by Mohab Ragab, Institute of Nutritional Medicine, University Hospital Schleswig-Holstein, Campus Lübeck, Germany. Due to differences in basal mRNA expression of targets of interest, expression data was normalized to B6-wt controls for each individual experiment.

Murine samples included in the result section 4.7 were obtained in the course of the PhD thesis and kindly provided by Kerstin Skibbe under the supervision of Dr. rer. nat Stefanie Derer, both from the Institute of Nutritional Medicine, University Hospital Schleswig-Holstein, Campus Lübeck, Germany. The author was involved in final sampling of the animals and performed subsequent molecular analyses. Glucose-free, high-protein (GFHP) and isocaloric control diet were purchased from Ssniff (Soest, Germany). Compositions of corresponding diets are specified in table 3. Female C57BL/6 mice were ordered with an age of 7-8 weeks from Charles River, were left to acclimatize on a standard chow diet until an age of 20 weeks and were then randomly distributed into GFHP-diet and isocaloric control (ctrl) diet receiving groups. Mice were kept on the corresponding diet for an average of 70 days before sampling. Food consumption and body weight were measured once a week. Dietary intervention was performed in two independent experimental rounds.

For colonoscopy utilizing high-resolution mouse video endoscopy, blood and tissue harvesting, mice were sedated intraperitoneal utilizing 100 mg/kg body weight Ketamin (Ketavet 10% w/v) and 10 mg/kg body weight Xylazin (Rompun 2% w/v). Before cervical dislocation, whole blood was taken directly from the heart after longitudinal opening of mice. For plasma retrieval, whole blood was first incubated on ice followed by centrifugation at 1,000 *xg*, 4°C for 5 minutes (min). Supernatant was

transferred to a new tube and frozen at -80°C. Colon tissue was flushed with 1x PBS and fixed in 4% w/v paraformaldehyde (PFA) or ready-to-use formaldehyde solution for immunohistochemistry staining. Additionally, samples were fixed in Carnoy's solution for preservation of the inner mucus layer. For RNA isolation and following analysis of transcript expression, tissue samples were frozen in liquid nitrogen and stored at -80°C.

Table 3: Chow composition for nutritional intervention experiments. Chow composition was provided by the manufacturer (Soest, Germany)

Diet composition	Isocaloric ctrl diet	Glucose-free, high-protein diet
Casein	20%	60%
Brewer`s yeast	-	2%
Corn starch	28%	-
Maltodextrin	14.5%	-
Sucrose	10%	-
Cellulose powder	15%	19.5%
L-Cystine	0.3%	0.3%
Vitamin premixture	1%	1%
Minerals & trace elements	6%	6%
Choline chloride	0.2%	0.2%
Soybean oil	5%	11%
Crude protein	17.7%	53.4%
Crude fat	5.1%	11.4%
Crude fibre	15.8%	20.3%
Crude ash	5.4%	5.9 %
Starch	26.9%	0.1%
Sugar	9.9%	-
NfE	51.7%	1.9%
Physiological fuel value	13.6 MJ/kg	13.6 MJ/kg
Protein	22 kcal%	66 kcal%
Fat	14 kcal%	32 kcal%
Carbohydrates	64 kcal%	2 kcal%

3.3 Cell biological methods

The human colorectal carcinoma cell lines HT29-MTX-E12 (Lesuffleur et al., 1990) and DiFi (Olive et al., 1993) were kept in DMEM medium supplemented with or without 1% non-essential amino acids,

respectively. The human colorectal carcinoma cell line T84 (Murakami and Masui, 1980) was grown in DMEM/F12 1:1 Medium containing 1.5% HEPES. The human chronic myelogenous leukemia cell lines HAP1 and CRISPR-Cas9 induced HAP1 *p32* knockout (HAP1-*p32*$^{-/-}$) were kept in IMDM medium. All cell culture media were supplemented with 10% heat-inactivated fetal bovine serum (FBS), 100 U/ml penicillin, and 100 mg/ml streptomycin. Cells were incubated at 37°C and 5% CO_2 in a humidified incubator and passaged two times per week. For experiments, cells were cultivated up to a maximum of 20 passages and confirmed to be negative for mycoplasma contamination every three months and when freshly thawed. If not otherwise indicated, cell count for seeding of cells or as a read-out for cell proliferation was obtained by manual counting of living cells utilizing a Neubauer chamber. Trypan blue solution stained dead cells and was applied as an indicator for cell viability.

In order to induce terminal differentiation of goblet cell-like cell lines in cell culture, cells were either stimulated with sodium butyrate solution or grown post confluent for 9 days as described previously (Navabi et al., 2013). For differentiation *via* butyrate, HT29-MTX, Difi and T84 cells were seeded with a density of 2 x 10^5 cells/well in 2 ml in 12-well plates and were stimulated with 1.25 mM butyrate for 72 hours. To mimic an inflammatory environment, 1 µg/ml LPS-EB ultrapure was added during the last 24 hours of stimulation. For post confluent growth, cells were seeded in standard medium with a density of 2 x 10^5 cells/well in 2 ml in a 24 well plate and medium was changed daily from day four onwards. Oligomycin or 2,4-Dinitrophenol were applied at indicated concentrations for the last 24 hours before sampling to inhibit mitochondrial respiration. For Glucose and non-essential amino acid (NEAA)-titration experiments, HT29-MTX cells were seeded with a density of 2 x 10^5 cells/well in a final volume of 1 ml glucose-free DMEM medium supplemented with 10% FBS, 100 U/ml penicillin and 100 mg/ml streptomycin in 24 well plates. Glucose and NEAA solution were added at indicated concentrations and cells were cultivated for 72 hours before harvest.

3.3.1 Stable and transient transfection experiments

For stable transfection of HAP1 *p32*$^{-/-}$ with mutated p32 (generation described in section 3.4.1 and 3.4.2), original p32 or mock pCMV3 plasmids (vector maps provided in supplementary figure 1A and B), cells were seeded with a density of 0.8 x 10^6 cells per well in a 6-well plate in 2 ml IMDM supplemented with 10% FBS. After 24 hours of growth, cells were transfected by lipofection utilizing the Lipofectamin™3000 kit according to manufacturer's instructions. Transfection was conducted with 2.5 µg corresponding plasmid, 7.5 µl lipofectamin 3000 and 5 µl P3000 reagents per well. One well was left non-transfected and served as a negative control. The next day, medium was substituted with fresh IMDM medium containing 10% FBS, 100 U/ml penicillin, 100 mg/ml streptomycin and 200 µg/ml Hygromcin B as selection pressure. Medium was changed twice a week until all cells of the non-

transfected negative control had died. Then, stable transfectants were moved to T25 cell culture flasks and further expanded under constant selection pressure.

Stable transfection of generated HAP1-*p32*-wt, HAP1-p32-D77E, HAP1-p32-D229E, HAP1-p32-D77E/D229E or HAP1-pCMV3-mock cells with pUNO1-hNLRP3, pUNO1-hASC and pUNO1-CASP1α or a mock plasmid was performed *via* lipofection as described above. The corresponding vector map is displayed in supplementary figure 1C. Again, a total amount of 2.5 µg plasmid DNA (0.83 µg of each transfected plasmid) was added per well. Blasticidin served as selection pressure for pUNO1 plasmids and stable transfectants were selected and cultivated in the presence of both Hygromycin B and Blasticidin.

HT29-MTX cells were transiently transfected with 50 µM siRNA specific for human *p32* (exon 3) or control siRNA by reverse lipofection using Lipofectamine 3000 reagent for 96 hours or were left untreated. For this, lipofectamin was mixed with DMEM medium without penicillin/streptavidin and FBS (DMEM -/-) and incubated for 5 min at room temperature (RT). Equal volumes of DMEM -/- containing siRNA against *p32* exon3 or respective negative control (listed in supplementary table 8) were added and the mixture was incubated for another 20 min at RT before 500 µl were added to respective wells. Finally, 0.5 x 10^6 cells in 2 ml medium without penicillin/streptavidin were added slowly to each well. After 24 hours, cells were stimulated with 1.25 mM butyrate for 72 hours or were left untreated. Transient transfection of HT29-MTX cells with pUNO1-hNLRP3, pUNO1-hASC and pUNO1-CASP1α or a mock plasmid was performed accordingly with a total amount of 2.5 µg plasmid DNA per well.

3.3.2 Seahorse assay

The Seahorse XF24 Cell Mito Stress Test was performed with parental HAP1 cells, HAP1-*p32*$^{-/-}$ cells as well as HAP1-*p32*-NAC transfectants. In order to achieve a similar cell density 24 hours after seeding, parental HAP1 cells were seeded with 3 × 10^4 cells/well in Seahorse XF24 cell culture plates, while HAP1-*p32*$^{-/-}$ cells were seeded with 6 × 10^4 cells/well. In the case of HAP1-mock-NAC (4 × 10^4 cells/well), HAP1-*p32*-wt-NAC (2 × 10^4 cells/well), and HAP1-p32-D77E/D229E-NAC (2 × 10^4 cells/well), cells were seeded 48 h before running the Seahorse XF24 Cell Mito Stress Test. The assay was performed according to manufacturer's instructions on a Seahorse XF24 extracellular flux analyser. Oxygen consumption rates (OCR) and extracellular acidification rates (ECAR) were measured every 8 min and oligomycin (1 µM final), FCCP (0.5 µM final) and rotenone/antimycin A (0.5 µM final) were injected after 3 consecutive measurements, each. Optimal cell numbers as well as oligomycin and FCCP concentrations were titrated before running the assay. Cells were counted at the end of the assay and

OCR and ECAR were normalized to cell count. The Seahorse wave software was utilized for data analysis.

In the case of HT29-MTX cells, 5 × 10^3 cells/well were seeded in 5 mM glucose containing DMEM medium and were left untreated or stimulated with 1.25 mM butyrate for 72 h. OCR and ECAR were determined in standard Seahorse medium on day three after seeding before and after injection of 2 µM oligomycin per well (final concentration).

3.3.3 Lactate assay

L-lactate levels were measured in serum or plasma samples and in cell culture supernatants according to manufacturer's instructions of the L-lactic Acid Assay Kit. Assays in human serum and plasma samples were performed and data were kindly provided by Annika Raschdorf, Institute of Nutritional Medicine, University Hospital Schleswig-Holstein, Campus Lübeck, Germany. Serum samples for measurement of L-lactate in ATP8-mutant and B6-wt mice were kindly provided by Dr. rer. nat Misa Hirose, Institute of Experimental Dermatology and Center for Research on Inflammation of the Skin, University of Lübeck, Schleswig-Holstein, Germany. Serum and plasma samples were applied diluted 1:5, while cell culture supernatants were diluted 1:10 in PBS. The absorbance was measured at a wavelength of 340 nm on a spectrophotometer before and after addition of L-lactate dehydrogenase.

3.3.4 Extracellular oxygen consumption assay

The extracellular oxygen consumption assay was performed in HAP1-p32 wt and mutant cell lines as a measurement for OXPHOS activity. Cells were seeded in 96-well-microtiter plates with a density of 1 x 10^5 cells per well in 150 µl IMDM medium supplemented with 10% FBS, 100 U/ml penicillin and 100 µg/ml streptomycin. Supplemented IMDM w/o cells served as a background control. Cells were incubated for 4 to 6 hours in a humidified incubator at 37°C, 5% CO_2 before real-time measurement of oxygen consumption was performed according to manufacturer's instructions applying the MitoXpress Xtra Oxygen Consumption Assay.

3.3.5 MTS assay

In order to measure metabolic activity in parental HAP1 cells and HAP1-*p32*$^{-/-}$ cells, the CellTiter 96® AQueous Non-Radioactive Cell Proliferation MTS Assay was performed. Cells were seeded in a 96-well-microtiter plate with a density of 5 × 10^3 cells per well in IMDM supplemented with 10% FBS, 100 U/ml penicillin, and 100 mg/ml streptomycin and were incubated for 72 hours in a humidified incubator at 37°C, 5% CO_2. The MTS assay was performed according to the manufacturer's instructions by addition of 20 µl substrate solution, incubation at 37°C for 30 min and measurement of absorbance at a wavelength of 490 nm against a reference wavelength of 670 nm on a spectrophotometer.

3.3.6 Neutral red assay

Viable cell mass was determined in HAP1-p32 wt and mutant cell lines by utilizing the neutral-red cytotoxicity assay. For this, 5 x 10^3 cells per well were seeded in 100 µl corresponding cell culture medium into a 96-well-microtiter plate and incubated for 96 hours in a humidified incubator at 37°C and 5% CO_2. After incubation, cells were stained by adding 150 µl neutral red dye per well for 2 hours at 37°C, 5% CO_2 in a humidified incubator. The corresponding neutral red stock solution was diluted 1:100 in IMDM medium without supplements the day before usage and filtrated using a 0.2 µm syringe filter. After two consecutive washing steps with PBS, 150 µl destain solution was added per well and incubated for 15 min on a microplate shaker at RT. 100 µl supernatant of each well was transferred to a new 96-well-microtiter plate and neutral-red dye uptake was analyzed by measuring the absorbance at 540 nm against a reference wavelength of 690 nm on a spectrophotometer.

3.4 Molecular biology

3.4.1 Site-directed mutagenesis

In order to generate HAP1 cells stably expressing p32 mutated at its caspase-1 cleavage sites, the cDNA expression plasmid for human p32 was first mutated at nucleotide position 231 or 687 utilizing the QuickChange II XL site-directed mutagenesis kit. For this, 10 ng pCMV3 plasmid containing the cDNA sequence for human wt p32 was amplified in a PCR reaction according to manufacturer's instructions utilizing specific primers containing a C > G nucleotide exchange (position 231) or a T > G nucleotide exchange (position 687). The corresponding vector map is displayed in supplementary figure 1A and B. To digest unmutated, parental DNA, incubation with the restriction enzyme *DpnI* was performed applying 1 µl *Dpn*I to the PCR product for 1 hour at 37°C. Transformation into ultra-competent XL-1 bacterial cells was conducted by mixing 2 µl of *Dpn*I digested PCR product with 50 µl bacteria and incubation for 30 min on ice followed by 42°C for 45 seconds (sec). In order to generate a plasmid carrying both mutations of interest, mutagenesis PCR for c.687 T > G was performed utilizing a plasmid preparation after cloning, where the c. 231 C > G exchange was already introduced and confirmed. All following steps were conducted accordingly.

3.4.2 Transformation of plasmids

Following, XL-1 bacterial cells carrying p32-mutated, wt or empty plasmids where amplified in two consecutive steps with intermediate quality control. For this, transformed bacteria where first incubated in 250 µl S.O.C. medium for 1 hour at 37°C. Then, 100 µl of the corresponding suspensions were plated on lysogeny broth-agar plates containing 100 µg/ml ampicillin. Following incubation overnight (ON) at 37°C, 10 clones were picked and added each to 3 ml 2YT-medium containing 100 µg/ml ampicillin. Transformed bacterial cells were amplified ON at 37°C on a shaking incubator. The

next day, plasmids were isolated from 2 ml bacterial suspension utilizing the NucleoSpin® plasmid DNA purification kit according to manufacturer's instructions. Plasmids were eluted in 70 µl PCR-grade H_2O after 20 min incubation on the spin column and concentration was determined by absorbance measurement on a spectrophotometer at 260 nm. For quality control, approximately 400 ng of plasmid preparations and original plasmid were separated by agarose gel electrophoresis on a 1% w/v agarose gel. One clone for each mutation was chosen according to its appearance on the gel and 100 µl of the corresponding bacterial suspension was again amplified in 250 ml 2YT-medium supplemented with 100 µg/ml ampicillin. After incubation ON at 37°C on a shaking incubator, plasmids were isolated using the NucleoBond® Xtra Maxi kit according to manufacturer's instructions and DNA concentrations were determined photometrically at 260 nm. Finally, 15 µl of mutated plasmids were diluted to 80 ng/µl and were sent to Eurofins Genomics GmbH (Ebersberg, Germany) for Sanger sequencing together with 2 µl 10 pmol/µl primer T7_forward or BGH_reverse. Sequences were aligned applying the BioEdit alignment editor.

3.4.3 RNA isolation

Isolation of total RNA from tissue biopsies or cell pellets was performed using the innuPREP RNA Mini Kit according to manufacturer's guidelines. Human and murine biopsies were disrupted by mechanical force with a pellet pestle on ice. To protect tissue samples from RNAse degradation, 1% β-mercaptoethanol was added to the lysis buffer. Additional DNA digestion was performed twice for all samples after binding of RNA to RNA-column with 4 units (U) DNase, 4 µl 10x DNase reaction buffer and 32 µl nuclease free H_2O for 20 min at RT. RNA was eluted with 40 µl nuclease free H_2O and RNA concentration of filtrate was determined by measurement on the NanoDrop 2000c spectrophotometer. Samples were kept on ice or stored at -20°C until cDNA synthesis.

3.4.4 Reverse transcription

For cDNA synthesis, 1 µg of isolated RNA was transcribed with 100 pmol $Oligo(dt)_{18}$, 20 U RiboLock™ RNase inhibitor, dNTP Mix (0.2 mM for each dNTP), 200 U RevertAid H Minus reverse transcriptase and 4 µl 5x reaction buffer. Reaction mixture was added up to 20 µl with nuclease free H_2O. After thorough mixing by resuspension and brief centrifugation, cDNA synthesis was performed at 42°C for 60 min and reaction was terminated by enzyme inactivation at 70°C for 10 min. Finally, 20 µl cDNA samples were diluted with 80 µl nuclease free H_2O and stored at -20°C until further analysis *via* semi-quantitative polymerase chain reaction (PCR) or quantitative reverse transcriptase PCR (qPCR).

3.4.5 Primer design, semi-quantitative PCR and agarose gel electrophoresis

To control for primer specificity, a semi-quantitative PCR followed by agarose gel electrophoresis was performed and PCR product size was compared to expected product size from *in situ* PCR. Specific oligonucleotides were designed based on coding sequence of the transcript of interest using the primer 3 algorithm (*https://primer3.ut.ee/*). A oligonucleotide melting temperature between 57°C and 62°C, a guanidine and cytosine percentage of 50% to 60%, a oligonucleotide size of 18 to 23 nucleotides and a product size range of 250 to 500 nucleotides were applied. Specific oligonucleotides with minimal probability for hairpin formation or self-complementarity were chosen for further testing.

For PCR experiments, 2 µl of transcribed cDNA was mixed with 10 µl 2x Dream Taq Master Mix and 0.5 µM oligonucleotides each in a total volume of 20 µl on ice. According oligonucleotide sequences are listed in supplementary table 9. PCR reactions were run using the following cycling conditions: initial denaturation for 5 min at 95°C; 35 cycles of denaturation at 95°C for 30 sec, annealing at 55°C for 30 sec, elongation at 72°C for 1 min and final elongation at 72 °C for 5 min on the Tgradient thermocycler. Samples were kept at 4°C until agarose gel electrophoresis.

Finally, PCR amplicons were separated at 80 V for 30 min on a 2% w/v agarose gel containing 0.004% Midori green advanced DNA stain in 1x TAE running buffer. For this, 10 µl of PCR products were mixed with 2 µl 6x Tritrack DNA loading buffer and were applied to the gel. Generuler 100 bp DNA ladder served as a reference value for molecular size. For visualization of bands, gels were illuminated with an UV-lamp at 266 nm and band size and intensity were photographically recorded using the Quantum ST4 gel documentation system. Samples which passed *β-actin* quality control and primer which displayed specific binding were further utilized for qPCR experiments.

3.4.6 Quantitative PCR

In order to quantify mRNA expression levels in cells or tissue biopsies of interest, SYBR qPCR was performed on the StepOne real-time system. For this, 2 µl of cDNA was added to a PCR grade 96-well plate placed on ice. To every well 18 µl of Master Mix was added, containing 10 µl 2x Pefecta SYBR Green Super-Mix, 0.5 µM forward and reverse primer each and 8 µl nuclease free H_20. Applied primer sequences are listed in supplementary table 9. QPCR was run using the following cycling conditions: initial denaturation at 95°C for 5 min; 40 cycles of denaturation at 95°C for 45 sec, annealing at 55°C for 30 sec and elongation at 72°C for 30 sec. Melting curves of PCR products served as quality control and were obtained by the following cycling conditions: 95°C for 15 sec, 60°C for 20 sec and 95°C for 15 sec. Ct-Values were acquired by data analysis *via* the StepOne system software, whereby baseline for each primer was set to cycle of first amplification beyond background – 3 cycles and the threshold was set to 0.2 ΔRn. Ct-Values of targets were normalized to *β-actin* as internal housekeeper.

3.4.7 TaqMan® assay

For human biopsies, TaqMan® probes for exon 1 and every exon-exon junction of *p32* were additionally run for transcript expression analysis. Applied TaqMan® probes are listed in supplementary table 10. For this, 2 µl of according cDNA were mixed with 1 µl TaqMan® probe of interest, 10 µl 2x TaqMan® master mix and 7 µl nuclease free H_2O without direct exposure to light. Samples were run in PCR grade 96-well plates on the StepOne system with following cycling conditions: 50°C for 2 min, 95°C for 10 min; 40 cycles at 95°C for 15 sec, 60°C for 1 min. Ct-Values were acquired by data analysis *via* the OneStep system software, whereby baseline for each primer was set to cycle of first amplification beyond background – 3 cycles and the threshold was set to 0.1 ΔRn. Ct-Values of targets were normalized to the *β-actin* TaqMan® probe as internal housekeeper. qPCR amplificates were applied to gel electrophoresis and product size was verified as quality control. TaqMan® assays with the *p32*-wt-pCMV3 plasmid diluted to 10 pg/µl served as binding control for applied human TaqMan® probes.

3.5 Biochemical methods

3.5.1 Protein isolation and quantification

In order to quantify expression of targets of interest on protein level western blot, enzyme-linked immunosorbent assay (ELISA), immunohistochemistry and/or immunofluorescent stainings were performed. For western blot or ELISA experiments, proteins were extracted from tissue samples or cell pellets applying a denaturating lysis buffer (DLB) or non-denaturating lysis buffer (NLB) respectively. For tissue samples, frozen biopsies were first crushed with a pestle and then resuspended in 200 µl DLB or NLB buffer containing 2% protease inhibitor and 1% phosphatase inhibitor II and III, each. Cell pellets were resuspended in 100 to 150 µl of corresponding buffer depending on pellet size. For further cell lysis, samples were first heated at 100°C for 5 min, shortly cooled on ice followed by two times ultrasound sonication for 20 sec. Finally, proteins were separated from cell membranes and organelles by centrifugation for 15 min at 12 000 *xg* at 4°C. Protein concentration in supernatants was quantified according to Bradford by Roti®Quant assay, applying a 1:10 dilution for proteins from cell pellets and a 1:20 dilution for proteins from tissue samples in duplicates. OD was measured at 490 nm against a reference wavelength of 690 nm on a microplate reader and concentrations were calculated using a BSA standard curve. Protein samples were stored at – 20°C until further analysis.

3.5.2 SDS-PAGE, electrotransfer and immunodetection of proteins

For SDS-PAGE and immunoblotting experiments, 15 to 40 µg of isolated, denatured protein were first mixed with a reducing 5x SDS buffer containing 10% β-mercaptoethanol, heated at 95°C for 5 min and shortly cooled on ice. Protein samples or 7 µl of a prestained protein standard were then applied to a 4-15% precast polyacrylamide gel. Proteins were separated according to size by gel electrophoresis in

electrophoresis buffer at 230 V for approximately 30 min. Before blotting, methanol activated 0.2 µm polyvinylidene difluoride (PVDF) membranes as well as blotting paper and polyacrylamide gel were equilibrated in blotting buffer for 10 min. Blotting was performed in a semi-dry blotting system at 100 mA for 1 hour at RT. For this membranes were stacked onto 2 sheets of blotting paper, followed by the polyacrylamide gel and another two layers of blotting paper. After blotting, membranes were blocked in 5% w/v non-fat milk in Tween-TBS (T-TBS) for 1 hour at RT. Primary antibodies were diluted to working concentration (listed in supplementary table 11) in 5% non-fat milk or 5% BSA in T-TBS, applied to membranes and incubated at 4°C ON. Before and after applying horse-radish peroxidase (HRP) conjugated secondary antibodies (listed in supplementary table 11) for 1 hour at RT, membranes were washed two times in T-TBS buffer for 20 min. Finally, HRP substrate solution was evenly distributed on membranes and chemiluminescence was detected under UV light in the ChemiDocTM XRS+ imaging system using the ImageLabTM software. Following, membranes were prepared for reprobing *via* stripping of applied antibodies. Membranes were either incubated with a self-made stripping buffer, containing β-mercaptoethanol, for 20 min at 56°C or with a ready-to-use buffer for 15 min at RT. Stripping buffer was washed off for 1 hour under regular changing of washing buffer. After blocking, membranes were reprobed with another antibody of interest and detected as described above. Intensity of chemiluminescence was quantified *via* the Fiji plugin of the imageJ software and expression levels of proteins of interest were normalized to housekeeper proteins.

3.5.3 Enzyme-linked immunosorbant assay

Detection of human Muc5AC in HT29-MTX cell culture supernatant or native protein isolates was performed *via* direct enzyme-linked immunosorbant assay (ELISA). For this, 50 µl of pure supernatant or native proteins diluted 1:1 in bicarbonate/carbonate buffer were coated to a flat bottom high binding plate in triplicates and incubated on a shaker at 4°C ON. Following, plates were washed three times with 0.5% Tween in PBS and blocked with 300 µl 1% BSA in PBS for 1 hour at RT. Then, 100 µl anti-MUC5AC detection antibody was applied for 90 min at RT, plates were washed three times and 100 µl of corresponding secondary HRP-conjugated antibody was applied to each well. Antibodies used in ELISA experiments are listed in supplementary table 11. After a final washing step, 100 µl of TMB substrate was added per well and plates were incubated in the dark for 10 to 20 min, depending on the intensity of color development. Finally the reaction was stopped with 50 µl 3 M HCL per well and absorbance at 450 nm was measured against a reference wavelength of 540 nm on a microplate reader. Wells which were probed with cell culture medium or 1:1 NLB and coating buffer served as background controls for supernatants or native protein isolates, respectively.

P32 release into the cell culture supernatant of p32 transfected HAP1 cells was determined by direct ELISA. Methodology was performed as described above, with the exception of the following changes.

For coating, supernatant was diluted 1:1 in bicarbonate/carbonate buffer and anti-p32 exon 3 antibody with corresponding HRP-conjugated secondary antibody was applied for detection.

In order to quantify IgA in mouse fecal pellets sandwich ELISA was performed. Fecal protein was extracted by homogenisation in 10 x volume PEN-buffer [ml]/[g] faeces, separated from sediment by centrifugation at 20.000 *xg* for 10 min at 4°C and stabilized with 0.045% w/v NaN_3. Coating of capture antibody against anti-mouse Ig light chain κ and λ was performed with 50 µl/well at 4°C ON. After washing with 0.05% Tween-20 in 1x PBS and blocking with 3% w/v BSA in PBS, fecal protein extracts and IgA RSG ELISA standard were applied in triplicates with 50 µl/well for 2 hours at room temperature. Fecal protein was diluted 1:250 in 0.5% w/v BSA, 0.05% Tween-20 in 1x PBS. Between the following steps, wells were thoroughly washed 5x with washing buffer. An anti-mouse IgA α-chain specific detection antibody followed by the respective HRP-conjugated secondary antibody were applied with 100 µl/well at RT for 1 hour or 30 min, respectively. HRP-substrate and stop solution were added and optical density was measured as described above. Applied antibodies and corresponding concentrations are listed in supplementary table 11.

3.5.4 Immunohistochemical methods

Preparation of colonic sections for immunohistochemistry was performed according to standard protocols. Briefly, whole colons were rinsed with 1x PBS, sections were transferred to embedding cassettes and fixed in 4% w/v PFA fixative or ready-to-use formalin solution for 24 hours at RT. After rinsing of tissue with tap water for 2 to 4 hours, samples were dehydrated by sequentially transferring embedding cassettes three times to 70% isopropanol, followed by 80%, 90% and three times 100% isopropanol for 6 to 24 hours at RT. Then, samples were added to 1:1 paraffin/100% isopropanol mixture and three times to paraffin for 6 to 24 h each at 60°C. Colonic tissue pieces were finally embedded in an upright position in paraffin. In the case of human colon samples, paraffin-embedded tissue was kindly provided by the Institute of Pathology, University Hospital Schleswig-Holstein, Campus Lübeck, Germany.

Microtome sections were generated from paraffin blocks precooled to -20°C with a thickness of 4-6 µm. Sections were first collected in a 20°C water bath and then transferred to a 45°C water bath for flat mounting on slides. Finally, mounted slides were dried at 37°C ON before proceeding with histochemical staining.

For deparaffinization and rehydration, slides were sequentially transferred to staining jars as follows: three times xylene for 5 to 10 min each, two times 100% ethanol, 96% ethanol, 80% ethanol and two times 70% ethanol for 3 min each followed by two times rinsing in ddH_2O. Antigen retrieval was performed for 30 min in citrate buffer utilizing a steamer. Washing twice with PBS for 10 min was

performed before slides were treated with endogenous peroxidase blockage for 10 min and between all of the following steps. Following additional blockage with 2% BSA in PBS, slides were probed with specific primary antibodies or isotype control antibodies in 1% BSA in PBS and incubated in wet chambers for 45 min at RT. In the case of anti-KLF4 antibodies slides were incubated with primary antibodies ON. After washing with PBS, HRP-conjugated secondary antibodies or HRP-labelled polymers were applied for 45 min at RT in wet chambers. All applied antibodies and corresponding concentrations are listed in supplementary table 11. Tissue slides were incubated for 5 to 20 min at RT with DAB substrate solution depending on staining intensity. Finally, samples were counterstained with Mayer's hemalum solution or Alcian-blue solution, mounted with Aquatex® solution and analyzed on an Axio Scope.A1 microscope. If appropriate, stained areas were quantified *via* the color deconvolution plugin for the software ImageJ (Rasband, 1997-2018).

For Muc2 immunofluorescent staining and quantification of mucus layer thickness, colonic biopsies were fixed in Carnoy's solution before paraffin-embedding. Tissue samples were transferred to freshly prepared Carnoy's fixative solution for 4 to 24 hours and solution was refreshed 4 times. Following, samples were dehydrated by sequentially transferring embedding capsules two times to 100% methanol for 30 min, to 100% isopropanol for 30 min and again to fresh 100% isopropanol for 1 to 24 hours. Paraffin-embedding, deparaffinization, rehydration and antigen retrieval were performed as described above. Contrasting immunohistochemistry, blocking solution with goat or mouse serum, depending on the entity of the primary antibody, was applied for 20 min at RT. Following incubation with the primary antibody of interest, respective fluorochrome-labelled IgG secondary antibody was applied (both listed in supplementary table 11). Samples were counterstained with 4',6-Diamidino-2-phenylindole (DAPI). Mucus layer thickness was measured at least at four different representative positions per slide per animal using the AxioCam software.

In order to perform immunohistochemistry staining in cell lines, cells were embedded in PFA as follows. After detaching with accutase solution and washing with PBS, cells were fixed with 4.5% formalin solution under continuous shaking at 4°C for 30 min. Following another washing step, cells were resuspended in 200 µl buffer containing casein, thrombin and fibrinogen and treated in cryovials at 4°C ON. Serial dehydration was performed in isopropanol as described above for 30 min each. Finally, cells were embedded in paraffin.

3.5.5 Cell fractionation

In order to obtain protein fractions from nucleus, cytosol and mitochondria/cell membrane of paternal HAP1 cells or HAP1-p32$^{-/-}$ cells serial centrifugation was performed. After detachment of cells by accutase, cell pellets were washed with PBS and resuspended in 250 µl cold non-denaturing

resuspension buffer (RSB; buffer compositions are listed in supplementary table 4). All steps from here on were performed on ice. After incubation for 5 min, cells were disrupted by shear force through resuspension of cells with a 26 G needle. The cell suspension was centrifuged at 1,000 *xg* at 4°C for 10 min. The resulting supernatant was again centrifuged at 16,400 *xg* at 4°C for 30 min, resulting in a cytosolic protein fraction in the supernatant of the second centrifugation step. The corresponding pellet was resuspended in 30 µl PBS and contained mitochondrial/cell membrane proteins. The pellet of the first centrifugation step was resuspended in 40 µl buffer C and incubated for 2 hours. Finally, this cell nuclei-containing fraction was centrifuged at 16,400 *xg* at 4°C for 10 min and resulting supernatant contained the nuclear proteins.

3.5.6 Caspase-1 cleavage assay

To verify predicted caspase-1 cleavage sides in the human p32 protein, an *in vitro* cleavage assay was performed utilizing recombinant proteins, followed by identification of cleavage fragments by mass spectrometry. In more detail, 100 ng of recombinant human mature His-tagged p32 protein (aa 74-282) were incubated in the absence or presence of 0.5 U or 2 U human active caspase-1 at 37°C for 1, 4, 8 or 24 hours. Alternatively, 20 µg of native protein isolates from HAP1-p32 transfectants were incubated with 12 U caspase-1 at 37°C for 4 hours. In both cases, reactions were performed in a total volume of 20 µl in caspase-1 reaction buffer and was stopped by addition of 5 µl reducing SDS buffer with β-mercaptoethanol and heating at 95°C for 5 min. Samples were applied to SDS-PAGE and immunoblotting for further analysis.

Additionally, recombinant human full-length GST-tagged p32 protein (aa 1-282) was applied to the caspase-1 cleavage assay as described above utilizing 2 U of active human caspase-1 and 4 hours of incubation. Two reactions were mixed and 200 ng of cleaved p32 protein was separated by SDS-PAGE and stained with Coomassi-blue. Stained bands were cut from the gel and sent to the Proteome Factory AG (Berlin, Germany), where protein spots were in-gel digested by trypsin and analyzed by nanoHPLC-ESI-MS/MS method. Proteins were identified by the company, which performed database search against the sequence of the applied recombinant p32 and caspase-1 protein and a database with known protein contaminants using MS/MS ion search of the Mascot search engine (Matrix Science, London, England). Only peptides matches with a score of 20 or above were accepted.

3.6 Microbiological methods

3.6.1 Quantification of mucosa attached bacteria

Quantification of MAB by flow cytometry was performed as previously described by the author (Sünderhauf et al., 2017). Small tissue pieces from the proximal colon were weighed and MAB were extracted from epithelial cells as follows (protocol adopted from Swidsinski *et al.*, 2002 (Swidsinski et

al., 2002)). Intestinal mucus was first removed by incubation with 0.016 % DTT in PBS at 800 *xg* for 1 min. After washing of samples three times with PBS, hypotonic lysis was performed with 500 µl ddH_2O at 800 *xg* for 30 min. Finally, bacteria and cell debris were pelletized by centrifugation at 12,000 *xg* for 3 min at 4°C and resuspended in 16% glycerol in PBS. Samples were frozen in liquid nitrogen and stored at −80°C until analysis *via* flow cytometry. For this, MAB were thawed on ice, washed with FACS buffer, pelletized by centrifugation at 12,000 *xg* for 3 min and incubated with 50 µl, 10 µM Syto BC green fluorescent nucleic acid stain in FACS buffer for 20 min on ice in the dark. Flow cytometry was performed on an Attune NxT cytometer with a forward scatter threshold set to 10,000 to exclude cell debris from measurement. The FlowJo™ software was utilized to quantify SYBR-stained bacterial cells. Numbers were normalized to weight of the initial colon specimen.

3.6.2 Microbiome analysis

Extraction of fecal DNA, 16S ribosomal RNA (rRNA) amplification and next generation sequencing was performed by the author under the supervision of Dr. rer. nat. Misa Hirose and Prof. Dr. med Saleh Ibrahim at the Institute of Experimental Dermatology and Center for Research on Inflammation of the Skin, University of Lübeck, Schleswig-Holstein, Germany. Data were generated in the course of an internship as part of the author's Master degree in 2014/2015. Microbiome analysis was performed as previously described (Hirose et al., 2017; Pagel et al., 2017). In more detail, DNA was extracted from frozen fecal samples with the PowerSoil® DNA Isolation kit. Homogenization of feces was performed with the Precellys®24 homogenizer three times for 15 sec at a speed of 5,000 rpm. The hypervariable regions V1 and V2 of the 16S rRNA genes were amplified by PCR utilizing the forward primer 27F 5'-*AATGATACGGCGACCACCGAGATCTACAC* XXXXXXXX **TATGGTAATT *GT*** AGAGTTTGATCCTGGCTCAG-3': in italics the 5' Illumina MiSeq adaptor, the 8 X's represent unique indices; bold, primer pad; bold and italics, primer linker; underscored residues, primer 27F. For the reverse primer 338R 5'-*CAAGCAGAAGACGGCATACGAGAT* XXXXXXXX **AGTCAGTCAG *CC*** TGCTGCCTCCC GTAGGAGT-3': in italics the 3' reverse complement sequence of the Illumina MiSeq adaptor; the 8 X's represent the unique indices; bold, primer pad; bold and italics, primer linker; underscored residues, primer 338R. Forward and reverse primers were tagged with 16 and 24 unique indices, respectively. PCR reactions (20 µl), containing 1 µl 1:10 diluted template DNA, 4 µL forward and reverse primer (0.28 µM) each, 0.25 µL of Phusion Hot Start II DNA polymerase (0.5 U), 0.5 µL dNTPs (200µM each) and 5 µL of HF buffer, were performed with the following cycling conditions: 98°C for 30 sec, followed by 30 cycles at 98°C for 9 sec, 55°C for 60 sec, 72°C for 90 sec, and a final extension at 72°C for 10 min. PCR products were quantified on 1.5% agarose gels *via* the Quantum ST4 system with a 100 bp DNA ladder serving as internal standard for band intensity measurement. One subpool per gel with PCR products of equimolar ratios was prepared. Subpools were applied on a gel, extracted with the GeneJET Gel

Extraction Kit and quantified with the Quant-iT^{TM} dsDNA BR Assay Kit on a Qubit fluorometer. Subpools were again pooled in equimolar amounts and purified by Agencourt AMPure Beads. The PerfeCTa® NGS Library Quantification Kit was used for quantification of the final library, which was sequenced with the Illumina MiSeq system (paired-end reads, V3 chemistry). Data analysis was performed according to published methodology (Hirose et al., 2017) and kindly provided by Dr. rer. nat Axel Künstner, Group for Medical Systems Biology, Institute of Experimental Dermatology, University of Lübeck, Germany.

3.7 Statistical analysis

Statistical analysis was performed using the GraphPad Prism version 6. Outliers were identified by Grubbs' test (significant level $\alpha = 0.05$). The F test was used to compare variances and D'Agostino–Pearson test was applied to test for normal distribution. Statistical differences between two groups were analyzed by unpaired t-test or paired t-test (normally distributed data), unpaired t-test with Welch's correction (significant different variances) or Mann–Whitney U-test (not-normally distributed data). For comparison of more than two groups one-way analysis of variances (ANOVA) with Tukey's post-hoc test for multiple comparisons was applied. Uncorrected Fisher's Least Significant Difference (LSD) test or two-way ANOVA with Sidac's post-hoc test was employed for data sets with two variables. *P*-values were calculated and null hypotheses were rejected when $p \leq 0.05$. Data are shown as mean with 95% confidence interval (mean ± 95% CI), as mean ± standard deviation for small data sets (mean ± SD) or median with interquartile range for data sets with large variances.

4 Results

4.1 Loss of p32 expression results in deficient OXPHOS and proliferation activity

Silencing of *p32* has been previously proposed to regulate mitochondrial energy metabolism and cell proliferation (Chowdhury et al., 2008; Fogal et al., 2010; Hu et al., 2013; Muta et al., 1997), both of which are highly important for intestinal crypt architecture (Ito and Suda, 2014; Kaiko et al., 2016; Stringari et al., 2012; Xu et al., 2013). Here, *p32*-deficient HAP1 cells (HAP1 $p32^{-/-}$ cells), which were commercially generated by CRISPR/Cas9 technology, and the corresponding parental *p32* expressing cell line were applied to study functional consequences of loss of p32 expression *in vitro*. Complete knock-out of p32 in HAP1 $p32^{-/-}$ cells was verified by western blot experiments and resulted in cell morphology alterations as compared to HAP1 p32 wild-type cells (HAP1 *p32*-wt cells) (Figure 5A and B). In line with the literature (Hu et al., 2013), Seahorse experiments performed with HAP1 $p32^{-/-}$ cells revealed loss of respiratory OXPHOS capacity and a shift towards energy generation *via* anaerobic glycolysis as compared to HAP1 *p32*-wt cells (Figure 5C and D). In depth analysis of mitochondrial function employing the Seahorse XF Cell Mito Stress test displayed a reduction of basal, maximal and non-mitochondrial respiration as well as an overall decrease in ATP production in HAP1 $p32^{-/-}$ cells compared to the parental cell line (Figure 5E). Differences in metabolic activity, cell proliferation and cell viability were further reflected by diminished level in MTS assay activity and low p44/42 and AKT but high AMP-activated protein kinase (AMPK) activation in HAP1 $p32^{-/-}$ cells in western blot experiments (Figure 5F and G). Upon growth factor-mediated activation/phosphorylation the p44/42 mitogen-activated protein kinase (MAPK) and AKT are kinases that inhibit apoptosis and support cell proliferation (Alberts et al., 2015). Phosphorylation of AMPK is induced upon high intracellular AMP/ATP or ADP/ATP ratios indicating low cellular energy level (Alberts et al., 2015). Together, p32 expression appeared to be indispensable in the maintenance of mitochondrial OXPHOS and cell proliferation.

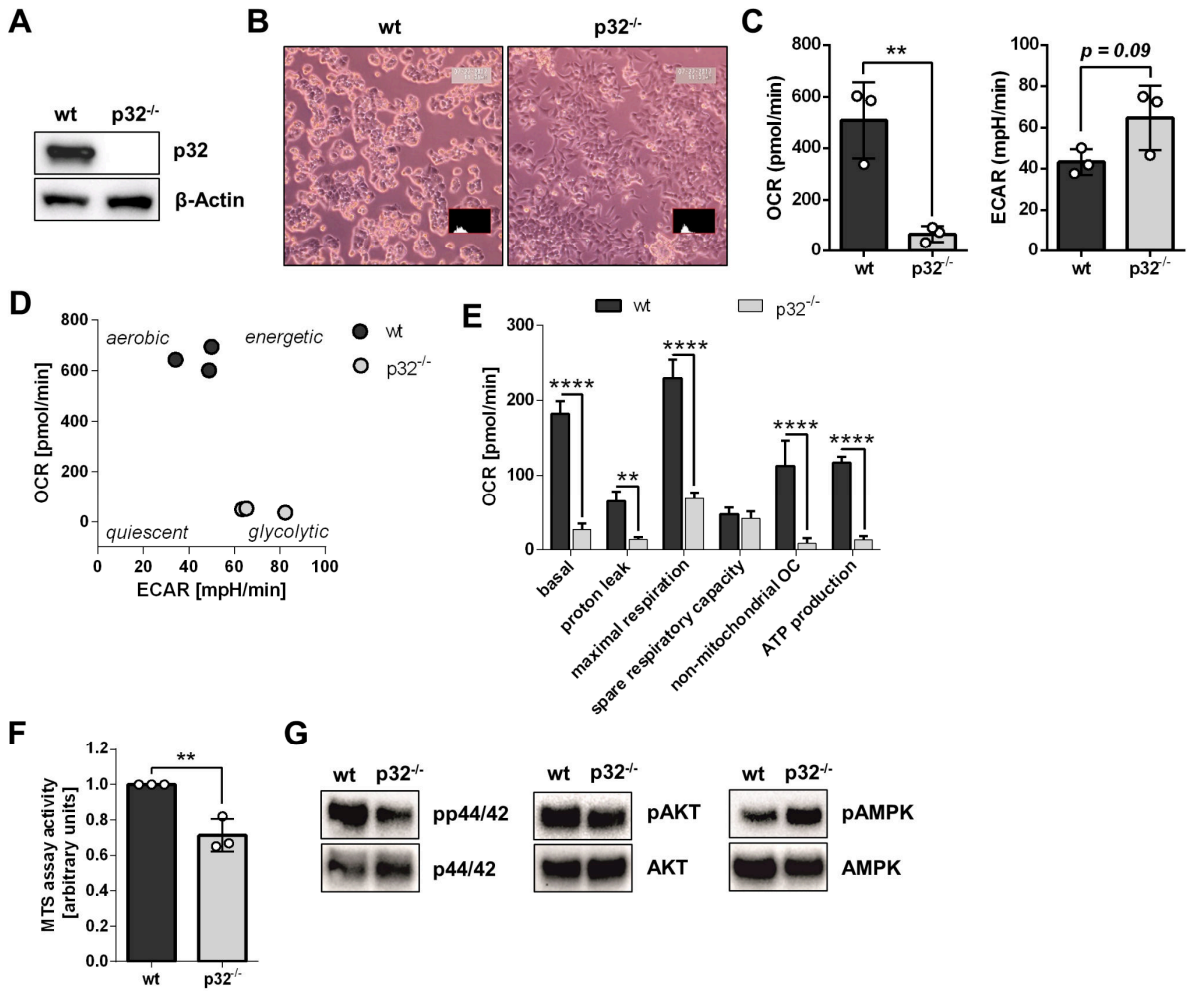

Figure 5: HAP1 *p32-/-* cells display loss of OXPHOS and proliferation activity. A) and **G)** Denaturing western blot analysis of reduced whole protein extracts from HAP1 *p32*-wt and HAP1 *p32*$^{-/-}$ cells was performed applying primary antibodies against p32, β-Actin, pp44/42, p44/42, pAKT, pAMPK and AMPK. **B)** Cellular morphology after 72h of growth under normal cell culture conditions was visualized by light microscopy. **C)** to **E)** Oxygen consumption rate (OCR) and extracellular acidification rate (ECAR) in HAP1 *p32*-wt and HAP1 *p32*$^{-/-}$ cells were assessed by Seahorse measurement applying the Mito stress test. Corresponding rates were calculated according to manufacturer's instructions. **F)** The MTS assay was applied as an indicator of metabolic activity, cell proliferation and cell viability. Absorbance was measured at OD = 490 nm against a reference wavelength of OD = 670 nm after 72 h of growth. Statistical significance was determined by unpaired t-tests. Results are expressed as mean ± SD from at least three independent experiments. ***p* ≤ 0.01, *****p* ≤ 0.0001.

4.2 P32 mainly localizes to the mitochondria

In the literature, p32 has been reported to localize to several subcellular localizations including mitochondria, cytosol, nucleus and the cell surface (Ghebrehiwet et al., 1994; Saha and Datta, 2018). Exon 1 of the human full-length p32 pre-protein (282 amino acids (aa); 31.4 kDa) encodes a signal leader sequence for mitochondrial import (Ghebrehiwet et al., 1994). Meanwhile, the mature p32 protein (aa 74-282), which lacks the mitochondrial leader sequence, has been isolated from the surface of the lymphoblast-like Raji cell line and was reported to appear in the mitochondrial matrix of

endothelial cells (Dedio et al., 1998; Ghebrehiwet et al., 1994) (Figure 6A). Here, cell fractionation followed by western blot experiments displayed p32 to localize to the mitochondria-including cellular organelle fraction in HAP1 *p32*-wt cells when detected by an antibody specific for the residues 213-226 encoded by exon 5 (clone EPR8871) (Figure 6A and B). The strong association between p32 and mitochondria was supported by data from HAP1 *p32*$^{-/-}$ cells. They presented with a decrease in mitochondrial load compared to the parental cell line, as displayed by antibody binding to voltage-dependent anion channel 1 (VDAC-1), a marker for mitochondria (Figure 6B). Mitochondrial localization of p32 detected by antibody clone EPR8871 was further validated by overlapping fluorescence signals of p32 and mitochondria-localized HSP60 (Figure 6c). To study localization of p32 in a mucus producing goblet cell-like colorectal carcinoma cell line, immunohistochemical staining was performed in HT29-MTX cells (Figure 6D and E). Again, anti-p32 antibody clone EPR8871 detected p32 localized to the mitochondria, while an anti-p32 antibody directed against the *N*-terminal aa residues 76-93 (clone 60.11) detected mitochondrial and cytosolic p32 (Figure 6A and E). Differences in staining patterns were most likely a result of preferential antibody binding either to the mitochondria-associated variant (clone EPR8871) or both the cytosolic- and mitochondria-associated variants (clone 60.11) of p32 due to epitope availability upon distinct protein folding.

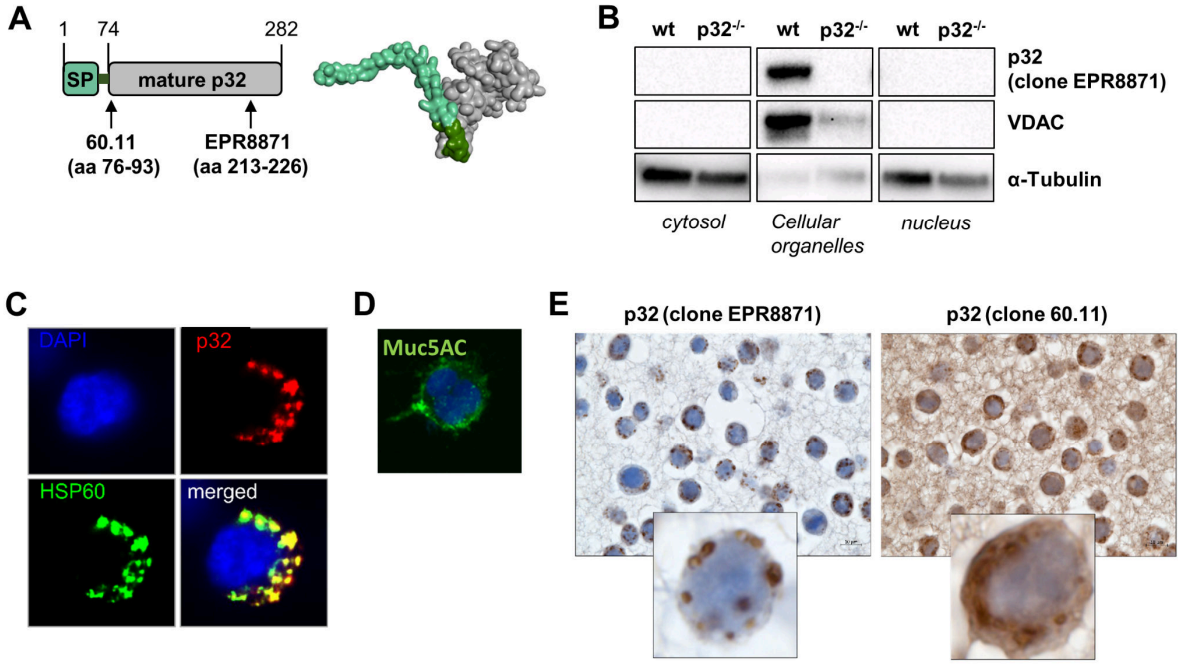

Figure legend follows on next page

Figure 6: Mature p32 localizes to the mitochondria in HAP1 and HT29-MTX cells. A) Schematic model of p32 and corresponding antibody binding sites of anti-p32 clone 60.11 and EPR8871. The homology model was generated using the PHYRE2 server (Kelley et al., 2015) and kindly provided by Stefanie Derer, Institute of Nutritional Medicine, University Hospital Schleswig-Holstein, Campus Lübeck, Germany. SP, light green: predicted signaling peptide for mitochondrial import; dark green: residual amino acids (aa) of exon 1; gray: mature p32. **B)** Denaturating western blot experiments of reduced protein samples generated from HAP1 *p32*-wt and HAP1 *p32*$^{-/-}$ cells following cell fractionation. Anti-p32 (clone EPR8871), anti-VDAC and anti-α-tubulin antibodies were applied. **C)** Co-localization of p32 (antibody clone EPR8871) with mitochondrial HSP60 protein in HAP1 *p32*-wt cells and **D)** detection of Muc5AC in HT29-MTX cells was assessed by fluorescence microscopy. **E)** Immunohistochemstry was performed to stain p32 in paraffin-embedded HT29-MTX cells utilizing anti-p32 antibody clone EPR8871 and clone 60.11.

4.3 UC patients in remission display decreased colonic p32 expression and metabolic imbalance.

Stem cells in the lower part of the colonic crypt are mainly dependent on glycolysis, while there is a gradient towards an increase in energy generation *via* OXPHOS and a decrease in glycolysis towards differentiated cells at the tip of the crypt (Ito and Suda, 2014; Stringari et al., 2012; Xu et al., 2013). Cellular differentiation occurs alongside this gradient of shifting energy source (Figure 2 and 3). P32 as a main driver of mitochondrial OXPHOS was therefore postulated to be involved in its maintenance. Indeed, p32 was found to be highly expressed in the upper part of the colonic crypt, together with the mitochondrial marker TOMM22 (translocase of the outer membrane of mitochondria 22) and goblet cell differentiation marker KLF4 (Figure 7A and B). Since mitochondrial dysfunction has been previously proposed as a hallmark of UC (Roediger, 1980a), *p32* mRNA expression was analyzed in intestinal biopsies (ileum to sigmoidal colon) from non-IBD controls and UC patients in remission. Of main interest, significantly reduced p32 mRNA expression was found in the colon (unpaired t-test with Welch's correction, p = 0.0033) but not in the terminal ileum (unpaired t-test: p = 0.0733) of UC patients (Table 1 and Figure 7C and D). Besides the reference mRNA sequence NM_001212, different splice variants have been proposed for the *p32* gene locus (ENSG00000108561) (Ponten et al., 2008). Hence, we investigated exon expression in a subset of intestinal biopsies from ten non-IBD controls and nine UC patients in remission. MRNA expression of all exons, and therefore most likely all potential isoforms, of the *p32* transcript was reduced in the intestine of UC patients compared to non-IBD controls (Figure 7E). Detection rates of the *p32* exon 1 and exon 1-2 transcripts were more than 100-fold lower than for all other *p32* exons when quantified by the ΔCt method. This was at least partially due to low binding capacity of corresponding p32 TaqMan® probes as revealed by binding assays of these probes against a human full-length *p32* encoding plasmid (Figure 7F).

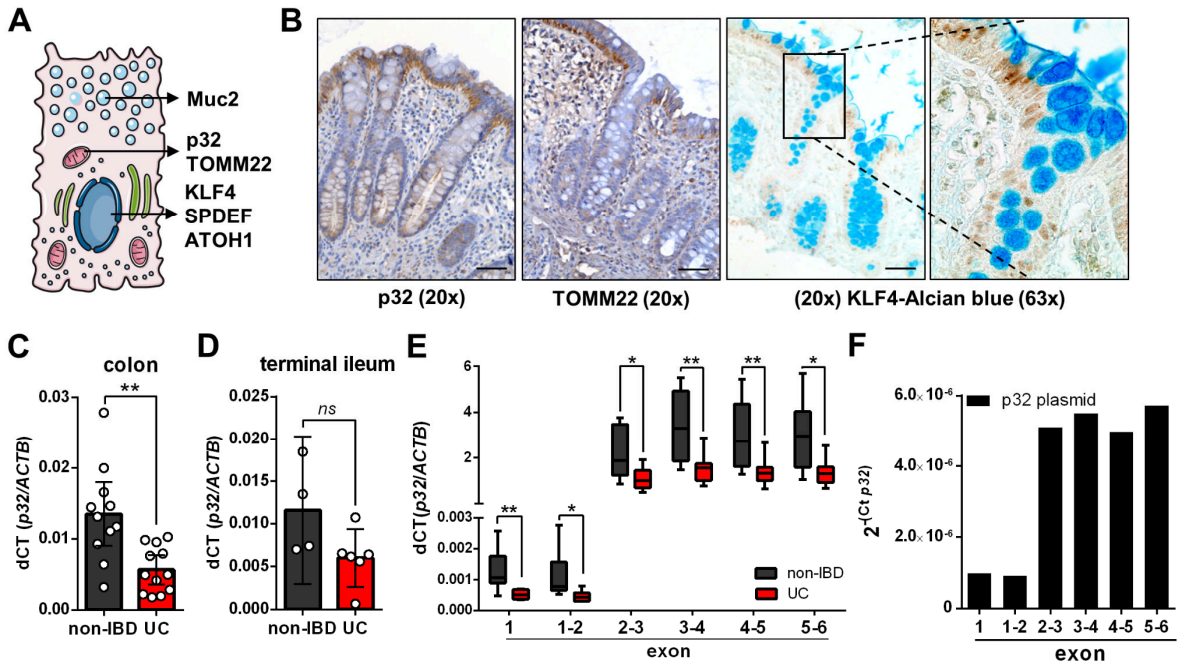

Figure 7: UC patients in remission display reduced intestinal *p32* expression. A) Schematic overview of subcellular localization of proteins of interest were generated by modifying images from Servier Medical Art (Reef et al., 2007). **B)** Representative immunohistochemistry of p32 (clone EPR8871), TOMM22 and KLF4 stained in PFA-fixed, paraffin-embedded human colonic biopsies. Scale bar = 50 µM. Expression of the *p32* transcript was measured by qPCR in **C)** colonic and **D)** ileal biopsies from non-IBD controls and UC patients in remission. *P32* exon expression was analyzed in **E)** colonic biopsies from non-IBD controls and UC patients in remission and **F)** a human full-length p32 encoding plasmid by TaqMan® assay. Patients treated with azathioprine were excluded from data in subfigure **C)** to **E)**. **C)**, **D)** and **E)** *P32* mRNA expression was related to β-Actin mRNA applying the ΔCt method. Statistical significance for **C), D)** and **E)** was determined by unpaired t-test with Welch's correction. Results are shown as **C)** and **D)** mean ± 95% CI; **F)** Box & whiskers plot minimum to maximum. *$p \leq 0.05$, **$p \leq 0.01$.

Due to the fact that mitochondrial function is highly affected by ageing (Sun et al., 2016) and potentially by various therapeutic regiments, *p32* mRNA expression was related to patients' age and tested for potential influences of commonly prescribed therapeutics within our cohort such as prednisolone, mesalazine and azathioprine. *P32* mRNA expression did not correlate with age in either non-IBD controls or UC patients (Figure 8A). In line with previous studies, which reported azathioprine to impair cell proliferation (Schroll et al., 2005), azathioprine treatment was associated with an increase in *p32* mRNA expression in UC patients, an effect neither observed under mesalazine nor prednisolone therapy (Figure 8B and C). Therefore, biopsies from patients receiving azathioprine treatment were excluded from the statistical analysis of data presented in Figure 7, 9 and 10.

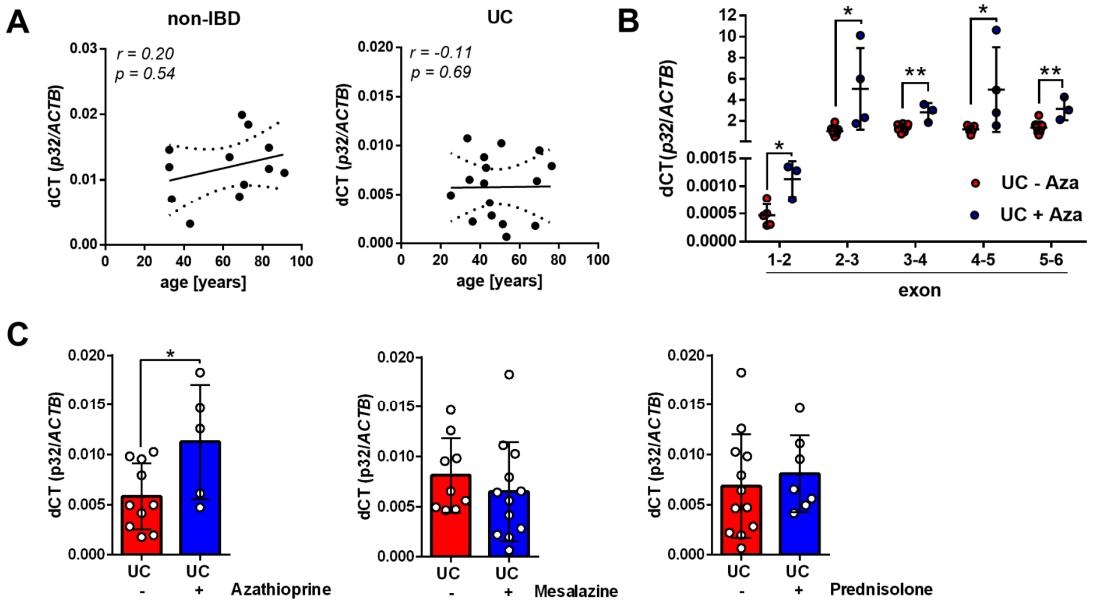

Figure 8: Azathioprine treatment is associated with increased p32 expression in UC patients. A) Intestinal *p32* transcript expression was correlated against age in non-IBD and UC patients. **B)** Measurement of *p32* mRNA level in colonic biopsies from patients receiving azathioprine or control treatment applying TaqMan® probes for every exon-exon junction. **C)** *P32* transcript expression in colonic biopsies from UC patients in remission treated with or without azathioprine, mesalazine or prednisolone was measured by SYBR qPCR. *P32* mRNA expression was normalized to β-Actin applying the dCt method. Statistical significance was determined by **A)** Spearman's rank correlation coefficient**, B)** multiple unpaired t-tests and **C)** unpaired t-test. **B)** and **C)** Results are shown as mean ± SD. ** $p \leq 0.05$, ** $p \leq 0.01$.*

To investigate whether differences in *p32* mRNA expression are also reflected on protein level, a set of ten colonic biopsies collected from non-IBD patients was compared to nine colonic biopsies collected from UC patients in remission (Table 1). Immunohistochemical staining of p32 protein (anti-p32 antibody clone EPR8871) was quantified densitometrical in the upper third of the crypt and revealed a significantly lower p32-positive area in UC patients compared to non-IBD controls (Figure 9A). Further, UC patients in remission displayed increased L-lactate level in plasma/serum samples compared to non-IBD controls as well as high phosphorylation of AMPK in colonic biopsies, pointing to increased glycolysis activity and mucosal energy deficiency in UC patients already during quiescent disease (Table 2 and Figure 9B and C).

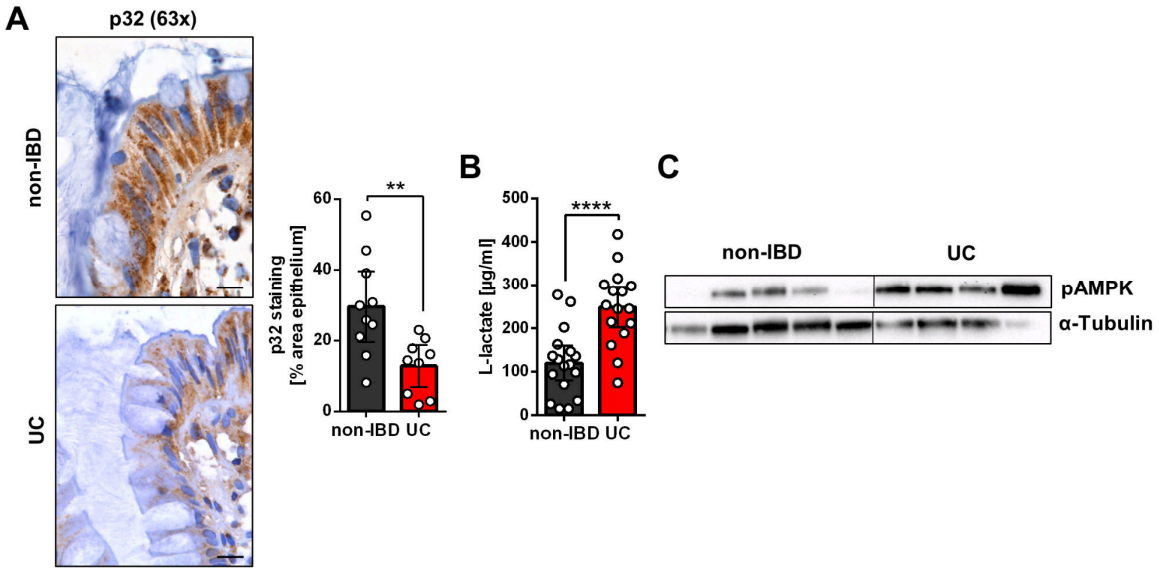

Figure 9: Low colonic p32 level in UC patients in remission are associated with high glycolytic activity and mucosal energy deficiency. A) Representative immunhistochemistry stainings utilizing anti-p32 antibody clone EPR8871 in PFA-fixed, paraffin-embedded biopsies from non-IBD controls and UC patients in remission not treated with azathioprine. Corresponding quantification of p32 expression in the upper part of the colonic crypt was performed applying the deconvolution plugin for ImageJ (Rasband, 1997-2018). Scale bar = 10 µM **B)** L-lactate level were measured in serum or plasma samples collected from non-IBD controls and UC patients in remission. Data were kindly provided by Annika Raschdorf, Institute of Nutritional Medicine, University Hospital Schleswig-Holstein, Campus Lübeck, Germany. **C)** Western blot experiments were performed with colonic biopsies from non-IBD controls and UC patients in remission. Whole protein extracts were separated under denaturing and reducing conditions and membranes were probed with primary antibodies against pAMPK and α-Tubulin. Statistical significance was determined by unpaired t-test. Results are shown as mean ± 95% CI. ** $p \leq 0.01$, **** $p \leq 0.0001$.

4.4 Low p32 expression correlates with impaired goblet cell differentiation in UC patients in remission

High glycolytic activity characterizes cell metabolism in proliferating precursor cells rather than in non-dividing differentiated cells (Ito and Suda, 2014). Since goblet cell function has been previously proposed to be impaired in UC (Gersemann et al., 2009; Johansson, 2014; Roediger, 1980a), the focus of the present study was to analyze differentiation status of this cell entity. Of main interest, expression of terminal goblet cell differentiation marker *KLF4* was significantly downregulated in colonic biopsies (hepatic flexure to sigmoid colon) from UC patients in remission compared to non-IBD controls (Figure 10A). Additionally, colonic *KLF4* mRNA expression significantly correlated with *p32* mRNA expression (Figure 10B), supporting the hypothesis, that impaired terminal goblet cell differentiation in UC is a result of diminished energy generation *via* p32-driven OXPHOS. Meanwhile, transcript levels of goblet cell precursor markers *ATOH1* and *SPDEF1* were not statistically different when comparing UC patients in remission and non-IBD controls (Figure 10A).

To examine whether the correlation between *p32* and *KLF4* expression would also transfer to protein levels, PAS-Alcian blue staining was performed in non-inflamed tissue sections from nine UC patients in remission *versus* 10 non-IBD controls. These samples were already quantified for their p32 staining intensity in figure 9A. Blinded evaluation of PAS-Alcian blue staining revealed reduced staining intensity of goblet cell granules and an overall reduction in goblet cell numbers in UC patients compared to non-IBD controls (Figure 10C).

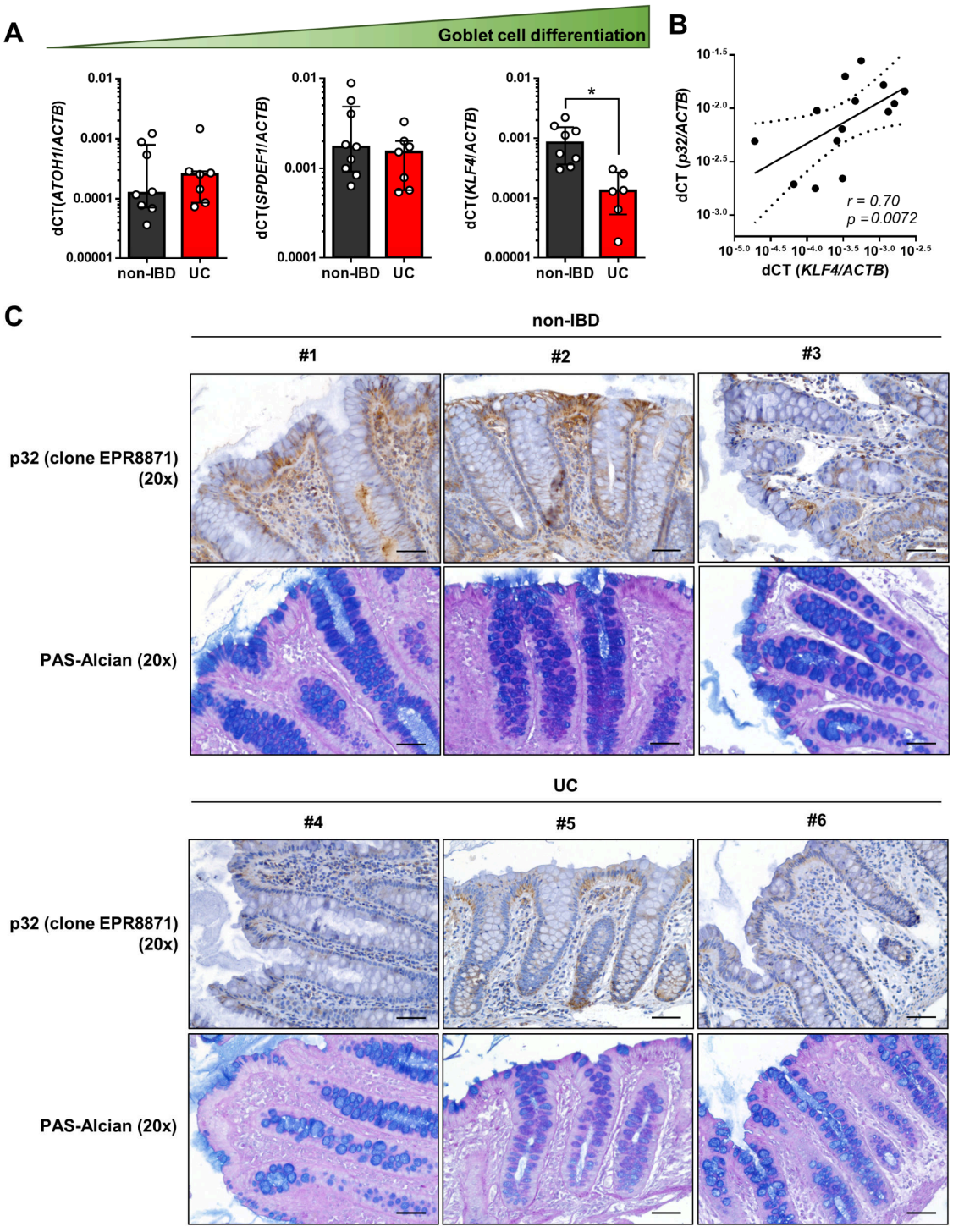

Figure legend follows on next page

Figure 10: UC patients in remission present with abnormal goblet cell differentiation. A) Transcript expression of goblet cell differentiation factors *ATOH1*, *SPDEF1* and *KLF4* was assessed by qPCR in biopsies taken distal from the ascending colon from non-IBD controls and UC patients in remission. **B)** Colonic *p32* mRNA expression was correlated against *KLF4* mRNA expression in non-IBD controls and UC patients in remission. **C)** Representative p32 (clone EPR8871) immunohistochemistry and corresponding PAS-Alcian blue stainings in paraffin-embedded biopsies from the descending colon or sigma. #1: healthy control; #2: antibiotic-associated colitis non-inflammed; #3: infectious colitis non-inflammed; #4-6: UC patients in remission. Scale bar = 50 µM. **A)** and **B)** Target expression data were normalized to β-Actin. Statistical significance was determined by **A)** Unpaired t-test with Welch's correction and **B)** Spearman's rank correlation coefficient. Results are shown as **A)** median ± interquartile range. * $p \leq 0.05$.

4.5 Goblet cell differentiation is dependent on OXPHOS and p32 expression *in vitro*

To test the hypothesis that OXPHOS-driven goblet cell differentiation in the intestinal crypt is dependent on p32 expression *in vitro*, a range of human colorectal carcinoma cell lines were screened for expression of goblet cell differentiation markers *SPDEF1*, *ATOH1*, *KLF4*, *MUC2, MUC5AC* and *p32*. HT29-MTX cells displayed high basal mRNA level of *SPDEF1*, indicating a goblet cell precursor phenotype as well as *MUC5AC* but not *MUC2*. While DiFi cells expressed high levels of both *ATOH1* and *KLF4*, the analyses of T84 cells indicated terminal differentiation reflected by high expression of *KLF4* and *MUC2*. All three goblet cell-like cell lines similarly expressed *p32* mRNA (Figure 11A). To find an inducible cell line model to study dependency of goblet cell differentiation on mitochondrial activity *in vitro*, β-oxidation and hence OXPHOS in HT29-MTX, T84 and DiFi cells was boosted through stimulation with the SCFA butyrate. LPS, a proinflammatory stimulus which is frequently present in the intestine, was applied as a co-stimulus to mimic an inflammatory milieu (Figure 11B). Butyrate stimulation induced terminal goblet cell differentiation of HT29-MTX but not of T84 or DiFi cells, reflected by induction of KLF4 protein expression, which was abrogated in the presence of LPS (Figure 11C and H). Butyrate-triggered terminal goblet cell differentiation of HT29-MTX cells was accompanied by an increase in oxygen consumption rate but not in extracellular acidification rate (Figure 11D), underlining the importance of a metabolic switch towards OXPHOS in goblet cell differentiation. Furthermore, differentiated HT29-MTX cells displayed increased mucin granule formation, decreased cell proliferation and enhancement of Muc5AC secretion (Figure 11E-H).

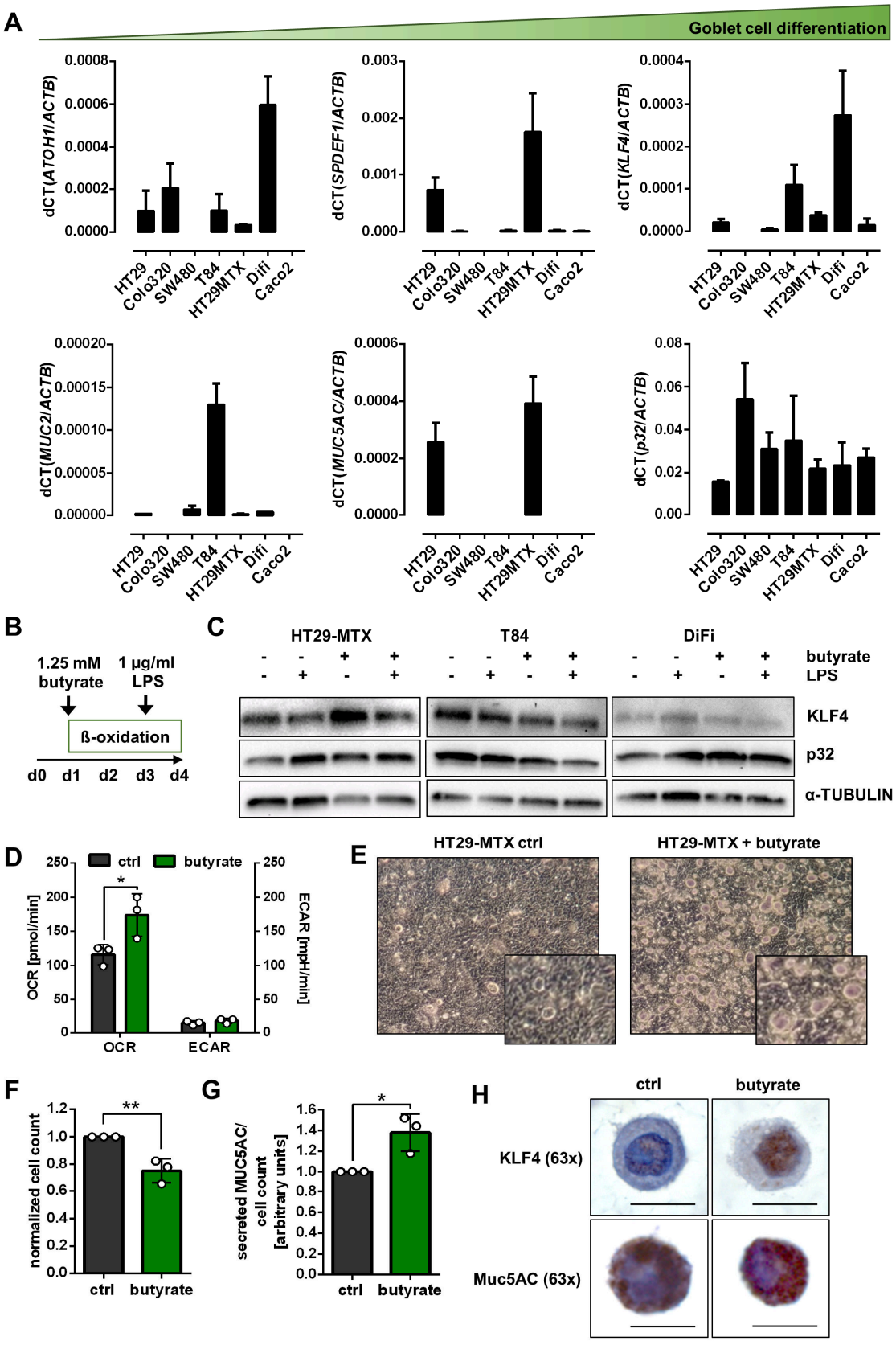

Figure legend follows on next page

Figure 11: HT29-MTX cells develop towards differentiated goblet cells upon butyrate stimulation. A) Expression of *ATOH1*, *SPDEF1*, *KLF4*, *MUC2*, *MUC5AC* and *p32* was assessed in HT29, Colo320, SW480, T84, HT29-MTX, DiFi and Caco2 cells by qPCR. Data were normalized to corresponding *β-Actin* levels and are shown as mean ± SEM. **B)** Graphical setup of cell stimulation experiments. **C)** Western blot experiments were performed under denaturing and reducing conditions with whole protein extracts of untreated HT29-MTX, T84 or Difi cells or cells stimulated with 1.25 mM butyrate and/or 1 µg/ml LPS. Membranes were probed with primary anti-KLF4, anti-p32 (clone EPR8871) or anti-α-tubulin antibodies. **D)** Basal oxygen consumption rate (OCR) and extracellular acidification rate (ECAR) were assessed by Seahorse measurement of HT29-MTX cells stimulated with or without butyrate. **E)** Representative images of growth characteristics, **F)** cell counts and **G)** levels of secreted Muc5AC of HT29-MTX cells in the presence or absence of 72h butyrate stimulation. Cell counts are presented as fold-change for each individual experiment. Muc5AC levels in the supernatant were measured by ELISA, normalized to cell count and are displayed as fold-change for each individual experiment. **H)** Immunohistochemistry staining against KLF4 and MUC5AC was performed in paraffin-embedded HT29-MTX cells grown in the absence or presence of butyrate. Scale bar = 10 µM. Statistical significance was determined by **D)** paired t-test and **F)** and **G)** unpaired t-test. Data are shown from at least 3 independent experiments and if not differently indicated presented as mean ± SD. * $p \leq 0.05$, ** $p \leq 0.01$.

As a next step, siRNA-induced silencing experiments in HT29-MTX cells were performed to verify that goblet cell differentiation is indeed dependent on p32 expression. Of main interest, induction of goblet cell differentiation *via* butyrate was abrogated in *p32*-silenced HT29-MTX cells accompanied by increased L-lactate level, indicating a switch in energy metabolism towards aerobic glycolysis. Thus, supporting the idea that p32 maintains mitochondrial function and thereby ensures goblet cell differentiation (Figure 12).

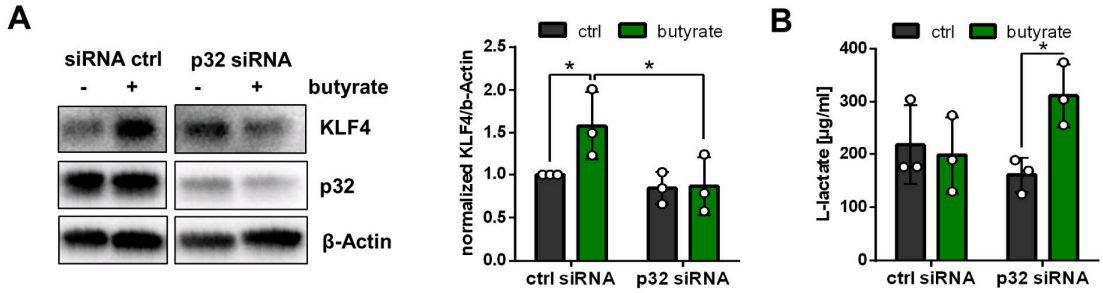

Figure 12: Induction of goblet cell differentiation depends on p32 expression in HT29-MTX cells. A) Denaturing western blot experiments applying anti-KLF4, anti-p32 clone 60.11 or anti-β-actin primary antibodies were performed with HT29-MTX whole protein extracts under reducing conditions. Cells were stimulated with siRNA targeting p32 exon 3 or corresponding control siRNA for 96 hours in the presence or absence of butyrate during the last 72 hours of the experiment. Representative western blot and corresponding quantification of n=3 independent experiments are shown. **B)** L-Lactate level were measured in respective cell culture supernatants. Statistical significance was determined by applying an uncorrected Fisher's LSD test. Results are presented as mean ± SD. * $p \leq 0.05$.

OXPHOS is a lot more efficient in the production of ATP compared to aerobic glycolysis (Alberts et al., 2015; Cooper, 2000) and exocytosis of mucus granules is presumably a highly energy demanding mechanism. Therefore, a pivotal role for cellular energy supplied by the mitochondrial OXPHOS system

not only for goblet cell differentiation, but also for mucus secretion was proposed. To test this hypothesis, HT29-MTX cells were first terminally differentiated by post-confluent growth (Navabi et al., 2013), followed by stimulation with OXPHOS complex V blocker oligomycin or the uncoupling agent 2,4-Dinitrophenol (DNP) (Figure 13A and B). As expected, blocking of OXPHOS function by oligomycin resulted in a shift of cellular energy metabolism from OXPHOS to anaerobic glycolysis (Figure 13C). Moreover, mucus secretion was impaired by oligomycin as well as by DNP, reflected by a dose-dependent downregulation of secreted but not intracellular Muc5AC (Figure 13D and E), supporting the idea that mucus secretion is a highly energy demanding process enabled by efficient OXPHOS activity. *Vice versa*, we tested how cultivation of HT29-MTX cells under different glucose concentrations for 72 hours would affect growth, secretion of MUC5AC and metabolism. In line with the literature describing glucose metabolism as a rapid pathway to generate ATP, NADPH and 5-carbon sugars required for anabolic pathways (Alfarouk et al., 2020; Vander Heiden et al., 2009; Warburg, 1956), depletion of glucose in HT29-MTX cell culture media resulted in a significant decrease in cell proliferation. A maximum in cell growth was achieved applying 10 mM glucose in the media, with no further increase in proliferation beyond this dose (Figure 13F). Interestingly, MUC5AC secretion into the cell culture supernatant was even enhanced in HT29-MTX cells grown in glucose-free medium compared to 10 mM glucose medium, accompanied by an expected reduction of L-lactate production as an indirect method to measure glycolysis activity (Figure 13G and H). Together, data strengthen the idea that not glycolysis but mitochondrial OXPHOS is the primary pathway of energy generation required for mucus secretion in goblet cells.

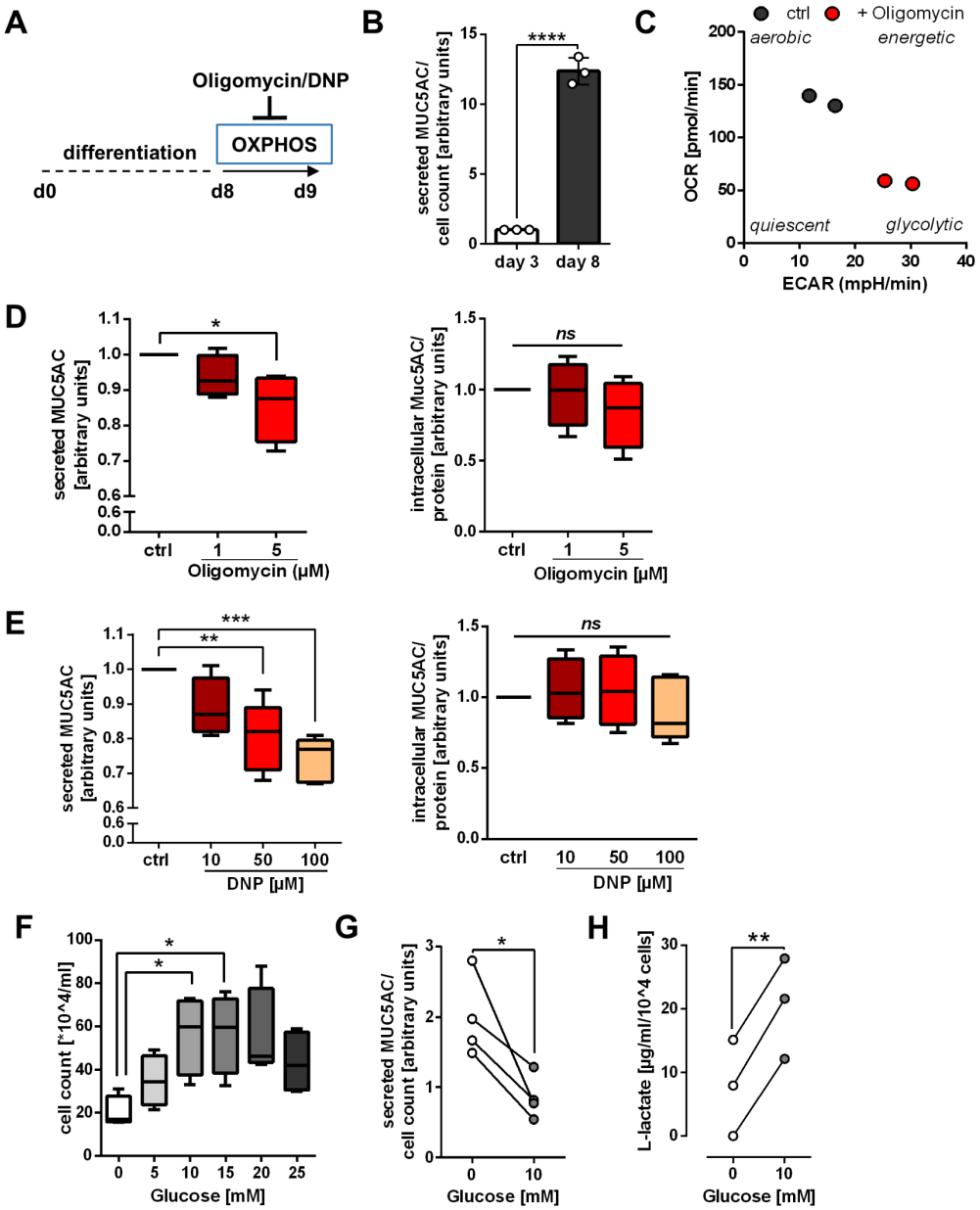

Figure 13: MUC5AC secretion of HT29-MTX cells is dependent on the OXPHOS system. Graphical setup of cell culture experiments applying an ATPase synthase inhibitor/uncoupler. **B)** Muc5AC was measured by direct ELISA in cell culture supernatant from HT29-MTX cells grown for three or eight days. Data were normalized to cell count and presented as fold change. **C)** Oxygen consumption rate (OCR) and extracellular acidification rate (ECAR) were determined in HT29-MTX cells *via* Seahorse measurement by applying the Mito stress assay. Values were obtained from two independent experiments before and after 2 µM oligomycin injection. Intracellular and extracellular Muc5AC level of **D)** oligomycin or **E)** DNP stimulated HT29-MTX cells were obtained by direct ELISA with native protein isolates or cell culture supernatants. Results are shown as fold change for each individual experiment and intracellular Muc5AC level were normalized to according total protein concentrations. **F)** HT29-MTX cells were grown for 72 hours with different glucose concentrations. Cell count was determined by manual counting utilizing a Neubauer chamber. **G)** Muc5AC and **H)** L-lactate levels in cell culture supernatants of HT29-MTX cells grown in 0 or 10 mM glucose medium were determined by direct ELISA or commercial L-lactate assay, respectively. Muc5AC and L-lactate levels were normalized to cell count for each individual experiment.

Figure legend continuous on next page

F) to **H)** Data were generated in the course of the Bachelor thesis of Joyce Preira under the supervision of the author at the Institute of Nutritional Medicine, University Hospital Schleswig-Holstein, Lübeck, Germany. Statistical significance was determined by **B)** unpaired t-test, **D)** to **F)** ordinary one-way ANOVA with Tukey's post hoc test for multiple comparisons and **G)** and **H)** paired t-test. Results are shown from **D)** and **F)** four and **E)** five individual experiments and data are presented as **B)** mean **±** SEM and **D)** to **F)** Box and whiskers blots minimum to maximum. ** $p \leq 0.05$, ** $p \leq 0.01$, *** $p \leq 0.001$, **** $p \leq 0.0001$.*

4.6 ATP8-mutant mice with low intestinal p32 expression display defective goblet cell differentiation and alterations in microbiome composition

To investigate the observed UC phenotype of low colonic p32 level, energy deficiency and defective goblet cell differentiation in a mouse model, conplastic respiratory chain complex V-mutant mice were applied. These mice carry a mutation in the mitochondria encoded ATP8-synthase resulting in diminished respiratory capacity and ATP production with parallel induction of energy generation *via* non-mitochondrial glycolysis in various cell entities (Hirose et al., 2017; Schroder et al., 2016; Yu et al., 2009a) (Figure 14A). ATP8-mutant mice did not exhibit signs of colonic inflammation under basal conditions, as defined by an inconspicuous colonoscopy and similar mRNA expression of *cxcl1*/*keratinocyte chemoattractant* (*kc*) in colonic biopsies compared to B6-wt mice (Figure 14B and C). Furthermore, intestinal barrier integrity was still intact, with comparable level of immunoglobulin A (IgA) in fecal samples of ATP8-mutant compared to B6-wt mice and similar amounts of mucosa attached bacteria (MAB) in colonic biopsies (Figure 14D and E). Specifically, ATP8-mutant mice were found to display reduced *p32* mRNA expression and diminished p32 protein levels especially in differentiated IECs in the upper part of colonic crypts (Figure 14F and G), while serum L-lactate levels were similar between strains (Figure 14H).

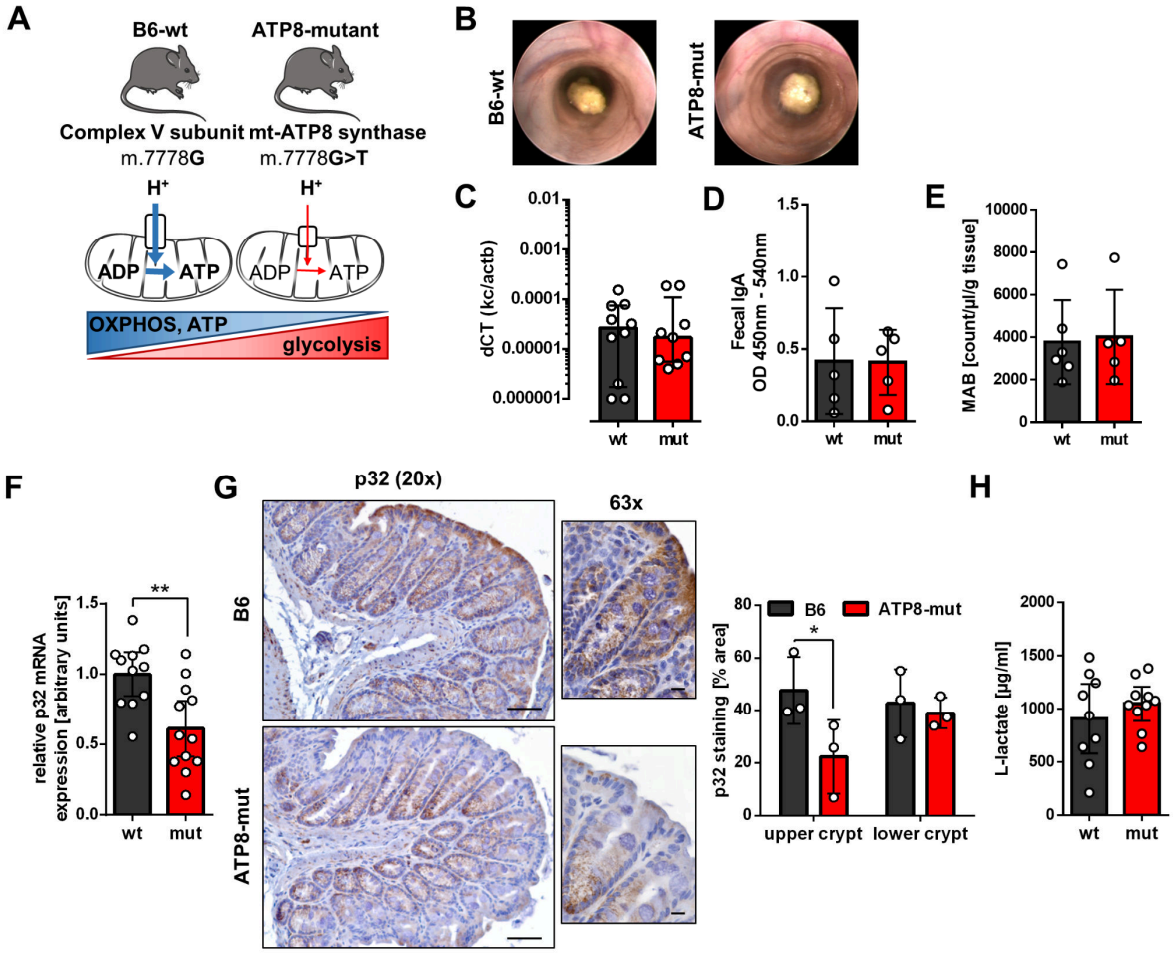

Figure 14: OXPHOS-deficient ATP8-mutant mice present with low colonic p32 expression. A) Schematic overview of the mutation in subunit 8 of the ATP-synthase in ATP8-mutant mice and published metabolic imbalance (Hirose et al., 2017; Reef et al., 2007; Schroder et al., 2016). **B)** Representative colonoscopy images (n = 3 mice per group). **C)** *Kc* mRNA expression was measured by qPCR. **D)** Fecal IgA was measured by ELISA. **E)** Mucosa attached bacteria (MAB) were extracted from colonic tissue by hypotonic cell lysis, stained with a commercial bacterial stain, quantified by fluorescence-activated cell sorting analysis, and normalized to tissue weight. **F)** *P32* mRNA expression was measured by qPCR in colonic biopsies from B6-wt and ATP8-mutant mice. Data were normalized to ß-actin and are displayed as relative values to B6-wt mice for each sampling round. **G)** Immunohistochemistry staining against p32 (antibody clone EPR8871) was performed in paraffin-embedded colonic biopsies of B6-wt and ATP8-mutant mice. Quantification of staining was performed utilizing the colour deconvolution plugin in ImageJ (Rasband, 1997-2018). Representative images are shown. Scale bar (20x) = 50 µM, scale bar (63x) = 10 µM. **H)** L-Lactate levels were measured in serum samples from B6-wt and ATP8-mutant mice. Statistical significance was determined by **F)** unpaired t-test and **G)** uncorrected Fisher's LSD test. Data are presented as **C)** median with interquartile range, **C)** to **E)** and **F)** mean ± SD and **F)** and **H)** mean ± 95% CI. * $p \leq 0.05$, ** $p \leq 0.01$.

In line with the phenotype observed in UC patients, reduced p32 expression in ATP8-mutant mice was associated with altered colonic goblet cell differentiation represented by decreased *klf4* mRNA expression, diminished mucus filling of goblet cells and a reduced thickness of the colonic mucus layer. Further, *klf4* mRNA expression significantly correlated with *p32* mRNA expression in colonic samples from B6-wt and ATP8-mutant mice (Figure 15A to C). Expression of the transcription factors *atoh1* and

spdef1 was not altered, which was comparable to observations in UC patients (Figure 15A and 9A). Finally, mRNA expression of the proliferation marker *ki67* and the stem cell marker *lgr5* was similar in colonic biopsies from ATP8-mutant and B6-wt mice (Figure 15D). These results strengthen the idea, that terminal goblet cell differentiation rather than proliferation or stemness is highly dependent on mitochondrial function.

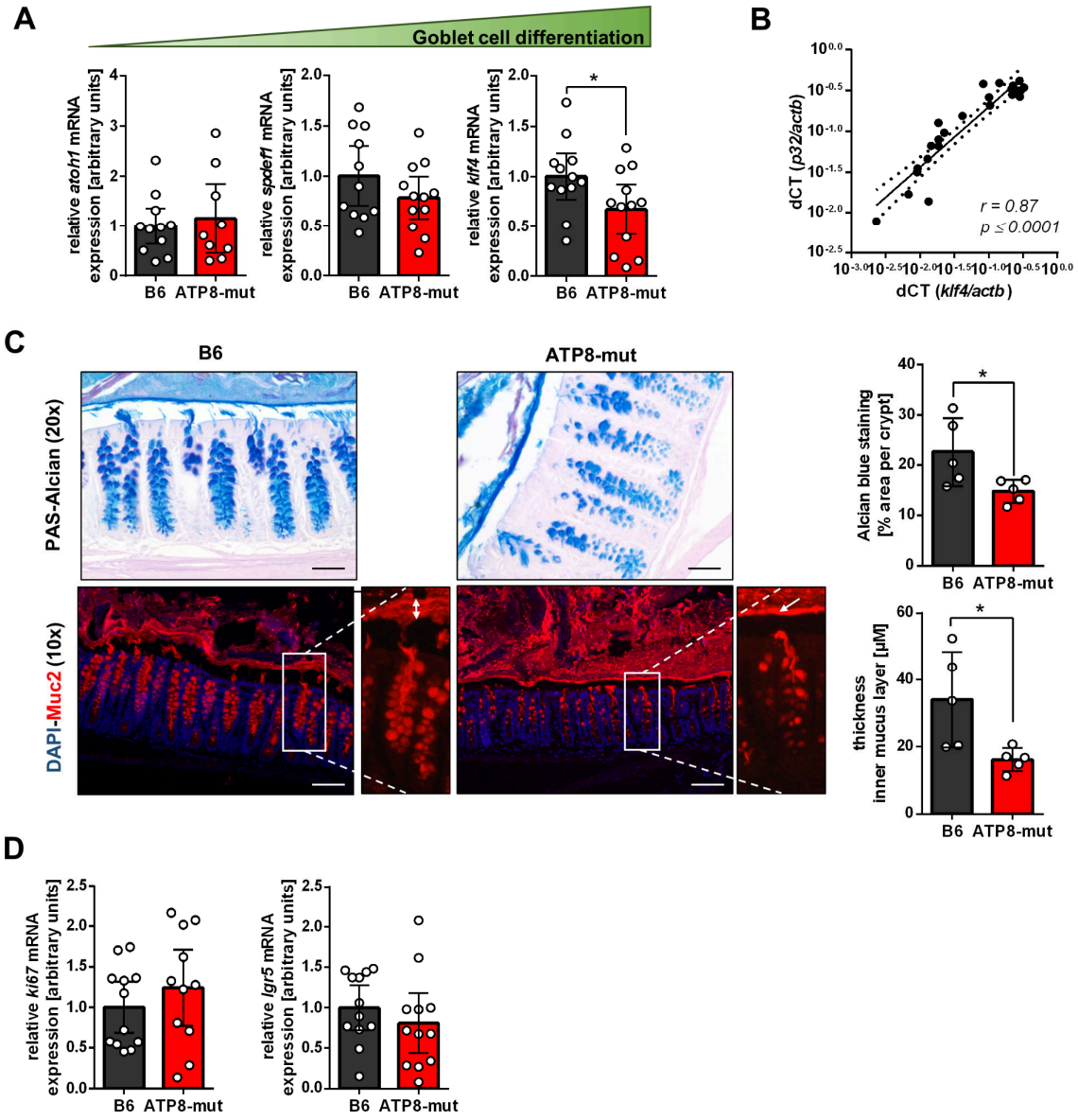

Figure legend follows on next page

Figure 15: Low p32 expression correlates with impaired goblet cell differentiation in ATP8-mutant mice. Expression of **A)** goblet cell transcription factors *atoh1*, *spdef1* and *klf4* and **D)** proliferation marker *ki67* and stem cell marker *lgr5* was quantified by qPCR in colonic biopsies from B6-wt and ATP8-mut mice. Data were normalized to *ß-actin* and are displayed as relative values to B6-wt mice for each sampling round. **B)** Colonic *p32* mRNA expression (Figure 13B) was correlated against *klf4* mRNA expression data (Figure 14A) in B6-wt and ATP8-mut mice. **C)** PAS-Acian and Muc2 immunofluorescent staining with DAPI counterstain was performed in Carnoy's fixed colonic tissue samples from B6-wt and ATP8-mutant mice. Alcian blue staining was quantified utilizing the colour deconvolution tool in ImageJ (Rasband, 1997-2018) and thickness of the inner mucus layer was measured applying the ZEN software (blue edition; Zeiss). Representative Images are shown. Scale bar (20x) = 50 µM, scale bar (10x) = 100 µM. Statistical significance was determined by **A)** unpaired t-test, **B)** Spearman's rank correlation coefficient and **C)** unpaired t-test with Welch's correction. Results are presented as **A)** and **D)** mean ± 95% CI and **C)** mean ± SD. * $p \leq 0.05$.

The intestinal mucus layer is in direct contact with the luminal microbiota, constantly shaping each other (Ouwerkerk et al., 2013). The microbiome composition in ATP8-mutant and B6-wt mice was analyzed to unravel potentially mucus-associated alterations between strains. Indeed, sequencing of two variable regions of 16S rRNA in fecal samples revealed distinct clustering of strains in terms of differences in microbial abundance (β-diversity), displayed by Capscale analysis (ANOVA-like permutation test for Constrained Correspondence Analysis corrected for sex and housing unit p = 0.0001) (Figure 16A). PERMANOVA analysis revealed a strain effect of R2 = 0.14238 with a p-value of p = 0.0001 translating to an overall effect of 14.2% on the microbiome composition between B6-wt and ATP8-mutant mice. Meanwhile, alpha-diversity as a measurement of equal abundance of species within samples revealed no differences between strains (Wilcoxon test Shannon index: p = 0.7454) (Figure 16B). In-depth taxonomic analysis revealed significant strain-specific differences ($p < 0.05$) in the abundance of Bacteroidetes, Deferribacteres, Firmicutes, Proteobacteria and Tenericutes (Figure 16C). Furthermore, ATP8-mutant mice displayed a significantly higher Firmicutes to Bacteroidetes ratio compared to B6-wt mice (p = 4.679e-05) (Figure 16D). A finding which is of special interest, since an increased Firmicutes to Bacteroidetes ratio has been repeatedly associated with obesity and the metabolic syndrome in mice and humans (Ley et al., 2006; Turnbaugh et al., 2006).

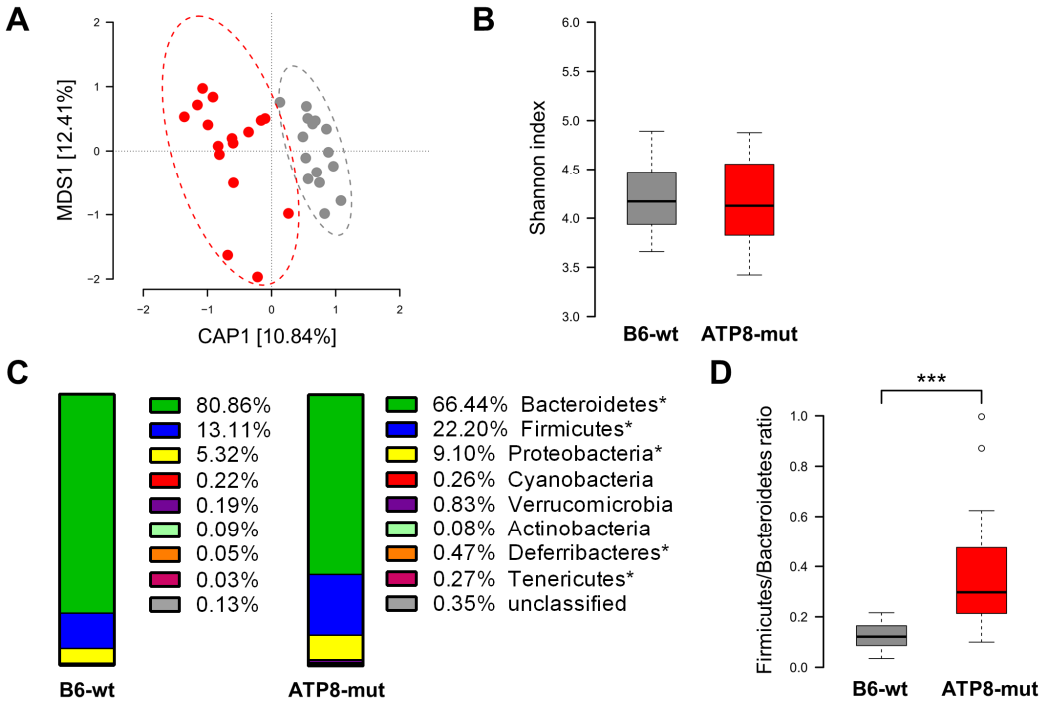

Figure 16: The fecal microbiome composition significantly differs between B6-wt and ATP8-mutant mice. A) Microbiome composition was analyzed in fecal samples of B6-wt (gray) and ATP8-mutant (red) mice by 16S rRNA next generation sequencing. β-diversity is displayed as Capscale analysis. **B)** α-diversity was analyzed by applying the Shannon index. **C)** The six most abundant phyla and **D)** the Firmcutes to Bacteroidetes ratio was plotted for both strains. In total, 16 age and sex matched individuals were sequenced per strain. The author performed the experiments. Bioinformatics' analysis was conducted according to published methodology (Hirose et al., 2017) and kindly provided by Axel Künstner, Group for Medical Systems Biology, Institute of Experimental Dermatology, University of Lübeck, Germany. Statistical significance was determined by **C)** Mann-Whitney *U* test and **D)** Wilcoxon test. $*p \leq 0.05$, $***p \leq 0.001$.

Taken together, data presented display a mouse model with low intestinal p32 level and diminished energy generation *via* OXPHOS to depict reduced numbers of terminally differentiated goblet cells in the colon, strengthening the notion that especially goblet cell differentiation is highly sensitive to mitochondrial dysfunction. Alterations in the colonic epithelium were accompanied by fecal microbiome alterations, which are frequently observed in UC (Duvallet et al., 2017; Walters et al., 2014).

4.7 Glucose-free, high-protein diet induces colonic p32 expression and goblet cell differentiation

Regulation of goblet cell differentiation *via* the enhancement of colonic p32 expression was finally studied in a glucose-free, high-protein nutritional intervention in mice. Availability of nutrients critically affects cellular metabolism (Palm and Thompson, 2017). Therefore, withdrawal of glucose and replacement by protein as an energy source was hypothesized to result in a metabolic shift from glycolysis towards mitochondrial oxidation, accompanied by induction of goblet cell differentiation.

Underlying cell culture experiments in goblet cell-like HT29-MTX cells supported this theory. HT29-MTX cells cultured for 72 hours in 0 mM glucose, 10% NEAA medium compared to HT29-MTX cells grown in 10 mM glucose, 1% NEAA medium presented with a significant reduction in cell growth and glycolysis activity as displayed by low levels of L-lactate in the cell culture supernatant (Figure 17A and B). Further, *klf4* mRNA expression and MUC5AC secretion into the supernatant was induced in HT29-MTX cells supplemented with 0 mM glucose, high NEAA containing medium as compared to controls (Figure 17C and D). Results further support the notion that the type of substrate available for cellular energy metabolism is important for goblet cell differentiation.

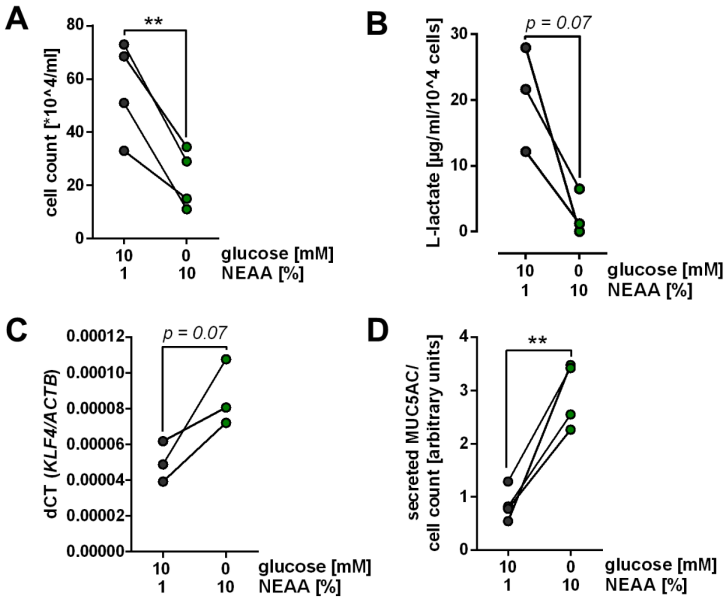

Figure 17: Substitution of glucose by non-essential amino acids in cell culture medium drives goblet cell differentiation in HT29-MTX cells. A) HT29-MTX cells were grown for 72 hours in 10 mM glucose, 1% non-essential amino acids (NEAA) or 0 mM glucose, 10% NEAA containing media. Cell count was determined by manual counting utilizing a Neubauer chamber. **B)** L-lactate and **D)** Muc5AC levels in cell culture supernatants of HT29-MTX cells grown in corresponding media were obtained by commercial L-lactate assay or direct ELISA, respectively. L-lactate and Muc5AC levels were normalized to cell count for each individual experiment. **C)** Expression of *KLF4* was assessed by qPCR and normalized to corresponding *ß-Actin* levels. Data were generated in the course of the Bachelor thesis of Joyce Preira under the supervision of the author at the Institute of Nutritional Medicine, University Hospital Schleswig-Holstein, Lübeck, Germany. Statistical significance was determined by **A)**, **B)** and **D)** paired t-test and **C)** ratio paired t-test. ** $p \leq 0.01$.

To transfer the results obtained in cell culture experiments to an *in vivo* nutritional intervention model, 20 weeks old C57BL/6 female mice were fed a glucose-free, high-protein (GFHP) or an isocaloric control diet (ctrl) for an average of 70 days before organ sampling and molecular analysis (Figure 18A, Table 3). Food consumption, body weight, serum glucose and lactate levels were similar between diets (Figure 17B to E). Of main interest, GFHP diet fed mice exhibited increased p32 protein level in the upper part of the colonic crypt which were not due to elevated *p32* mRNA level (Figure 18F to H) but accompanied by high colonic energy level reflected by low phosphorylation of AMPK (Figure 18G).

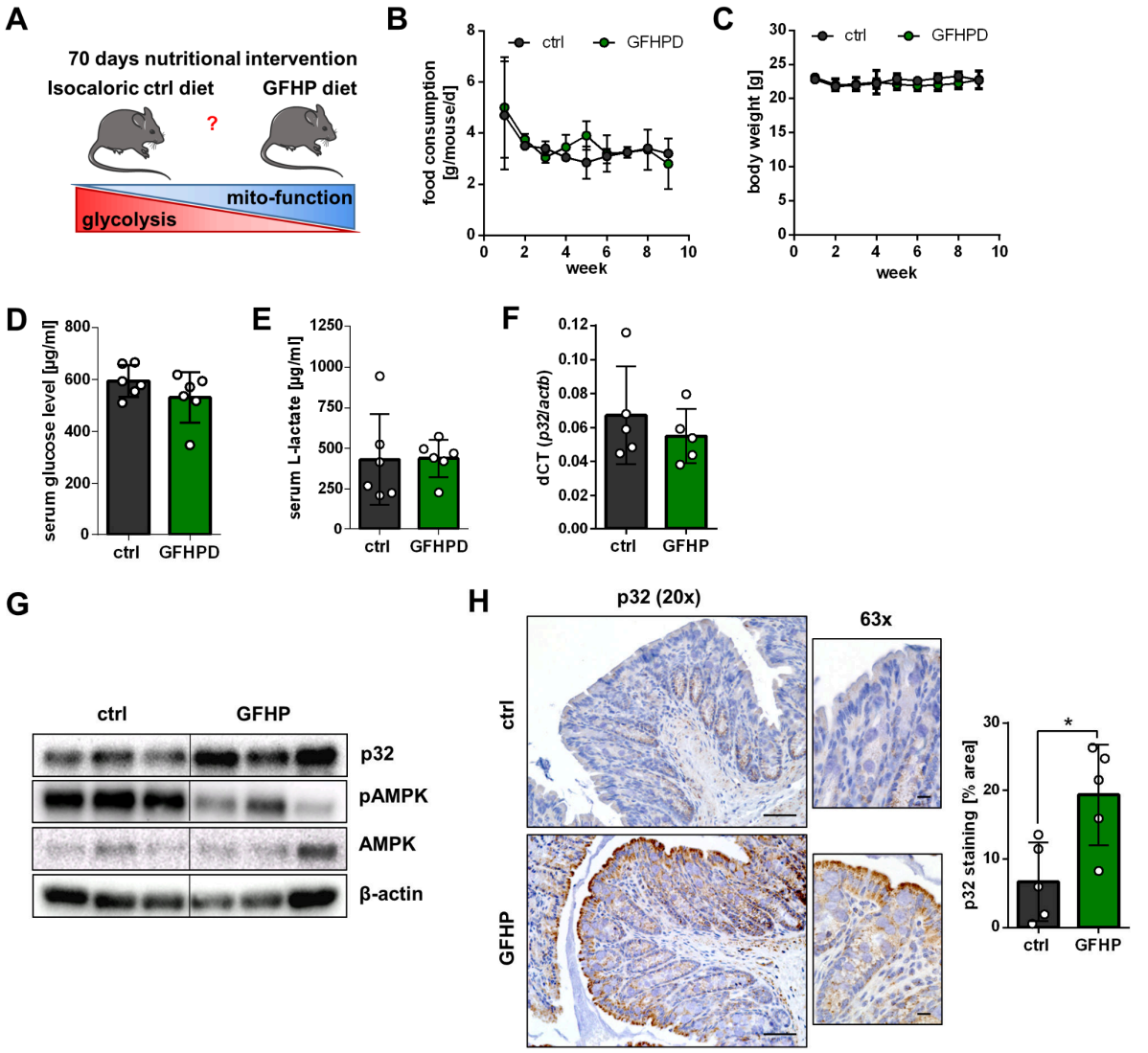

Figure 18: A glucose-free, high-protein diet drives colonic p32 protein expression in mice. A) Hypothesized metabolic switch upon glucose-free, high-protein (GFHP) dietary intervention in mice (Reef et al., 2007). Weekly, **B)** food consumption and **C)** mice body weight was determined (n = 6 mice from two independent experiments). Data were obtained by Kerstin Skibbe, Institute of Nutritional Medicine, University Hospital Schleswig-Holstein, Campus Lübeck, Germany with support of the author. **D)** Glucose and **E)** L-lactate levels were measured in serum samples from control (ctrl) and GFHP diet mice. **F)** Expression level of *p32* mRNA was determined *via* TaqMan® probes for *p32* exon 3-4 by qPCR in colonic biopsies from ctrl and GFHP diet mice. **G)** Denaturating western blot experiments were performed utilizing whole protein extracts from colonic samples from ctrl and GFHP mice under reducing conditions. Primary antibodies against p32 (clone EPR8871), pAMPK, AMPK and β-actin were applied. **H)** Immunohistochemisty staining against p32 (clone EPR8871) was conducted in paraffin-embedded colonic tissue samples of ctrl and GFHP diet fed mice. Corresponding area of staining was quantified utilizing the colour deconvolution tool in ImageJ (Rasband, 1997-2018) and representative images are shown. Scale bar (20x) = 50 µM, scale bar (63x) = 10 µM. Statistical significance was determined by unpaired t-test. Results are presented as mean ± SD. * $p \leq 0.05$.

Eventually, it was tested whether enhanced p32 protein expression in GFHP diet fed mice would also result in enhanced goblet cell differentiation. In comparison to control mice, increased KLF4 mRNA and protein expression, enhanced mucus filling of goblet cells and a thicker colonic mucus layer were

potent indicators for induction of terminal differentiation of goblet cells under GFHP diet (Figure 19A and B). Further, *spdef1* as a marker for secretory progenitor cells tended to be reduced in GFHP diet fed mice (unpaired t-test, $p = 0.06$) supporting the idea, that p32 expression is pivotal for the transition from secretory precursors towards terminally differentiated goblet cells (Figure 19A). Expression of proliferation marker *ki67* and intestinal stem cell marker *lgr5* was unaltered upon GFHP diet (Figure 19C). Taken together, nutritional intervention by glucose restriction in the presence of high protein intake appears as a promising tool to enhance colonic p32, thereby improving cellular energy supply and finally promoting goblet cell differentiation.

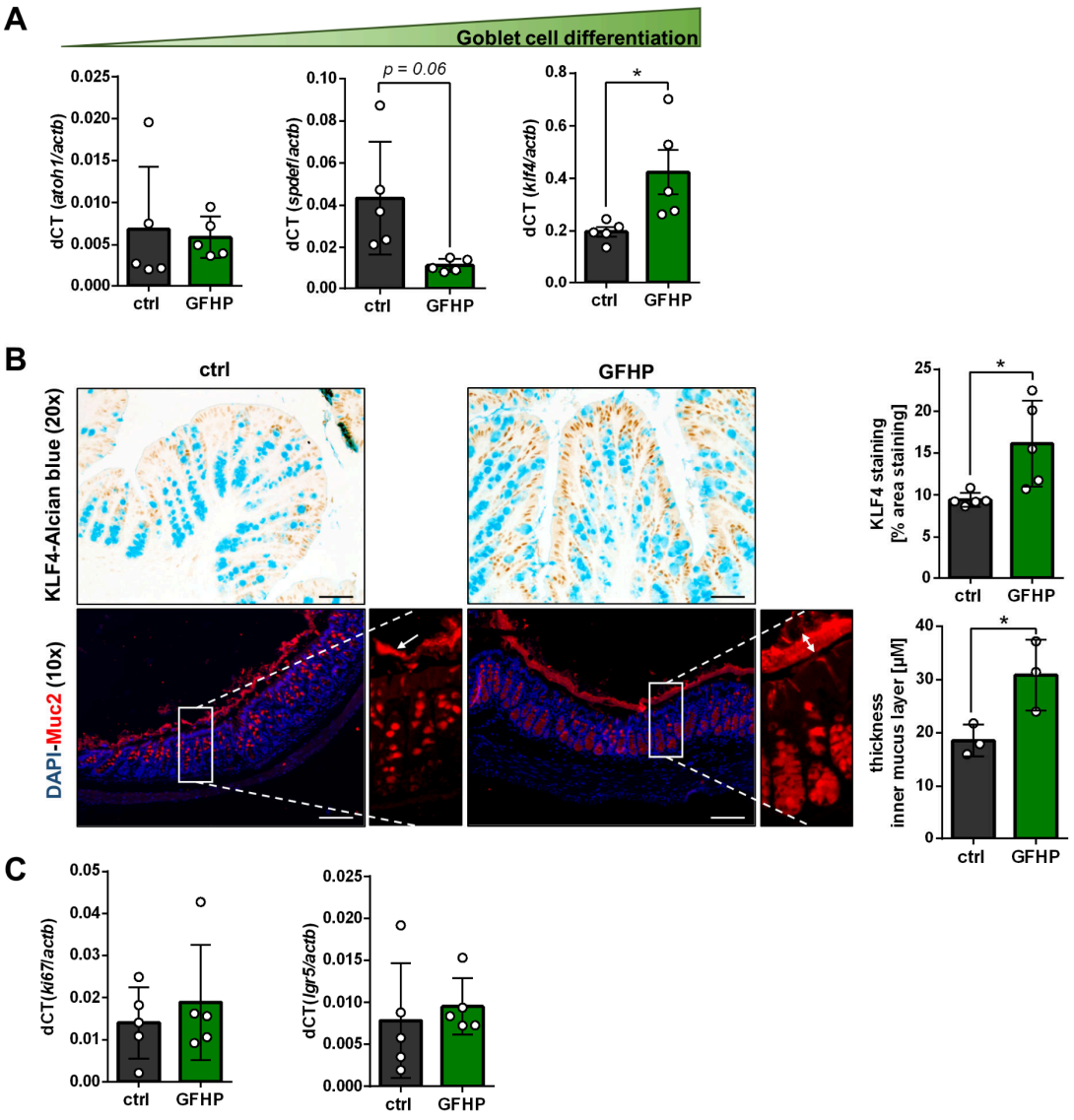

Figure legend follows on next page

Figure 19: A glucose-free, high-protein diet results in enhanced goblet cell differentiation in mice. Expression of **A)** goblet cell transcription factors *atoh1*, *spdef1* and *klf4,* **C)** proliferation marker *ki67* and stem cell marker *lgr5* was quantified by qPCR in colonic biopsies from B6-wt mice fed a glucose-free, high-protein (GFHP) or an isocaloric control (ctrl) diet. Data were normalized to *ß-actin*. **B)** Immunohistochemistry against KLF4 with Alcian blue counterstain and MUC2 immunofluorescent staining with DAPI counterstain was performed in formalin- or Carnoy-fixed, paraffin-embedded colonic tissue, respectively. Corresponding area of staining was quantified utilizing the colour deconvolution tool in ImageJ (Rasband, 1997-2018) and thickness of the inner mucus layer was measured applying the ZEN software (blue edition; Zeiss). Representative images are shown. Scale bar (20x) = 50 µM, scale bar (10x) = 100 µM. Statistical significance was determined by **A)** and **B)** (thickness of the inner mucus layer) unpaired t-test with Welch's correction and **B)** (KLF4 staining) unpaired t-test. Results are presented as mean ± SD. * $p \leq 0.05$.

4.8 The p32 protein is cleaved by caspase-1 during inflammation

After having delineated the importance of p32 in the context of goblet cell differentiation in non-inflamed colonic tissue, a second major aim of this thesis was to study the role of p32 in the context of intestinal inflammation. Cell proliferation, differentiation and metabolism are highly important during intestinal inflammation in UC by ensuring functional cell renewal and regain of barrier integrity (Clevers, 2013). Considering the results obtained during this thesis, presenting p32 as a key regulator of mitochondrial OXPHOS and as indispensable for cell proliferation, p32 was proposed to regulate goblet cell fate also under inflammatory conditions. Surprisingly, p32 level were not altered in UC tissue biopsies from inflamed *versus* non-inflamed regions, when analyzing mRNA expression in paired biopsies or p32 protein expression utilizing an anti-p32 antibody directed against epitopes encoded by exon 5 (Table 1, Figure 20A and B). Gersemann *et al*. published in 2009, that induction of goblet cell differentiation during inflammation is impaired in UC but not CD (Gersemann et al., 2009). In line with these data, similar *KLF4* expression was observed in biopsies obtained from inflamed regions of patients with active UC and non-inflamed biopsies from UC patients in remission (Table 1 and Figure 20C).

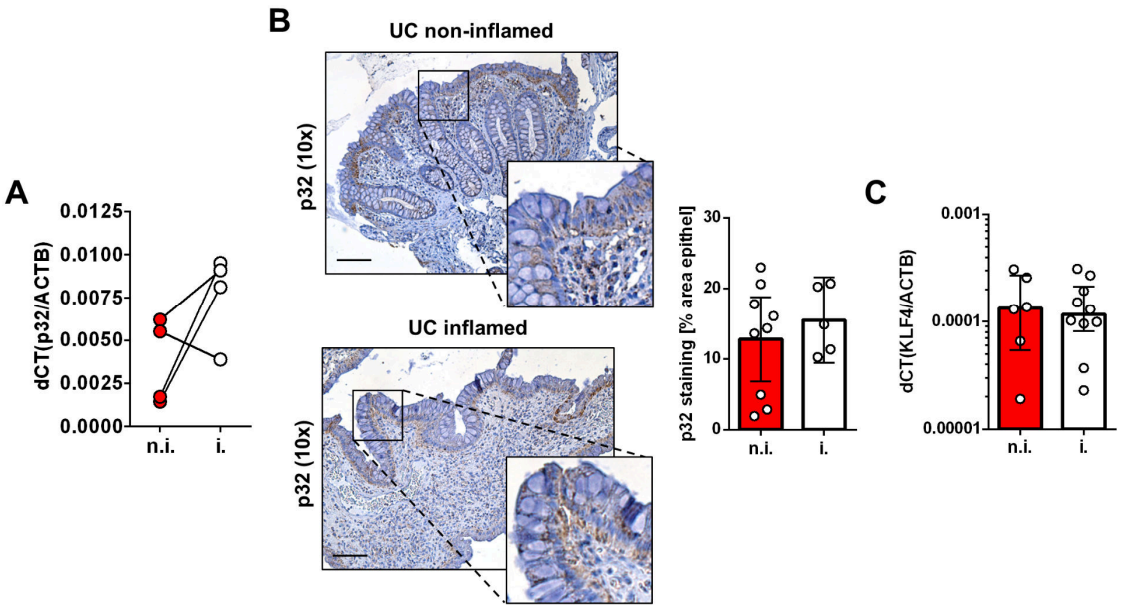

Figure 20: P32 mRNA and protein expression is unchanged during active inflammation in UC. A) *P32* mRNA expression in paired biopsies from non-inflamed and inflamed colonic tissue sections was quantified by qPCR and normalized to *ß-Actin*. **B)** Representative immunohistochemistry staining and corresponding quantification (Ruifrok and Johnston, 2001) of p32 protein expression (clone EPR8871, anti-p32 exon 5) in the upper part of the colonic crypt in paraffin-embedded biopsies from non-inflamed and inflamed colonic tissue sections from UC patients. Scale bar = 100 µM. Representative images from 10 non-IBD controls, 9 UC non-inflamed and 5 UC inflamed biopsies are shown. **C)** KLF4 mRNA expression was quantified by qPCR in non-inflamed colonic biopsies from UC patients in remission and inflamed colonic biopsies from UC patients with active disease. Data were normalized to *ß-Actin*.

Taking into consideration, that an antibody binding to epitopes encoded by exon 5 might not detect all possible alterations of the p32 protein and considering that p32 has been proposed to appear in various forms (full-length and mature protein, monomer, dimer, trimer) and at various intra- or extracellular localizations (mitochondria, cytoplasm, nucleus, cell surface, extracellular space), we still proposed potential cleavage of the p32 protein during inflammation. Hence, an *in silico* prediction analysis of potential protease cleavage sites was performed in human full-length p32 protein utilizing the PeptideCutter server (*https://web.expasy.org/peptide_cutter/*). Surprisingly, caspase-1 as part of the inflammasome complex was predicted to cleave p32 at two specific sites within its protein sequence besides conventional protease cleavage. The first target sequence for caspase-1 mediated cleavage was identified *N*-terminally directly after exon 1 (aa residues 1-77) between aa 77 and 80 (DGDK) and the second one *C*-terminally in exon 5 (aa 193-233) between aa 229 and 232 (DSLD) resulting in proposed cleavage at amino acid residues 77 and 229 (Figure 21A). To verify results from the *in silico* prediction analysis, an *in vitro* cleavage assay was performed. Indeed, western blot experiments revealed time- and concentration-dependent cleavage of recombinant human p32, when incubated with recombinant active human caspase-1 (Figure 21B). Caspase-1 mediated *in vitro* cleavage was additionally performed in GST-tagged recombinant human full-length p32. To examine

p32 cleavage products in detail, the four resulting protein bands (sample A-D) were visualized by Coomassie blue staining after SDS-gel electrophoresis, extracted and analyzed by mass spectrometry-based peptide sequencing (Figure 21C and D). Sample A mainly contained GST-tag alone (~26 kDA) or full-length p32 lacking the GST-tag (~32 kDA), both of which were already present in the commercially obtained recombinant p32 (Figure 21E). In sample B, large fractions of caspase-1 p20 were detected accompanied by untagged p32 which was lacking peptide sequences *C*-terminal of aa 229 (~25.2 kDA). Sample C predominantly contained *N*- and *C*-terminal cleaved p32, with no p32 peptide sequences detected *N*-terminally of aa 77 or *C*-terminal of aa 229 (~17.2 kDA). Finally, sample D mainly included peptide sequences matching caspase-1 p10 and small amounts of peptides located between aa 162 and 229 of the full-length p32 protein (Figure 21C and D).

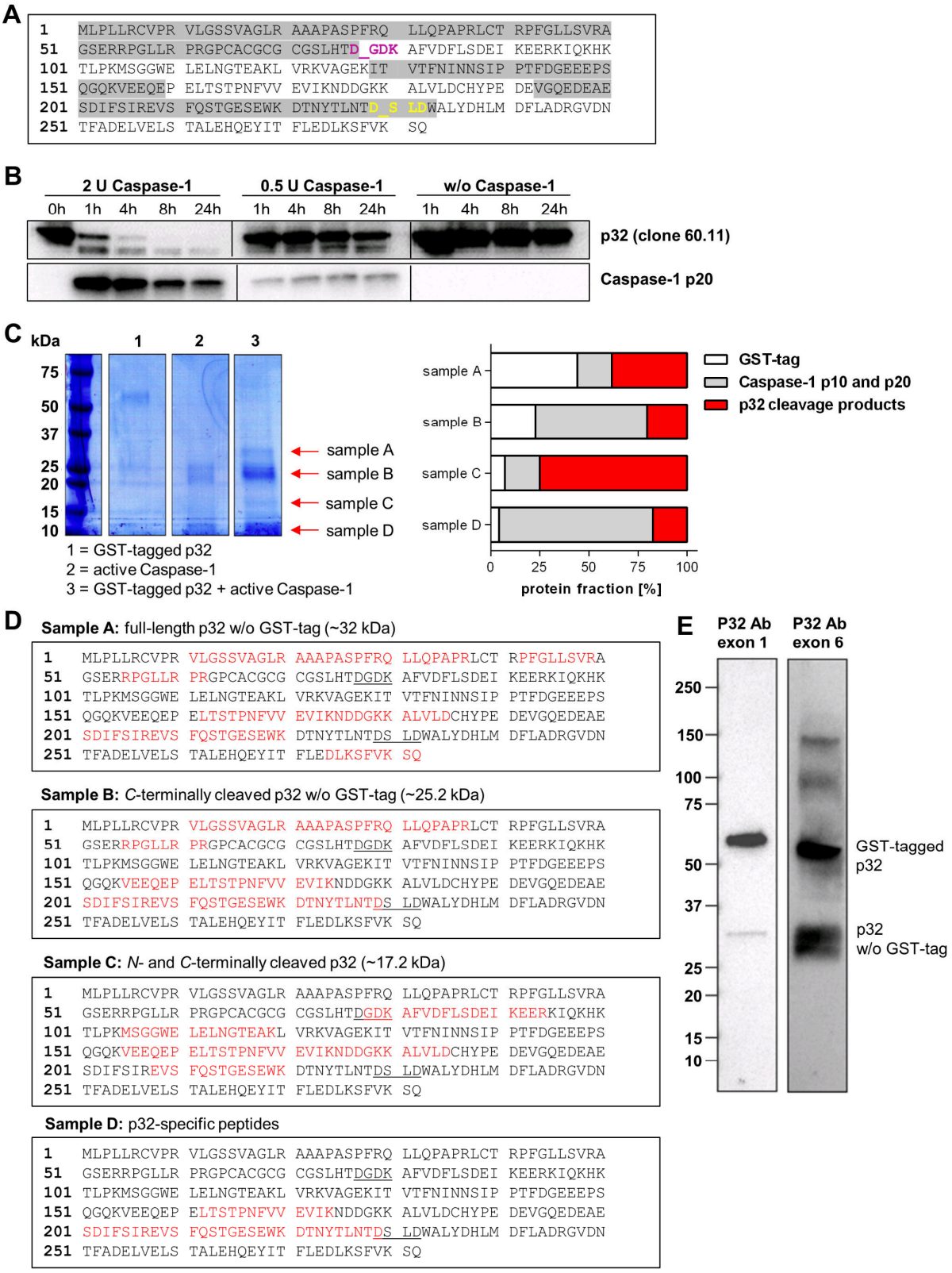

Figure legend follows on next page

Figure 21: Active caspase-1 cleaves human p32 at amino acid residues 77 and 229. A) Caspase-1 was predicted to cleave full-length p32 after amino acid residue (aa) 77 and 229 utilizing the PeptideCutter server (*https://web.expasy.org/peptide_cutter/*). Gray and white background: alternating exons; pink and yellow writing: Caspase-1 consensus sequences; underscore: predicted cleavage sites. **B)** *In vitro* cleavage assay was performed by incubating recombinant mature human p32 (aa 74-282) with active recombinant human caspase-1 at 37°C for indicated time periods. Corresponding protein samples were separated by denaturing SDS-PAGE and visualized by western blotting applying antibodies against p32 epitope aa 76-93 (clone 60.11) and caspase-1 p20 subunit. **C)** *N*-terminally GST-tagged full-length recombinant human p32 and active recombinant human caspase-1 were incubated together or separately at 37°C for 24 hours. Samples were separated by SDS-PAGE and stained with coomassie blue. Indicated samples A to D were cut out of the gel and sent to analysis *via* nanoHPLC-ESI-MS/MS method following in-gel digestion by trypsin. Corresponding fractions of peptides specific for cleaved or non-cleaved human p32, for active caspase-1 or for the GST-tag were visualized. **D)** Detected peptide sequences within sample A to D are marked in red and caspase-1 target sequences are underlined. **E)** Denaturing western blot experiments of human recombinant full-length p32 applying primary antibodies against epitopes of p32 encoded by exon 1 or exon 6.

4.9 P32 cleavage by caspase-1 results in a metabolic switch from OXPHOS towards glycolysis

The first exon of full-length p32 encodes a signaling peptide for mitochondrial import and active caspase-1 appears to cleave the p32 protein directly after the first exon at aspartic acid residue D77. To study functional consequences of caspase-1 mediated cleavage of p32, a cDNA plasmid encoding human wt full-length p32 was mutated at nucleotide position 231 C > G and/or nucleotide position 687 T > G, resulting in an exchange from aspartic acid (D) to glutamic acid (E) at aa position 77 and/or 229 in the translated protein (Figure 22A). Following, HAP1 *p32*$^{-/-}$ cells were stably transfected with either a mock plasmid, wt p32, mutant p32-D77E, mutant p32-D229E or mutant p32-D77E/D229E. Addition of recombinant human active caspase-1 to native protein isolates from HAP1-*p32*-wt or HAP1-*p32*- D77E/D229E cells resulted in cleavage of the *p32*-wt protein, while this was not the case in mutant p32-D77E/D229E cells (Figure 22B). To study metabolic consequences of inflammasome-mediated p32 cleavage, the inflammasome components human NLRP3 (N), human ASC (A) and human caspase-1 (C) were constantly overexpressed in HAP1 transfectants (Figure 22C). NAC overexpression resulted in a significant decrease in oxygen consumption in HAP1-*p32*-wt but not in HAP1-p32-D77E/D229E cells, supporting the idea that loss of the mitochondrial signaling peptide through caspase cleavage at aa position 77 would impair mitochondrial import of p32 and therefore its OXPHOS-driving function (Figure 22D). Overall, HAP1-p32-D77E/D229E-NAC cells appeared metabolically less active than its non-mutated counterpart, since both OCR and ECAR were reduced in Seahorse measurements. Meanwhile, HAP1-mock-NAC cells displayed high anaerobic glycolysis activity, which was similar to the findings obtained for HAP1 *p32*$^{-/-}$ cells in figure 4C to E (Figure 22E). In line with the literature describing proliferating cells to rely on energy supplied by glycolysis rather than on OXPHOS, NAC overexpression in HAP1-*p32*-wt cells was accompanied by induction of cell proliferation, which was not the case for

HAP1-p32-D77E/D229E cells. Meanwhile, mock transfected HAP1 cells died in the presence of NAC overexpression, supporting the idea that p32 is indispensable for maintaining efficient energy supply under stress conditions (Figure 22F). Finally, activated cells during inflammatory response have been proposed to release soluble p32 due to a yet unknown mechanism (Peterson et al., 1997). First experiments, quantifying p32 in cell culture supernatants of HAP1-*p32*-wt or HAP1-p32-mutant cells overexpressing NAC, resulted in significantly higher release of p32 from HAP1-p32-*wt*-NAC cells compared to those carrying the D77E mutation (Figure 22G). Taken together, cleavage of p32 by caspase-1 appears not only to regulate cell metabolism and proliferation during inflammasome activation, but also p32 secretion.

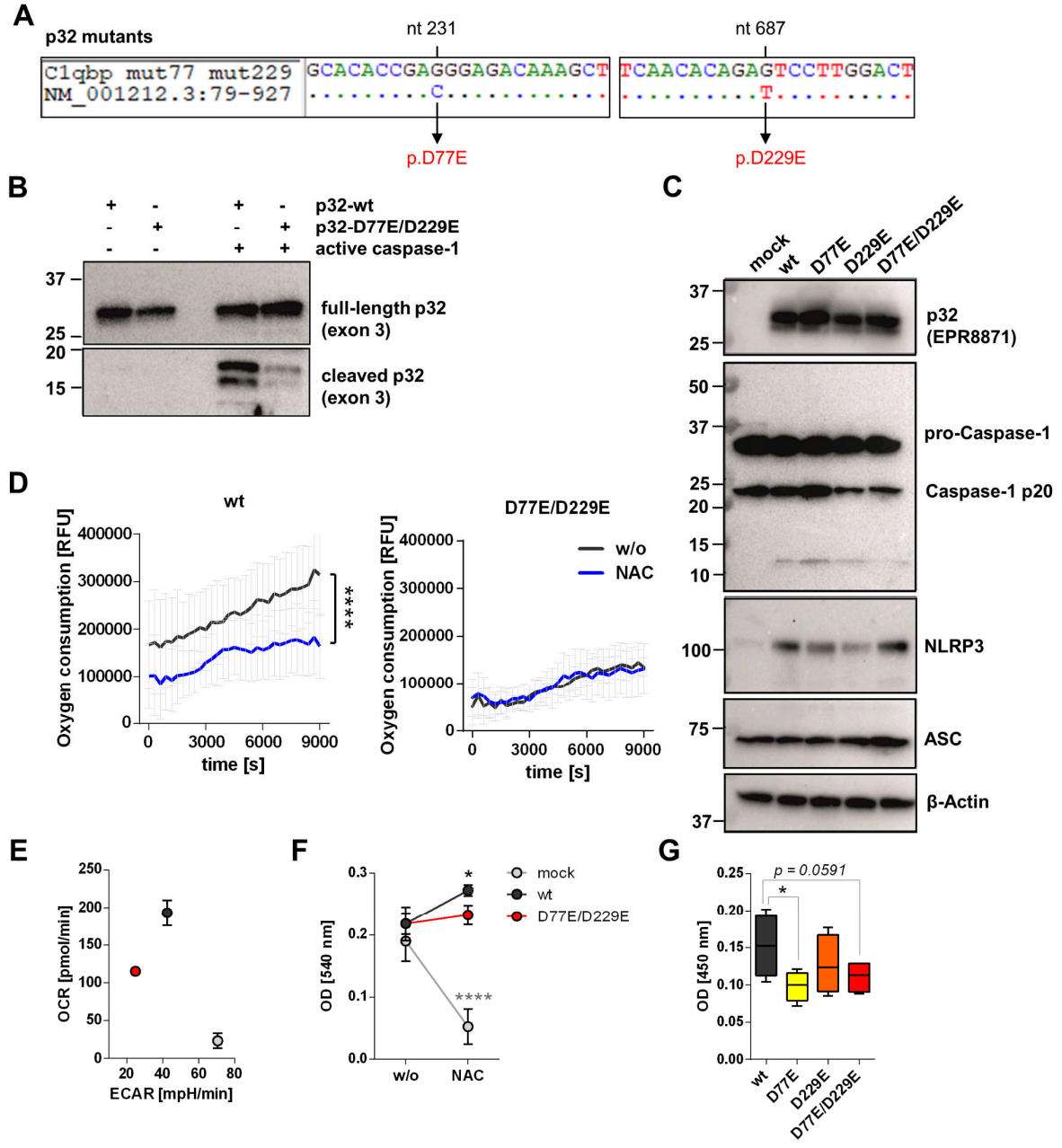

Figure legend follows on next page

Figure 22: Caspase-1 mediated p32 cleavage induces a metabolic switch towards glycolysis, cell proliferation and p32 secretion in HAP1 cells. A) Plasmids encoding human p32 were transformed at nucleotide (nt) position 231 and 681 by site-directed mutagenesis to generate p32-D77E, p32-D229E and p32-D77E/D229E plasmids. Sequences obtained from sequencing were aligned with BioEdit (*www.bioedit.software.informer.com*). NM_001212.3: p32 GenBank accession number. **B)** Whole native protein isolates from HAP1 *p32*$^{-/-}$ cells stably transfected with the *p32*-wt or mutant p32-D77E/D229E plasmid were treated with or without active caspase-1 at 37°C for 4h. Reduced protein extracts were separated by SDS-PAGE and western blot experiments were performed applying a primary antibody against p32 exon 3. **C)** HAP1-*p32*-mock, HAP1-*p32*-wt and HAP1-p32-mutant cells were stably transfected with inflammasome components NLRP3 (N), ASC (A) and caspase-1 (C). Transfection efficacy was confirmed by denaturing western blot analysis of whole protein extracts under reducing conditions applying primary antibodies against p32 (clone EPR8871), caspase-1, NLRP3, ASC and β-Actin. Statistical difference of the column factor (+/- NAC), including all time points, is visualized. **D)** Oxygen consumption was measured over time in HAP1-*p32*-wt and HAP1-p32-D77E/D229E mutant cells transfected with or without NAC. **E)** Oxygen consumption rate (OCR) and extracellular acidification rate (ECAR) were obtained from Seahorse experiments utilizing HAP1-*p32*-wt, HAP1-*p32*-mock and mutant HAP1-p32-D77E/D229E cells transfected with NAC. Results from one experiment with technical triplicates are shown. **F)** For estimation of viable cell mass, a neutral red assay was performed with HAP1-*p32*-wt, HAP1-*p32*-mock and mutant HAP1-p32-D77E/D229E cells with or without NAC overexpression after 72 h of incubation. **G)** Extracellular p32 was quantified in cell culture supernatants of HAP1-*p32*-NAC transfected cells cultivated for 72 h utilizing a direct p32 exon 3 ELISA. Data were generated with great technical support from Maren Hicken, Institute of Nutritional Medicine, University Hospital Lübeck, Germany. If not differently indicated results are presented from at least 3 individual experiments as **D)** mean ± SEM, **E)** and **F)** mean ± SD and **G)** Box and whiskers blot minimum to maximum. Statistical significance was determined by **D)** and **F)** Two-way ANOVA with Sidac multiple comparison test and **G)** matched one-way ANOVA w/o Geisser-Greenhouse correction and Fisher's LSD post test. * $p \leq 0.05$, **** ≤ 0.0001.

4.10 Caspase-1 is activated during inflammation in UC resulting in p32 cleavage and loss of goblet cells

After having shown that caspase-1 mediated cleavage of p32 results in a metabolic shift towards glycolysis the question remained, whether this mechanism is indeed relevant in the context of goblet cell differentiation and colonic inflammation in UC. Immunohistochemical staining revealed that pro-caspase-1 was expressed in lamina propria leucocytes and in the upper part of the colonic crypt in non-IBD controls as well as UC patients in remission (Figure 23A). Of note, epithelial expression pattern of pro-caspase-1 was similar to the ones obtained for p32, mitochondrial marker TOMM22 and goblet cell differentiation marker KLF4 (Figure 7C) indicating potential interactions between those proteins. Goblet cell differentiation is especially sensitive to alterations in cellular energy metabolism (Figure 11 and 13), caspase-1 mediated cleavage of p32 shifts the cell from mitochondrial OXPHOS towards energy generation *via* glycolysis (Figure 22) and proteins of the inflammasome complex have been previously reported to be highly expressed in colonic goblet cells (Wlodarska et al., 2014). Therefore, HT29-MTX cells were utilized to study goblet cell differentiation during inflammasome activation. Endogenously, HT29-MTX cells only expressed low levels of the inflammasome components caspase-

1 and NLRP3 (Figure 23B and C). Therefore, NLRP3, ASC and Caspase-1 were transiently overexpressed before induction of cell differentiation *via* butyrate (Figure 23C and Figure 11). Differentiation of H29MTX cells with butyrate let to a significant downregulation of *NALP3* mRNA expression, while expression of *ASC* and *Caspase-1* were induced, supporting the notion that the inflammasome plays a critical role in goblet cell differentiation. Of note, constant and butyrate-induced goblet cell differentiation was decreased in the presence of active NLRP3 inflammasome, indicated by reduced expression of the goblet cell differentiation marker KLF4 (Figure 23E). Together, results highlight the importance of inflammasome-mediated, p32-controlled abrogation of goblet cell differentiation.

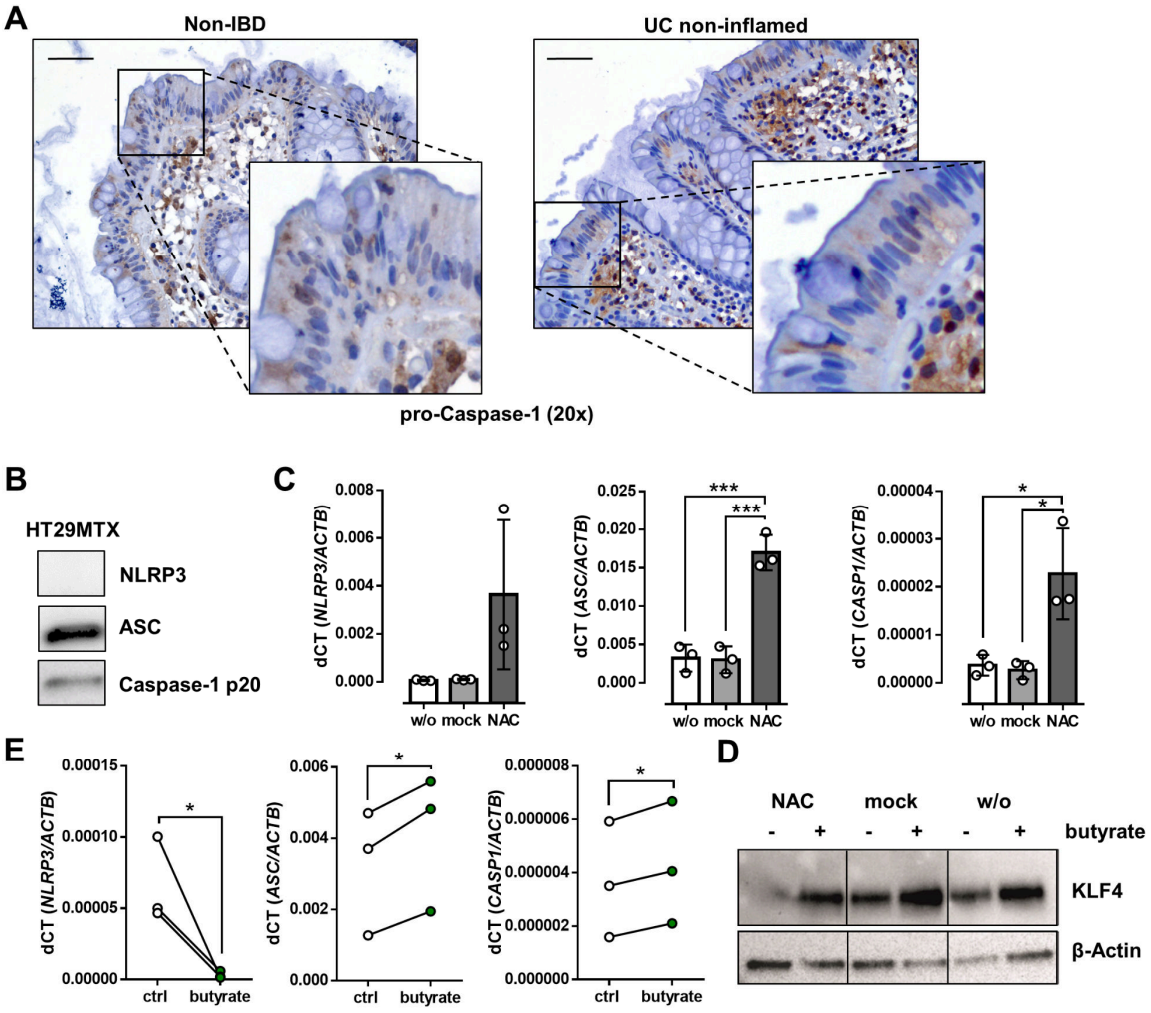

Figure legend follows on next page

Figure 23: Goblet cell differentiation is abrogated upon inflammasome activation in HT29-MTX cells. A) Immunohistochemistry applying an anti-pro-Caspase-1 antibody was performed in paraffin embedded non-inflamed sigmoidal biopsies from 10 non-IBD controls and 9 UC patients. Representative images are shown. Scale bar = 50 µM. **B)** Expression of inflammasome components Caspase-1, ASC and NLRP3 in untreated HT29-MTX was quantified by **B)** denaturing, reducing western blot experiments**.** One western blot experiments from two independent experiments is shown. Data were generated under the support of the author in the course of the Dr. med. thesis from Franziska Fetzer, Institute of Nutritional Medicine, University Hospital Lübeck, Germany. **C)** and **D)** HT29-MTX cells were transiently transfected with human NLRP3 (N), human ASC (A) and human Caspase-1 (C) or with a mock plasmid for 96 hours. Transfected or untransfected (w/o) cells were additionally stimulated with 1.25 mM butyrate for the last 72 hours of the experiment. **C)** Transfection efficacy was controlled by qPCR. **D)** Whole protein extracts were separated by SDS-PAGE under reducing conditions and western blot experiments were performed applying primary antibodies against human KLF4 and ß-Actin. Representative western blot of three individual experiments is shown. **E)** The effect of butyrate treatment on expression of inflammasome components NAC was measured by qPCR. Statistical significance was determined by **C)** ordinary one-way ANOVA with Tukey's post hoc test for multiple comparisons and **E)** ratio paired t-test (N) and paired t-test (A, C). ** $p \leq 0.05$*, ***** ≤ 0.001.

To finally transfer data obtained *in vitro* on caspase-1 mediated p32 cleavage and resulting loss of goblet cell differentiation to the human system, colonic biopsies from non-IBD controls as well as non-inflamed and inflamed tissue sections from UC patients were stained for pro-caspase-1, p32 exon 6 and PAS Alcian (Figure 24, partially combining data from Figure 10C and 23A). Of note, protein expression of pro-caspase 1 was reduced in inflamed but not non-inflamed tissue areas of UC patients indicating inflammasome activation in respective regions. Consistent with reported caspase-1 induced p32 cleavage (Figure 21), binding of an antibody against p32 exon 6 was reduced in UC inflamed tissue sections compared to non-IBD controls in a disease activity dependent manner. As presented in detail in Figure 9, the staining intensity of goblet cell granules was lower in UC non-inflamed tissue compared to non-IBD controls under basal conditions (see also Figure 10). Of special interest, the amount of mucus-filled goblet cells was reduced under low grade inflammation and further decreased with increasing degree of mucosal inflammation (Figure 24). Overall, these findings support the observation in Figure 22 that caspase-1 mediated cleavage of p32 leads to abrogation of goblet cell differentiation, thereby further reducing mitochondria-localized and functional p32 as well as differentiated goblet cells in the colonic crypt of UC patients.

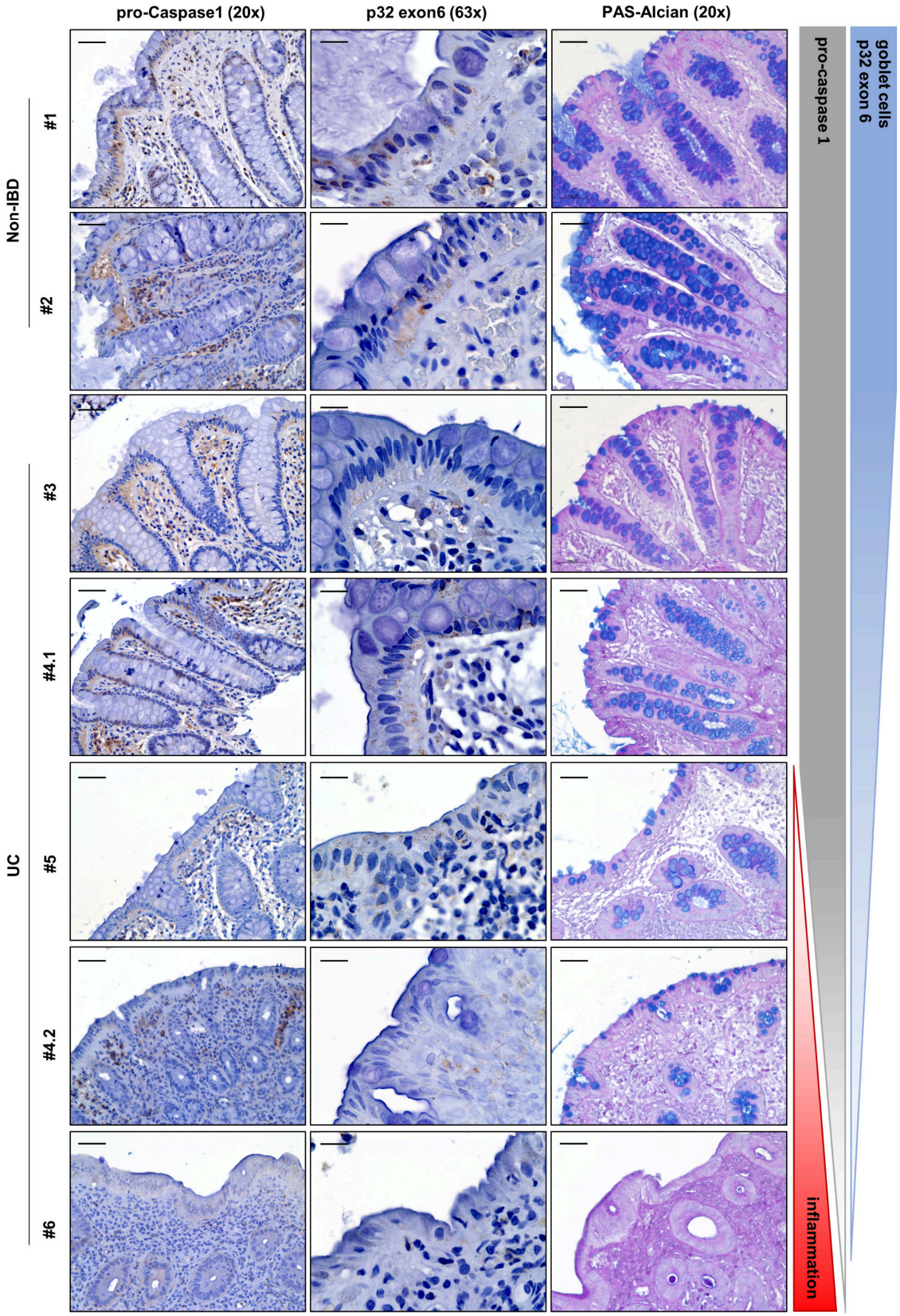

Figure legend follows on next page

Figure 24: Goblet cell numbers decrease with increasing degree of caspase-1 mediated p32 cleavage in UC. Immunohistochemical staining against pro-caspase-1 or p32 exon 6 as well as PAS-Alcian blue staining was performed in paraformaldehyde-embedded biopsies obtained from the descending colon or sigma from non-IBD controls and UC patients in remission or active disease. Representative images from 8 biopsies categorized as non-IBD controls or UC non-inflamed and 5 UC inflamed samples are displayed. #1 and #2: non-IBD non-inflamed; #3 and #4.1 UC non-inflamed; #5 UC low grade inflammation; #4.2 UC medium-grade inflammation; #6 UC high grade inflammation. #4.1 and #4.2 were obtained from different areas of the same patient. Scale bar = 50 µM.

5 Discussion

5.1 Mucosal p32 enables goblet cell differentiation *via* regulation of mitochondrial OXPHOS – a novel molecular mechanism impaired in UC

Mitochondrial disturbance and malfunction of goblet cells are frequently observed in UC, which presents as a multifactorial disease, where inflammation is caused by a disruption of the colonic epithelial and mucus barrier (Gersemann et al., 2009; Johansson, 2014; Khaloian et al., 2020; McCormick et al., 1990; Pullan et al., 1994; Rath et al., 2018; Roediger, 1980a, 1993; Santhanam et al., 2012; Sifroni et al., 2010). Terminally differentiated goblet cells have a pivotal role in the maintenance of intestinal barrier integrity and their differentiation is presumably regulated by a metabolic switch from glycolysis to mitochondrial OXPHOS (Katz et al., 2002; Stringari et al., 2012). In order to understand the molecular basis and disease origin of UC, it is necessary to find the underlying cause of mitochondrial dysfunction and to unravel a potential link to impaired goblet cell function.

P32 has been previously published to be highly important in the maintenance of OXPHOS in various experimental knockdown models, including yeast cells with disrupted *p32*-homologue, human and murine cell lines treated with short hairpin or siRNA against the *p32* transcript and heterozygous $p32^{-/-}$ mice (Fogal et al., 2010; Hu et al., 2013; Liu et al., 2017; Muta et al., 1997). In the present work the commercially available human haploid chronic myelogenous leukemia HAP1 cell line system in which *p32* was knocked-out by CRISPR/Cas9 technology and the corresponding paternal cell line were utilized to investigate molecular function of p32. Contrasting homozygous $p32^{-/-}$ mice which are embryonic lethal (Yagi et al., 2012), HAP1-$p32^{-/-}$ cells were culturable, but presented with growth retardation, diminished OXPHOS capacity, metabolic imbalance and energy deficiency. These results are in line with the supportive function of p32 in mitochondrial ribosome assembly, enabling protein translation of mitochondria encoded subunits of the respiratory complexes I, III, IV and V (Hillman and Henry, 2019; Yagi et al., 2012).

While the impact of p32 on cellular metabolism is rather consistent among studies, described subcellular localization for p32 are diverse (Ghebrehiwet et al., 1994; Muta et al., 1997; Saha and Datta, 2018). Here, p32 mainly localized to the mitochondria, but was also detected in the cytoplasm and the extracellular space, depending on the antibody and the methodology applied. Ghebrehiwet *et al.* first described p32 as a cell surface glycoprotein that binds to the globular heads of C1q on B-cells in 1994 (Ghebrehiwet et al., 1994). Even if the present study did not specifically detect cell surface-localized p32, it does not exclude the corresponding localization in human cancer cell lines and epithelial cells. Future research on p32 has to carefully take into account tertiary (protein folding of full-length or mature protein lacking the mitochondrial leader) and quaternary (monomer, dimer, trimer) protein

structure, applied antibodies (target epitope) and methodological approach (ELISA, Western blotting, IHC/IF, crystallography).

After having verified that p32 is indispensable for mitochondrial OXPHOS function, and bearing in mind that mitochondrial disturbance is a hallmark of UC pathology (Roediger, 1980a, 1993; Santhanam et al., 2012; Sifroni et al., 2010), p32 expression was hypothesized to be altered in the colon of UC patients. Both IBD subtypes, UC and CD, are disorders of the gastrointestinal tract, which display dysfunctional mitochondria (Khaloian et al., 2020; Rath et al., 2018). While the reason for mitochondrial dysfunction in CD is still unknown, data presented here suggest that low expression level of p32 is the underlying cause for metabolic dysfunction in UC. Of note, p32 level were decreased in colonic but not ileal samples from non-inflamed UC patients in remission compared to non-IBD controls, supporting the notion that low p32 level are not a result but rather an underlying source for intestinal inflammation. The question whether p32 expression is also aberrant in CD and plays a role in corresponding disease phenotype remains to be answered. So far, disease-associated variations in p32 expression have been focused on studies on cancer development and progression, as p32 level are frequently upregulated in various tumors (Bar et al., 2013; Chen et al., 2009; Gao et al., 2016; Kim et al., 2017; Rubinstein et al., 2004; Yu et al., 2013). The present work for the first time presents *p32*-deficiency as a potential cause for an immune-mediated inflammatory disorder. Meanwhile, underlying reasons for low colonic p32 level observed in UC still remain unresolved and future research on this topic will be discussed in section 5.5 of this thesis.

In line with published data on mitochondrial dysfunction in UC (Roediger, 1980a, 1993; Santhanam et al., 2012; Sifroni et al., 2010) and in accordance with observed p32 downregulation, phosphorylation of AMPK as a sensor for energy deficiency was strongly increased in colonic biopsies of UC patients in remission. Furthermore, L-lactate level as a sign of glycolytic activity were measured in serum or plasma samples and displayed significantly higher level in UC patients in remission compared to non-IBD controls. In line, metabolomics studies have previously shown increased lactate level in serum, urine and fecal samples for both UC and CD, when compared to healthy controls (Dawiskiba et al., 2014; Schicho et al., 2012; Vernia et al., 1988; Williams et al., 2012). Hereby, high lactate level were especially observed during active disease or when no distinction between remission and active disease state was made. Nevertheless, two of the studies also reported a moderate increase for UC patients in remission (Dawiskiba et al., 2014; Vernia et al., 1988).

When analyzing the spatial distribution of p32 protein expression in the colonic crypt, p32 was found to be highly expressed in the upper part of the crypt together with mitochondrial marker TOMM22 and KLF4, a marker for terminal differentiated goblet cells. Differentiated cells in the upper part of the crypt have been previously reported to be highly dependent on energy supplied by mitochondria

(Stringari et al., 2012). Similar spatial distribution of TOMM22, p32 and KLF4 expression in the colonic crypt does not prove interaction between these proteins. Nevertheless, since reduced numbers of goblet cells and a defective colonic mucus barrier was already published for UC patients in remission (Johansson, 2014; Johansson et al., 2014; McCormick et al., 1990; Pullan et al., 1994), p32 was hypothesized to impact goblet cells. While mitochondrial disturbance results in aberrant development of Paneth Cells in CD (Khaloian et al., 2020), this work presents abrogation of goblet cell differentiation through insufficient mitochondrial respiration as a potential cause for disease development in UC. Impaired induction of goblet cell differentiation in inflamed UC but not CD has been previously reported (Gersemann et al., 2009). Data presented here indicate that defective differentiation of goblet cells is already present in non-inflamed colonic tissue of UC patients in remission, defined by diminished mucus filling of goblet cells and reduced expression of terminal goblet cell differentiation marker *KLF4* compared to non-IBD controls. Despite the fact, that p32 interacts with a range of different binding partners (Saha and Datta, 2018) and that *p32* transcript expression correlated with *klf4* mRNA level in human and murine colonic biopsies, there is no evidence to date supporting direct interaction of p32 with KLF4 (*https://string-db.org/*). Data generated in the course of this study rather support the idea that changes in cellular metabolism upon alterations in p32 expression result in aberrant cell differentiation. Additionally, p32 might be generally involved in the maintenance of the metabolic gradient within the intestinal crypt. A hypothesis, which will be difficult to prove since *p32*$^{-/-}$ mice are embryonic lethal (Yagi et al., 2012) and even an intestine-specific *p32*-knockout mouse will most likely results in severe morphological and functional alterations in the crypt, due to the lack of energy generated *via* OXPHOS.

Next to the observation that low p32 expression is accompanied by mitochondrial dysfunction and defective goblet cell maturation in UC, this work provides experimental evidence that induction of goblet cell differentiation is dependent on p32-regulated mitochondrial function *in vitro.* Stimulation of a mucus producing goblet cell-like cell line with the short chain fatty acid butyrate resulted in induction of OXPHOS and terminal differentiation. Interestingly, HT29 cells are described in the literature to be fully differentiated mucin-secreting cells after differentiation with MTX (Dahiya et al., 1992). Here, data support the notion, that HT29-MTX are not *per se* differentiated goblet cells, but rather secretory precursor cells, as depicted by high expression of *SPDEF1* but not *KLF4*. Formation of an adherent cell layer coated with a mucus layer has been previously published for HT29-MTX cells, when cultured post-confluent in a semi-wet interface with mechanical stimulation and a Notch γ-secretase inhibitor treatment for 28 days (Navabi et al., 2013). The present work provides a novel, more convenient method to achieve differentiation of HT29-MTX cells. Shifting the cells metabolism towards energy generation *via* mitochondrial oxidation by supplementation with butyrate for three days, resulted in terminal differentiation as defined by induction of mucus secretion, increased vacuole

formation and high expression of KLF4. Kaiko *et al.* previously demonstrated that the butyrate oxidation pathway is especially active in differentiated colonocytes in the upper part of the crypt (Kaiko et al., 2016). Thereby, a metabolic gradient for butyrate is built, resembling the OXPHOS gradient in the intestinal crypt described by Stringari *et al.* in 2012 (Stringari et al., 2012) as well as the spatial distribution of p32 in the human and murine colonic epithelium observed in this work. Interestingly, Roedinger *et al.* already published in 1980, that colonocytes from UC patients with both quiescent and active disease have a significant lower ability to oxidize butyrate compared to healthy controls (Roediger, 1980a). Whether butyrate-producing bacteria and butyrate itself is reduced in patients with UC is still a topic of discussion with partially contradictory studies present in the literature (Machiels et al., 2014; Takaishi et al., 2008; Zhuang et al., 2019). Additionally, it is difficult to judge whether potential changes in microbiome and metabolome composition are a result of alterations of the inflammatory state or *vice versa*. Data generated in the context of this work support the idea, that the colonic epithelium itself is responsible for reduced oxidative capacity, due to diminished expression of p32.

Supporting the hypothesis that p32-dependent OXPHOS is indispensable for goblet cell differentiation, butyrate-induced differentiation of HT29-MTX cells was abrogated upon p32 silencing. P32 has been previously published to be a critical regulator of dendritic cell maturation. Gotoh *et al.* suggested dendritic cell maturation to be regulated by citrate production *via* p32-dependent PDH activity (Gotoh et al., 2018). Again, loss of maturation in p32-deficient cells can be ascribed to the chaperone function of p32 in mitochondria.

Of note, while p32 is indispensable for the differentiation process of goblet cells, differentiated goblet cells did not necessarily express high p32 level. This observation is most likely due to the fact, that fully differentiated cells are in a more quiescent, less metabolic active state and therefore require lower overall energy level (Vander Heiden et al., 2009). In addition to its importance for cellular differentiation, this thesis presents data demonstrating that especially energy generated by OXPHOS is important for the process of mucus secretion itself. Mucus secreted into the cell culture supernatant was significantly decreased when HT29-MTX cells were treated with OXPHOS-inhibitors targeting complex V of the respiratory chain, but not when glucose was deprived from the cell culture medium. Even if there is no data available to date demonstrating level of energy required for exocytosis of mucin-containing granules, the latter can be assumed to be a highly energy demanding process due to the vast size of highly O-glycosylated mucin proteins. In line, mast cell degranulation is especially dependent on mitochondrial OXPHOS but not glycolysis in a mechanism involving mitochondrial signal transducer and activator of transcription 3 (Erlich et al., 2014). One major drawback of the cell model applied in this work is, that HT29-MTX cells produce MUC5AC rather than MUC2, the major gel-forming

mucin in the intestine. Even if HT29-MTX cell are derived from a colorectal cancer cell line, they produce and secrete a mucin protein that is primarily found in the lung and stomach (Ponten et al., 2008). Nevertheless, MUC2 and MUC5AC are structurally and functionally rather similar entities of high molecular weights (human MUC2: 5179 AA and 540 kDA; human MUC5AC: 5654 AA and 586 kDA), intensive O-glycosylation and the ability to form gel-like layers upon secretion (Holmen Larsson et al., 2013). Potential alterations in MUC5AC glycosylation also have to be considered in the context of ELISA experiments performed in this study. Differences in glycosylation pattern of mucin proteins have been previously published to alter binding of corresponding antibodies (Uray et al., 2014). Taken together, data generated in HT29-MTX cells underline the adaptability of goblet cells to its metabolic environment through regulation of their differentiation state, their level of mucus secretion and potentially their glycosylation pattern.

After having shown, that inhibition of respiratory chain complex V, the ATP-synthase, results in diminished mucus secretion *in vitro*, ATP8-mutant mice, carrying a mutation in the corresponding complex were utilized to study functional consequences of diminished OXPHOS activity *ex vivo*. ATP8-mutant mice presented as a suitable model for quiescent UC, sharing features like reduction of p32 expression, metabolic impairment and correlating loss of Klf4-expressing differentiated goblet cells as well as a thinned mucus layer. ATP8-mutant mice have been previously demonstrated to be particularly susceptible to experimentally-induced metabolic diseases, such as insulin resistance and non-alcoholic steatohepatitis (Schroder et al., 2016; Weiss et al., 2012). On the other hand, ATP8-mutant mice appear phenotypically inconspicuous in the absence of metabolic stress. In line, ATP8-deficiency did not result in the development of spontaneous colitis. Bearing in mind, that *Muc2*$^{-/-}$ mice develop spontaneous colitis and considering that a thin, permeable mucus layer is a risk factor in the development of intestinal inflammation, it can be assumed, that ATP8-mutant mice will present with increased susceptibility to intestinal inflammation, when challenged with dextran sodium sulfate (DSS) or trinitrobenzenesulfonic acid. Supporting this hypothesis, polymorphisms in nuclear encoded mitochondrial genes involved in ATP generation, namely uncoupling protein 2 (*UCP2*) and *SLC22A5*, encoding the organic carnitine transporter 2 (OCNT2), have been described as risk factors for UC (Waller et al., 2006; Yu et al., 2009b). In addition, inhibition of intestinal fatty acid ß-oxidation as well as genetic ablation of *UCP2* or *OCNT2* in mice resulted in experimental colitis (Roediger, 1980a; Shekhawat et al., 2007; Zhang et al., 2012). Conversely, conplastic mice with high mucosal OXPHOS and ATP levels have been already demonstrated to be protected from experimental colitis (Bar et al., 2013). Furthermore, ATP8-mutant mice presented with alterations in the intestinal microbiome, in specific in the abundance of *Bacteroidetes, Deferribacteres, Firmicutes, Proteobacteria* and *Tenericutes*. Since the mucus layer and the intestinal microbiota shape each other (Earley et al., 2019; Johansson et al., 2015), again the question remains if alterations in bacterial composition in ATP8-

mutant mice are a result of or a cause for colonic mucus layer alterations. Even if no mutations in the mitochondrially encoded ATP8-gene have been described in the context of UC to date, ATP8-mutant mice remain a good model to study the impact of OXPHOS-deficiency in the intestine *in vivo*.

In the present work, high level of KLF4-expressing terminally differentiated goblet cells are presented as a healthy state and as necessary for mucus barrier integrity. The transcription factor KLF4 specifically controls goblet cell fate, since in mice with intestinal deletion of *klf4* both colonocytes and enteroendocrine cells appear to undergo normal maturation. Additionally, cell proliferation and cell death rates are unchanged in *klf4*-deficient mice, while goblet cell numbers are reduced by 90% (Katz et al., 2002). In general, goblet cells are recognized to be a major line of defense in the intestinal mucosa. The two-layered colonic mucus system separates bacteria from the host epithelium and the continuous self-renewal pushes bacteria out into the lumen (Johansson et al., 2008), while animals with a penetrable mucus layer develop spontaneous colitis (Johansson et al., 2014). Notably, high KLF4 levels suppress development and progression of intestinal neoplasia and colitis-associated colorectal cancer upon azoxymethane (AOM)/DSS treatment in mice (Yang et al., 2019). Surprisingly, the same working group reported mice with intestine-specific *klf4*-deletion to be significantly less sensitive to acute DSS-induced colitis possibly explained by an increased cellular proliferation response (Ghaleb et al., 2014). Nevertheless, since acute DSS-colitis is a highly artificial model and since we did not observe changes in proliferation marker *ki67* in mice expressing low or high level of intestinal KLF4 it is unlikely that high KLF4 expression *per se* negatively controls proliferation.

5.2 Nutritional intervention presents as a promising tool to modulate p32 expression and hence goblet cell differentiation

After having delineated the dependency of goblet cell differentiation on p32-mediated OXPHOS metabolism *ex vivo* in humans and mice as well as *in vitro* in HT29-MTX cells, the question remained how p32 expression and hence goblet cell differentiation can be modulated. The present study proposes dietary intervention as a regulator of p32 expression on protein level. A diet deprived of glucose as energy source, but with double the amount of kilocalorie (kcal) derived from fat and three times the amount of kcal derived from the protein source casein, which was isocaloric to the corresponding control diet, was composed to achieve reduction of energy generated *via* glycolysis and thereby induction of alternative energy generation *via* OXPHOS in mice. Surprisingly, intake of a diet deprived of glucose but high in protein for more than two month did not result in increased weight gain or weight loss, did not alter serum glucose or L-lactate level or result in aberrant behavior of mice, supporting the idea that mice are in principal capable of tolerating a nourishment, which is deprived of glucose and has a protein source as its major caloric supply. Nevertheless, it has to be kept in mind that a diet high in protein can induce alterations in renal function and kidney health. A protein-rich

diet has been previously shown to increase renal blood flow and elevating intraglomerular pressure leading to higher glomerular filtration rates (Fouque and Aparicio, 2007; Kalantar-Zadeh et al., 2016; Ko et al., 2017). In terms of modulating p32 level, a GFHP diet was highly successful, since mice on the corresponding diet exhibited induction of p32 protein expression in the colon. Interestingly, this was not due to elevated *p32* mRNA level compared to mice on a control diet and hence supported post-translational regulation of the target. In line with human and *in vitro* data as well as evidence from ATP8-mutant mice, GFHP-diet mice depicted high mucosal energy level, an increased number of KLF4-positive terminally differentiated goblet cells, and a thickening of the colonic mucus layer compared to controls. In the diet applied in this study, casein, a protein derived from cow's milk, served as the major source of energy. Obviously, this kind of diet cannot be directly transferred to the human situation. In general, positive health outcome have been attributed to the intake of milk protein by humans, especially due to its high percentage of branched-chain amino acids. A decrease in the prevalence of individual metabolic risk factors such as hypertension, dyslipidaemia, mild hyperglycaemia and overall decreased adiposity have been reported (McGregor and Poppitt, 2013). Nevertheless, the applied GFHP diet remains rather constructed and unbalanced in relation to its composition. Especially a westernized diet, rich in animal protein in the form of red meat, high in sugar and low in fibres has been associated with an increased risk for UC (Jantchou et al., 2010; Jowett et al., 2004; Racine et al., 2016). Taken together, dietary intervention low in glucose but high in plant-based protein appears as a promising tool to modulate p32 expression, mitochondrial function, and goblet cell differentiation in the human intestine.

Finally, the question remains if there are possibilities to medically induce energy generated *via* mitochondrial oxidation and hence goblet cell differentiation besides nutritional intervention. In the present study, the author presents a small, preliminary data set supporting increased *p32* mRNA level in colonic biopsies from UC patients receiving azathioprine treatment compared to those not having azathioprine included in their medical regimen. Azathioprine, a purine analogue inhibiting nucleic acid synthesis, is frequently applied in both UC and CD to maintain clinical remission, due to its immunosuppressive properties (Biancone et al., 2003; Timmer et al., 2016). Additionally, an *in vitro* study from Schroll *et al.* reported profound inhibition of epithelial cell proliferation upon treatment with azathioprine (Schroll et al., 2005). Whether inhibition of intestinal epithelial cell proliferation conversely supports cell differentiation and how azathioprine possibly alters *p32* expression will require further investigations. In general, novel interventions specifically aiming at improvement of mitochondrial function are rare and nearly absent in the context of IBD (Andreux et al., 2013). One of the most prominent and best studied modulators of mitochondrial function is resveratrol, an indirect activator of sirtuin histone deacetylases, which control the activity of various transcription factors and co-factors which govern mitochondrial biogenesis and function (Howitz et al., 2003; Imai et al., 2000).

Resveratrol is present in low levels in red grapes and wine and has been presented to improve mitochondrial function at least in obese patients (Timmers et al., 2011; Yoshino et al., 2012). Of special interest, resveratrol has been published by several independent studies to ameliorate experimental colitis is rodents ((Cui et al., 2010; Martin et al., 2006; Yao et al., 2010). Meanwhile, human clinical trials on the potential therapeutic effect of resveratrol are limited to one randomized, double-blinded, placebo-controlled pilot study. Here, patients with mild to moderate UC presented with a decrease in clinical colitis activity and improved quality of life after having received resveratrol for 6 weeks compared to the placebo group (Samsami-Kor et al., 2015; Samsamikor et al., 2016). Together, a substantial amount of further studies is required to delineate, whether modulators of mitochondrial function have indeed the potential to significantly ameliorate inflammation in UC.

5.3 Cleavage of p32 by caspase-1 induces a metabolic switch from OXPHOS towards glycolysis – a novel mechanism supporting proliferation upon mucosal damage?

While data discussed so far concentrated on p32 in the context of goblet cell differentiation in the absence of inflammation, the final part of this thesis explored the impact of a p32-driven metabolism on goblet cells in the presence of active inflammation. As described above, intestinal epithelial cells mainly rely on energy supplied by mitochondrial oxidation to ensure proper cell differentiation (Stringari et al., 2012). Conversely, for fast cell renewal at sides of mucosal damage during inflammation, cells most likely rely on aerobic glycolysis for ATP production rather than on OXPHOS. The latter describes a metabolic phenomenon which is also known as the Warburg effect, and which is of special importance in the context of tumor development (Vander Heiden et al., 2009; Warburg, 1956). In the present study cleavage of p32 upon inflammasome activation was found to mediate a metabolic switch towards aerobic glycolysis. Data generated in HAP1-*p32*$^{-/-}$, HAP1-*p32* mutant and the corresponding parental cell line presented clear evidence that human p32 is cleaved by caspase-1 at two distinct positions. Cleavage sides were located *N*-terminally after the mitochondrial leader and *C*-terminally in a sequence encoded by exon 5. The *N*-terminal cleavage side is of special interest since it prevents mitochondrial import of cleaved p32 resulting in a decrease in mitochondrial OXPHOS capacity and a compensatory elevation in glycolysis activity enabling increased proliferation rates. Of note, HAP1-p32 cells carrying mutations inhibiting cleavage by caspase-1 and overexpressing inflammasome components, displayed reduced level of secreted p32 in cell culture supernatant compared to HAP1-*p32*-wt-NAC cells. It can therefore be postulated, that p32 is released into the extracellular space upon caspase-1 mediated cleavage similar to Il1β and Il18 (Ghayur et al., 1997; Thornberry et al., 1992). These results provide a first reasonable explanation for data reporting p32 to be expressed extracellularly and potentially also on the cell surface (Ghebrehiwet et al., 1994; Peerschke et al., 1998; Peterson et al., 1997). Apart from its role as a regulator of cellular metabolism,

functions requiring non-mitochondrial and non-cytoplasmic localization have been attributed to p32. In this context, binding of cell-surface localized p32 to the globular heads of C1q reportedly inhibits complement activation (Ghebrehiwet et al., 1994). Furthermore, interaction of p32 with serum proteins involved in blood clotting (Peerschke et al., 1998) and fibrin polymerization (Lu et al., 1999) as well as binding to various bacterial or viral antigens (Peerschke and Ghebrehiwet, 2007), might play a role in the prevention of intestinal inflammation. In how far low expression of non-cleaved p32 in UC will also result in lower extracellular level of p32 during inflammation compared to non-IBD remains to be topic of further investigation.

The described mechanism of caspase-1 mediated p32 cleavage was indeed found to be relevant in the context of UC, since caspase-1 was activated in inflamed tissue sections. In line, an antibody binding to p32 epitope encoded by exon 6 depicted decreased staining during inflammation. Meanwhile, p32 mRNA and total p32 protein level – utilizing a p32 antibody binding to a central region of the protein - where unaltered. Inflammasome activation upon barrier breakdown and bacterial invasion have been previously reported for IBD. The NLRP3 inflammasome has been published to be especially upregulated in CD and in late disease stage also in UC (Lazaridis et al., 2017). Additionally, production of IL1β was found to be enhanced in mononuclear cells isolated from the mucosa of patients with active UC or CD (Mahida et al., 1989). In line with data obtained in other studies describing inflammasome components NLRC1, 2 and 4, NLRP1, 3 and 6, AIM, ASC, Caspase-1, 4 and 8 as well as IL1β and IL1α to be expressed not only in intestinal immune cells, but also in non-hematopoietic IECs (reviewed by Lei-Leston and Murphy *et al.* in 2017 (Lei-Leston et al., 2017)), this study observed high expression of pro-caspase 1 in the non-inflamed colonic epithelium of UC patients and non-IBD controls. Interestingly, spatial distribution of pro-caspase 1 in the colonic crypt was similar to p32, KLF4 and TOMM22 with elevated expression level in the upper part of the crypt. This expression pattern appears rather reasonable, given that corresponding IECs serve as a physical and immunological barrier between the host and its microbiota. The role of the inflammasome in contributing to the pathology of inflammatory diseases of the intestine has been discussed rather controversial. Mice deficient for specific components of the inflammasome cascade partially presented with increased susceptibility to colitis and partially with decreased pathology (Allen et al., 2012; Bauer et al., 2010; Carvalho et al., 2012; Couturier-Maillard et al., 2013; Davis et al., 2011; Elinav et al., 2011; Guo et al., 2020; Hirota et al., 2011; Seo et al., 2015; Zaki et al., 2010). Nevertheless, Dupaul-Chicoine *et al.* nicely demonstrated that *caspase1*-deficient mice were highly susceptible to DSS-induced colitis and presented with impaired epithelial regeneration and tissue repair (Dupaul-Chicoine et al., 2010). The work of the present thesis describes the underlying mechanism. High rates of cell proliferation, enabled by a glycolytic cell metabolism, is mediated by caspase-1 dependent p32 cleavage upon active inflammation.

Besides its importance during active inflammation, there is increasing evidence that the inflammasome is involved in mediating homeostatic conditions also in the absence of intestinal inflammation. Several microbiota-associated metabolites, like taurine, histamine and spermine modulate NLRP6 signaling and hence caspase-mediated IL18 secretion under basal conditions (Levy et al., 2015). Therefore, it can be postulated that also cleavage of p32 is not restricted to an inflammatory environment. The composition and the metabolic profile of the intestinal microbiota might hence be able to constantly modulate intestinal IEC metabolism *via* the inflammasome – p32 axis. Considering that the composition of the intestinal microbiota is strongly shaped by diet (David et al., 2014) and that the NLRP3 inflammasome is continuously activated by nutrient excess (Ahechu et al., 2018; Christ et al., 2018), again dietary intervention appears as a promising tool to balance cell proliferation and differentiation in the intestine. A cell type in the colonic crypt where NLRP6 and ASC have been found to be especially high expressed are mature goblet cells in the apical mucosal region (Wlodarska et al., 2014). Wlodarska et *al.* demonstrated NLRP6 deficiency to result in defective autophagy and abrogation of mucus secretion in mice. Further, *Nlrp6* deficient, *Caspase-1/11* knockout and *ASC* lacking mice depicted increased susceptibility to colitis, linking the inflammasome signaling cascade to goblet cell function and colitis (Wlodarska et al., 2014). Nevertheless, corresponding data are controversially discussed, since Volk *et al.* recently published the Nlrp6 inflammasome not to be required for baseline mucus layer formation in mice (Volk et al., 2019). Opposing data are most likely explained by differences in housing conditions of mice, strengthening the role of microbiota-controlled experiments in this field. In the present work, differentiation of goblet cells was found to be abrogated in the presence of overexpression of inflammasome components in both butyrate and non-stimulated HT29-MTX cells. These results add a new aspect to the field, since mucus secretion but not goblet cell differentiation has been published to be influenced by the inflammasome (Wlodarska et al., 2014). Finally, goblet cell numbers were found to be severely reduced in inflamed tissue section of UC patients, compared to non-inflamed section of UC patients and non-IBD controls. Hereby, loss of goblet cells positively correlated with p32 cleavage and activation of caspase-1. Reduced OXPHOS and thereby goblet cell differentiation through loss of mitochondrial-localized p32 upon caspase-1 cleavage might be one explanatory mechanism. On the other hand, goblet cells have been previously reported to appear reduced and empty during chronic manifestation of inflammation, most likely due to prior hypersecretion of mucins (Johansson, 2014; Specian and Neutra, 1980). To what extend both of these factors contribute to goblet cell loss yet remains to be determined.

Contrasting colonic inflammation, where regeneration of the epithelium depends on cell proliferation rather than on differentiation, increased cellular proliferation rates are detrimental in the context of colorectal cancer (CRC). The author recently published a study delineating the importance of caspase-1 mediated p32 cleavage and the resulting shift towards aerobic glycolysis and hence cell proliferation

in CRC (Sünderhauf et al., 2020). This metabolic switch might be of general importance in the context of inflammation-driven tumorigenesis, by providing first evidence on the underlying mechanism of aerobic glycolysis. Of note, p32 mutations present a rather frequent event in breast and colorectal cancer tissue (Jiang et al., 2017) (Raschdorf et al., 2020) and IBD patients are at increased risk for the development of CRC (Axelrad et al., 2016). Therefore, increased risk of tumor development has to be taken carefully into account, when discussing p32 cleavage as a potential therapeutic target to boost cell proliferation during active disease in IBD.

5.4 Conclusion

The present work verified p32 to be indispensable for mitochondrial OXPHOS function. With this knowledge, a new molecular pathway was identified whereby p32 regulates intestinal goblet cell differentiation and hence mucus secretion by modulating mitochondrial OXPHOS metabolism. This mechanism was presented to be of special interest in the context of UC, since already under remission, p32 level in the upper part of the colonic crypt were strongly reduced compared to non-IBD controls. Impairment of p32 expression in UC was associated with mucosal energy deficiency and correlated with loss of differentiated goblet cells. Nutritional intervention in the form of a low glucose, high protein diet presented as a promising tool to induce mucosal expression of p32 and hence differentiation of goblet cells in mice. These results open new alleys in the preventive treatment and therapy of UC. Finally, the present thesis demonstrates a novel molecular mechanism relevant to active inflammation in UC. Upon induction of inflammasome subunit caspase-1, p32 was found to be cleaved at two distinct sides resulting in the loss of its mitochondrial leader and a metabolic shift from mitochondrial OXPHOS towards aerobic glycolysis. This mechanism was found to induce proliferation and to diminish goblet cell differentiation *in vitro*, potentially explaining goblet cell loss observed in active UC. Results obtained in this study where graphically summarized in figure 25.

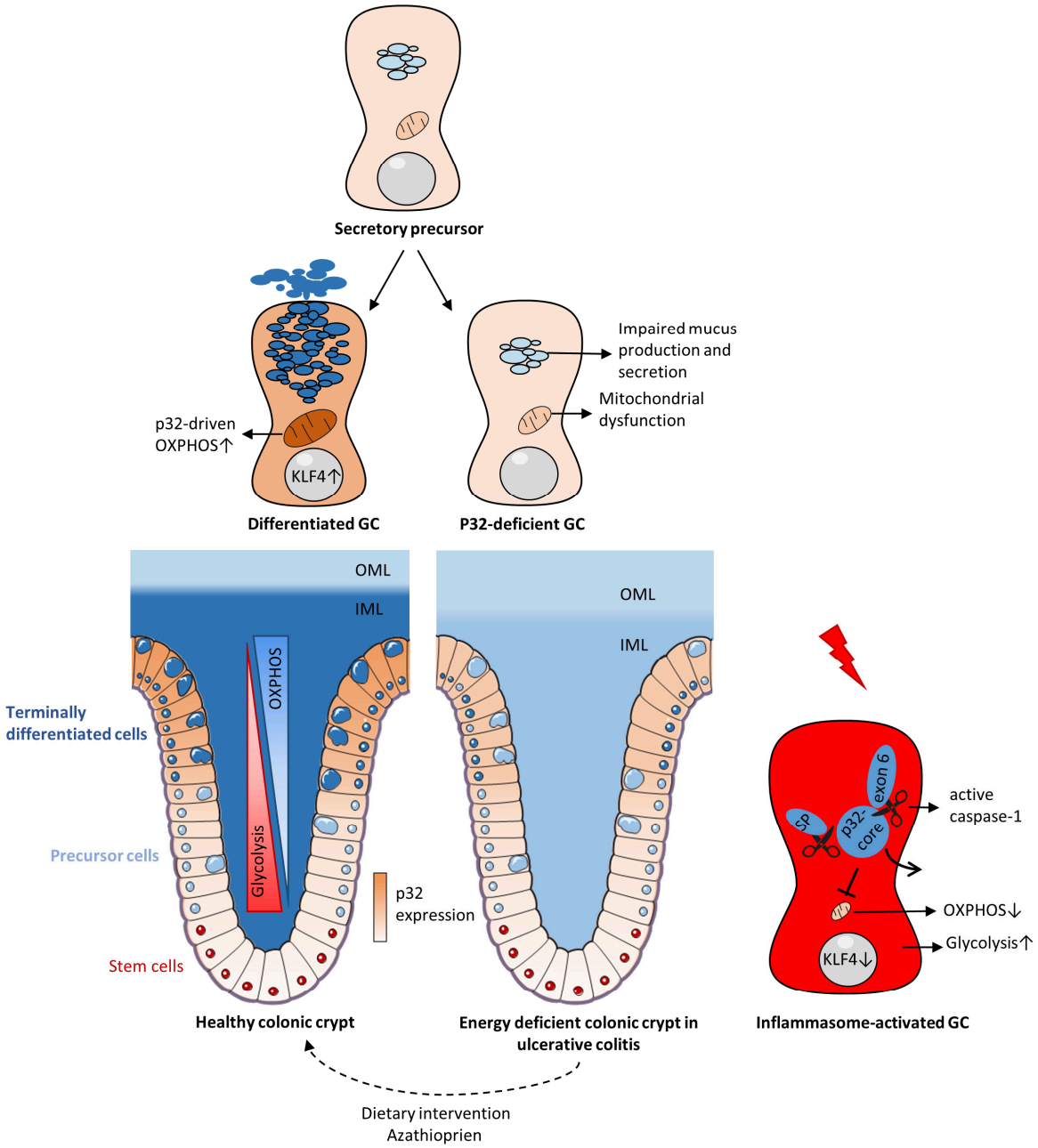

Figure 25: Graphical abstract of p32 mediated regulation of cell metabolism and differentiation in the colonic crypt. Mitochondrial OXPHOS metabolism and goblet cell (GC) differentiation is impaired in the colonic crypt of UC patients expressing low level of p32. Dietary intervention and treatment with azathioprine present two promising options to boost intestinal p32 expression, goblet cell differentiation and hence mucus secretion. During active UC, inflammasome activation leads to caspase-1 mediated cleavage of p32 resulting in a loss of mitochondrial localized p32, a metabolic shift towards aerobic glycolysis and hence abrogation of goblet cell differentiation.

5.5 Outlook

After having discussed the impact and context of data generated in this thesis, open questions remain presenting new perspectives for future research.

First of all, the presented data clearly display low expression level of p32 in the colonic crypt of UC patients and its consequences. Nevertheless, the origin of reduced p32 expression is still unsolved. Low p32 level were already observed in a state of quiescent disease and p32 has been previously proposed to be dysregulated before disease onset of UC but not CD (Torres, 2018), strengthening the notion that p32 is rather a causative factor in disease development than a result of active or chronic inflammation. Since mutations in the *p32* gene have not yet been described in the context of UC, it is unlikely that they are the underlying reason for reduced transcription or potentially increased degradation of *p32* mRNA. Detailed investigations of the promoter regions of the *p32* gene might be the most promising attempt to further delineate the origin of low p32 level in UC. Binding of the transcription factor SP1 to the SP1 binding site located upstream of the translation initiation codon are possibly involved in the transcription control of the human *p32* gene (Tye et al., 2001). Additionally, promoter hypermethylation as part of epigenetic regulation causes gene silencing (Alberts et al., 2015). Therefore, analysis of SP1 bound to the *p32* promoter region and determination of the promoter methylation status in UC patients *versus* non-IBD controls might unravel whether low p32 expression in UC is due to epigenetic events.

A second area of research which derives from data generated in this thesis is, how p32-driven mitochondrial respiration can be therapeutically induced. Nutritional intervention in the form of a diet low in glucose and potentially a medical regiment including azathioprine can be proposed to be supportive in increasing colonic p32 level. Nevertheless, further studies on the corresponding modes of action as well as additional data from animal experiments and finally human studies will be necessary to make reliable statements on therapeutic modulation of p32 expression. In the context of upcoming animal experiments, three aspects have to be taken strongly into consideration. Firstly, colonic mucus layer constitution has been previously shown to be strongly dependent on the composition of the intestinal microbiota (Johansson et al., 2015; Wlodarska et al., 2014). Potentially also goblet cell differentiation is regulated by certain microbial metabolites (Levy et al., 2015), resulting in a need for highly microbiota-controlled experiments in this field. Secondly, *p32*-knockout mice are embryonic lethal (Yagi et al., 2012) and even intestine-specific *p32*-deficient mice, if viable, will most likely present with to severe defects in crypt architecture to study mechanistic relationships. On the other hand, mice heterozygous for p32 have been recently reported by Liu *et al.* to be developmentally normal but to display a metabolic shift from mitochondrial OXPHOS towards glycolysis. Next to ATP8-mutant mice utilized in this thesis, $p32^{+/-}$ mice might be a promising tool to deepen the molecular

understanding and to study modulation of the p32 – goblet cell axis in the intestine. Thirdly, reviewer who assessed the two main publications derived from the data generated in this thesis (Sünderhauf et al., 2021; Sünderhauf et al., 2020) frequently asked for *in vivo* models to demonstrate impact of alterations in p32-driven metabolism and status of goblet cell differentiation on colitis as well as to verify caspase-1 mediated cleavage of p32. Even if the rat and mouse p32 cDNA present with 89.9% sequence identity compared to the human cDNA (Lynch et al., 1997), the *N*-terminal caspase-1 cleavage side is missing in rodents (*https://web.expasy.org/peptide_cutter/*). Therefore, caspase-1 mediated cleavage of p32 upon inflammasome activation during colitis or tumor induction in mice would only partially mimic the human situation. Inducing colitis in mice with a high degree of colonic goblet cell differentiation and a thick mucus layer might therefore answer if these factors protect from colitis. Nevertheless, the exact impact of p32 cleavage on cell metabolism and proliferation *versus* differentiation state will remain somewhat elusive. To overcome the described problem in the context of inflammation-driven tumor development, human tumor xenograft models might be the experiments of choice. Subcutaneous injection of human tumor cell lines, like *e.g.* HAP1-*p32*-wt and HAP1-*p32* cells with mutated caspase-1 cleavage sides, in genetically susceptible mice should result in solid tumor formation. Analyzing tumor development on macroscopic, microscopic and molecular level should provide rather detailed information on effects of p32-cleavage on tumor progression and metabolism *in vivo.*

Finally, future research in this field should carefully take mucus quality next to mucus quantity into account. The degree of impermeability of the inner mucus layer, rather than its thickness is the most important factor in shielding the colonic epithelium from the luminal microbiota (Bergstrom et al., 2017; Johansson et al., 2014; Johansson et al., 2008). *O*-linked glycosylation, characterized by covalent addition of glycans to the hydroxyl group of serine and threonine residues, account for up to 80% of the total molecular mass of Muc2 (Bergstrom and Xia, 2013; Johansson et al., 2011; Thomsson et al., 2012). Glycosylation patterns of mucins produced and secreted by goblet cells of differing differentiation state have not been investigated in this work. Additionally, dependency of intestinal mucin glycosylation on the metabolic status of goblet cells as well possible modulation by nutritional supplementation will be of special interest in the context of intestinal homeostasis and the field of nutritional medicine.

6 References

1 Abegunde, A.T., Muhammad, B.H., Bhatti, O., and Ali, T. (2016). Environmental risk factors for inflammatory bowel diseases: Evidence based literature review. World J Gastroenterol *22*, 6296-6317.

2 Ahechu, P., Zozaya, G., Marti, P., Hernandez-Lizoain, J.L., Baixauli, J., Unamuno, X., Fruhbeck, G., and Catalan, V. (2018). NLRP3 Inflammasome: A Possible Link Between Obesity-Associated Low-Grade Chronic Inflammation and Colorectal Cancer Development. Front Immunol *9*, 2918.

3 Alberts, B., Johnson, A., Lewis, J., Raff, M., Roberts, K., and Walter, P. (2015). Molecular biology of the cell (6th edition). New York: Garland Science.

4 Alfarouk, K.O., Ahmed, S.B.M., Elliott, R.L., Benoit, A., Alqahtani, S.S., Ibrahim, M.E., Bashir, A.H.H., Alhoufie, S.T.S., Elhassan, G.O., Wales, C.C., Schwartz, L.H., Ali, H.S., Ahmed, A., Forde, P.F., Devesa, J., Cardone, R.A., Fais, S., Harguindey, S., and Reshkin, S.J. (2020). The Pentose Phosphate Pathway Dynamics in Cancer and Its Dependency on Intracellular pH. Metabolites *10*.

5 Allen, I.C., Wilson, J.E., Schneider, M., Lich, J.D., Roberts, R.A., Arthur, J.C., Woodford, R.M., Davis, B.K., Uronis, J.M., Herfarth, H.H., Jobin, C., Rogers, A.B., and Ting, J.P. (2012). NLRP12 suppresses colon inflammation and tumorigenesis through the negative regulation of noncanonical NF-kappaB signaling. Immunity *36*, 742-754.

6 Ananthakrishnan, A.N., Khalili, H., Konijeti, G.G., Higuchi, L.M., de Silva, P., Fuchs, C.S., Willett, W.C., Richter, J.M., and Chan, A.T. (2014). Long-term intake of dietary fat and risk of ulcerative colitis and Crohn's disease. Gut *63*, 776-784.

7 Anderson, C.A., Boucher, G., Lees, C.W., Franke, A., D'Amato, M., Taylor, K.D., Lee, J.C., Goyette, P., Imielinski, M., Latiano, A., Lagace, C., Scott, R., Amininejad, L., Bumpstead, S., Baidoo, L., Baldassano, R.N., Barclay, M., Bayless, T.M., Brand, S., Buning, C., Colombel, J.F., Denson, L.A., De Vos, M., Dubinsky, M., Edwards, C., Ellinghaus, D., Fehrmann, R.S., Floyd, J.A., Florin, T., Franchimont, D., Franke, L., Georges, M., Glas, J., Glazer, N.L., Guthery, S.L., Haritunians, T., Hayward, N.K., Hugot, J.P., Jobin, G., Laukens, D., Lawrance, I., Lemann, M., Levine, A., Libioulle, C., Louis, E., McGovern, D.P., Milla, M., Montgomery, G.W., Morley, K.I., Mowat, C., Ng, A., Newman, W., Ophoff, R.A., Papi, L., Palmieri, O., Peyrin-Biroulet, L., Panes, J., Phillips, A., Prescott, N.J., Proctor, D.D., Roberts, R., Russell, R., Rutgeerts, P., Sanderson, J., Sans, M., Schumm, P., Seibold, F., Sharma, Y., Simms, L.A., Seielstad, M., Steinhart, A.H., Targan, S.R., van den Berg, L.H., Vatn, M., Verspaget, H., Walters, T., Wijmenga, C., Wilson, D.C., Westra, H.J., Xavier, R.J., Zhao, Z.Z., Ponsioen, C.Y., Andersen, V., Torkvist, L., Gazouli, M., Anagnou, N.P., Karlsen, T.H., Kupcinskas, L., Sventoraityte, J., Mansfield, J.C., Kugathasan, S., Silverberg, M.S., Halfvarson, J., Rotter, J.I., Mathew, C.G., Griffiths, A.M., Gearry, R., Ahmad, T., Brant, S.R., Chamaillard, M., Satsangi, J., Cho, J.H., Schreiber, S., Daly, M.J., Barrett, J.C., Parkes, M., Annese, V., Hakonarson, H., Radford-Smith, G., Duerr, R.H., Vermeire, S., Weersma, R.K., and Rioux, J.D. (2011). Meta-analysis identifies 29 additional ulcerative colitis risk loci, increasing the number of confirmed associations to 47. Nat Genet *43*, 246-252.

8 Andreux, P.A., Houtkooper, R.H., and Auwerx, J. (2013). Pharmacological approaches to restore mitochondrial function. Nat Rev Drug Discov *12*, 465-483.

9 Asquith, M., and Powrie, F. (2010). An innately dangerous balancing act: intestinal homeostasis, inflammation, and colitis-associated cancer. J Exp Med *207*, 1573-1577.

10 Atuma, C., Strugala, V., Allen, A., and Holm, L. (2001). The adherent gastrointestinal mucus gel layer: thickness and physical state in vivo. Am J Physiol Gastrointest Liver Physiol *280*, G922-929.

11 Axelrad, J.E., Lichtiger, S., and Yajnik, V. (2016). Inflammatory bowel disease and cancer: The role of inflammation, immunosuppression, and cancer treatment. World journal of gastroenterology *22*, 4794-4801.

12 Bansil, R., and Turner, B.S. (2018). The biology of mucus: Composition, synthesis and organization. Adv Drug Deliv Rev *124*, 3-15.

13 Bar, F., Bochmann, W., Widok, A., von Medem, K., Pagel, R., Hirose, M., Yu, X., Kalies, K., Konig, P., Bohm, R., Herdegen, T., Reinicke, A.T., Buning, J., Lehnert, H., Fellermann, K., Ibrahim, S., and Sina, C. (2013). Mitochondrial gene polymorphisms that protect mice from colitis. Gastroenterology *145*, 1055-1063 e1053.

14 Barker, N. (2014). Adult intestinal stem cells: critical drivers of epithelial homeostasis and regeneration. Nat Rev Mol Cell Biol *15*, 19-33.

15 Bauer, C., Duewell, P., Mayer, C., Lehr, H.A., Fitzgerald, K.A., Dauer, M., Tschopp, J., Endres, S., Latz, E., and Schnurr, M. (2010). Colitis induced in mice with dextran sulfate sodium (DSS) is mediated by the NLRP3 inflammasome. Gut *59*, 1192-1199.

16 Bergstrom, K., Fu, J., Johansson, M.E., Liu, X., Gao, N., Wu, Q., Song, J., McDaniel, J.M., McGee, S., Chen, W., Braun, J., Hansson, G.C., and Xia, L. (2017). Core 1- and 3-derived O-glycans collectively maintain the colonic mucus barrier and protect against spontaneous colitis in mice. Mucosal Immunol *10*, 91-103.

17 Bergstrom, K.S., and Xia, L. (2013). Mucin-type O-glycans and their roles in intestinal homeostasis. Glycobiology *23*, 1026-1037.

18 Biancone, L., Tosti, C., Fina, D., Fantini, M., De Nigris, F., Geremia, A., and Pallone, F. (2003). Review article: maintenance treatment of Crohn's disease. Aliment Pharmacol Ther *17 Suppl 2*, 31-37.

19 Birchenough, G.M., Nystrom, E.E., Johansson, M.E., and Hansson, G.C. (2016). A sentinel goblet cell guards the colonic crypt by triggering Nlrp6-dependent Muc2 secretion. Science *352*, 1535-1542.

20 Braun, L., Ghebrehiwet, B., and Cossart, P. (2000). gC1q-R/p32, a C1q-binding protein, is a receptor for the InlB invasion protein of Listeria monocytogenes. EMBO J *19*, 1458-1466.

21 Carvalho, F.A., Nalbantoglu, I., Aitken, J.D., Uchiyama, R., Su, Y., Doho, G.H., Vijay-Kumar, M., and Gewirtz, A.T. (2012). Cytosolic flagellin receptor NLRC4 protects mice against mucosal and systemic challenges. Mucosal Immunol *5*, 288-298.

22 Chen, Y.B., Jiang, C.T., Zhang, G.Q., Wang, J.S., and Pang, D. (2009). Increased expression of hyaluronic acid binding protein 1 is correlated with poor prognosis in patients with breast cancer. J Surg Oncol *100*, 382-386.

23 Cheng, H. (1974). Origin, differentiation and renewal of the four main epithelial cell types in the mouse small intestine. II. Mucous cells. Am J Anat *141*, 481-501.

24 Cheng, H., and Leblond, C.P. (1974). Origin, differentiation and renewal of the four main epithelial cell types in the mouse small intestine. V. Unitarian Theory of the origin of the four epithelial cell types. Am J Anat *141*, 537-561.

25 Chowdhury, A.R., Ghosh, I., and Datta, K. (2008). Excessive reactive oxygen species induces apoptosis in fibroblasts: role of mitochondrially accumulated hyaluronic acid binding protein 1 (HABP1/p32/gC1qR). Exp Cell Res *314*, 651-667.

26 Christ, A., Gunther, P., Lauterbach, M.A.R., Duewell, P., Biswas, D., Pelka, K., Scholz, C.J., Oosting, M., Haendler, K., Bassler, K., Klee, K., Schulte-Schrepping, J., Ulas, T., Moorlag, S., Kumar, V., Park, M.H., Joosten, L.A.B., Groh, L.A., Riksen, N.P., Espevik, T., Schlitzer, A., Li, Y., Fitzgerald, M.L., Netea, M.G., Schultze, J.L., and Latz, E. (2018). Western Diet Triggers NLRP3-Dependent Innate Immune Reprogramming. Cell *172*, 162-175 e114.

27 Clevers, H. (2013). The intestinal crypt, a prototype stem cell compartment. Cell *154*, 274-284.

28 Collaborators, G.B.D.I.B.D. (2020). The global, regional, and national burden of inflammatory bowel disease in 195 countries and territories, 1990-2017: a systematic analysis for the Global Burden of Disease Study 2017. Lancet Gastroenterol Hepatol *5*, 17-30.

29 Cone, R.A. (2009). Barrier properties of mucus. Adv Drug Deliv Rev *61*, 75-85.

30 Cong, L., Ran, F.A., Cox, D., Lin, S., Barretto, R., Habib, N., Hsu, P.D., Wu, X., Jiang, W., Marraffini, L.A., and Zhang, F. (2013). Multiplex genome engineering using CRISPR/Cas systems. Science *339*, 819-823.

31 Conrad, K., and Stöcker, W. (2014). Autoantibodies - Chapter 50 - Anti-intestinal Goblet Cell Antibodies. Elsevier *third edition*, 425-431.

32 Cooper, G.M. (2000). The cell: A Molecular Approach (The Mechanism of Oxidative Phosphorylation). Sinauer Associates *2nd Edition*.

33 Couturier-Maillard, A., Secher, T., Rehman, A., Normand, S., De Arcangelis, A., Haesler, R., Huot, L., Grandjean, T., Bressenot, A., Delanoye-Crespin, A., Gaillot, O., Schreiber, S., Lemoine, Y., Ryffel, B., Hot, D., Nunez, G., Chen, G., Rosenstiel, P., and Chamaillard, M. (2013). NOD2-mediated dysbiosis predisposes mice to transmissible colitis and colorectal cancer. J Clin Invest *123*, 700-711.

34 Cui, X., Jin, Y., Hofseth, A.B., Pena, E., Habiger, J., Chumanevich, A., Poudyal, D., Nagarkatti, M., Nagarkatti, P.S., Singh, U.P., and Hofseth, L.J. (2010). Resveratrol suppresses colitis and colon cancer associated with colitis. Cancer Prev Res (Phila) *3*, 549-559.

35 D'Souza, M., and Datta, K. (1985). Evidence for naturally occurring hyaluronic acid binding protein in rat liver. Biochem Int *10*, 43-51.

36 Dahiya, R., Lesuffleur, T., Kwak, K.S., Byrd, J.C., Barbat, A., Zweibaum, A., and Kim, Y.S. (1992). Expression and characterization of mucins associated with the resistance to methotrexate of human colonic adenocarcinoma cell line HT29. Cancer Res *52*, 4655-4662.

37 Darwich, A.S., Aslam, U., Ashcroft, D.M., and Rostami-Hodjegan, A. (2014). Meta-analysis of the turnover of intestinal epithelia in preclinical animal species and humans. Drug Metab Dispos *42*, 2016-2022.

38 David, L.A., Maurice, C.F., Carmody, R.N., Gootenberg, D.B., Button, J.E., Wolfe, B.E., Ling, A.V., Devlin, A.S., Varma, Y., Fischbach, M.A., Biddinger, S.B., Dutton, R.J., and Turnbaugh, P.J. (2014). Diet rapidly and reproducibly alters the human gut microbiome. Nature *505*, 559-563.

39 Davis, B.K., Wen, H., and Ting, J.P. (2011). The inflammasome NLRs in immunity, inflammation, and associated diseases. Annu Rev Immunol *29*, 707-735.

40 Dawiskiba, T., Deja, S., Mulak, A., Zabek, A., Jawien, E., Pawelka, D., Banasik, M., Mastalerz-Migas, A., Balcerzak, W., Kaliszewski, K., Skora, J., Barc, P., Korta, K., Pormanczuk, K., Szyber, P., Litarski, A., and Mlynarz, P. (2014). Serum and urine metabolomic fingerprinting in diagnostics of inflammatory bowel diseases. World J Gastroenterol *20*, 163-174.

41 de Lau, W., Kujala, P., Schneeberger, K., Middendorp, S., Li, V.S., Barker, N., Martens, A., Hofhuis, F., DeKoter, R.P., Peters, P.J., Nieuwenhuis, E., and Clevers, H. (2012). Peyer's patch M cells derived from Lgr5(+) stem cells require SpiB and are induced by RankL in cultured "miniguts". Mol Cell Biol *32*, 3639-3647.

42 Dedio, J., Jahnen-Dechent, W., Bachmann, M., and Muller-Esterl, W. (1998). The multiligand-binding protein gC1qR, putative C1q receptor, is a mitochondrial protein. J Immunol *160*, 3534-3542.

43 Derer, S., Brethack, A.K., Pietsch, C., Jendrek, S.T., Nitzsche, T., Bokemeyer, A., Hov, J.R., Schaffler, H., Bettenworth, D., Grassl, G.A., and Sina, C. (2020). Inflammatory Bowel Disease-associated GP2 Autoantibodies Inhibit Mucosal Immune Response to Adherent-invasive Bacteria. Inflamm Bowel Dis *26*, 1856-1868.

44 Desai, M.S., Seekatz, A.M., Koropatkin, N.M., Kamada, N., Hickey, C.A., Wolter, M., Pudlo, N.A., Kitamoto, S., Terrapon, N., Muller, A., Young, V.B., Henrissat, B., Wilmes, P., Stappenbeck, T.S., Nunez, G., and Martens, E.C. (2016). A Dietary Fiber-Deprived Gut Microbiota Degrades the Colonic Mucus Barrier and Enhances Pathogen Susceptibility. Cell *167*, 1339-1353 e1321.

45 Detmer, S.A., and Chan, D.C. (2007). Functions and dysfunctions of mitochondrial dynamics. Nat Rev Mol Cell Biol *8*, 870-879.

46 Dignass, A., and Esters, P. Colitis ulcerosa. Thieme.

47 Dotan, I. (2007). Serologic markers in inflammatory bowel disease: tools for better diagnosis and disease stratification. Expert Rev Gastroenterol Hepatol *1*, 265-274.

48 Duerr, R.H. (2007). Genome-wide association studies herald a new era of rapid discoveries in inflammatory bowel disease research. Gastroenterology *132*, 2045-2049.

49 Dupaul-Chicoine, J., Yeretssian, G., Doiron, K., Bergstrom, K.S., McIntire, C.R., LeBlanc, P.M., Meunier, C., Turbide, C., Gros, P., Beauchemin, N., Vallance, B.A., and Saleh, M. (2010). Control of intestinal homeostasis, colitis, and colitis-associated colorectal cancer by the inflammatory caspases. Immunity *32*, 367-378.

50 Duvallet, C., Gibbons, S.M., Gurry, T., Irizarry, R.A., and Alm, E.J. (2017). Meta-analysis of gut microbiome studies identifies disease-specific and shared responses. Nat Commun *8*, 1784.

51 Earley, H., Lennon, G., Balfe, A., Coffey, J.C., Winter, D.C., and O'Connell, P.R. (2019). The abundance of Akkermansia muciniphila and its relationship with sulphated colonic mucins in health and ulcerative colitis. Sci Rep *9*, 15683.

52 Elinav, E., Strowig, T., Kau, A.L., Henao-Mejia, J., Thaiss, C.A., Booth, C.J., Peaper, D.R., Bertin, J., Eisenbarth, S.C., Gordon, J.I., and Flavell, R.A. (2011). NLRP6 inflammasome regulates colonic microbial ecology and risk for colitis. Cell *145*, 745-757.

53 Erlich, T.H., Yagil, Z., Kay, G., Peretz, A., Migalovich-Sheikhet, H., Tshori, S., Nechushtan, H., Levi-Schaffer, F., Saada, A., and Razin, E. (2014). Mitochondrial STAT3 plays a major role in IgE-antigen-mediated mast cell exocytosis. J Allergy Clin Immunol *134*, 460-469.

54 Finucane, H.K., Reshef, Y.A., Anttila, V., Slowikowski, K., Gusev, A., Byrnes, A., Gazal, S., Loh, P.R., Lareau, C., Shoresh, N., Genovese, G., Saunders, A., Macosko, E., Pollack, S., Brainstorm, C., Perry, J.R.B., Buenrostro, J.D., Bernstein, B.E., Raychaudhuri, S., McCarroll, S., Neale, B.M., and Price, A.L. (2018). Heritability enrichment of specifically expressed genes identifies disease-relevant tissues and cell types. Nat Genet *50*, 621-629.

55 Fogal, V., Richardson, A.D., Karmali, P.P., Scheffler, I.E., Smith, J.W., and Ruoslahti, E. (2010). Mitochondrial p32 protein is a critical regulator of tumor metabolism via maintenance of oxidative phosphorylation. Mol Cell Biol *30*, 1303-1318.

56 Forbes, A., Escher, J., Hebuterne, X., Klek, S., Krznaric, Z., Schneider, S., Shamir, R., Stardelova, K., Wierdsma, N., Wiskin, A.E., and Bischoff, S.C. (2017). ESPEN guideline: Clinical nutrition in inflammatory bowel disease. Clin Nutr *36*, 321-347.

57 Fouque, D., and Aparicio, M. (2007). Eleven reasons to control the protein intake of patients with chronic kidney disease. Nat Clin Pract Nephrol *3*, 383-392.

58 Franzmann, E.J., Schroeder, G.L., Goodwin, W.J., Weed, D.T., Fisher, P., and Lokeshwar, V.B. (2003). Expression of tumor markers hyaluronic acid and hyaluronidase (HYAL1) in head and neck tumors. Int J Cancer *106*, 438-445.

59 Furusawa, Y., Obata, Y., Fukuda, S., Endo, T.A., Nakato, G., Takahashi, D., Nakanishi, Y., Uetake, C., Kato, K., Kato, T., Takahashi, M., Fukuda, N.N., Murakami, S., Miyauchi, E., Hino, S., Atarashi, K., Onawa, S., Fujimura, Y., Lockett, T., Clarke, J.M., Topping, D.L., Tomita, M., Hori, S., Ohara, O., Morita, T., Koseki, H., Kikuchi, J., Honda, K., Hase, K., and Ohno, H. (2013). Commensal microbe-derived butyrate induces the differentiation of colonic regulatory T cells. Nature *504*, 446-450.

60 Gao, H., Yao, Q., Lan, X., Li, S., Wu, J., Zeng, G., and Xue, Y. (2016). Elevated HABP1 protein expression correlates with progression and poor survival in patients with gastric cancer. Onco Targets Ther *9*, 6711-6718.

61 Geboes, K. (2008). What histologic features best differentiate Crohn's disease from ulcerative colitis? Inflamm Bowel Dis *14 Suppl 2*, S168-169.

62 Gersemann, M., Becker, S., Kubler, I., Koslowski, M., Wang, G., Herrlinger, K.R., Griger, J., Fritz, P., Fellermann, K., Schwab, M., Wehkamp, J., and Stange, E.F. (2009). Differences in goblet cell differentiation between Crohn's disease and ulcerative colitis. Differentiation *77*, 84-94.

63 Ghaleb, A.M., Laroui, H., Merlin, D., and Yang, V.W. (2014). Genetic deletion of Klf4 in the mouse intestinal epithelium ameliorates dextran sodium sulfate-induced colitis by modulating the NF-kappaB pathway inflammatory response. Inflamm Bowel Dis *20*, 811-820.

64 Ghayur, T., Banerjee, S., Hugunin, M., Butler, D., Herzog, L., Carter, A., Quintal, L., Sekut, L., Talanian, R., Paskind, M., Wong, W., Kamen, R., Tracey, D., and Allen, H. (1997). Caspase-1 processes IFN-gamma-inducing factor and regulates LPS-induced IFN-gamma production. Nature *386*, 619-623.

65 Ghebrehiwet, B., Lim, B.L., Peerschke, E.I., Willis, A.C., and Reid, K.B. (1994). Isolation, cDNA cloning, and overexpression of a 33-kD cell surface glycoprotein that binds to the globular "heads" of C1q. J Exp Med *179*, 1809-1821.

66 Gkouskou, K.K., Deligianni, C., Tsatsanis, C., and Eliopoulos, A.G. (2014). The gut microbiota in mouse models of inflammatory bowel disease. Front Cell Infect Microbiol *4*, 28.

67 Gotoh, K., Morisaki, T., Setoyama, D., Sasaki, K., Yagi, M., Igami, K., Mizuguchi, S., Uchiumi, T., Fukui, Y., and Kang, D. (2018). Mitochondrial p32/C1qbp Is a Critical Regulator of Dendritic Cell Metabolism and Maturation. Cell Rep *25*, 1800-1815 e1804.

68 Graham, D.B., and Xavier, R.J. (2020). Pathway paradigms revealed from the genetics of inflammatory bowel disease. Nature *578*, 527-539.

69 Greenfield, S.M., Punchard, N.A., Teare, J.P., and Thompson, R.P. (1993). Review article: the mode of action of the aminosalicylates in inflammatory bowel disease. Aliment Pharmacol Ther *7*, 369-383.

70 Gribble, F.M., and Reimann, F. (2019). Function and mechanisms of enteroendocrine cells and gut hormones in metabolism. Nat Rev Endocrinol *15*, 226-237.

71 Guo, H., Gibson, S.A., and Ting, J.P.Y. (2020). Gut microbiota, NLR proteins, and intestinal homeostasis. J Exp Med *217*.

72 Guo, N., Weremowicz, S., Lynch, N., Lim, B.L., Schwaeble, W., Peerschke, E.I., Morton, C.C., Reid, K.B., Ghebrehiwet, B., and Sastry, K.N. (1997). Assignment of C1QBP encoding the C1q globular domain binding protein (gC1q-R) to human chromosome 17 band p13.3 by in situ hybridization. Cytogenet Cell Genet *77*, 283-284.

73 Halme, L., Paavola-Sakki, P., Turunen, U., Lappalainen, M., Farkkila, M., and Kontula, K. (2006). Family and twin studies in inflammatory bowel disease. World J Gastroenterol *12*, 3668-3672.

74 Harusato, A., Abo, H., Ngo, V.L., Yi, S.W., Mitsutake, K., Osuka, S., Kohlmeier, J.E., Li, J.D., Gewirtz, A.T., Nusrat, A., and Denning, T.L. (2017). IL-36gamma signaling controls the induced regulatory T cell-Th9 cell balance via NFkappaB activation and STAT transcription factors. Mucosal Immunol *10*, 1455-1467.

75 Heller, F., Florian, P., Bojarski, C., Richter, J., Christ, M., Hillenbrand, B., Mankertz, J., Gitter, A.H., Burgel, N., Fromm, M., Zeitz, M., Fuss, I., Strober, W., and Schulzke, J.D. (2005). Interleukin-13 is the key effector Th2 cytokine in ulcerative colitis that affects epithelial tight junctions, apoptosis, and cell restitution. Gastroenterology *129*, 550-564.

76 Hillman, G.A., and Henry, M.F. (2019). The yeast protein Mam33 functions in the assembly of the mitochondrial ribosome. J Biol Chem *294*, 9813-9829.

77 Hirose, M., Kunstner, A., Schilf, P., Sunderhauf, A., Rupp, J., Johren, O., Schwaninger, M., Sina, C., Baines, J.F., and Ibrahim, S.M. (2017). Mitochondrial gene polymorphism is associated with gut microbial communities in mice. Sci Rep *7*, 15293.

78 Hirota, S.A., Ng, J., Lueng, A., Khajah, M., Parhar, K., Li, Y., Lam, V., Potentier, M.S., Ng, K., Bawa, M., McCafferty, D.M., Rioux, K.P., Ghosh, S., Xavier, R.J., Colgan, S.P., Tschopp, J., Muruve, D., MacDonald, J.A., and Beck, P.L. (2011). NLRP3 inflammasome plays a key role in the regulation of intestinal homeostasis. Inflamm Bowel Dis *17*, 1359-1372.

79 Hoffmann, J., Kroesen, A., and Klump, B. (2009). Chronisch entzündliche Darmerkrankungen - Handbuch für Klinik und Praxis. Thieme *2*.

80 Holmen Larsson, J.M., Thomsson, K.A., Rodriguez-Pineiro, A.M., Karlsson, H., and Hansson, G.C. (2013). Studies of mucus in mouse stomach, small intestine, and colon. III.

Gastrointestinal Muc5ac and Muc2 mucin O-glycan patterns reveal a regiospecific distribution. Am J Physiol Gastrointest Liver Physiol *305*, G357-363.

81 Honore, B., Madsen, P., Rasmussen, H.H., Vandekerckhove, J., Celis, J.E., and Leffers, H. (1993). Cloning and expression of a cDNA covering the complete coding region of the P32 subunit of human pre-mRNA splicing factor SF2. Gene *134*, 283-287.

82 Houten, S.M., and Wanders, R.J. (2010). A general introduction to the biochemistry of mitochondrial fatty acid beta-oxidation. J Inherit Metab Dis *33*, 469-477.

83 Howitt, M.R., Lavoie, S., Michaud, M., Blum, A.M., Tran, S.V., Weinstock, J.V., Gallini, C.A., Redding, K., Margolskee, R.F., Osborne, L.C., Artis, D., and Garrett, W.S. (2016). Tuft cells, taste-chemosensory cells, orchestrate parasite type 2 immunity in the gut. Science *351*, 1329-1333.

84 Howitz, K.T., Bitterman, K.J., Cohen, H.Y., Lamming, D.W., Lavu, S., Wood, J.G., Zipkin, R.E., Chung, P., Kisielewski, A., Zhang, L.L., Scherer, B., and Sinclair, D.A. (2003). Small molecule activators of sirtuins extend Saccharomyces cerevisiae lifespan. Nature *425*, 191-196.

85 Hu, M., Crawford, S.A., Henstridge, D.C., Ng, I.H., Boey, E.J., Xu, Y., Febbraio, M.A., Jans, D.A., and Bogoyevitch, M.A. (2013). p32 protein levels are integral to mitochondrial and endoplasmic reticulum morphology, cell metabolism and survival. Biochem J *453*, 381-391.

86 Hufford, M.M., and Kaplan, M.H. (2014). A gut reaction to IL-9. Nat Immunol *15*, 599-600.

87 Imai, S., Armstrong, C.M., Kaeberlein, M., and Guarente, L. (2000). Transcriptional silencing and longevity protein Sir2 is an NAD-dependent histone deacetylase. Nature *403*, 795-800.

88 Itahana, K., and Zhang, Y. (2008). Mitochondrial p32 is a critical mediator of ARF-induced apoptosis. Cancer Cell *13*, 542-553.

89 Ito, K., and Suda, T. (2014). Metabolic requirements for the maintenance of self-renewing stem cells. Nat Rev Mol Cell Biol *15*, 243-256.

90 James, S.L., Christophersen, C.T., Bird, A.R., Conlon, M.A., Rosella, O., Gibson, P.R., and Muir, J.G. (2015). Abnormal fibre usage in UC in remission. Gut *64*, 562-570.

91 Jantchou, P., Morois, S., Clavel-Chapelon, F., Boutron-Ruault, M.C., and Carbonnel, F. (2010). Animal protein intake and risk of inflammatory bowel disease: The E3N prospective study. Am J Gastroenterol *105*, 2195-2201.

92 Jiang, J., Zhang, Y., Krainer, A.R., and Xu, R.M. (1999). Crystal structure of human p32, a doughnut-shaped acidic mitochondrial matrix protein. Proc Natl Acad Sci U S A *96*, 3572-3577.

93 Jiang, Y., Wu, H., Liu, J., Chen, Y., Xie, J., Zhao, Y., and Pang, D. (2017). Increased breast cancer risk with HABP1/p32/gC1qR genetic polymorphism rs2285747 and its upregulation in northern Chinese women. Oncotarget *8*, 13932-13941.

94 Johansson, M.E. (2014). Mucus layers in inflammatory bowel disease. Inflamm Bowel Dis *20*, 2124-2131.

95 Johansson, M.E., Ambort, D., Pelaseyed, T., Schutte, A., Gustafsson, J.K., Ermund, A., Subramani, D.B., Holmen-Larsson, J.M., Thomsson, K.A., Bergstrom, J.H., van der Post, S., Rodriguez-Pineiro, A.M., Sjovall, H., Backstrom, M., and Hansson, G.C. (2011). Composition and functional role of the mucus layers in the intestine. Cell Mol Life Sci *68*, 3635-3641.

96 Johansson, M.E., Gustafsson, J.K., Holmen-Larsson, J., Jabbar, K.S., Xia, L., Xu, H., Ghishan, F.K., Carvalho, F.A., Gewirtz, A.T., Sjovall, H., and Hansson, G.C. (2014). Bacteria penetrate the normally impenetrable inner colon mucus layer in both murine colitis models and patients with ulcerative colitis. Gut *63*, 281-291.

97 Johansson, M.E., Jakobsson, H.E., Holmen-Larsson, J., Schutte, A., Ermund, A., Rodriguez-Pineiro, A.M., Arike, L., Wising, C., Svensson, F., Backhed, F., and Hansson, G.C. (2015). Normalization of Host Intestinal Mucus Layers Requires Long-Term Microbial Colonization. Cell Host Microbe *18*, 582-592.

98 Johansson, M.E., Phillipson, M., Petersson, J., Velcich, A., Holm, L., and Hansson, G.C. (2008). The inner of the two Muc2 mucin-dependent mucus layers in colon is devoid of bacteria. Proc Natl Acad Sci U S A *105*, 15064-15069.

99 Jostins, L., Ripke, S., Weersma, R.K., Duerr, R.H., McGovern, D.P., Hui, K.Y., Lee, J.C., Schumm, L.P., Sharma, Y., Anderson, C.A., Essers, J., Mitrovic, M., Ning, K., Cleynen, I., Theatre, E., Spain, S.L., Raychaudhuri, S., Goyette, P., Wei, Z., Abraham, C., Achkar, J.P., Ahmad, T., Amininejad, L., Ananthakrishnan, A.N., Andersen, V., Andrews, J.M., Baidoo, L., Balschun, T., Bampton, P.A., Bitton, A., Boucher, G., Brand, S., Buning, C., Cohain, A., Cichon, S., D'Amato, M., De Jong, D., Devaney, K.L., Dubinsky, M., Edwards, C., Ellinghaus, D., Ferguson, L.R., Franchimont, D., Fransen, K., Gearry, R., Georges, M., Gieger, C., Glas, J., Haritunians, T., Hart, A., Hawkey, C., Hedl, M., Hu, X., Karlsen, T.H., Kupcinskas, L., Kugathasan, S., Latiano, A., Laukens, D., Lawrance, I.C., Lees, C.W., Louis, E., Mahy, G., Mansfield, J., Morgan, A.R., Mowat, C., Newman, W., Palmieri, O., Ponsioen, C.Y., Potocnik, U., Prescott, N.J., Regueiro, M., Rotter, J.I., Russell, R.K., Sanderson, J.D., Sans, M., Satsangi, J., Schreiber, S., Simms, L.A., Sventoraityte, J., Targan, S.R., Taylor, K.D., Tremelling, M., Verspaget, H.W., De Vos, M., Wijmenga, C., Wilson, D.C., Winkelmann, J., Xavier, R.J., Zeissig, S., Zhang, B., Zhang, C.K., Zhao, H., International, I.B.D.G.C., Silverberg, M.S., Annese, V., Hakonarson, H., Brant, S.R., Radford-Smith, G., Mathew, C.G., Rioux, J.D., Schadt, E.E., Daly, M.J., Franke, A., Parkes, M., Vermeire, S., Barrett, J.C., and Cho, J.H. (2012). Host-microbe interactions have shaped the genetic architecture of inflammatory bowel disease. Nature *491*, 119-124.

100 Jowett, S.L., Seal, C.J., Pearce, M.S., Phillips, E., Gregory, W., Barton, J.R., and Welfare, M.R. (2004). Influence of dietary factors on the clinical course of ulcerative colitis: a prospective cohort study. Gut *53*, 1479-1484.

101 Kaiko, G.E., Ryu, S.H., Koues, O.I., Collins, P.L., Solnica-Krezel, L., Pearce, E.J., Pearce, E.L., Oltz, E.M., and Stappenbeck, T.S. (2016). The Colonic Crypt Protects Stem Cells from Microbiota-Derived Metabolites. Cell *167*, 1137.

102 Kalantar-Zadeh, K., Moore, L.W., Tortorici, A.R., Chou, J.A., St-Jules, D.E., Aoun, A., Rojas-Bautista, V., Tschida, A.K., Rhee, C.M., Shah, A.A., Crowley, S., Vassalotti, J.A., and Kovesdy, C.P. (2016). North American experience with Low protein diet for Non-dialysis-dependent chronic kidney disease. BMC Nephrol *17*, 90.

103 Katz, J.P., Perreault, N., Goldstein, B.G., Lee, C.S., Labosky, P.A., Yang, V.W., and Kaestner, K.H. (2002). The zinc-finger transcription factor Klf4 is required for terminal differentiation of goblet cells in the colon. Development *129*, 2619-2628.

104 Kelley, L.A., Mezulis, S., Yates, C.M., Wass, M.N., and Sternberg, M.J. (2015). The Phyre2 web portal for protein modeling, prediction and analysis. Nat Protoc *10*, 845-858.

105 Khaloian, S., Rath, E., Hammoudi, N., Gleisinger, E., Blutke, A., Giesbertz, P., Berger, E., Metwaly, A., Waldschmitt, N., Allez, M., and Haller, D. (2020). Mitochondrial impairment drives intestinal stem cell transition into dysfunctional Paneth cells predicting Crohn's disease recurrence. Gut.

106 Khan, K.J., Ullman, T.A., Ford, A.C., Abreu, M.T., Abadir, A., Marshall, J.K., Talley, N.J., and Moayyedi, P. (2011). Antibiotic therapy in inflammatory bowel disease: a systematic review and meta-analysis. Am J Gastroenterol *106*, 661-673.

107 Kim, K., Kim, M.J., Kim, K.H., Ahn, S.A., Kim, J.H., Cho, J.Y., and Yeo, S.G. (2017). C1QBP is upregulated in colon cancer and binds to apolipoprotein A-I. Exp Ther Med *13*, 2493-2500.

108 Knoop, K.A., Gustafsson, J.K., McDonald, K.G., Kulkarni, D.H., Kassel, R., and Newberry, R.D. (2017). Antibiotics promote the sampling of luminal antigens and bacteria via colonic goblet cell associated antigen passages. Gut Microbes *8*, 400-411.

109 Ko, G.J., Obi, Y., Tortorici, A.R., and Kalantar-Zadeh, K. (2017). Dietary protein intake and chronic kidney disease. Curr Opin Clin Nutr Metab Care *20*, 77-85.

110 Kobayashi, T., Siegmund, B., Le Berre, C., Wei, S.C., Ferrante, M., Shen, B., Bernstein, C.N., Danese, S., Peyrin-Biroulet, L., and Hibi, T. (2020). Ulcerative colitis. Nat Rev Dis Primers *6*, 74.

111 Kostic, A.D., Xavier, R.J., and Gevers, D. (2014). The microbiome in inflammatory bowel disease: current status and the future ahead. Gastroenterology *146*, 1489-1499.

112 Krainer, A.R., Mayeda, A., Kozak, D., and Binns, G. (1991). Functional expression of cloned human splicing factor SF2: homology to RNA-binding proteins, U1 70K, and Drosophila splicing regulators. Cell *66*, 383-394.

113 Kulkarni, D.H., McDonald, K.G., Knoop, K.A., Gustafsson, J.K., Kozlowski, K.M., Hunstad, D.A., Miller, M.J., and Newberry, R.D. (2018). Goblet cell associated antigen passages are inhibited during Salmonella typhimurium infection to prevent pathogen dissemination and limit responses to dietary antigens. Mucosal Immunol *11*, 1103-1113.

114 Lazaridis, L.D., Pistiki, A., Giamarellos-Bourboulis, E.J., Georgitsi, M., Damoraki, G., Polymeros, D., Dimitriadis, G.D., and Triantafyllou, K. (2017). Activation of NLRP3 Inflammasome in Inflammatory Bowel Disease: Differences Between Crohn's Disease and Ulcerative Colitis. Dig Dis Sci *62*, 2348-2356.

115 Ledder, O., and Turner, D. (2018). Antibiotics in IBD: Still a Role in the Biological Era? Inflamm Bowel Dis *24*, 1676-1688.

116 Lei-Leston, A.C., Murphy, A.G., and Maloy, K.J. (2017). Epithelial Cell Inflammasomes in Intestinal Immunity and Inflammation. Front Immunol *8*, 1168.

117 Lesuffleur, T., Barbat, A., Dussaulx, E., and Zweibaum, A. (1990). Growth adaptation to methotrexate of HT-29 human colon carcinoma cells is associated with their ability to differentiate into columnar absorptive and mucus-secreting cells. Cancer Res *50*, 6334-6343.

118 Levy, M., Thaiss, C.A., Zeevi, D., Dohnalova, L., Zilberman-Schapira, G., Mahdi, J.A., David, E., Savidor, A., Korem, T., Herzig, Y., Pevsner-Fischer, M., Shapiro, H., Christ, A., Harmelin, A., Halpern, Z., Latz, E., Flavell, R.A., Amit, I., Segal, E., and Elinav, E. (2015). Microbiota-Modulated Metabolites Shape the Intestinal Microenvironment by Regulating NLRP6 Inflammasome Signaling. Cell *163*, 1428-1443.

119 Ley, R.E., Turnbaugh, P.J., Klein, S., and Gordon, J.I. (2006). Microbial ecology: human gut microbes associated with obesity. Nature *444*, 1022-1023.

120 Lieberkühn, J.N. (1745). Dissertatio Anatomico Physiologica de fabrica et actione villorum intestinorum tenuium hominis. Lugduni Batavorum.

121 Liu, J.Z., van Sommeren, S., Huang, H., Ng, S.C., Alberts, R., Takahashi, A., Ripke, S., Lee, J.C., Jostins, L., Shah, T., Abedian, S., Cheon, J.H., Cho, J., Dayani, N.E., Franke, L., Fuyuno, Y., Hart, A., Juyal, R.C., Juyal, G., Kim, W.H., Morris, A.P., Poustchi, H., Newman, W.G., Midha, V., Orchard, T.R., Vahedi, H., Sood, A., Sung, J.Y., Malekzadeh, R., Westra, H.J., Yamazaki, K., Yang, S.K., International Multiple Sclerosis Genetics, C., International, I.B.D.G.C., Barrett, J.C., Alizadeh, B.Z., Parkes, M., Bk, T., Daly, M.J., Kubo, M., Anderson, C.A., and Weersma, R.K. (2015a). Association analyses identify 38 susceptibility loci for inflammatory bowel disease and highlight shared genetic risk across populations. Nat Genet *47*, 979-986.

122 Liu, Y., Leslie, P.L., Jin, A., Itahana, K., Graves, L.M., and Zhang, Y. (2017). p32 heterozygosity protects against age- and diet-induced obesity by increasing energy expenditure. Sci Rep *7*, 5754.

123 Liu, Z., Kato, A., Oyama, M., Kozuka-Hata, H., Arii, J., and Kawaguchi, Y. (2015b). Role of Host Cell p32 in Herpes Simplex Virus 1 De-Envelopment during Viral Nuclear Egress. J Virol *89*, 8982-8998.

124 Lu, P.D., Galanakis, D.K., Ghebrehiwet, B., and Peerschke, E.I. (1999). The receptor for the globular "heads" of C1q, gC1q-R, binds to fibrinogen/fibrin and impairs its polymerization. Clin Immunol *90*, 360-367.

125 Luciano, P., and Geli, V. (1996). The mitochondrial processing peptidase: function and specificity. Experientia *52*, 1077-1082.

126 Lynch, N.J., Reid, K.B., van den Berg, R.H., Daha, M.R., Leigh, L.A., Ghebrehiwet, B., Lim, W.B., and Schwaeble, W.J. (1997). Characterisation of the rat and mouse homologues of gC1qBP, a 33 kDa glycoprotein that binds to the globular 'heads' of C1q. FEBS Lett *418*, 111-114.

127 Mabbott, N.A., Donaldson, D.S., Ohno, H., Williams, I.R., and Mahajan, A. (2013). Microfold (M) cells: important immunosurveillance posts in the intestinal epithelium. Mucosal Immunol *6*, 666-677.

128 Machiels, K., Joossens, M., Sabino, J., De Preter, V., Arijs, I., Eeckhaut, V., Ballet, V., Claes, K., Van Immerseel, F., Verbeke, K., Ferrante, M., Verhaegen, J., Rutgeerts, P., and Vermeire, S. (2014). A decrease of the butyrate-producing species Roseburia hominis and Faecalibacterium prausnitzii defines dysbiosis in patients with ulcerative colitis. Gut *63*, 1275-1283.

129 Magallon-Tejada, A., Machevo, S., Cistero, P., Lavstsen, T., Aide, P., Rubio, M., Jimenez, A., Turner, L., Valmaseda, A., Gupta, H., De Las Salas, B., Mandomando, I., Wang, C.W., Petersen, J.E., Munoz, J., Gascon, J., Macete, E., Alonso, P.L., Chitnis, C.E., Bassat, Q., and Mayor, A. (2016). Cytoadhesion to gC1qR through Plasmodium falciparum Erythrocyte Membrane Protein 1 in Severe Malaria. PLoS Pathog *12*, e1006011.

130 Mahida, Y.R., Wu, K., and Jewell, D.P. (1989). Enhanced production of interleukin 1-beta by mononuclear cells isolated from mucosa with active ulcerative colitis of Crohn's disease. Gut *30*, 835-838.

131 Manichanh, C., Borruel, N., Casellas, F., and Guarner, F. (2012). The gut microbiota in IBD. Nat Rev Gastroenterol Hepatol *9*, 599-608.

132 Martin, A.R., Villegas, I., Sanchez-Hidalgo, M., and de la Lastra, C.A. (2006). The effects of resveratrol, a phytoalexin derived from red wines, on chronic inflammation induced in an experimentally induced colitis model. Br J Pharmacol *147*, 873-885.

133 Martinez-Medina, M., Denizot, J., Dreux, N., Robin, F., Billard, E., Bonnet, R., Darfeuille-Michaud, A., and Barnich, N. (2014). Western diet induces dysbiosis with increased E coli in CEABAC10 mice, alters host barrier function favouring AIEC colonisation. Gut *63*, 116-124.

134 Martini, E., Krug, S.M., Siegmund, B., Neurath, M.F., and Becker, C. (2017). Mend Your Fences: The Epithelial Barrier and its Relationship With Mucosal Immunity in Inflammatory Bowel Disease. Cellular and molecular gastroenterology and hepatology *4*, 33-46.

135 McCormick, D.A., Horton, L.W., and Mee, A.S. (1990). Mucin depletion in inflammatory bowel disease. J Clin Pathol *43*, 143-146.

136 McDole, J.R., Wheeler, L.W., McDonald, K.G., Wang, B., Konjufca, V., Knoop, K.A., Newberry, R.D., and Miller, M.J. (2012). Goblet cells deliver luminal antigen to CD103+ dendritic cells in the small intestine. Nature *483*, 345-349.

137 McGregor, R.A., and Poppitt, S.D. (2013). Milk protein for improved metabolic health: a review of the evidence. Nutr Metab (Lond) *10*, 46.

138 Mitsuyama, K., Niwa, M., Takedatsu, H., Yamasaki, H., Kuwaki, K., Yoshioka, S., Yamauchi, R., Fukunaga, S., and Torimura, T. (2016). Antibody markers in the diagnosis of inflammatory bowel disease. World J Gastroenterol *22*, 1304-1310.

139 Murakami, H., and Masui, H. (1980). Hormonal control of human colon carcinoma cell growth in serum-free medium. Proc Natl Acad Sci U S A *77*, 3464-3468.

140 Murphy, K., and Weaver, C. (2017). Janeway's Immunobiology, 9th edition. Garland Science, 99-101.

141 Muta, T., Kang, D., Kitajima, S., Fujiwara, T., and Hamasaki, N. (1997). p32 protein, a splicing factor 2-associated protein, is localized in mitochondrial matrix and is functionally important in maintaining oxidative phosphorylation. J Biol Chem *272*, 24363-24370.

142 Navabi, N., McGuckin, M.A., and Linden, S.K. (2013). Gastrointestinal cell lines form polarized epithelia with an adherent mucus layer when cultured in semi-wet interfaces with mechanical stimulation. PLoS One *8*, e68761.

143 Nguyen, T., Ghebrehiwet, B., and Peerschke, E.I. (2000). Staphylococcus aureus protein A recognizes platelet gC1qR/p33: a novel mechanism for staphylococcal interactions with platelets. Infect Immun *68*, 2061-2068.

144 Ni, J., Wu, G.D., Albenberg, L., and Tomov, V.T. (2017). Gut microbiota and IBD: causation or correlation? Nat Rev Gastroenterol Hepatol *14*, 573-584.

145 Noah, T.K., Kazanjian, A., Whitsett, J., and Shroyer, N.F. (2010). SAM pointed domain ETS factor (SPDEF) regulates terminal differentiation and maturation of intestinal goblet cells. Exp Cell Res *316*, 452-465.

146 Ohno, H., and Hase, K. (2010). Glycoprotein 2 (GP2): grabbing the FimH bacteria into M cells for mucosal immunity. Gut Microbes *1*, 407-410.

147 Olive, M., Untawale, S., Coffey, R.J., Siciliano, M.J., Wildrick, D.M., Fritsche, H., Pathak, S., Cherry, L.M., Blick, M., Lointier, P., Roubein, L.D., Levin, B., and Boman, B.M. (1993). Characterization of the DiFi rectal carcinoma cell line derived from a familial adenomatous polyposis patient. In Vitro Cell Dev Biol *29A*, 239-248.

148 Ouwerkerk, J.P., de Vos, W.M., and Belzer, C. (2013). Glycobiome: bacteria and mucus at the epithelial interface. Best Pract Res Clin Gastroenterol *27*, 25-38.

149 Pabst, O., and Mowat, A.M. (2012). Oral tolerance to food protein. Mucosal Immunol *5*, 232-239.

150 Pagel, R., Bar, F., Schroder, T., Sunderhauf, A., Kunstner, A., Ibrahim, S.M., Autenrieth, S.E., Kalies, K., Konig, P., Tsang, A.H., Bettenworth, D., Divanovic, S., Lehnert, H., Fellermann, K., Oster, H., Derer, S., and Sina, C. (2017). Circadian rhythm disruption impairs tissue homeostasis and exacerbates chronic inflammation in the intestine. FASEB J *31*, 4707-4719.

151 Palm, W., and Thompson, C.B. (2017). Nutrient acquisition strategies of mammalian cells. Nature *546*, 234-242.

152 Palmer, C.S., Osellame, L.D., Stojanovski, D., and Ryan, M.T. (2011). The regulation of mitochondrial morphology: intricate mechanisms and dynamic machinery. Cell Signal *23*, 1534-1545.

153 Paramsothy, S., Paramsothy, R., Rubin, D.T., Kamm, M.A., Kaakoush, N.O., Mitchell, H.M., and Castano-Rodriguez, N. (2017). Faecal Microbiota Transplantation for Inflammatory Bowel Disease: A Systematic Review and Meta-analysis. J Crohns Colitis *11*, 1180-1199.

154 Pednekar, L., Valentino, A., Ji, Y., Tumma, N., Valentino, C., Kadoor, A., Hosszu, K.K., Ramadass, M., Kew, R.R., Kishore, U., Peerschke, E.I., and Ghebrehiwet, B. (2016). Identification of the gC1qR sites for the HIV-1 viral envelope protein gp41 and the HCV core protein: Implications in viral-specific pathogenesis and therapy. Mol Immunol *74*, 18-26.

155 Peerschke, E.I., and Ghebrehiwet, B. (2007). The contribution of gC1qR/p33 in infection and inflammation. Immunobiology *212*, 333-342.

156 Peerschke, E.I., Jesty, J., Reid, K.B., and Ghebrehiwet, B. (1998). The soluble recombinant form of a binding protein/receptor for the globular domain of C1q (gC1qR) enhances blood coagulation. Blood Coagul Fibrinolysis *9*, 29-37.

157 Peerschke, E.I., Yin, W., Grigg, S.E., and Ghebrehiwet, B. (2006). Blood platelets activate the classical pathway of human complement. J Thromb Haemost *4*, 2035-2042.

158 Peters, L.A., Perrigoue, J., Mortha, A., Iuga, A., Song, W.M., Neiman, E.M., Llewellyn, S.R., Di Narzo, A., Kidd, B.A., Telesco, S.E., Zhao, Y., Stojmirovic, A., Sendecki, J., Shameer, K., Miotto, R., Losic, B., Shah, H., Lee, E., Wang, M., Faith, J.J., Kasarskis, A., Brodmerkel, C., Curran, M., Das, A., Friedman, J.R., Fukui, Y., Humphrey, M.B., Iritani, B.M., Sibinga, N., Tarrant, T.K., Argmann, C., Hao, K., Roussos, P., Zhu, J., Zhang, B., Dobrin, R., Mayer, L.F., and Schadt, E.E. (2017). A functional genomics predictive network model identifies regulators of inflammatory bowel disease. Nat Genet *49*, 1437-1449.

159 Petersen-Mahrt, S.K., Estmer, C., Ohrmalm, C., Matthews, D.A., Russell, W.C., and Akusjarvi, G. (1999). The splicing factor-associated protein, p32, regulates RNA splicing by inhibiting ASF/SF2 RNA binding and phosphorylation. EMBO J *18*, 1014-1024.

160 Peterson, K.L., Zhang, W., Lu, P.D., Keilbaugh, S.A., Peerschke, E.I., and Ghebrehiwet, B. (1997). The C1q-binding cell membrane proteins cC1q-R and gC1q-R are released from activated cells: subcellular distribution and immunochemical characterization. Clin Immunol Immunopathol *84*, 17-26.

161 Png, C.W., Linden, S.K., Gilshenan, K.S., Zoetendal, E.G., McSweeney, C.S., Sly, L.I., McGuckin, M.A., and Florin, T.H. (2010). Mucolytic bacteria with increased prevalence in IBD mucosa augment in vitro utilization of mucin by other bacteria. Am J Gastroenterol *105*, 2420-2428.

162 Ponten, F., Jirstrom, K., and Uhlen, M. (2008). The Human Protein Atlas--a tool for pathology. J Pathol *216*, 387-393.

163 Potten, C.S. (1977). Extreme sensitivity of some intestinal crypt cells to X and gamma irradiation. Nature *269*, 518-521.

164 Pullan, R.D., Thomas, G.A., Rhodes, M., Newcombe, R.G., Williams, G.T., Allen, A., and Rhodes, J. (1994). Thickness of adherent mucus gel on colonic mucosa in humans and its relevance to colitis. Gut *35*, 353-359.

165 Quinton, J.F., Sendid, B., Reumaux, D., Duthilleul, P., Cortot, A., Grandbastien, B., Charrier, G., Targan, S.R., Colombel, J.F., and Poulain, D. (1998). Anti-Saccharomyces cerevisiae mannan antibodies combined with antineutrophil cytoplasmic autoantibodies in inflammatory bowel disease: prevalence and diagnostic role. Gut *42*, 788-791.

166 Racine, A., Carbonnel, F., Chan, S.S., Hart, A.R., Bueno-de-Mesquita, H.B., Oldenburg, B., van Schaik, F.D., Tjonneland, A., Olsen, A., Dahm, C.C., Key, T., Luben, R., Khaw, K.T., Riboli, E., Grip, O., Lindgren, S., Hallmans, G., Karling, P., Clavel-Chapelon, F., Bergman, M.M., Boeing, H., Kaaks, R., Katzke, V.A., Palli, D., Masala, G., Jantchou, P., and Boutron-Ruault, M.C. (2016). Dietary Patterns and Risk of Inflammatory Bowel Disease in Europe: Results from the EPIC Study. Inflamm Bowel Dis *22*, 345-354.

167 Rao, J.N., and Wang, J.Y. (2010). Intestinal Architecture and Development. In Regulation of Gastrointestinal Mucosal Growth (San Rafael (CA): Morgan & Claypool Live Sciences).

168 Rasband, W.S. (1997-2018). ImageJ, U. S. National Institutes of Health, Bethesda, Maryland, USA.

169 Raschdorf, A., Sünderhauf, A., Skibbe, K., Ghebrehiwet, B., Peerschke, E.I., Sina, C., and Derer, S. (2020). Heterozygous P32/C1QBP/HABP1 Polymorphism rs56014026 Reduces Mitochondrial Oxidative Phosphorylation and Is Expressed in Low-grade Colorectal Carcinomas. Front Oncol *10*, 631592.

170 Rath, E., Moschetta, A., and Haller, D. (2018). Mitochondrial function - gatekeeper of intestinal epithelial cell homeostasis. Nat Rev Gastroenterol Hepatol *15*, 497-516.

171 Reef, S., Shifman, O., Oren, M., and Kimchi, A. (2007). The autophagic inducer smARF interacts with and is stabilized by the mitochondrial p32 protein. Oncogene *26*, 6677-6683.

172 Reese, G.E., Constantinides, V.A., Simillis, C., Darzi, A.W., Orchard, T.R., Fazio, V.W., and Tekkis, P.P. (2006). Diagnostic precision of anti-Saccharomyces cerevisiae antibodies and perinuclear antineutrophil cytoplasmic antibodies in inflammatory bowel disease. Am J Gastroenterol *101*, 2410-2422.

173 Roediger, W.E. (1980a). The colonic epithelium in ulcerative colitis: an energy-deficiency disease? Lancet *2*, 712-715.

174 Roediger, W.E. (1980b). Role of anaerobic bacteria in the metabolic welfare of the colonic mucosa in man. Gut *21*, 793-798.

175 Roediger, W.E. (1993). Colonic epithelial metabolism in ulcerative colitis. Gut *34*, 1646.

176 Rogler, G., Bernstein, C.N., Sood, A., Goh, K.L., Yamamoto-Furusho, J.K., Abbas, Z., and Fried, M. (2012). Role of biological therapy for inflammatory bowel disease in developing countries. Gut *61*, 706-712.

177 Rubinstein, D.B., Stortchevoi, A., Boosalis, M., Ashfaq, R., Ghebrehiwet, B., Peerschke, E.I., Calvo, F., and Guillaume, T. (2004). Receptor for the globular heads of C1q (gC1q-R, p33, hyaluronan-binding protein) is preferentially expressed by adenocarcinoma cells. Int J Cancer *110*, 741-750.

178 Ruifrok, A.C., and Johnston, D.A. (2001). Quantification of histochemical staining by color deconvolution. Anal Quant Cytol Histol *23*, 291-299.

179 Saha, P., and Datta, K. (2018). Multi-functional, multicompartmental hyaluronan-binding protein 1 (HABP1/p32/gC1qR): implication in cancer progression and metastasis. Oncotarget *9*, 10784-10807.

180 Samsami-Kor, M., Daryani, N.E., Asl, P.R., and Hekmatdoost, A. (2015). Anti-Inflammatory Effects of Resveratrol in Patients with Ulcerative Colitis: A Randomized, Double-Blind, Placebo-controlled Pilot Study. Arch Med Res *46*, 280-285.

181 Samsamikor, M., Daryani, N.E., Asl, P.R., and Hekmatdoost, A. (2016). Resveratrol Supplementation and Oxidative/Anti-Oxidative Status in Patients with Ulcerative Colitis: A Randomized, Double-Blind, Placebo-controlled Pilot Study. Arch Med Res *47*, 304-309.

182 Santhanam, S., Rajamanickam, S., Motamarry, A., Ramakrishna, B.S., Amirtharaj, J.G., Ramachandran, A., Pulimood, A., and Venkatraman, A. (2012). Mitochondrial electron transport chain complex dysfunction in the colonic mucosa in ulcerative colitis. Inflamm Bowel Dis *18*, 2158-2168.

183 Sartor, R.B. (2001). Intestinal microflora in human and experimental inflammatory bowel disease. Curr Opin Gastroenterol *17*, 324-330.

184 Scheibe, K., Kersten, C., Schmied, A., Vieth, M., Primbs, T., Carle, B., Knieling, F., Claussen, J., Klimowicz, A.C., Zheng, J., Baum, P., Meyer, S., Schurmann, S., Friedrich, O., Waldner, M.J., Rath, T., Wirtz, S., Kollias, G., Ekici, A.B., Atreya, R., Raymond, E.L., Mbow, M.L., Neurath, M.F., and Neufert, C. (2019). Inhibiting Interleukin 36 Receptor Signaling Reduces Fibrosis in Mice With Chronic Intestinal Inflammation. Gastroenterology *156*, 1082-1097 e1011.

185 Schicho, R., Shaykhutdinov, R., Ngo, J., Nazyrova, A., Schneider, C., Panaccione, R., Kaplan, G.G., Vogel, H.J., and Storr, M. (2012). Quantitative metabolomic profiling of serum, plasma, and urine by (1)H NMR spectroscopy discriminates between patients with inflammatory bowel disease and healthy individuals. J Proteome Res *11*, 3344-3357.

186 Schroder, T., Kucharczyk, D., Bar, F., Pagel, R., Derer, S., Jendrek, S.T., Sunderhauf, A., Brethack, A.K., Hirose, M., Moller, S., Kunstner, A., Bischof, J., Weyers, I., Heeren, J., Koczan, D., Schmid, S.M., Divanovic, S., Giles, D.A., Adamski, J., Fellermann, K., Lehnert, H., Kohl, J., Ibrahim, S., and Sina, C. (2016). Mitochondrial gene polymorphisms alter hepatic cellular energy metabolism and aggravate diet-induced non-alcoholic steatohepatitis. Mol Metab *5*, 283-295.

187 Schroeder, K.W., Tremaine, W.J., and Ilstrup, D.M. (1987). Coated oral 5-aminosalicylic acid therapy for mildly to moderately active ulcerative colitis. A randomized study. N Engl J Med *317*, 1625-1629.

188 Schroll, S., Sarlette, A., Ahrens, K., Manns, M.P., and Goke, M. (2005). Effects of azathioprine and its metabolites on repair mechanisms of the intestinal epithelium in vitro. Regul Pept *131*, 1-11.

189 Schulz, O., and Pabst, O. (2013). Antigen sampling in the small intestine. Trends Immunol *34*, 155-161.

190 Sengupta, A., Ghosh, I., Mallick, J., Thakur, A.R., and Datta, K. (2004). Presence of a human Hyaluronan binding protein 1 (HABP1) pseudogene-like sequence in Methanosarcina barkeri suggests its linkage in evolution. DNA Cell Biol *23*, 301-310.

191 Seo, S.U., Kamada, N., Munoz-Planillo, R., Kim, Y.G., Kim, D., Koizumi, Y., Hasegawa, M., Himpsl, S.D., Browne, H.P., Lawley, T.D., Mobley, H.L., Inohara, N., and Nunez, G. (2015). Distinct Commensals Induce Interleukin-1beta via NLRP3 Inflammasome in Inflammatory Monocytes to Promote Intestinal Inflammation in Response to Injury. Immunity *42*, 744-755.

192 Shekhawat, P.S., Srinivas, S.R., Matern, D., Bennett, M.J., Boriack, R., George, V., Xu, H., Prasad, P.D., Roon, P., and Ganapathy, V. (2007). Spontaneous development of intestinal and colonic atrophy and inflammation in the carnitine-deficient jvs (OCTN2(-/-)) mice. Mol Genet Metab *92*, 315-324.

193 Sifroni, K.G., Damiani, C.R., Stoffel, C., Cardoso, M.R., Ferreira, G.K., Jeremias, I.C., Rezin, G.T., Scaini, G., Schuck, P.F., Dal-Pizzol, F., and Streck, E.L. (2010). Mitochondrial respiratory chain in the colonic mucosal of patients with ulcerative colitis. Mol Cell Biochem *342*, 111-115.

194 Silverberg, M.S., Satsangi, J., Ahmad, T., Arnott, I.D., Bernstein, C.N., Brant, S.R., Caprilli, R., Colombel, J.F., Gasche, C., Geboes, K., Jewell, D.P., Karban, A., Loftus, E.V., Jr., Pena, A.S., Riddell, R.H., Sachar, D.B., Schreiber, S., Steinhart, A.H., Targan, S.R., Vermeire, S., and Warren, B.F. (2005). Toward an integrated clinical, molecular and serological classification of inflammatory bowel disease: report of a Working Party of the 2005 Montreal World Congress of Gastroenterology. Can J Gastroenterol *19 Suppl A*, 5A-36A.

195 Sinha, A., Nightingale, J., West, K.P., Berlanga-Acosta, J., and Playford, R.J. (2003). Epidermal growth factor enemas with oral mesalamine for mild-to-moderate left-sided ulcerative colitis or proctitis. N Engl J Med *349*, 350-357.

196 Sjolund, K., Sanden, G., Hakanson, R., and Sundler, F. (1983). Endocrine cells in human intestine: an immunocytochemical study. Gastroenterology *85*, 1120-1130.

197 Smith, S.A., Ogawa, S.A., Chau, L., Whelan, K.A., Hamilton, K.E., Chen, J., Tan, L., Chen, E.Z., Keilbaugh, S., Fogt, F., Bewtra, M., Braun, J., Xavier, R.J., Clish, C.B., Slaff, B., Weljie, A.M., Bushman, F.D., Lewis, J.D., Li, H., Master, S.R., Bennett, M.J., Nakagawa, H., and Wu, G.D. (2020). Mitochondrial dysfunction in inflammatory bowel disease alters intestinal epithelial metabolism of hepatic acylcarnitines. J Clin Invest.

198 Snoeck, V., Goddeeris, B., and Cox, E. (2005). The role of enterocytes in the intestinal barrier function and antigen uptake. Microbes Infect *7*, 997-1004.

199 Specian, R.D., and Neutra, M.R. (1980). Mechanism of rapid mucus secretion in goblet cells stimulated by acetylcholine. J Cell Biol *85*, 626-640.

200 Spence, J.R., Mayhew, C.N., Rankin, S.A., Kuhar, M.F., Vallance, J.E., Tolle, K., Hoskins, E.E., Kalinichenko, V.V., Wells, S.I., Zorn, A.M., Shroyer, N.F., and Wells, J.M. (2011). Directed differentiation of human pluripotent stem cells into intestinal tissue in vitro. Nature *470*, 105-109.

201 Staff, M.C. (2020). Ulcerative Colitis.

202 Stringari, C., Edwards, R.A., Pate, K.T., Waterman, M.L., Donovan, P.J., and Gratton, E. (2012). Metabolic trajectory of cellular differentiation in small intestine by Phasor Fluorescence Lifetime Microscopy of NADH. Sci Rep *2*, 568.

203 Sun, N., Youle, R.J., and Finkel, T. (2016). The Mitochondrial Basis of Aging. Mol Cell *61*, 654-666.

204 Sünderhauf, A., Hicken, M., Schlichting, H., Skibbe, K., Ragab, M., Raschdorf, A., Hirose, M., Schaffler, H., Bokemeyer, A., Bettenworth, D., Savitt, A.G., Perner, S., Ibrahim, S., Peerschke, E.L., Ghebrehiwet, B., Derer, S., and Sina, C. (2021). Loss of mucosal p32/gC1qR/HABP1 triggers energy deficiency and impairs goblet cell differentiation in ulcerative colitis. Cellular and molecular gastroenterology and hepatology.

205 Sünderhauf, A., Raschdorf, A., Hicken, M., Schlichting, H., Fetzer, F., Brethack, A.K., Perner, S., Kemper, C., Ghebrehiwet, B., Sina, C., and Derer, S. (2020). GC1qR Cleavage by Caspase-1 Drives Aerobic Glycolysis in Tumor Cells. Front Oncol *10*, 575854.

206 Sünderhauf, A., Skibbe, K., Preisker, S., Ebbert, K., Verschoor, A., Karsten, C.M., Kemper, C., Huber-Lang, M., Basic, M., Bleich, A., Buning, J., Fellermann, K., Sina, C., and Derer, S. (2017). Regulation of epithelial cell expressed C3 in the intestine - Relevance for the pathophysiology of inflammatory bowel disease? Mol Immunol *90*, 227-238.

207 Swidsinski, A., Ladhoff, A., Pernthaler, A., Swidsinski, S., Loening-Baucke, V., Ortner, M., Weber, J., Hoffmann, U., Schreiber, S., Dietel, M., and Lochs, H. (2002). Mucosal flora in inflammatory bowel disease. Gastroenterology *122*, 44-54.

208 Takaishi, H., Matsuki, T., Nakazawa, A., Takada, T., Kado, S., Asahara, T., Kamada, N., Sakuraba, A., Yajima, T., Higuchi, H., Inoue, N., Ogata, H., Iwao, Y., Nomoto, K., Tanaka, R., and Hibi, T. (2008). Imbalance in intestinal microflora constitution could be involved in the pathogenesis of inflammatory bowel disease. Int J Med Microbiol *298*, 463-472.

209 Tatiya-Aphiradee, N., Chatuphonprasert, W., and Jarukamjorn, K. (2018). Immune response and inflammatory pathway of ulcerative colitis. J Basic Clin Physiol Pharmacol *30*, 1-10.

210 Thomsson, K.A., Holmen-Larsson, J.M., Angstrom, J., Johansson, M.E., Xia, L., and Hansson, G.C. (2012). Detailed O-glycomics of the Muc2 mucin from colon of wild-type, core 1- and core 3-transferase-deficient mice highlights differences compared with human MUC2. Glycobiology *22*, 1128-1139.

211 Thornberry, N.A., Bull, H.G., Calaycay, J.R., Chapman, K.T., Howard, A.D., Kostura, M.J., Miller, D.K., Molineaux, S.M., Weidner, J.R., Aunins, J., and et al. (1992). A novel heterodimeric

cysteine protease is required for interleukin-1 beta processing in monocytes. Nature *356*, 768-774.

212 Timmer, A., Patton, P.H., Chande, N., McDonald, J.W., and MacDonald, J.K. (2016). Azathioprine and 6-mercaptopurine for maintenance of remission in ulcerative colitis. Cochrane Database Syst Rev, CD000478.

213 Timmers, S., Konings, E., Bilet, L., Houtkooper, R.H., van de Weijer, T., Goossens, G.H., Hoeks, J., van der Krieken, S., Ryu, D., Kersten, S., Moonen-Kornips, E., Hesselink, M.K.C., Kunz, I., Schrauwen-Hinderling, V.B., Blaak, E., Auwerx, J., and Schrauwen, P. (2011). Calorie restriction-like effects of 30 days of resveratrol supplementation on energy metabolism and metabolic profile in obese humans. Cell Metab *14*, 612-622.

214 Torres, J. (2018). CAN WE PREDICT / PREVENT IBD? DDW, 20. https://static.livemedia.gr/livemedia/documents/al26698_us26680_20190601172921_20190601172901.torres.pdf.

215 Turnbaugh, P.J., Ley, R.E., Mahowald, M.A., Magrini, V., Mardis, E.R., and Gordon, J.I. (2006). An obesity-associated gut microbiome with increased capacity for energy harvest. Nature *444*, 1027-1031.

216 Tye, A.J., Ghebrehiwet, B., Guo, N., Sastry, K.N., Chow, B.K., Peerschke, E.I., and Lim, B.L. (2001). The human gC1qR/p32 gene, C1qBP. Genomic organization and promoter analysis. J Biol Chem *276*, 17069-17075.

217 Ungaro, R., Mehandru, S., Allen, P.B., Peyrin-Biroulet, L., and Colombel, J.F. (2017). Ulcerative colitis. Lancet *389*, 1756-1770.

218 Uray, K., Mizuno, M., Inazu, T., Goto, K., and Hudecz, F. (2014). The effect of glycosylation on the antibody recognition of a MUC2 mucin epitope. Biopolymers *102*, 390-395.

219 Van der Sluis, M., De Koning, B.A., De Bruijn, A.C., Velcich, A., Meijerink, J.P., Van Goudoever, J.B., Buller, H.A., Dekker, J., Van Seuningen, I., Renes, I.B., and Einerhand, A.W. (2006). Muc2-deficient mice spontaneously develop colitis, indicating that MUC2 is critical for colonic protection. Gastroenterology *131*, 117-129.

220 van der Valk, M.E., Mangen, M.J., Leenders, M., Dijkstra, G., van Bodegraven, A.A., Fidder, H.H., de Jong, D.J., Pierik, M., van der Woude, C.J., Romberg-Camps, M.J., Clemens, C.H., Jansen, J.M., Mahmmod, N., van de Meeberg, P.C., van der Meulen-de Jong, A.E., Ponsioen, C.Y., Bolwerk, C.J., Vermeijden, J.R., Siersema, P.D., van Oijen, M.G., Oldenburg, B., group, C.s., the Dutch Initiative on, C., and Colitis (2014). Healthcare costs of inflammatory bowel disease have shifted from hospitalisation and surgery towards anti-TNFalpha therapy: results from the COIN study. Gut *63*, 72-79.

221 van Es, J.H., van Gijn, M.E., Riccio, O., van den Born, M., Vooijs, M., Begthel, H., Cozijnsen, M., Robine, S., Winton, D.J., Radtke, F., and Clevers, H. (2005). Notch/gamma-secretase inhibition turns proliferative cells in intestinal crypts and adenomas into goblet cells. Nature *435*, 959-963.

222 van Gennep, S., Evers, S.W., Rietdijk, S.T., Gielen, M.E., de Boer, N.K.H., Gecse, K.B., Ponsioen, C.I.J., Duijvestein, M., D'Haens, G.R., de Boer, A., and Lowenberg, M. (2020). High Disease Burden Drives Indirect Costs in Employed Inflammatory Bowel Disease Patients: The WORK-IBD Study. Inflamm Bowel Dis.

223 Van Scoy, S., Watakabe, I., Krainer, A.R., and Hearing, J. (2000). Human p32: a coactivator for Epstein-Barr virus nuclear antigen-1-mediated transcriptional activation and possible role in viral latent cycle DNA replication. Virology *275*, 145-157.

224 Vander Heiden, M.G., Cantley, L.C., and Thompson, C.B. (2009). Understanding the Warburg effect: the metabolic requirements of cell proliferation. Science *324*, 1029-1033.

225 Vernia, P., Caprilli, R., Latella, G., Barbetti, F., Magliocca, F.M., and Cittadini, M. (1988). Fecal lactate and ulcerative colitis. Gastroenterology *95*, 1564-1568.

226 Vigsnaes, L.K., Brynskov, J., Steenholdt, C., Wilcks, A., and Licht, T.R. (2012). Gram-negative bacteria account for main differences between faecal microbiota from patients with ulcerative colitis and healthy controls. Benef Microbes *3*, 287-297.

227 Volk, J.K., Nystrom, E.E.L., van der Post, S., Abad, B.M., Schroeder, B.O., Johansson, A., Svensson, F., Javerfelt, S., Johansson, M.E.V., Hansson, G.C., and Birchenough, G.M.H. (2019). The Nlrp6 inflammasome is not required for baseline colonic inner mucus layer formation or function. J Exp Med *216*, 2602-2618.

228 Waller, S., Tremelling, M., Bredin, F., Godfrey, L., Howson, J., and Parkes, M. (2006). Evidence for association of OCTN genes and IBD5 with ulcerative colitis. Gut *55*, 809-814.

229 Walters, W.A., Xu, Z., and Knight, R. (2014). Meta-analyses of human gut microbes associated with obesity and IBD. FEBS Lett *588*, 4223-4233.

230 Wang, H., Shi, P., Zuo, L., Dong, J., Zhao, J., Liu, Q., and Zhu, W. (2016). Dietary Non-digestible Polysaccharides Ameliorate Intestinal Epithelial Barrier Dysfunction in IL-10 Knockout Mice. J Crohns Colitis *10*, 1076-1086.

231 Warburg, O. (1956). On the origin of cancer cells. Science *123*, 309-314.

232 Weiss, H., Wester-Rosenloef, L., Koch, C., Koch, F., Baltrusch, S., Tiedge, M., and Ibrahim, S. (2012). The mitochondrial Atp8 mutation induces mitochondrial ROS generation, secretory dysfunction, and beta-cell mass adaptation in conplastic B6-mtFVB mice. Endocrinology *153*, 4666-4676.

233 Williams, H.R., Willsmore, J.D., Cox, I.J., Walker, D.G., Cobbold, J.F., Taylor-Robinson, S.D., and Orchard, T.R. (2012). Serum metabolic profiling in inflammatory bowel disease. Dig Dis Sci *57*, 2157-2165.

234 Wlodarska, M., Thaiss, C.A., Nowarski, R., Henao-Mejia, J., Zhang, J.P., Brown, E.M., Frankel, G., Levy, M., Katz, M.N., Philbrick, W.M., Elinav, E., Finlay, B.B., and Flavell, R.A. (2014). NLRP6 inflammasome orchestrates the colonic host-microbial interface by regulating goblet cell mucus secretion. Cell *156*, 1045-1059.

235 Wu, G.D., Chen, J., Hoffmann, C., Bittinger, K., Chen, Y.Y., Keilbaugh, S.A., Bewtra, M., Knights, D., Walters, W.A., Knight, R., Sinha, R., Gilroy, E., Gupta, K., Baldassano, R., Nessel, L., Li, H., Bushman, F.D., and Lewis, J.D. (2011). Linking long-term dietary patterns with gut microbial enterotypes. Science *334*, 105-108.

236 Xu, X., Duan, S., Yi, F., Ocampo, A., Liu, G.H., and Izpisua Belmonte, J.C. (2013). Mitochondrial regulation in pluripotent stem cells. Cell Metab *18*, 325-332.

237 Xu, X.R., Liu, C.Q., Feng, B.S., and Liu, Z.J. (2014). Dysregulation of mucosal immune response in pathogenesis of inflammatory bowel disease. World J Gastroenterol *20*, 3255-3264.

238 Yagi, M., Uchiumi, T., Takazaki, S., Okuno, B., Nomura, M., Yoshida, S., Kanki, T., and Kang, D. (2012). p32/gC1qR is indispensable for fetal development and mitochondrial translation: importance of its RNA-binding ability. Nucleic Acids Res *40*, 9717-9737.

239 Yang, H., McElree, C., Roth, M.P., Shanahan, F., Targan, S.R., and Rotter, J.I. (1993). Familial empirical risks for inflammatory bowel disease: differences between Jews and non-Jews. Gut *34*, 517-524.

240 Yang, V.W., Liu, Y., Kim, J., Shroyer, K.R., and Bialkowska, A.B. (2019). Increased Genetic Instability and Accelerated Progression of Colitis-Associated Colorectal Cancer through Intestinal Epithelium-specific Deletion of Klf4. Mol Cancer Res *17*, 165-176.

241 Yao, J., Wang, J.Y., Liu, L., Li, Y.X., Xun, A.Y., Zeng, W.S., Jia, C.H., Wei, X.X., Feng, J.L., Zhao, L., and Wang, L.S. (2010). Anti-oxidant effects of resveratrol on mice with DSS-induced ulcerative colitis. Arch Med Res *41*, 288-294.

242 Yoshino, J., Conte, C., Fontana, L., Mittendorfer, B., Imai, S., Schechtman, K.B., Gu, C., Kunz, I., Rossi Fanelli, F., Patterson, B.W., and Klein, S. (2012). Resveratrol supplementation does not improve metabolic function in nonobese women with normal glucose tolerance. Cell Metab *16*, 658-664.

243 Yu, H., Liu, Q., Xin, T., Xing, L., Dong, G., Jiang, Q., Lv, Y., Song, X., Teng, C., Huang, D., Li, Y., Shen, W., Teng, C., Jin, Y., and Zhang, F. (2013). Elevated expression of hyaluronic acid binding protein 1 (HABP1)/P32/C1QBP is a novel indicator for lymph node and peritoneal metastasis of epithelial ovarian cancer patients. Tumour Biol *34*, 3981-3987.

244 Yu, X., Gimsa, U., Wester-Rosenlof, L., Kanitz, E., Otten, W., Kunz, M., and Ibrahim, S.M. (2009a). Dissecting the effects of mtDNA variations on complex traits using mouse conplastic strains. Genome Res *19*, 159-165.

245 Yu, X., Wieczorek, S., Franke, A., Yin, H., Pierer, M., Sina, C., Karlsen, T.H., Boberg, K.M., Bergquist, A., Kunz, M., Witte, T., Gross, W.L., Epplen, J.T., Alarcon-Riquelme, M.E., Schreiber, S., and Ibrahim, S.M. (2009b). Association of UCP2 -866 G/A polymorphism with chronic inflammatory diseases. Genes Immun *10*, 601-605.

246 Zaki, M.H., Boyd, K.L., Vogel, P., Kastan, M.B., Lamkanfi, M., and Kanneganti, T.D. (2010). The NLRP3 inflammasome protects against loss of epithelial integrity and mortality during experimental colitis. Immunity *32*, 379-391.

247 Zhang, H., Kuai, X.Y., Yu, P., Lin, L., and Shi, R. (2012). Protective role of uncoupling protein-2 against dextran sodium sulfate-induced colitis. J Gastroenterol Hepatol *27*, 603-608.

248 Zhuang, X., Li, T., Li, M., Huang, S., Qiu, Y., Feng, R., Zhang, S., Chen, M., Xiong, L., and Zeng, Z. (2019). Systematic Review and Meta-analysis: Short-Chain Fatty Acid Characterization in Patients With Inflammatory Bowel Disease. Inflamm Bowel Dis *25*, 1751-1763.

7 Appendix

7.1 Material

7.1.1 Reagents

Supplementary table 1: List of reagents

Reagent	Company (headquarter)
2,4-Dinitrophenol (DNP)	SantaCruz (Dallas, Texas, US)
2-Mercaptoethanol (≥ 99.0%)	Sigma-Aldrich Inc. (St. Louis, Missouri, USA)
2-Propanol (≥ 99.5%, for synthesis)	Carl Roth GmbH + Co. KG (Karlsruhe, Germany)
3,3',5,5'-Tetramethylbenzidine (TMB) single solution	Thermo Fisher Scientific Inc. (Waltham, Massachusetts, USA)
3-[(3-cholamidopropyl)dimethylammonio]-1-propanesulfonate (CHAPS)	Sigma-Aldrich Inc. (St. Louis, Missouri, USA)
4-(2-Hydroxyethyl)-1-piperazineethane-sulfonic acid (HEPES) ultrapure	Biomol Feinchemikalien GmbH (Hamburg, Germany)
4',6-Diamidino-2-phenylindole (DAPI)	Sigma-Aldrich Inc. (St. Louis, Missouri, USA)
Acetic acid (100%, extra pure)	Carl Roth GmbH + Co. KG (Karlsruhe, Germany)
Agarose LE	Biozym Scientific GmbH (Hessisch Oldendorf, Germany)
Agencourt AMPure Beads	Beckman Coulter, Krefeld, Germany
Alcian blue 8 GX	Merck KGaA (Darmstadt, Germany)
Ampicillin (sodium salt)	Carl Roth GmbH + Co. KG (Karlsruhe, Germany)
Aquatex® mounting solution	Merck KGaA (Darmstadt, Germany)
BactoTM Agar	BD Biosciences (San José, California, USA)
Blasticidin (solution) (10 mg/ml)	InvivoGen Inc. (San Diego, California, USA)
Blocking solution with goat serum	GeneTex (Irvine, California, USA)
Bromophenol blue sodium salt	Merck KGaA (Darmstadt, Germany)
Bovin Serum Albumin (BSA) Fraction V (pH 7.0)	AppliChem GmbH (Darmstadt, Germany)
Casein (≥ 95%)	Carl Roth GmbH + Co. KG (Karlsruhe, Germany)
Chloroform	Carl Roth GmbH + Co. KG (Karlsruhe, Germany)
Citrate Buffer, pH 6.0, 10x	Sigma-Aldrich Inc. (St. Louis, Missouri, USA)
Coomassie® Brilliant Blue G250	SERVA Electrophoresis GmbH (Heidelberg, Germany)
DAB+ chromogen substrate system	Dako (Jena, Germany)
Dimethyl sulfoxide (DMSO, sterile filtered)	Sigma-Aldrich Inc. (St. Louis, Missouri, USA)
Dithiothreitol (DTT)	Sigma-Aldrich Inc. (St. Louis, Missouri, USA)
DNA Gel Loading Dye (6x)	Thermo Fisher Scientific Inc. (Waltham, Massachusetts, USA)
dNTP-Set peqGOLD (dATP, dCTP, dGTP, dTTP, 100 mM)	VWR International LLC. (Radnor, Pennsylvania, USA)
Dual endogenous enzyme block	Dako (Jena, Germany)
Dulbecco's Phosphate Buffered Saline (DPBS) (w/o CaCl2 and MgCl2)	Sigma-Aldrich Inc. (St. Louis, Missouri, USA)

Ethanol absolute, EMPLURA®	Merck KGaA (Darmstadt, Germany)
Ethanol denatured (≥ 99.8%)	Carl Roth GmbH + Co. KG (Karlsruhe, Germany)
Ethylenediaminetetraacetic acid (EDTA) (disodium salt dihydrate) (99.0 – 101.0%)	Sigma-Aldrich Inc. (St. Louis, Missouri, USA)
Fetal bovine serum (FBS)	Thermo Fisher Scientific Inc. (Waltham, Massachusetts, USA)
Fibrinogen from human plasma	Merck KGaA (Darmstadt, Germany)
Formaldehyde solution 4.5%	Th. Geyer GmbH & Co. KG (Renningen, Germany)
GeneRuler 1 kb Plus DNA Ladder	Thermo Fisher Scientific Inc. (Waltham, Massachusetts, USA)
GeneRuler 100 bp DNA Ladder	Thermo Fisher Scientific Inc. (Waltham, Massachusetts, USA)
Glucose Solution (D-Glucose at 200 g/l)	Thermo Fisher Scientific Inc. (Waltham, Massachusetts, USA)
Glycerine (anhydrous puriss., ≥ 99.0%)	Th. Geyer GmbH & Co. KG (Renningen, Germany)
Glycerine, fluorescent free	Merck KGaA (Darmstadt, Germany)
Glycine	AppliChem GmbH (Darmstadt, Germany)
Hydrochloric acid (HCl) (35 - 38%)	Th. Geyer GmbH & Co. KG (Renningen, Germany)
Hygromycin B (50 mg/ml in PBS)	Thermo Fisher Scientific Inc. (Waltham, Massachusetts, USA)
IgA RSG ELISA standard	Affymetrix (Santa Clara, California, USA)
Ketavet 10%	Pfizer (New York City, New York, USA)
LPS-EB ultrapure	InvivoGen (San Diego, California, USA)
Magnesium chloride hexahydrate ($MgCl2 \cdot 6 H2O$) (99.0 – 102.0%)	Sigma-Aldrich Inc. (St. Louis, Missouri, USA)
Mayer's hemalum solution	Merck KGaA (Darmstadt, Germany)
Methanol (≥ 99%)	Carl Roth GmbH + Co. KG (Karlsruhe, Germany)
Midori Green Advance	Nippon Genetics Europe GmbH (Düren, Germany)
Millipore Immobilon® Western Chemiluminescent HRP Substrate	Merck KGaA (Darmstadt, Germany)
Minimum Essential Medium Non-Essential Amino Acids Solution (MEM NEAA) (100X)	Thermo Fisher Scientific Inc. (Waltham, Massachusetts, USA)
Mowiol 4-88	Carl Roth GmbH + Co. KG (Karlsruhe, Germany)
Mouse serum (fraction)	Dako (Jena, Germany)
MTS substrate	Promega (Madison, Wisconsin, USA)
Neutral Red (≥ 90%)	Sigma-Aldrich Inc. (St. Louis, Missouri, USA)
Nonfat dried milk powder	AppliChem GmbH (Darmstadt, Germany)
Oligomycin	Agilent (Santa Clara, California, US)
Paraplast Plus® (Paraffin)	Carl Roth GmbH + Co. KG (Karlsruhe, Germany)
Paraformaldehyde	Merck KGaA (Darmstadt, Germany)
Penicillin/Streptomycin (100x), for cell culture	Th. Geyer GmbH & Co. KG (Renningen, Germany)
PerfeCTa SYBR Green FastMix	Quanta BioSciences Inc. (Gaithersburg, Maryland, USA)
Phosphatase Inhibitor Cocktail III (DMSO solution)	Sigma-Aldrich Inc. (St. Louis, Missouri, USA)
Phosphatase Inhibitor Cocktail II	Th. Geyer GmbH & Co. KG (Renningen, Germany)
Potassium chloride (KCl) (for analysis)	Merck KGaA (Darmstadt, Germany)
Precision Plus Protein™ Dual Color Standards	Bio-Rad Laboratories Inc. (Hercules, California, USA)

Protease Inhibitor Cocktail (DMSO solution)	Sigma-Aldrich Inc. (St. Louis, Missouri, USA)
Restore™ Plus Western Blot Stripping Buffer	Thermo Fisher Scientific Inc. (Waltham, Massachusetts, USA)
RiboLock RNase Inhibitor (40 U/µl)	Thermo Fisher Scientific Inc. (Waltham, Massachusetts, USA)
Rompun 2%	Bayer (Leverkusen, Germany)
Roti®Quant universal (reagents 1 and 2)	Carl Roth GmbH + Co. KG (Karlsruhe, Germany)
Sodium azide (NaN_3) (≥ 99.5%)	Sigma-Aldrich Inc. (St. Louis, Missouri, USA)
Sodium Butyrate Solution (500 mM)	Merck KGaA (Darmstadt, Germany)
Sodium chloride (NaCl) (≥ 99.8%), with anticaking	Carl Roth GmbH + Co. KG (Karlsruhe, Germany)
Sodium dodecyl sulfate (SDS) ultrapure	AppliChem GmbH (Darmstadt, Germany)
Sodium fluoride (NaF) BioXtra (≥ 99%)	Sigma-Aldrich Inc. (St. Louis, Missouri, USA)
Sodium Hydroxide pellets (for analysis)	AppliChem GmbH (Darmstadt, Germany)
Syto BC green fluorescent nucleic acid stain	Thermo Fisher Scientific Inc. (Waltham, Massachusetts, USA)
Thrombin from human plasma	Merck KGaA (Darmstadt, Germany)
Tris	Merck KGaA (Darmstadt, Germany)
Tris ultrapure	AppliChem GmbH (Darmstadt, Germany)
Trypan Blue solution (0.4%)	Sigma-Aldrich Inc. (St. Louis, Missouri, USA)
Tween® 20	AppliChem GmbH (Darmstadt, Germany)
UltraPureTM DNase/RNase-free distilled water	Thermo Fisher Scientific Inc. (Waltham, Massachusetts, USA)

7.1.2 Kits

Supplementary table 2: List of kits

Kit	Company (headquarter)
CellTiter 96® AQueous Non-Radioactive Cell Proliferation Assay (MTS)	Promega (Madison, Wisconsin, USA)
GeneJET Gel Extraction Kit	Thermo Fisher Scientific (Waltham, Massachusetts, USA)
InnuPREP RNA Mini Kit 2.0	Analytik Jena AG (Jena, Germany)
Lipofectamine™ 3000 Reagent	Thermo Fisher Scientific (Waltham, Massachusetts, USA)
L-Lactic Acid (L-Lactate) Assay Kit	Megazyme Corp. (Bray, Ireland)
MiSeq® Reagent Kit v3	Illumina (San Diego, California, USA)
MitoXpress Xtra Oxygen Consumption Assay (MitoXpress Xtra reagent + MitoXpress mineral oil)	Agilent Technologies Inc. (Santa Clara, California, USA)
NucleoBond® Xtra Maxi Kit	Macherey-Nagel GmbH & Co. KG (Düren, Germany)
NucleoSpin® plasmid DNA purification kit	Macherey-Nagel GmbH & Co. KG (Düren, Germany)
PerfeCTa® NGS Library Quantification Kit	Quanta BioSciences (Beverly, Massachusetts, USA)
PowerSoil® DNA Isolation kit	MoBio (Vancouver, British Columbia, Canada)
Quant-iT™ dsDNA Broad-Range Assay Kit	Thermo Fisher Scientific (Waltham, Massachusetts, USA)
QuikChange II XL Site-Directed Mutagenesis Kit (containing Dpn I restriction enzyme and XL-10 Gold bacterial cells)	Agilent Technologies Inc. (Santa Clara, California, USA)
Seahorse XF Cell Mito Stress Test kit	Agilent (Santa Clara, California, USA)

7.1.3 Media, buffer and solutions

Supplementary table 3: List of Media

Medium	Company (headquarter)
2xYT Medium	Carl Roth GmbH + Co. KG (Karlsruhe, Germany)
Dulbecco's Modified Eagle Medium (DMEM) (1x) [+] L-Glutamine [-] D-Glucose [-] Sodium Pyruvate	Thermo Fisher Scientific Inc. (Waltham, Massachusetts, USA)
DMEM (1x) [+] 4.5 g/l D-Glucose [+] L-Glutamine [-] Sodium Pyruvate	Thermo Fisher Scientific Inc. (Waltham, Massachusetts, USA)
Iscove's Modified Dulbecco's Medium (IMDM) (1x) [+] L-Glutamine [+] 25 mM HEPES	Thermo Fisher Scientific Inc. (Waltham, Massachusetts, USA)
S.O.C. Medium	Thermo Fisher Scientific Inc. (Waltham, Massachusetts, USA)

Supplementary table 4: List of buffers and solutions

Buffer	Composition
Alcian-blue staining solution	0.1% w/v Alcian blue 3% acetic acid *ad* ddH_2O
Bicarbonate/carbonate coating buffer, pH 9.6	0.3% w/v NAH_2CO_3 + 0.6% w/v $NAHCO_3$ *ad* ddH_2O
Blotting buffer (10x)	0.25 M Tris 1.92 M Glycine
Blotting buffer (1x) + Methanol	10% Blotting buffer (10x) 20% Methanol *ad* ddH_2O
Buffer C	20 mM HEPES (adjust to pH 7.9) 420 mM NaCl 1.5 mM MgCl2 0.2 mM EDTA 25% Glycerine (≥ 99.0%) 10 mM Sodium fluoride (NaF) 1:100 Phosphatase Inhibitor Cocktail II
Carnoy's fixative solution	300 ml Methanol 150 ml Chloroform 50 ml Acetic acid
Caspase-1 cleavage buffer	50 mM HEPES (adjust to pH 7.2) 50 mM NaCl 0.1% w/v CHAPS 10 mM EDTA 5% Glycerine (≥ 99.0%) 10 mM DTT *ad* ddH_2O
Cell embedding solution	75 µl Thrombin 200 µl Fibrinogen 375 µl Casein
Citrate buffer, pH 6.0	2.1% w/v Citric acid *ad* ddH_2O
Coomassie blue solution	1 g Comassie® Brilliant Blue

	500 ml Methanol 100 ml Acetic acid 400 ml ddH_2O Filtration after 3 to 4 hours
Denaturing lysis buffer (DLB) (2x), pH 7.4	20 mM Tris 2% SDS *ad* ddH_2O
Electrophoresis buffer (5x)	1.25 mM Tris 960 mM Glycine 0.5% SDS *ad* ddH_2O
ELISA blocking buffer	1% w/v BSA *ad* PBS
ELISA washing buffer	0.05% Twenn 20 *ad* PBS
FACS buffer	1% w/v BSA 0.1% w/v NaN_3 *ad* PBS
Mowiol mounting media, pH 8.5	0.2 M Tris-HCL buffer, pH 8.5 12 g Mowiol in 30 ml ddH_2O Mix Mowiol solution and Tris-HCL buffer 1:2 Stear 45 min at 90°C, cool to 50°C 26,7% fluorescent free glycerin
Native lysis buffer (NLB) (1x), pH 7.4	1 mM EDTA 20 mM Tris 150 mM NaCl
Neutral Red destaining solution	50% Ethanol (≥ 99.8%) 1% Acetic acid (100%) *ad* ddH_2O
Neutral Red stock solution (0.4%)	40 mg Neutral Red 10 ml PBS
Paraformaldehyde (PFA) fixation buffer, pH 7,4	4% PFA *ad* ddH_2O, 60°C until dissolved
RSB Buffer	10 mM Tris, pH 7.4 10 mM NaCl 1.5 mM MgCl2 10 mM Sodium fluoride (NaF) 1:100 Phosphatase Inhibitor Cocktail II
SDS buffer (5x) + 10% 2-Mercaptoethanol	1563 µl Tris (1 M, pH 6.8) 2500 µl Glycerine (≥ 99.0%) 500 µl 2-Mercaptoethanol 0.5 g SDS 437 µl ddH_2O Bromophenol blue sodium salt (spatula tip)
Stripping buffer with 2-Mercaptoethanol	2% SDS 62.5 mM Tris 0.5% 2-Mercaptoethanol *ad* ddH_2O
TAE buffer (50x), pH 8	1M Tris 5.7% Acetic acid (100%) 0.5 M EDTA *ad* ddH_2O

TBS buffer (10x)	200 mM Tris 1.4 M NaCl *ad* ddH_2O
T-TBS buffer (1x)	TBS (10x) *ad* ddH_2O 0.1% Tween 20

7.1.4 Mice

Supplementary table 5: List of mice

Cell line	Company (headquarter)
C57BL/6	Charles River (Wilmington, Massachusetts, US)
C57BL/6J	Jackson Laboratory (Bar Harbor, Maine, US)
C57BL/6J-$mt^{FVB/NJ}$	Generated as described previously(Yu et al., 2009a), maintained in the animal facility at the University of Lübeck, Germany and kindly provided by the Institute of Dermatology.

7.1.5 Cells

Supplementary table 6: List of cells

Cell line	Company (headquarter)
HAP1 (+/- CRISPR/Cas9 induced p32 knockout)	Horizon Discovery Group plc (Cambridge, United Kingdom)
HT29-MTX-E12	Sigma Aldrich, St. Louis, US
Difi	described by Olive et al in 1993 (Olive et al., 1993)
T84	kindly provided by Markus Huber-Lang, University Hospital Ulm, Ulm , Germany

7.1.6 Enzymes

Supplementary table 7: List of enzymes

Enzyme	Company (headquarter)
Accutase® solution	Th. Geyer GmbH & Co. KG (Renningen, Germany)
Caspase-1, active (600 U/ml)	Enzo Life Sciences GmbH, Lörrach, Germany
DNase I Amplification Grade	Sigma-Aldrich Inc. (St. Louis, Missouri, USA)
DreamTaq PCR Master Mix (2x)	Thermo Fisher Scientific Inc. (Waltham, Massachusetts, USA)
Phusion Hot Start II DNA polymerase	Thermo Fisher Scientific Inc. (Waltham, Massachusetts, USA)
RevertAid H Minus Reverse Transcriptase (200 U/µl)	Thermo Fisher Scientific Inc. (Waltham, Massachusetts, USA)

7.1.7 Plasmids, recombinant proteins and siRNAs

Supplementary table 8: List of plasmids, recombinant proteins and siRNAs

Plasmid	Company (headquarter)
Human p32 siRNA (exon 3; s2138)	Thermo Fisher Scientific (Waltham, Massachusetts, USA)
Negative control siRNA	Thermo Fisher Scientific (Waltham, Massachusetts, USA)
P32, human GST-tagged (aa 1-282)	Abnova (Walnut, California, USA)
P32, human HIS-tagged (aa 74-282)	Prospec (East Brunswick, New Jersey, USA)
pCMV3-p32	Sino Biological Inc. (Beijing, China)

pCMV3-untagged-NCV (negative control vector)	Sino Biological Inc. (Beijing, China)
pUNO1-hASCa	InvivoGen Inc. (San Diego, California, USA)
pUNO1-hCASP1a	InvivoGen Inc. (San Diego, California, USA)
pUNO1-hNALP3a	InvivoGen Inc. (San Diego, California, USA)
pUNO1-mcs (negative control vector)	InvivoGen Inc. (San Diego, California, USA)

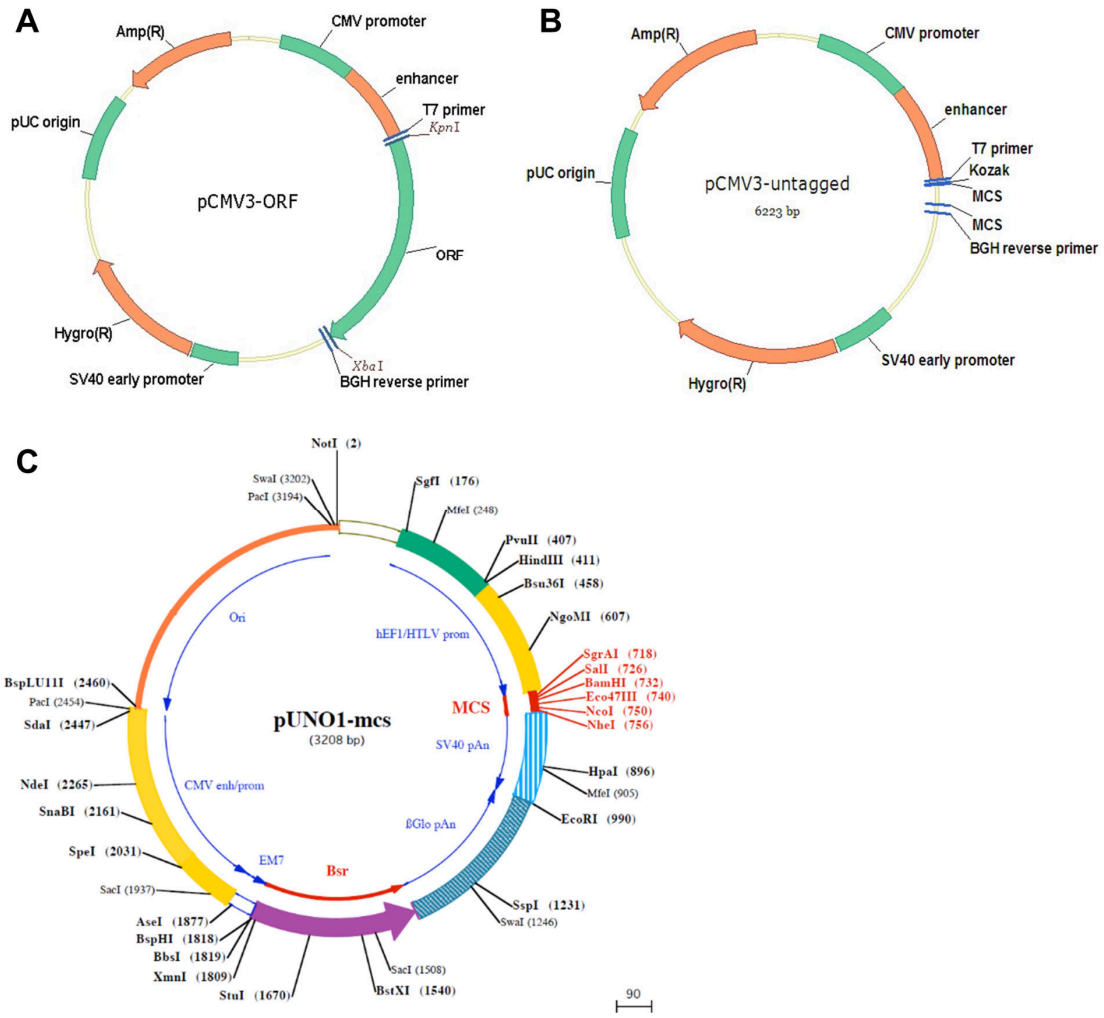

Supplementary figure 1: Vector maps of applied plasmids. A) Vector map of pCMV3-p32, carrying the full-length cDNA of human p32 (849 bp) between two multiple cloning sides. **B)** Vector map of pCMV3-untagged containing two multiple cloning sites (MCS). **A)** and **B)** pCMV3 vectors contain antibiotic resistance genes for hygromycin (Hygro(R)) and ampicillin (AMP(R)) and were ordered from Sino Biological Inc. (Beijing, China). Vector maps were provided from Sino Biological Inc. (Beijing, China). **C)** Vector map of p-UNO-1-mcs containing a MCS and a blasticidin S resistant gene (Bsr). Plasmids were ordered with inserted full-length cDNA for human NALP3 isoform 1 (3,143 bp), human ASC isoform (633 bp) or human CASP1 isoform α (1,266 bp) from InvivoGen Inc. (San Diego, California, USA).

7.1.8 Oligonucleotides and TaqMan® probes

Supplementary table 9: List of oligonucleotides. The following primers were produced by and ordered from Metabion international AG (Planegg, Germany).

Target genes human:	Forward primer (5‘-3‘)	Reverse primer (5‘-3‘)
ASC	GAGAACCTGACCGCCGAG	CCTTCCCGTACAGAGCATCC
ATOH1	CCAGCTGCGCAATGTTATCC	TGCTGTTTTCCTCCTGCACT
ß-ACTIN	ACATCCGCAAAGACCTGTACG	TTGCTGATCCACATCTGCTGG
Caspase-1	CAAGACCTCTGACAGCACGT	GCATCTGCGCTCTACCATCT
KLF4	CCATCTTTCTCCACGTTCG	ATCGGATAGGTGAAGCTGCA
Muc2	GACGGAGCTGAAGTTGGAAG	GGACACGGAGATGTTGGAGT
Muc5AC	CTGTGTCAAAGTGTGCCTGC	TTGATCACCACCACCGTCTG
NLRP3	CGTTCCAGGGAGTCGTTTGA	GGCCTTCCTTTTCCTCCTCC
P32	CTGCACACCGACGGAGACAA	CATATAAGGCCCAGTCCAAG
P32_nt231-mut	GGCTCGCTGCACACCGAGGGAGACAAAGCTTTTG	CAAAAGCTTTGTCTCCCTCGGTGTGCAGCGAGCC
P32_nt687-mut	CACTCAACACAGAGTCCTTGGACTGGG	CCCAGTCCAAGGACTCTGTGTTGAGTG
SPDEF1	GATTCACTACTGTGCCTCGAC	ATGTCTGGCTTCCGGATGAT
T7_for; BGH_rev	TAATACGACTCACTATAGGG	TAGAAGGCACAGTCGAGG
Target genes mouse:	**Forward primer (5‘-3‘)**	**Reverse primer (5‘-3‘)**
atoh1	GTGGGGTTGTAGTGGACGAG	GTTGCTCTCCGACATTGGG
ß-actin	GATGCTCCCCGGGCTGTATT	GGGGTACTTCAGGGTCAGGA
cxcl1/kc	GCTGGGATTCACCTCAAGAA	TGGGGACACCTTTTAGCATC
ki67	CCTGCCCGACCCTACAAAAT	TTGCTCACACTCGATGCAGT
klf4	GATTAAGCAAGAGGCGGT	GGTAAGGTTTCTCGCCTGTG
lgr5	CGGCAACAGTGTGGACGACCT	GCGAGCACTGCACCGAGTGA
muc2	GCTGACGAGTGGTTGGTGAATG	GATGAGGTGGCAGACAGGAGAC
p32	CGCTCTGCACACGGAAGGAG	CGGCCTCATCTTCGTGTCCA
spdef1	GGAGAAGGCAGCATCAGGA	CCAGGGTCTGCTGTGATGT

Supplementary table 10: List of TaqMan® probes

Target genes	Exon-exon junction	Assay ID (Thermo Fisher Scientific)
Human ß-ACTIN	Exon 1	Hs99999903_m1
Human p32	Exon 1	Hs05053979_g1
Human p32	Exon 1-2	Hs00241825_m1
Human p32	Exon 2-3	Hs00911223_g1
Human p32	Exon 3-4	Hs00911220_g1
Human p32	Exon 4-5	Hs00911221_g1
Human p32	Exon 5-6	Hs00911222_g1
Murine ß-actin	Exon 2-3	Mm01205647_g1
Murine p32	Exon 3-4	Mm01245770_m1

7.1.9 Antibodies

Supplementary table 11: List of antibodies

Primary antibodies	Species	Company	Working concentration
Anti-AKT (#9272)	rabbit	Cell Signaling (Danvers, Massachusetts, USA)	1:1000 (WB)[a]
Anti-AMPKα (#2532)	rabbit	Cell Signaling (Danvers, Massachusetts, USA)	1:1000 (WB)[a]
Anti-ASC (#13833)	rabbit	Cell Signaling (Danvers, Massachusetts, USA)	1:1000 (WB)[a]
Anti-α-Tubulin (#2125)	rabbit	Cell Signaling (Danvers, Massachusetts, USA)	1:1000 (WB)[a]
Anti-β-Actin (#4967)	rabbit	Cell Signaling (Danvers, Massachusetts, USA)	1:1000 (WB)[a]
Anti-Caspase-1 (#2225)	rabbit	Cell Signaling (Danvers, Massachusetts, USA)	1:100 (IHC); 1:1000 (WB)[a]
Anti-mouse IgA α-chain (PAB9360)	rabbit	Abnova, Taipei, Taiwan	0.5 µg/ml (ELISA)
Anti-mouse Ig light chain κ (407201)	rat	Biolegend, San Diego, CA, US	1 µg/ml (ELISA)
Anti-mouse Ig light chain λ (407302)	rat	Biolegend, San Diego, CA, US	1 µg/ml (ELISA)
Anti-human KLF4 (AF3640)	goat	R&D Systems (Minneapolis, Minnesota, USA)	4 µg/ml (IHC); 1 µg/ml (WB)
Anti-murine KLF4 (AF3158)	goat	R&D Systems (Minneapolis, Minnesota, USA)	3.3 µg/ml (IHC)
Anti-Muc2 (clone H-300)	rabbit	Santa Cruz Biotechnologie (Dallas, Texas, USA)	2 µg/ml (IF)
Anti-Muc5AC (clone 45M1)	mouse	Bioss (Woburn, Massachusetts, USA)	2 µg/ml (IHC); 1 µg/ml (ELISA)
Anti-NLRP3 (clone D4D8T)	rabbit	Cell Signalling (Danvers, Massachusetts, USA)	1:1000 (WB)[a]
Anti-p32 (clone EPR8871)	rabbit	Abcam (Cambridge, UK)	2 µg/ml (IHC); 0.4 µg/ml (WB)
Anti-p32 (clone 60.11)	mouse	Abcam (Cambridge, UK)	1 µg/ml (WB)
Anti-p32 (clone 74.5.2)	mouse	Hycult Biotech (Uden, Netherlands)	0.5 µg/ml (ELISA)
Anti-p32 exon 1	rabbit	kindly provided by Berhane Ghebrehiwet	1 µg/ml (WB)
Anti-p32 exon 3	rabbit	kindly provided by Berhane Ghebrehiwet	1 µg/ml (ELISA)
Anti-p32 exon 6	rabbit	kindly provided by Berhane Ghebrehiwet	5 µg/ml (IHC); 1 µg/ml (WB)
Anti-p44/42 MAPK (clone 137F5)	rabbit	Cell Signalling (Danvers, Massachusetts, USA)	1:1000 (WB)[a]
Anti-pAKT (Ser473, clone D9E)	rabbit	Cell Signaling (Danvers, Massachusetts, USA)	1:1000 (WB)[a]
Anti-pAMPKα (Thr 172, clone 40H9)	rabbit	Cell Signalling (Danvers, Massachusetts, USA)	1:1000 (WB)[a]

Anti-pp44/42 MAPK (Thr202/Tyr204, clone D13.14.4E)	rabbit	Cell Signalling (Danvers, Massachusetts, USA)	1:1000 (WB)[a]
Anti-TOMM22	rabbit	Sigma-Aldrich (St. Louis, Missouri, US)	2.5 µg/ml (IHC)
Immunoglobulin Fraction	rabbit	Agilent (Santa Clara, California, USA)	[b]
Isotype control	goat	R&D Systems (Minneapolis, Minnesota, USA)	[b]
Isotype control	mouse	Biotech (Onsala, Sweden)	[b]
Secondary antibodies/ labelled polymers		**Company**	**Working concentration**
AlexaFluor 594 goat anti-rabbit IgG		Thermo Fisher Scientific Inc. (Waltham, Massachusetts, USA)	8 µg/ml (IF)
AlexaFluor 594 goat anti-rabbit IgG		Thermo Fisher Scientific Inc. (Waltham, Massachusetts, USA)	8 µg/ml (IF)
Anti-mouse IgG HRP		Cell Signalling (Danvers, Massachusetts, USA)	1:1000 (ELISA); 1:4000 (WB)[a]
Anti-rabbit IgG HRP		Cell Signalling (Danvers, Massachusetts, USA)	1:1000 (ELISA); 1:4000 (WB)[a]
Anti-goat IgG HRP		Agilent (Santa Clara, California, USA)	1 µg/ml (IHC); 0.5 µg/ml (WB)
EnVision+ System- HRP Labelled polymer Anti-Rabbit		Agilent (Santa Clara, California, USA)	Not applicable
EnVision+ System- HRP Labelled polymer Anti-Rabbit		Agilent (Santa Clara, California, USA)	Not applicable

[a] Antibody dilution was listed, if concentration was not provided by the manufacturer.
[b] Isotype controls were applied in concentrations of corresponding primary antibody of interest.

7.1.10 Instruments

Supplementary table 12: List of instruments

Instrument	Company (headquarter)
Accu-jet® pro pipetting aid	BRAND GmbH + Co. KG (Wertheim, Germany)
Accurpette pipetting aid	VWR International LLC. (Radnor, Pennsylvania, USA)
Attune NxT cytometer	Thermo Fisher Scientific Inc. (Waltham, Massachusetts, USA)
Autoclave VX-75	Systec GmbH (Linden, Germany)
Axio Scope.A1 microscope Axiocam 503 color microscope camera	Carl Zeiss AG (Oberkochen, Germany)
BarnsteadTM GenPureTM Pro UV/UF – TOC system for bidistilled water	Thermo Fisher Scientific Inc. (Waltham, Massachusetts, USA)
Bottle-top dispenser CalibrexTM 520 (10 ml)	Socorex Isba S.A. (Ecublens, Switzerland)
Centrifuge MC 6	Sarstedt AG & Co. KG (Nümbrecht, Germany)
Centrifuge Sigma 2K 15	Sigma Laborzentrifugen GmbH (Osterode am Harz, Germany)
ChemiDocTM XRS+ Imaging System	Bio-Rad Laboratories Inc. (Hercules, California, USA)
CriterionTM Cell 135BR gel electrophoresis system	Bio-Rad Laboratories Inc. (Hercules, California, USA)
Electrophoresis power supply 3000Xi	Bio-Rad Laboratories Inc. (Hercules, California, USA)
Endoscope camera Tricam SL II	KARL STORZ (Tuttlingen, Germany)

Endoscope light source Xenon 175	KARL STORZ (Tuttlingen, Germany)
Endoscope-optic HOPKINS® II 64019 BA	KARL STORZ (Tuttlingen, Germany)
Film sealing device FS 3604	SEVERIN Elektrogeräte GmbH (Sundern, Germany)
Fluorometer Quibit 2.0	Thermo Fisher Scientific Inc. (Waltham, Massachusetts, USA)
FormaTM Steri-CycleTM i160 CO2 Incubator	Thermo Fisher Scientific Inc. (Waltham, Massachusetts, USA)
Freezers (- 20°C)	Liebherr-International AG (Bulle, Switzerland) Robert Bosch GmbH (Gerlingen, Germany) Siemens (München, Germany)
Freezers (- 80°C)	Liebherr-International AG (Bulle, Switzerland) Sanyo Electric Co. Ltd. (Watford, United Kingdom)
Gel documentation system Quantum ST4	Vilber Lourmat Deutschland GmbH (Eberhardzell, Germany)
Glassware (bottles, Erlenmeyer flasks)	DWK Life Sciences GmbH (Wertheim, Germany)
Gyratory rocker SSL3	Cole-Parmer Instrument Company, LLC. (Vernon, Illinois, USA)
Heraeus Multifuge X3 FR	Thermo Fisher Scientific Inc. (Waltham, Massachusetts, USA)
Hotplate Stirrer RT2 Basic	Thermo Fisher Scientific Inc. (Waltham, Massachusetts, USA)
Ice Machine UFF-0350A	Manitowoc Ice Inc. (Manitowoc, Wisconsin, USA)
Incubator HeracellTM VIOS 160i	Thermo Fisher Scientific Inc. (Waltham, Massachusetts, USA)
Incubator INCU-Line®	VWR International LLC. (Radnor, Pennsylvania, USA)
Incubator Heratherm	Thermo Fisher Scientific Inc. (Waltham, Massachusetts, USA)
Inverted microscope Primovert	Carl Zeiss AG (Oberkochen, Germany)
Laminar flow cabinet NU-425-600E (Class II Type A/B3)	NuAire Inc. (Plymouth, Minnesota, USA)
Liquid nitrogen tank LocatorTM 8 Plus	Thermo Fisher Scientific Inc. (Waltham, Massachusetts, USA)
Microcentrifuge, MiniStar silverline	VWR International LLC. (Radnor, Pennsylvania, USA)
Microplate Reader SpectraMax® iD3	Molecular Devices, LLC. (San José, California, USA)
Microtome Hn-40	Jung (Heidelberg, Germany)
Microwave HMT702C	Robert Bosch GmbH (Gerlingen, Germany)
Minishaker MS1 and MS2	IKA Werke GmbH & Co. KG (Staufen im Breisgau, Germany)
MiSeq™-System	Illumina (San Diego, California, USA)
Multifuge X3R	Thermo Fisher Scientific Inc. (Waltham, Massachusetts, USA)
Multipette® M4	Eppendorf AG (Hamburg, Germany)
Multipette® plus repetitive pipette	Eppendorf AG (Hamburg, Germany)
Multi-Tube Vortexer	SMI
NalgeneTM Cryo 1°C Freezing Container	Thermo Fisher Scientific Inc. (Waltham, Massachusetts, USA)
NalgeneTM Cryogenic Storage Boxes	Thermo Fisher Scientific Inc. (Waltham, Massachusetts, USA)
NanoDropTM 2000c Spectrophotometer	Thermo Fisher Scientific Inc. (Waltham, Massachusetts, USA)
Neubauer-improved counting chamber	Paul Marienfeld GmbH & Co. KG (Lauda-Königshofen, Germany)
NucleoBondTM Xtra Combi Rack	Macherey-Nagel GmbH & Co. KG (Düren, Germany)
Orbital microplate shaker Type HKS 250	Behring Shaker Optoelectronic Control (Germany)
Orbital shaker TCR 170	Heidolph Instruments GmbH & Co. KG (Schwabach, Germany)
OwlTM EasyCastTM horizontal electrophoresis system (models B1A and B2) with trays and combs	Thermo Fisher Scientific Inc. (Waltham, Massachusetts, USA)
pH meter pH3110 + pH electrode SenTix® 41	WTW GmbH (Weilheim, Germany)
Piston-operated pipettes Research® plus (0.5 – 10 µl, 10 – 100 µl, 100 – 1,000 µl)	Eppendorf AG (Hamburg, Germany)
PowerPacTM Basic Power Supply	Bio-Rad Laboratories Inc. (Hercules, California, USA)
Precellis® 24 homogenizer	Bertin Instruments (Montigny-le-Bretonneux, France)
Precision scales ABS 120-4	KERN & SOHN GmbH (Balingen, Germany)
Precision scales PFB 200-3	KERN & SOHN GmbH (Balingen, Germany)

Refrigerators	Liebherr-International AG (Bulle, Switzerland) Robert Bosch GmbH (Gerlingen, Germany)
Rocking platform Mini Rocker	Bio-Rad Laboratories Inc. (Hercules, California, USA)
Seahorse XF24 analyzer	Agilent (Santa Clara, California, USA)
Shaking incubator MaxQTM 4000	Thermo Fisher Scientific Inc. (Waltham, Massachusetts, USA)
Sigma 1-14 centrifuge	Sigma Laborzentrifugen GmbH (Osterode am Harz, Germany)
Single channel pipettes, Ultra High-Performance (0.5 – 10 µl, 10 – 100 µl, 100 – 1,000 µl)	VWR International LLC. (Radnor, Pennsylvania, USA)
Sonorex RK 102 Transistor	BANDELIN electronic GmbH & Co. KG (Berlin, Germany)
Standard Power Pack P25 Power Supply	Biometra GmbH (Göttingen, Germany)
Steamer	Braun (Kronberg in Taunus, Germany)
StepOnePlus Real-Time PCR System	Thermo Fisher Scientific Inc. (Waltham, Massachusetts, USA)
Stereo microscope Leica S6 E + Leica KL300 LED fiber optic light source	Leica Microsystems GmbH (Wetzlar, Germany)
Thermoblock Biometra® TB1	Biometra GmbH (Göttingen, Germany)
Thermocycler T1	Biometra GmbH (Göttingen, Germany)
Thermocycler TGradient	Biometra GmbH (Göttingen, Germany)
Thermomixer Compact	Eppendorf AG (Hamburg, Germany)
Trans-Blot® SD Semi-Dry Transfer Cell	Bio-Rad Laboratories Inc. (Hercules, California, USA)
Transferpette® -8 (30 – 300 µl)	BRAND GmbH + Co. KG (Wertheim, Germany)
Vortex Mixer Advanced ZX3	VELP Scientifica Srl (Usmate, Italy)
Vortex mixer REAX 2000	Heidolph Instruments GmbH & Co. KG (Schwabach, Germany)
Vortex-Genie 2	Scientific Industries Inc. (Bohemia, New York, USA)
Waterbath Type 1007	Gesellschaft für Labortechnik (GFL) mbH (Burgwedel, Germany)
Waterbath Type 3048	Köttermann GmbH & Co. KG (Uetze, Germany)
Waterbath WNB 29	Memmert GmbH & Co. KG (Schwabach, Germany)

7.1.11 Supplies

Supplementary table 13: List of supplies

Product	Company (headquarter)
96 fast PCR Plate half skirt	Sarstedt AG & Co. KG (Nümbrecht, Germany)
96-Well Assay Plates Costar® (black, clear bottom, with lid, tissue culture treated)	Corning Inc. (Corning, New York, USA)
Acetate Foils for 96-Well Plates	Sarstedt AG & Co. KG (Nümbrecht, Germany)
AmershamTM HybondTM PVDF blotting membrane (0.2 µm)	GE Healthcare (Chicago, Illinois, USA)
Bacillol® AF surface disinfectant	Bode Chemie GmbH (Hamburg, Germany)
Biosphere® Filter Tips (0.1 – 20 µl, 2 – 100 µl, 100 – 1000 µl)	Sarstedt AG & Co. KG (Nümbrecht, Germany)
Blot filter paper (extra thick, 19.0 x 18.5 cm)	Bio-Rad Laboratories Inc. (Hercules, California, USA)
Cannulae Sterican® (20 G, 24 G, 26 G)	B. Braun Melsungen AG (Melsungen, Germany)
Combitips advanced® (5 ml, 1 ml, 0.2 ml)	Eppendorf AG (Hamburg, Germany)
Combitips advanced® Eppendorf Biopur® (sterile) (5 ml)	Eppendorf AG (Hamburg, Germany)
Cover glasses, 24x32 mm	Th. Geyer GmbH & Co. KG (Renningen, Germany)
Cover glasses, Haemacytometer	Th. Geyer GmbH & Co. KG (Renningen, Germany)
CriterionTM TGXTM 4 – 15% Precast Midi Protein Gel (18 well, 30 µl and 26 well, 15 µl)	Bio-Rad Laboratories Inc. (Hercules, California, USA)
CryoPure tubes (1.0 ml, white)	Sarstedt AG & Co. KG (Nümbrecht, Germany)

+ color coded inserts	
Filtropur S 0.2 syringe filtration unit (pore size 0.2 µm)	Sarstedt AG & Co. KG (Nümbrecht, Germany)
Gel Releaser	Bio-Rad Laboratories Inc. (Hercules, California, USA)
Helipur®	B. Braun Melsungen AG (Melsungen, Germany)
Injekt®-F single-use syringes (1 ml)	B. Braun Melsungen AG (Melsungen, Germany)
Inoculating loops (disposable, 1 µl)	VWR International LLC. (Radnor, Pennsylvania, USA)
Micro tubes (1.5 ml, 2.0 ml)	Sarstedt AG & Co. KG (Nümbrecht, Germany)
Micro tubes (1.5 ml, 2.0 ml) (sterile, DNase/RNase free)	Sarstedt AG & Co. KG (Nümbrecht, Germany)
MicroAmpTM Optical Adhesive Film (for 384- or 96-Well Plates)	Thermo Fisher Scientific Inc. (Waltham, Massachusetts, USA)
Microtest plate (96 Well, canonical bottom)	Sarstedt AG & Co. KG (Nümbrecht, Germany)
Microtest Plates 96 Well, F	Sarstedt AG & Co. KG (Nümbrecht, Germany)
MICRO-TOUCH® Nitra-Tex® nitrile gloves (powder-free)	Ansell Ltd. (Yarra City, Australia)
Mini-Protean® Cassette Opening Lever	Bio-Rad Laboratories Inc. (Hercules, California, USA)
Multiply®-µStrip Pro 4-strips (0.2 ml tubes, DNase/RNase free)	Sarstedt AG & Co. KG (Nümbrecht, Germany)
Multitex® Wipes	Zellstoff-Vertriebs-GmbH & Co. KG (Troisdorf, Germany)
Parafilm® M	Carl Roth GmbH + Co. KG (Karlsruhe, Germany)
Pipette tips with microcapillary for loading gels (1 – 200 µl)	VWR International LLC. (Radnor, Pennsylvania, USA)
Pellet Pestle™	Kimble Chase, Life Science (Vineland, New Jersey, USA)
Pipette tips without filter (10 – 200 µl)	Th. Geyer GmbH & Co. KG (Renningen, Germany)
Pipette tips without filter (10 µl, 1000 µl)	Sarstedt AG & Co. KG (Nümbrecht, Germany)
Plastic film (transparent, 0.1 mm)	Th. Geyer GmbH & Co. KG (Renningen, Germany)
Protran® BA83 nitrocellulose membrane (0.2 µm)	Whatman GmbH (Dassel, Germany)
RNaseZapTM RNase Decontamination Wipes	Thermo Fisher Scientific Inc. (Waltham, Massachusetts, USA)
Seahorse FluxPaks	Agilent (Santa Clara, California, USA)
Serological pipettes (sterile) (5 ml, 10 ml, 25 ml, 50 ml)	Sarstedt AG & Co. KG (Nümbrecht, Germany)
Slides, Menzel Superfrost®	Thermo Fisher Scientific Inc. (Waltham, Massachusetts, USA)
Staining Jars	Carl Roth GmbH + Co. KG (Karlsruhe, Germany)
Sterillium® classic pure hand disinfectant	Bode Chemie GmbH (Hamburg, Germany)
Syringe with BD Luer-LokTM Tip	Becton, Dickinson & Company (Franklin Lakes, New Jersey, USA)
TC dishes 100 (standard)	Sarstedt AG & Co. KG (Nümbrecht, Germany)
TC dishes 100 (suspension)	Sarstedt AG & Co. KG (Nümbrecht, Germany)
Tissue culture flasks (T25, T75) (Cell+, Vented Cap)	Sarstedt AG & Co. KG (Nümbrecht, Germany)
Tissue culture plates (6 Well, Standard, F)	Sarstedt AG & Co. KG (Nümbrecht, Germany)
Tissue culture plates (96 Well, Cell+, F)	Sarstedt AG & Co. KG (Nümbrecht, Germany)
Tissue embedding casettes	Carl Roth GmbH + Co. KG (Karlsruhe, Germany)
Transfer pipettes (3 ml)	Sarstedt AG & Co. KG (Nümbrecht, Germany)
Tubes (15 ml, 50 ml)	Sarstedt AG & Co. KG (Nümbrecht, Germany)

7.1.12 Software and Databases

Supplementary table 14: List of software and databases

Software	Company (headquarter)
BioEdit 7.2	Bioedit company (Manchester, UK)
FlowJo™ V10	Becton, Dickinson & Company (Franklin Lakes, New Jersey, USA)
GIMP 2.10.18	GIMP-Team (*https://www.gimp24.de/)*
ImageJ	National Institutes of Health (NIH) (Bethesda, Maryland, USA)
ImageLab™	Bio-Rad Laboratories Inc. (Hercules, California, USA)
NanoDrop 2000/2000c	Thermo Fisher Scientific Inc. (Waltham, Massachusetts, USA)
Quantum-Capt software for gel imaging	Vilber Lourmat Deutschland GmbH (Eberhardzell, Germany)
Primer3web version 4.1.0 (primer3.ut.ee)	Whitehead Institute for Biomedical Research (Cambridge, Massachusetts, USA)
GraphPad Prism 6.0	GraphPad Software Inc. (San Diego, California, USA)
Seahorse Wave	Agilent (Santa Clara, California, USA)
StepOneTM S v2.3	Thermo Fisher Scientific Inc. (Waltham, Massachusetts, USA)
ZEN 2.3 lite	Carl Zeiss AG (Oberkochen, Germany)
Database	**Website**
GTExPortal	*https://gtexportal.org/home/*
NCBI (National Center for Biotechnology Information)	*https://www.ncbi.nlm.nih.gov/*
Nucleotide BLAST	*https://blast.ncbi.nlm.nih.gov/Blast.cgi?PAGE_TYPE=BlastSearch*
PeptideCutter Expasy	*https://web.expasy.org/peptide_cutter/*
Phyre2	*http://www.sbg.bio.ic.ac.uk/phyre2/html/page.cgi?id=index*
Primer3	*https://primer3.ut.ee/*
STRING database	*https://string-db.org/*
TargetP 1.1	*http://www.cbs.dtu.dk/services/TargetP-1.1/index.php*
The Human Protein Atlas	*https://www.proteinatlas.org/*
UCSC genome browser	*https://genome.ucsc.edu/cgi-bin/hgGateway*

7.2 Publications

- Loss of mucosal p32/gC1qR/HABP1 triggers energy deficiency and impairs goblet cell differentiation in ulcerative colitis.

Sünderhauf A, Hicken M, Schlichting H, Skibbe K, Ragab M, Raschdorf A, Hirose M, Schäffler H, Bokemeyer A, Bettenworth D, Savitt AG, Ibrahim S, Perner S, Peerschke E, Ghebrehiwet B, Derer S, Sina C. Cell Mol Gastroenterol Hepatol. 2021 Jan 27;S2352-345X(21)00023-0. doi: 10.1016/j.jcmgh.2021.01.017. PMID: 33515804

- Heterozygous P32/ C1QBP/ HABP1 Polymorphism rs56014026 Reduces Mitochondrial Oxidative Phosphorylation and Is Expressed in Low-grade Colorectal Carcinomas.

Raschdorf A, **Sünderhauf A**, Skibbe K , Ghebrehiwet B, Peerschke EI, Sina C, Derer S. Front Oncol. 2021 Feb 8;10:631592. doi: 10.3389/fonc.2020.631592. eCollection 2020. PMID: 33628739

- GC1qR Cleavage by Caspase-1 Drives Aerobic Glycolysis in Tumor Cells.

Sünderhauf A, Raschdorf A, Hicken M, Schlichting H, Fetzer F, Brethack AK, Perner S, Kemper C, Ghebrehiwet B, Sina C, Derer S. Front Oncol. 2020 Sep 30;10:575854. doi: 10.3389/fonc.2020.575854. eCollection 2020. PMID: 33102234.

- Saccharin Supplementation Inhibits Bacterial Growth and Reduces Experimental Colitis in Mice.

Sünderhauf A, Pagel R, Künstner A, Wagner AE, Rupp J, Ibrahim SM, Derer S, Sina C. Nutrients. 2020 Apr 17;12(4):1122. doi: 10.3390/nu12041122. PMID: 32316544.

- Short-term high-fat diet feeding protects from the development of experimental allergic asthma in mice.

Schröder T, Wiese AV, Ender F, Quell KM, Vollbrandt T, Duhn J, **Sünderhauf A**, Künstner A, Moreno-Fernandez ME, Derer S, Aherrahrou Z, Lewkowich I, Divanovic S, Sina C, Köhl J, Laumonnier Y. Clin Exp Allergy. 2019 Sep;49(9):1245-1257. doi: 10.1111/cea.13454. Epub 2019 Aug 13. PMID: 31265181.

- Mitochondrial gene polymorphism is associated with gut microbial communities in mice.

Hirose M, Künstner A, Schilf P, **Sünderhauf A**, Rupp J, Jöhren O, Schwaninger M, Sina C, Baines JF, Ibrahim SM. Sci Rep. 2017 Nov 10;7(1):15293. doi: 10.1038/s41598-017-15377-7. PMID: 29127319.

- Regulation of epithelial cell expressed C3 in the intestine - Relevance for the pathophysiology of inflammatory bowel disease?

Sünderhauf A, Skibbe K, Preisker S, Ebbert K, Verschoor A, Karsten CM, Kemper C, Huber-Lang M, Basic M, Bleich A, Büning J, Fellermann K, Sina C, Derer S. Mol Immunol. 2017 Oct;90:227-238. doi: 10.1016/j.molimm.2017.08.003. Epub 2017 Aug 24. PMID: 28843904.

- Circadian rhythm disruption impairs tissue homeostasis and exacerbates chronic inflammation in the intestine.

Pagel R, Bär F, Schröder T, **Sünderhauf A**, Künstner A, Ibrahim SM, Autenrieth SE, Kalies K, König P, Tsang AH, Bettenworth D, Divanovic S, Lehnert H, Fellermann K, Oster H, Derer S, Sina C. FASEB J. 2017 Nov;31(11):4707-4719. doi: 10.1096/fj.201700141RR. Epub 2017 Jul 14. PMID: 28710114.

- Thermoneutral housing exacerbates nonalcoholic fatty liver disease in mice and allows for sex-independent disease modeling.

Giles DA, Moreno-Fernandez ME, Stankiewicz TE, Graspeuntner S, Cappelletti M, Wu D, Mukherjee R, Chan CC, Lawson MJ, Klarquist J, **Sünderhauf A**, Softic S, Kahn CR, Stemmer K, Iwakura Y, Aronow BJ, Karns R, Steinbrecher KA, Karp CL, Sheridan R, Shanmukhappa SK, Reynaud D, Haslam DB, Sina C, Rupp J, Hogan SP, Divanovic S. Nat Med. 2017 Jul;23(7):829-838. doi: 10.1038/nm.4346. Epub 2017 Jun 12. PMID: 28604704.

- Mitochondrial gene polymorphisms alter hepatic cellular energy metabolism and aggravate diet-induced non-alcoholic steatohepatitis.

Schröder T, Kucharczyk D, Bär F, Pagel R, Derer S, Jendrek ST, **Sünderhauf A**, Brethack AK, Hirose M, Möller S, Künstner A, Bischof J, Weyers I, Heeren J, Koczan D, Schmid SM, Divanovic S, Giles DA, Adamski J, Fellermann K, Lehnert H, Köhl J, Ibrahim S, Sina C. Mol Metab. 2016 Feb 2;5(4):283-295. doi: 10.1016/j.molmet.2016.01.010. eCollection 2016 Apr. PMID: 27069868.

7.3 Conference contributions

7.3.1 Talks

06/2017 – Meeting of the German research foundation on inflammatory bowel diseases (DACED), Mainz, Germany. **Sünderhauf A**, Künstner A, Pagel R, Wagner AE, Ibrahim S, Derer S, Sina C. Saccharin: not as bad as its reputation?

07/2015 – Meeting of the DFG priority Program Intestinal microbiota", Seeon, Germany. **Sünderhauf A**, Bär F, Hirose M, Künstner A, Pagel R, Ibrahim S, Derer S, Sina C. Delineating mechanisms linking altered mitochondrial metabolism with microbiome changes and colitis susceptibility.

7.3.2 Poster

02/2020 – 15th Congress of Eurpean Crohn's and Colitis Organisation (ECCO), Vienna, Austria. **Sünderhauf A**, Hicken M, Schlichting H, Skibbe K, Hirose M, Perner S, Ibrahim S, Derer S, Sina C. GC1qR driven oxidative phosphorylation is essential for intestinal goblet cell differentiation.

01/2018 – Falk Symposium: Liver-Gut-Microbiome Interactions, Hamburg, Germany. **Sünderhauf A**, Bär F, Hirose M, Künstner A, Pagel R, Ibrahim S, Derer S, Sina C. Linking mucus depletion and microbiome alterations in Ulcerative Colitis to mucosal energy supply.

01/2018 – Falk Symposium: Liver-Gut-Microbiome Interactions, Hamburg, Germany. **Sünderhauf A**, Künstner A, Pagel R, Wagner AE, Ibrahim S, Derer S, Sina C. Saccharin supplementation modulates the intestinal microbiome and is protective in early stages of experimental colitis.

01/2017 – Keystone Symposium, Dublin, Ireland. **Sünderhauf A**, Künstner A, Pagel R, Wagner AE, Ibrahim S, Derer S, Sina C. Saccharin supplementation modulates the intestinal microbiome and is protective in early stages of experimental colitis.

06/2016 – Meeting of the German Research Foundation priority Program Intestinal microbiota", Seeon, Germany. **Sünderhauf A**, von Medem K, Künstner A, Bär F, Pagel R, Sadik C, Derer S, Sina C. 12/15-Lipoxygenase contributes to the resolution of experimental colitis in mice.

7.4 Acknowledgements

First of all, I would like to express my sincere gratitude to my supervisor Prof. Christian Sina. I deeply thank you for giving me the opportunity to work on this project as part of your research team. Your continuous support from Master to PhD and your guidance throughout the last five years enabled me to realize this work and made me the researcher I am know. Besides providing scientific knowledge and endless ideas for new scientific goals you always had an open ear for every matter whatsoever.

Secondly, my deepest gratefulness belongs to Dr. Stefanie Derer. You have been an excellent supervisor throughout the time of my PhD thesis, before and hopefully beyond. Each time I talked to you I was impressed by your scientific knowledge as well as by the time and effort you dedicate to your work. You taught me scientific accuracy, scientific thinking and that humanity and science are not two different pair of shoes.

This work would not have been possible without the continuous technical help from Maren Hicken and Heidi Schlichting as well as Ann-Kathrin Brethack and Miriam Freitag. You told me every step along the way from keeping order in my chaos to complex transfection, staining and sequencing procedures. Beside this, you always filled the lab with joy and laughter, so that it was seldom hard to get up and get to work.

I am very thankful to have had Annika Raschdorf, Kerstin Skibbe, Katharina Schlumm, Anna-Lena Thiel, Mohab Ragab and René Pagel as my PhD-colleges. Not only because you were always willing to share samples, data and laughter but also because you always had time to help or discuss content.

I also want to use the opportunity to thank Prof. Saleh Ibrahim, Dr. Misa Hirose as well as Prof. Berhane Ghebrehiwet. This work would not have been possible without the mice, antibodies and knowledge you provided.

My very personal thanks go to my wonderful husband, Paul Simon. You were always there to talk every detail of the day through and share every thought. You and our marvelous daughter, Anuk Lia Simon were always capable, at any time and in any situation, to make me think of something else than work. I also thank the unborn to keep its feet still and let me finish of this thesis.

I deeply want to say thank you to my mom, Sabine Sünderhauf, my dad, Andreas Sünderhauf and my brother, Jan-Ole Sünderhauf. I knew that I would be always able to call you whenever I needed help with whatsoever. You always had my back, caught me when I was overworked and remembered me to take a break when it was necessary.